MOLECULAR SELF-ASSEMBLY STUDY OF PEG BASED UNCONVENTIONAL AMPHIPHILES IN WATER AT ROOM TEMPERATURE

Thesis submitted to the

Indian Institute of Technology Kharagpur

For award of the degree

of

Doctor of Philosophy

by

Rita Ghosh

Under the guidance of

Prof. Joykrishna Dey

DEPARTMENT OF CHEMISTRY

INDIAN INSTITUTE OF TECHNOLOGY KHARAGPUR

FEBRUARY 2018

To my parents…

.

CERTIFICATE OF APPROVAL

Date: 07/02/2018

Certified that the thesis entitled ***"Molecular Self-assembly Study of PEG Based Unconventional Amphiphiles in Water at Room Temperature"*** *submitted by* ***Miss. Rita Ghosh*** *to Indian Institute of Technology, Kharagpur, for the award of the degree Doctor of Philosophy has been accepted by the external examiners and that the student has successfully defended the thesis in the viva-voce examination held today.*

----------	----------	----------
Prof. Nilmoni Sarkar (Member of the DSC)	Prof. Dibakar Dhara (Member of the DSC)	Prof. Tapas Kumar Maiti (Member of the DSC)
----------	----------	----------
Prof. Joykrishna Dey (Supervisor)	Prof. G. Krishnamoorthy (External Examiner)	Prof. Manish Bhattacharjee (Chairman)

Prof. Joykrishna Dey
Professor
Biophysical and Analytical Laboratory
Department of Chemistry
Indian Institute of Technology Kharagpur

CERTIFICATE

This is to certify that the thesis entitled ***"Molecular Self-assembly Study of PEG Based Unconventional Amphiphiles in Water at Room Temperature"*** *submitted by* ***Miss. Rita Ghosh*** *for the award of Doctor of Philosophy in Science (Chemistry) to Indian Institute of Technology, Kharagpur, India, is a bonafide research work carried out by her under my supervision. The thesis in my opinion has reached the requirements of the Institute's regulations relating to the award of the PhD degree. The contents of this thesis, in full or in parts, have not been submitted to any other Institute or University for the award of any degree or diploma.*

February, 2018
Indian Institute of Technology
Kharagpur

Prof. Joykrishna Dey
(Supervisor)

DECLARATION

I certify that

a. *The work contained in the thesis is original and has been done by myself under the general supervision of Prof. Joykrishna Dey, in the Department of Chemistry, Indian Institute of Technology, Kharagpur, India. .*

b. *The work has not been submitted to any other Institute for any degree or diploma.*

c. *I have followed the guidelines provided by the Institute in writing the thesis.*

d. *I have conformed to the norms and guidelines given in the Ethical Code of Conduct of the Institute.*

e. *Whenever I have used materials (data, theoretical analysis, and text) from other sources, I have given due credit to them by citing them in the text of the thesis and giving their details in the references.*

f. *Whenever I have quoted written materials from other sources, I have put them under quotation marks and given due credit to the sources by citing them and giving required details in the references.*

Kharagpur *Rita Ghosh*
February, 2018

Rita Ghosh
Email: ritag@chem.iitkgp.ernet.in
Born on March 4th, 1989 at Galsi of
Burdwan district under the state of West Bengal (India)
Graduation (B.Sc.) from Vivekananda Mahavidyalaya, Burdwan (W.B.) (2010)
Post Graduation (M. Sc.) from University of Burdwan (W.B.) (2012)
Joined in the Department of Chemistry, Indian Institute of Technology Kharagpur, Kharagpur, India in the year 2012 as a Junior Research Fellow.

ACKNOWLEDGEMENT

First of all, I would like to express my deep sense of gratitude to my research supervisor ***Prof. Joykrishna Dey****, Department of Chemistry, Indian Institute of Technology Kharagpur, India for his wise and valuable guidance without which my research work could never get a shape and this dissertation would not be complete.*

Sir; I am grateful to you for your continued interest and encouragement during my research work.

I wish to express my regards to Prof. M. Bhattacharjee, Head, Prof. T. Pathak and Prof. D. Mal, former Head of the Department of Chemistry for providing me all the departmental facilities during my research work.

I would also like to acknowledge the members of my doctoral scrutiny committee Prof. N. Sarkar, Prof. D. Dhara and Prof. T. K, Maiti for their valuable suggestions during my research work.

I would like to specially thank the Central Research Facility, IIT Kharagpur for providing me enormous research facilities, and IIT Kharagpur for providing me research fellowship.

I am grateful to Prof. N. Sarkar and Prof. D. Dhara, Department of Chemistry, IIT Kharagpur for DLS and zeta potential measurements.

I would like to thank all the faculty members, office staffs of the Chemistry Department and all the instrument operators for their help and co-operation.

I sincerely thank my colleagues Amritadi, Subhajitda, Parthada, Trilochanda, Ritadi, and Deepnath for their help and co-operation.

I also thank my friends, Kanika, Munmundi, Debarati, Aditya, Ruma, Sonali, Supriti, Sipradi, Rimpa, Sukanya, Krishnadi, Krishna, Sudipta, Sourav, Biswajit, Suman, Raka, Palashda, Animeshda, Biswajitda and all the well wishers who have always extended their helping hands when needed.

I convey my acknowledgement to my elder sister Munmun, my brother Amit, brother-in-law Sujitda, my uncles, aunts and my in-laws for their love, affection, and encouragement without which I would not be able to come up to this stage.

Finally, I would like to thank ***my father*** *Shri Mrinal Kanti Ghosh,* ***my mother*** *Smt. Bhaggyabati Ghosh,* ***my grandfather*** *late Shri Modan Mohan Ghosh, and* ***my grandmother*** *late Smt. Gita Ghosh for their unconditional love, care and encouragement throughout my life. I owe special thanks to the very special person, my husband,* ***Debasis****, for his incredible love, endless motivation and support in each step throughout the last two years. Without their sacrifices and prayers, I would not have had the opportunity to pursue my dreams.*

Thank you so much!

Rita Ghosh

Chapter 1 Introduction

Chapter 2 Materials and Methods

Chapter 4 pH-Responsive Self-Assembly Formation

4.1 Vesicle Formation Followed by Vesicle to Micelle Transition by Hydrocarbon and PEG-containing Double-Headed Amphiphiles

4.2 Self-assembly Behavior of Cholesterol and PEG Chain-Containing Amphiphiles at Room Temperature

Abbreviations

AFM	Atomic Force Microscopy
C 153	Coumarin 153
cac	Critical aggregation concentration
Cal	Calceine
CPP	Critical packing parameter
Chol	Cholesterol
cmc	Critical micelle concentration
CHN	Carbon Hydrogen Nitrogen
CFM	Confocal fluorescence microscopy
CTAB	Cetyltrimethylammonium bromide
DBU	1,8-diazabicycloundec-7-ene
DCE	Dichloroethane
DCM	Dichloromethane
DLS	Dynamic light scattering
DPH	1,6-diphenyl-1,3,5-hexatriene
DTAB	Dodecyltrimethylammonium bromide
EA	Ethyl acetate
FT IR	Fourier transforms infrared
ITC	Isothermal titration calorimetry
H-bonding	Hydrogen bonding
MB	Methylene blue
Mesna	Sodium-2-mercapto ethane sulfonate
MLM	Monolayer membrane
MLV	Multilamellar vesicle
mPEG	Methoxy poly(ethylene glycol) monomethacrylate
M.P.	Melting point
MVV	Multivesicular vesicle
NHS	N-hydroxysuccinimide
NMR	Nuclear Magnetic Resonance

NOESY	Nuclear Overhauser Effect Spectroscopy
NPN	N-Phenyl-1-naphthyl amine
PE	Pet ether
PEO	Poly(ethylene oxide)
PPO	Poly(propylene oxide)
Py	Pyrene
SDS	Sodium dodecyl sulfate
ST	Surface tension
TEA	Triethylamine
TEM	Transmission electron microscope
THF	Tetrahydrofuran
ULV	Unilamellar vesicle
UV	Ultraviolet

Symbols

C_s	Concentration of surfactant
^oC	Degree Celsius
r	Fluorescence anisotropy
g	Gram
γ	Surface/interfacial tension
Γ_{max}	Surface excess concentration
A_0	Area of head-group
κ	Specific Conductance
δ	Chemical shift
gL^{-1}	Gram per litre
h	Hour
d_h	Hydrodynamic diameter
lc	Critical chain length

mPa s	Mili pascal second
T	Temperature
T_m	Phase transition temperature
mM	Millimolar
mol	Mole
M	Molar
M_w	Weight average molecular weight
M_n	Number average molecular weight
N_A	Avogadro number
N_{agg}	Aggregation number
nm	Nanometer
θ	Scattering angle
s	Second
λ	Wavelength
ζ	Zetapotential
[η]	Intrinsic viscosity
τ_f	Fluorescence lifetime
μM	Micromolar

The work presented in this dissertation is focused on self-assembly behavior of PEG based unconventional amphiphiles. The objective of this study is to see how conventional surfactants containing hydrocarbon tail(s) would behave when their hydrophobic tail(s) is (are) substituted by so-called polar poly(ethylene glycol) (PEG) chain. With this in mind, a series of molecules consisting of a single or double PEG tails or a combination of a PEG and a hydrocarbon tail covalently linked to an anionic (sulfonate) or zwitterionic (L-cysteine) head was synthesized and characterized. Molecules with two zwitterionic heads connected by a PEG chain were also designed and developed. The self-assembly properties of these molecules in water at room temperature were investigated by use of a number of methods including surface tension, fluorescence, NMR, dynamic light scattering, transmission electron microscopy, atomic force microscopy and isothermal titration calorimetry. The surface tension measurements indicated that the molecules with only PEG chains as tail or spacer are less surface active in comparison to conventional surfactant molecules. But the molecules containing typical hydrophobe (hydrocarbon or cholesterol) and PEG chains were found to be surface active like conventional surfactants. However, fluorescence probe studies suggested that both single and double PEG-tailed molecules self-assemble in water at room temperature to spontaneously form stable vesicles. The results of fluorescence as well as 2D NOESY ^{1}H-NMR studies indicated that the vesicle bilayer is constituted by the PEG chains. The thermodynamic parameters also suggest that spontaneous vesicle formation is entropy driven process. This means as in the case conventional surfactants the hydrophobic interaction among the PEG chains is the major driving force for aggregate formation. In other words, the PEG chains behave like hydrocarbon chains. Interestingly, molecules containing both hydrocarbon and PEG chains, the latter acts as a polar head group. In other words, these molecules behave like conventional surfactants. In fact, these molecules exhibit thermodynamically stable vesicle formation followed by vesicle-to-micelle transition in concentrated solution. However, these amphiphiles exhibit LCST behavior at acidic pH. Zwitterionic bolaamphiphiles with low-molecular-weight PEG as spacer were also observed to spontaneously self-assemble in water at room temperature. Despite having so called polar spacer the bolaamphiphiles produce stable monolayer vesicles in water. The stability of monolayer and bilayer vesicle under physiological conditions suggests that they can be applied for encapsulating hydrophilic as well as hydrophobic guest molecules. The encapsulation and release of hydrophilic as well as hydrophobic guest molecules have been demonstrated in this work. Thus the vesicles can have potential applications in drug delivery.

Keywords: Amphiphiles, poly(ethylene glycol), bolaamphiphiles, vesicles, calorimetry, fluorescence, microscopy

Chapter 1
Introduction

1.1 What are amphiphiles?

Amphiphilic molecules are generally composed of a long hydrophobic tail and a hydrophilic head. The amphiphilic molecules upon adsorption at the air/water interface reduce surface tension (γ) of water and behave like surface-active agents. Since surfactant molecules consist of both hydrophilic (water-loving) and lipophiliic (fat-loving) groups, they are often termed as amphiphiles. When an amphiphile is dissolved in water, the hydrophobic tail causes disruption of water structure thereby increasing the overall free energy of the system. In order to avoid such unfavorable interactions the amphiphilic molecules preferentially adsorb at the air/water interface. But above a critical concentration the amphiphiles prefer to undergo self-assembly formation which results in a net decrease in free energy of the system as a whole. Thus, molecular self-assembly is a spontaneous organization of molecules driven by noncovalent forces such as hydrophobic effect, van der Waals, dipole-dipole, electrostatic and hydrogen-bonding interactions. The self-assembly is also well identified in biological systems such as lipid bilayer, DNA duplex, tertiary and quaternary structure of proteins. The spontaneous aggregate formation by amphiphilic molecules in solution into larger structures is also very important in our daily life as well as in bio-medical and drug delivery applications. There has been extensive fundamental and applied research about the properties of amphiphilic molecules in aqueous solution because of their widespread applications in chemistry, biochemistry, pharmaceuticals, petroleum recovery, detergents, cosmetics, paints, coatings, photographic films, mineral processing, food science, and also in drug design and drug delivery [1-3].

1.1.1 Classification of amphiphiles

Cartoon structure of different types of amphiphiles has been featured in **Figure 1.1.1**. The classification of amphiphiles is done mainly based on the nature of the polar head group (or hydrophile). The head group may be anionic (e.g., carboxylate ($-COO^-$), sulfonate ($-SO_3^-$), sulfate ($-OSO_3^-$), or phosphate ($-OPO_3^-$)), cationic (e.g., quaternary

ammonium ($-NR_3^+$) group, or salt of amine ($-NH_3^+$)) or nonionic (e.g., polyoxyethylene (POE), sugar or other polyol groups) and accordingly the amphiphiles are classified as anionic, cationic or nonionic. There are also amphiphilic molecules that contain both anionic and cationic centers at the head group (e.g. sulfobetaines ($-N^+(CH_3)_2CH_2CH_2SO_3^-$), long-chain amino acids ($RN^+H_2CH_2COO^-$), imidazoline derivatives, etc.) and have been referred to as zwitterionic surfactants. On the other hand, the hydrophobic group is generally a long saturated or unsaturated hydrocarbon chain (C_8-C_{22}), a branched alkyl chain (C_8-C_{22}), an alkyl aromatic group, a high-molecular-weight poly(propylene oxide) chain ($-O(-CH(CH_3)CH_2O)_n$), long-chain fluoroalkyl group ($CF_3(CF_2)_n$-), a polysiloxane group ($-CH_3(OSi(CH_3)_2O)_n$-), derivatives of natural or synthetic polymers, etc. However, recently, new structures have also been taken into consideration for enhanced surface and aggregation behavior of surfactants [4-7]. Surfactants can also have two or three tails attached to a polar head and are called as double or triple-chain surfactants. Surfactants having two hydrophilic heads and two hydrophobic tails linked by a short spacer at or near the head groups are referred to as "gemini" surfactants. Further, surfactants can also have two head groups (both anionic, both cationic or one anionic and the other cationic) joined by one hydrophobic spacer. These types of molecules are termed as "bolaamphiphiles" or "bolaforms". Solution behavior of amphiphilic molecules depends on both the hydrophobic spacer and the nature of hydrophilic head group(s).

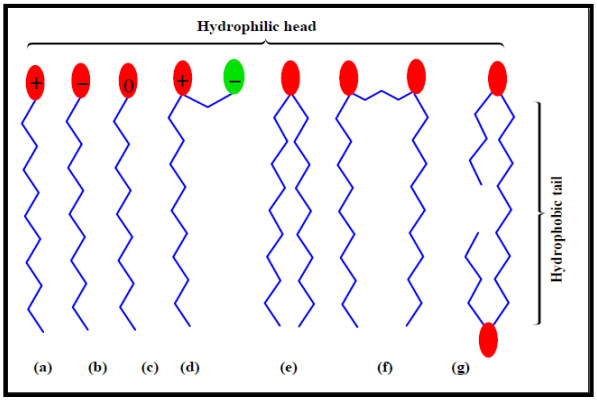

Figure 1.1.1 Cartoon presentation of (a) cationic, (b) anionic, (c) nonionic, (d) zwitterionic, (e) double tailed, (f) gemini, and (g) bolaamphiphiles.

1.1.2 Surface activity of amphiphiles

Surface activity is an essential property of an amphiphilic molecule, which is measured by its ability to reduce surface tension of water at 25 ^{o}C (γ = 71.99±0.05 mNm^{-1}). It has been observed that with the addition of surfactant in water a monolayer is formed at air/water interface leading to a decrease in γ value of water. With increasing surfactant concentration the γ value continues to decrease until the air/water interface becomes saturated with surfactant molecules. With further increase of surfactant concentration the γ value remains unaltered and the surfactant molecules start to self-assemble in the bulk water phase to form aggregates like micelles, vesicles, etc. The critical concentration of surfactant above which micelle formation starts to occur is referred to as critical micelle concentration (*cmc*) or in general, critical aggregation concentration (*cac*). The efficiency of a surfactant to reduce γ value of water is generally determined by pC_{20} value (negative logarithm of the concentration (C) required to reduce γ by 20 units). Surfactants with higher hydrophobic tail exhibit greater surface activity and hence have higher pC_{20} values.

The surface activity can also be measured in terms of surface excess concentration (Γ_{max}) that is, the maximum number of surfactant molecules adsorbed per unit area of air/water interface and can be obtained from Gibbs adsorption equation [8]:

$$\Gamma_{max} = -(1/nRT)(d\gamma/d\ln C) \qquad (1.1)$$

where n is the number of molecular species. Higher value of Γ_{max} means higher surface activity. The adsorption efficiency of an amphiphilic molecule, however, depends on the effective cross-sectional area (A_o) of the polar head group. When A_o is small more amphiphiles can be accommodated in the interface which means Γ_{max} value will be higher. A_o can be successfully calculated from the Gibbs adsorption isotherm:

$$A_o = 1/(N_A\Gamma_{max}) \qquad (1.2)$$

where N_A is Avogadro's number. Thus, amphiphiles with small A_o value and long hydrophobic tail will have higher surface activity or in other words, will have greater tendency to self-assemble in water to produce tightly packed aggregates.

1.1.3 Self-assembly formation by amphiphiles

As already mentioned, molecular self-assembly is the spontaneous and reversible arrangement of molecules to higher order structure or pattern by some local non-covalent or weak interactions (e.g. hydrophobic, van der Waals, π−π, electrostatic, hydrogen-bonding or metal coordination). Among these, hydrophobic effect plays a predominant role in molecular self-assembly formation. Hydrophobic effect is mainly related to hydrophobic hydration, hydrophobic interactions and aqueous cohesiveness [9-12]. The hydrophobic tail(s) of the surfactant monomer is/are being highly hydrated in aqueous solution involves increased hydrogen bond interactions. During aggregation the van der Waals interaction between the hydrophobic tails gives a considerable decrease in the hydrophobic hydration. The consequent breaking of the extra hydrogen bonds results in an unfavorable enthalpy effect ($\Delta H > 0$), which is compensated by a large entropy gain ($\Delta S > 0$) due to increased freedom of the water molecules. This favorable entropy effect also compensates for two smaller effects: the entropy loss for the tails themselves and the enthalpy increase due to head group repulsion, especially in the case of ionic surfactants. However, the binding of counter ions also relieves this repulsion by decreasing the overall surface charge.

1.1.4 Thermodynamics of self-assembly formation

In order to evaluate the spontaneity of self-assembly formation study of thermodynamics of the self-assembly process has become an important objective. Thermodynamics of self-assembly (micelle/vesicle) formation in water involves mainly three thermodynamic parameters, enthalpy change of micellization (ΔH_m), entropy change of micellization (ΔS_m), free energy change of micellization (ΔG_m). There are a number of methods including surface tension (ST) measurement and isothermal titration calorimetry (ITC) to determine the thermodynamic parameters. However, the ultimate requirement of

spontaneous self-assembly formation is the decrease in free energy ($\Delta G_m < 0$). According to the pseudo-phase separation model [13,14], the ΔG_m can be calculated from the following [15]:

$$\Delta G_m = (1 + \beta)\, RT \ln(x_{cmc}) \qquad (1.3)$$

where x_{cmc} is the mole fraction of the surfactant at the *cmc* and β is the degree of counterion association to micelle. The latter can be calculated from the degree of ionization of counterion, α ($\beta = 1 - \alpha$), obtained from the conductivity measurement. On the other hand, ΔS_m can be obtained from the equation:

$$\Delta G_m = \Delta H_m - T\Delta S_m \qquad (1.4)$$

Thus, ΔG_m is a consequence of the change in enthalpy (ΔH_m), and entropy (ΔS_m) of the system. In most of the thermodynamic calculations, it has been found that for adsorption and micellization the positive entropy change ($\Delta S_m > 0$) is the major contributor to the negative values of the ΔG_m [2, 3]. The ΔH_m of micellization, on the other hand, can be positive or negative, depending on the nature of the amphiphile and physical parameters like temperature, concentration and pH of the solution. During self-assembly formation the disturbance in water structure by the amphiphiles induces increase in entropy of the system as a whole. Therefore, the hydrophobic interactions which arise from the increase in entropy of the system induce aggregate formation and growth of aggregates to larger size.

1.2 Self-assembled structures of the amphiphiles in water

Amphiphilic molecules start to self-assemble in aqueous solution above a concentration equal to *cmc* [1-3]. Extensive research on the structure-property relationship reveals that the size and shape of the self-assemblies mainly depend on (i) concentration of the amphiphile, (ii) the length of the hydrophobic tail, (iii) geometric and packing constraints deriving from the particular molecular structure involved, (iv) presence of additives in the solution, (v) nature of counterion (for ionic surfactants), (vi) temperature of the solution,

and (vii) the concentration of electrolyte (in the case of ionic surfactants) [4]. Kunitake and co-workers examined over 60 amphiphles to identify relationships between aggregate morphology and structure of amphiphile [16]. They recognized that the flexible tail, rigid segment, and hydrophilic head group were the essential elements for stable self-assemblies.

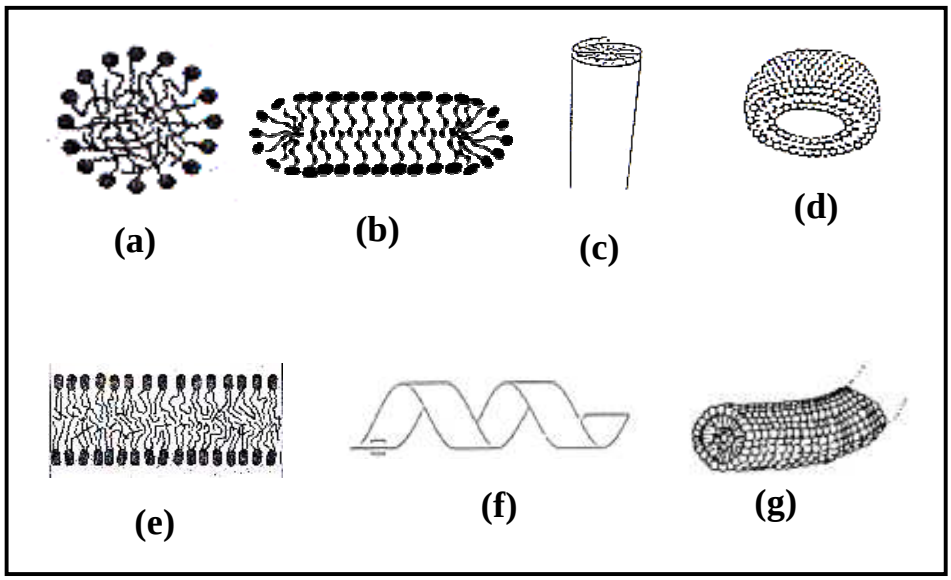

Figure 1.2.1 Shapes of different types of self-assemblies in aqueous solution (a) spherical micelle (b) disk (c) rod (d) vesicle (e) planar bilayer (f) twisted (or helical) ribbon and (g) tube.

Micelles are the simplest and most extensively studied microstructure among the various aggregates that are formed in aqueous solutions. Micelles are generally considered as dynamic aggregate of around 30-200 amphiphiles to a small spherical structure with hydrodynamic diameter $\leq 2l$ (where l is the extended length of surfactant tail). The interior of a micelle is made up of hydrophobic tail, while the surface consisted of the polar head groups. Thus, the microenvironment of the interior rigid hydrophobic core of micelles differs from the polar hydrophilic surface [17]. Although, theoretically

the most proposed structure for micelle is that of a sphere, but the more commonly encountered shapes of micelle are elongated, disk-like, rod-like and worm-like structures. Indeed, depending on the shape and size of the microstructures formed by amphiphilic molecules they are called as spherical, and rod-, disk- and worm-like micelles, planar and flexible bilayer, tubules, ribbons, monolayer and multilayer vesicles, etc. (see **Figure 1.2.1**).

1.2.1 Geometric factors influencing the shape of the aggregates

The types of the aggregates formed in aqueous solution can be predicted by calculating critical packing parameter (CPP) or shape factor (P). According to Israelachvili, the CPP of an amphiphile is given by $P = v / l_c A_o$, where 'A_o' is the surface area of the head group when the amphiphilic molecules are packed so as to maximize the attractive forces and minimize the repulsive forces, 'v' is the volume of the hydrophobic tail and critical chain length 'l_c' is the maximum effective length the tail can assume [18-20]. The model predicts formation of spherical micelles for $P < 1/3$, cylindrical micelles for $1/3 < P < 1/2$, vesicles or flexible bilayer for $1/2 < P < 1$. On the other hand, in nonaqueous medium, inverted micelles are formed when $P > 1$.

Thus, according to Israelachvili usually cone-shaped amphiphilic molecules with large polar head group (higher A_o value) tend to form micelles in water. In other words, single-tail amphiphiles form spherical micelles. On the other hand, truncated cone-shaped amphiphiles with small head group (lower A_o value) and /or large hydrocarbon tail (higher v value) tend to form vesicles [21-23]. Cylindrical molecules, however, form planar bilayer (lamellar) structures in water. This means amphiphiles with double hydrocarbon tails and one head form vesicles. Thus structure of the aggregate could be changed by varying the length of the tail or flexible linker, or both.

1.2.2 Vesicles

The most important type of self-assembly, which is truly essential to life, is the formation of bilayer vesicles. Vesicles also called liposomes, are the most versatile and most useful

self-assembly. They generally consist of alternating layers of lipid or surfactant bilayers separated by aqueous compartments arranged in approximately concentric circles [24]. That is vesicles have two distinct domains one is the hydrophobic membrane and the other is the interior aqueous cavity.

Vesicles can be of different types. The vesicles composed of alternating circular layers of lipid or surfactant bilayers and separated by aqueous layers are called multilamellar vesicle (MLVs), whereas those consisted of single circular bilayer assembly are termed as unilamellar vesicles (ULVs). The different types of vesicles which are generally formed by the amphiphiles in aqueous solution are depicted in **Figure 1.2.2**. The ULVs may also be of different sizes. ULVs of diameter in the range of 20-100 nm are generally named as small unilamellar vesicles (SUVs). ULVs of diameter in between 100-1000 nm are named as large unilamellar vesicles (LUVs), whereas ULVs of diameter greater than 1000 nm generally called as giant unilamellar vesicles (GUVs). Thus, the structural difference of the micelles and vesicles are prominent. Generally the surface of micelles is a lipid monolayer, while the surface of liposomes is a lipid bilayer (monolayer) and the inner core of micelles is composed of hydrocarbon chains, while the inner core of vesicles is consisted of aqueous pool. Micelles can only solubilize hydrophobic molecules while vesicles can encapsulate hydrophilic as well as hydrophobic molecules (drugs). In dilute lipid solution mainly ULVs dominate. However, at very high concentrations transformation from ULVs to MLVs or planner bilayer is observed [25]. MLVs are widely used in drug delivery but the disadvantage of using MLVs is their heterogeneous size distribution. However, there are various methods of preparation of vesicles of different kind reported in the literature [26]. Another kind of vesicular body named as multi vesicular vesicle (MVV) has also been found in many biological systems. It is a multistructural object in which a number of smaller vesicles are entrapped within the aqueous interior of a larger vesicle. MVV plays important role in protein sorting, degradation, and recycling during endocytosis and exocytosis [27-28].

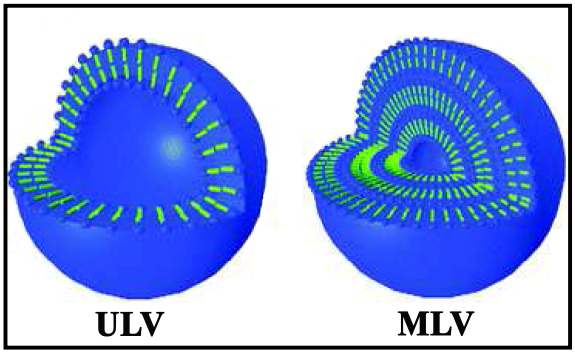

Figure 1.2.2 Different types of vesicles formed in aqueous solution.

Vesicles are also significantly thermodynamically stable and their lifetimes can be from a few days to several months. In most of the cases, it involves some external stimuli to formulate and stabilize the vesicles [29]. Therefore, spontaneous and stable vesicle formation without any external stimuli in aqueous solution has attracted much attention recent time. In most of the cases, spontaneous vesicle formation was found in "catanionic" mixtures or in case of double-tailed surfactants. The well-known examples of double-tailed surfactants are phospholipids which form liposomes (vesicles) in water [30]. There are also a number of reports which describe vesicle formation by synthetic, double-tailed surfactants [31-33]. In 1977, Kunitake et al. reported vesicle formation by tetraalkylammonium salts with two long alkyl residues similar to those of phospholipids [34]. Di-dodecyl dimethylammonium bromide (DDAB) also forms vesicles which is the first example of a synthetic bilayer membrane [35]. Bhattacharya et al. also have developed vesicle-forming double-tailed cationic surfactants [36, 37]. The gemini surfactants consisting of two hydrophobic and two hydrophilic groups have also been observed to form vesicles spontaneously [38-41].

Similarly, bolaamphiphiles composed of two polar head groups joined by hydrophobic spacer chain are getting increased attention as building blocks for structures, such as monolayer membranes and vesicles [42-55]. Kunitake et al. first reported monolayer membrane formation by bolaamphiphiles [45]. Bharadwaj et al. have reported the spontaneous formation of vesicles by cryptand-based bolaamphiphiles [56]. Takakura

et al. developed new class of bolaamphiphiles which formed self-reproducing giant vesicles [57].

On the other hand, single-tailed surfactants, as predicted by Israelichville, tend to form micelles in water. However, single-tailed surfactants whose conformation has been restricted by incorporation of rigid segments (e.g. biphenyl unit, azobenzene unit, diphenyl azomethine unit, etc.) or by intermolecular interactions, usually form stable bilayer aggregates [58-72]. For a spontaneous and reversible vesicle formation by single-tailed surfactants can be induced by tuning of packing parameter by some physical factor(s), such as variation in solution pH, change in temperature and addition of additives. With the variation of pH and ionic strength of the solution, head group area of the amphiphile also varies. Introduction of an electric charge generally increases the average curvature and facilitates the formation of vesicles from lamellar phase. Dey and coworkers have developed a number of vesicle-forming amino acid based single-tailed amphiphiles and have extensively studied their aggregation behavior in aqueous solution [73-76].

1.3 Applications of surfactants

Surfactants are widely used in our daily-life in various ways. We are greatly dependent to surfactant from the very early morning to the late night. Surfactants are mostly used in personal care products like detergents, shampoos, soaps, body spray, body lotion, perfume, and also in all kind of cosmetics. Some of such examples are gathered in **Figure 1.3.1**. Now-a-days, extensive fundamental research on surfactant self-assemblies is going on for the enhanced role of surfactants in biochemistry, polymer chemistry, pharmaceuticals, food science, cosmetics and personal care products, mineral processing, petroleum recovery, textiles, leather, paper, paints and coating industries [77-79]. Micellar aggregates are widely employed to solubilize hydrophobic drugs and water-insoluble materials into solvent system [80]. On the other hand, vesicles that are structurally similar to biomembranes have the higher capacity to encapsulate both polar and non polar drugs in comparison to other aggregates of amphiphilic molecules. Thus, vesicles have become the most promising and demanding vehicles for drug and gene

delivery [81]. Vesicles have been observed to be the most promising model system for investigating basic biological phenomena, like membrane fusion [82], ion channelling [83], photosynthetic processes [84], and proton gradient formation [85]. They are also widely used in waste water treatment [86], and separation of biomolecules [87, 88]. Some vesicle-forming amino acid-derived surfactants also show sufficient antimicrobial activity towards gram-positive bacteria and some fungi [75, 78]. Gemini surfactants are widely used in enhanced oil recovery, for solublization of hydrophobic drugs, and in personal care products [89-91]. Bolaamphiphiles have also widespread applications in drug delivery and gene therapy to design vesicular systems, hydrogels, and micellar systems. Hydrogel forming bolaamphiphiles were found as carriers for vitamin C and vitamin B12. Monolayer vesicles obtained from bolaamphiphiles have been found to be more efficient over phospholipid based vesicles in some cases. Grinsberg S. *et al* has reported vernonia oil-based bolaamphiphiles capable of forming vesicles that can be enzymatically disrupted by acetylcholine esterases [34, 39]. These types of vesicles were found to possess potential of site specific delivery with decapsulation taking place at enzymatically active anatomical region. Monolayer vesicles were found be more stable and cell membrane permeable due to lesser fusion due to lipid exchange in comparison to liposomes.

Figure 1.3.1 Applications of surfactants in daily life.

1.4 Biocompatible surfactants

As surfactants are now extensively used in detergents, cosmetics, pharmaceutical industries, laboratories and other fields, it becomes important to reduce the toxic effects of the surfactants on humans as well as on the environment. That is why, the biodegradability and biocompatibility of the surfactants used in various products have become very important. Nowadays, the surfactants must have properties of not only detergency and foaming power but also mildness and biodegradability. Consequently, new compounds, analogs of natural products, have been synthesized and their physical, chemical and biological properties have been studied [92-102]. Many methods have also been developed for designing and formulation of novel surfactants that are biodegradable and yield the desired effect with the least toxicity [103]. Rosen [104] and Swisher [105] have shown that biodegradability of surfactants mainly depends on the nature of the hydrophobic group, whereas the hydrophilic group plays a minor role. It has been found that the linear and single hydrocarbon chain containing surfactants are more biodegradable than the branched and multi-chain surfactants. Particularly, amino acid-derived surfactants are well known to be mild, non-irritating to human skin and highly biodegradable and hence are currently used as detergents, foaming agents and shampoos.

On the other hand, biocompatible amphiphiles are the most demanding in these days because the self-assemblies obtained from the biocompatible amphiphiles are proved to be the promising candidate for wider applications in biological and phatmaceutical applications [106]. Therefore, it becomes a challenge to the researchers to develop biocompatible, mild and less toxic amphiphilic molecules. For this, in the last few years, many novel amphiphilic molecules bearing carbohydrates, amino acids, alkylglucosides, acylglucosamines, chitosan, lipo-amino acid, peptides and of other small biomolecules like bile salts, choline, carnitine, steroids, urea etc. have been developed [107-121]. These molecules have been found to be biocompatible and biodegradable in nature and hence are suitable for biochemical applications. To further ensure the biocompatibility, poly(ethylene glycol) (PEG) molecule has been incorporated into the structure of amphiphilic molecules.

1.5 Poly(ethylene glycol) (PEG)

PEG, (HO–[CH_2–CH_2–O–]$_n$–CH_2–CH_2–OH), is the most versatile and the most used polymer in the emerging field of drug delivery [122-130]. PEG is considered to be a hydrophilic polymer consisting of a repeating unit of –(O–CH_2–CH_2)– and is synthesized from ethylene oxide in a wide range of molecular weights. Since PEG is highly water soluble at room temperature, it is considered to be a hydrophilic polymer. On the other hand, poly-(propylene oxide), –[CH(CH_3)–CH_2–O–]$_n$–, having a methyl (–CH_3) substitution is hydrophobic and is insoluble in water. Interestingly, poly(methylene oxide), –[CH_2– O–]$_n$– having one methylene group (–CH_2) less is also hydrophobic. However, PEG also possesses some hydrophobic character. In fact, PEG shows excellent solubility in different organic solvents such as, acetone, methanol, ethanol, tetrahydrofuran (THF), toluene, chloroform, and other chlorinated solvents etc. [131]. PEG was also found to have good solubility even in hydrocarbons like *n*-pentane, *n*-hexane, *n*-octane, *n*-decane etc [132]. Thus, PEG is a very good combination of both hydrophilic and hydrophobic properties. This is illustrated by its adsorption at the air-water interface forming a thin monolayer, which is a property of amphiphilic molecules that have distinct hydrophilic and hydrophobic regions. Furthermore, the hydrophobic force was found to be the driving force for the distinct aggregation behavior of the PEG-conjugated molecules at elevated temperatures.

It is believed that the increase of *trans-gauch-trans* (*tgt*) conformer of PEG in water is the main reason of its higher solubility in water. A number of reports describing the conformational behavior of PEG in water and organic solvents can be found in literature. The preferred conformations around the C−C and C−O bond of PEG in aqueous solutions were examined using several techniques like, X-ray (1964), NMR (1965) and IR spectroscopy (1969) [133-136]. All the techniques suggest that PEG in aqueous solution preferentially adopts the *tgt* conformation (*trans-gauch-trans*). In 1969, Blandamer et al., on the basis of the distances between oxygen atoms in the *tgt* conformer of PEG, demonstrated that PEG molecules form hydrogen-bond (H-bond) with the surrounding water molecules in aqueous solution [136]. This indeed implies good fitting

of the *tgt* conformer into the H-bonded networks in the aqueous solution and thus the high solubility of PEG in water. Results of Raman spectroscopic and molecular dynamics (MD) studies also implied that PEG in aqueous solution forms helical structure because of the *tgt* conformation in the C−O−C−C−O−C segments [137, 138].

1.5.1 Uses of PEG

Potential applications of PEG in modern medication, health care and in our daily life are summarized in Figure 1.5.1. PEG is an essential daily consumer product, and an omnipresent in our everyday life. PEG when attached with hydrophobic units, like oleic acid or others, acts as nonionic surfactant, which is found to be surface-active, skin-conditioning agents, viscosity-increasing agent etc. These type of non-ionic surfactants have wide applications in all kinds of cosmetics including toothpaste, cleansing agents, shampoos, fragrance, aftershave lotion, face powder, and eye shadow [139-141].

On the other hand, high solubility in both polar and non-polar solvents and less intrinsic toxicity makes PEG ideal for biological applications. PEG is very essential in medicinal field. It is utilized in blood and organ storage. It mainly minimizes the aggregation of red blood cells and enhances the blood compatibility of poly(vinyl chloride) bags [142-144]. Multi-arm PEG derivatives are widely used in the formation of hydrogels for controlled release of therapeutics, for use in medical devices, regenerative medicine, and also in other applications such as cell culture, wound healing etc [145-159].

Furthermore, PEG is widely employed in pharmaceutical applications behaving as an excipient for parenteral, nasal, ocular, and topical importance. In laxatives, PEG is employed as the active principal. When PEG is attached with hydrophobic drugs or carriers the solubility of the drugs or carriers also increases in water. Thus, the aggregation of the drugs in vivo is hindered resulting high physical and thermal stability of the drugs in body system. The PEGylation (the covalent attachment of a PEG derivative onto molecules) of drug carriers not only increases its aqueous solubility and makes its renal clearance faster, but also reduces its enzymatic degradation and elimination and opsonization by the reticular endothelial system (RES) [160-176]. Davies

and Abuchowski first reported PEGylation in 1970 for albumin and catalase modification [177,178]. Indeed, binding of drug conjugates with PEG result in prolonged blood circulation time [179-181]. Thus PEGylation has a high impact to drug development and drug delivery [182-186]. Consequently, PEG derivatives are frequently employed for the PEGylation of peptides [187-189], proteins [190,191], small molecules like mannose, prodrugs [192], oligo nucleotides [193], cells [194], nanoparticles and virus particles [195-200]. It should be mentioned here that all polymer-based stealth drug-delivery systems that are available in market up to now contain PEG-containing compounds.

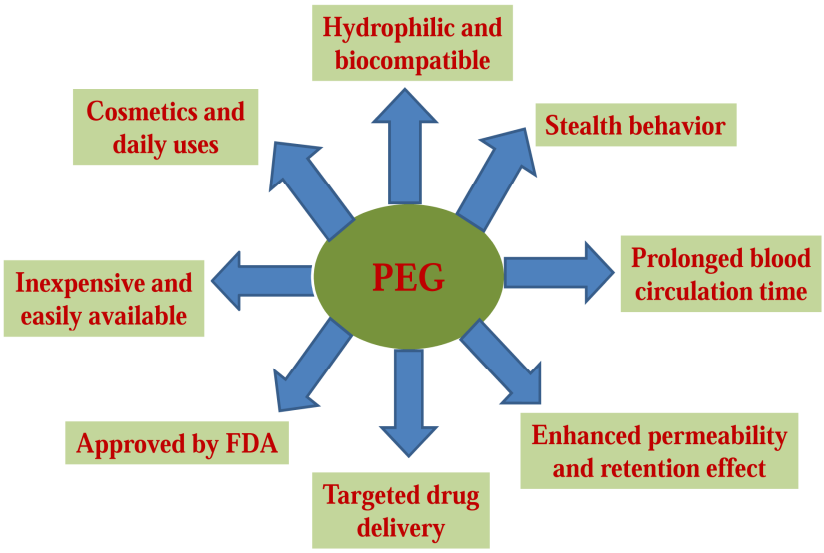

Figure 1.5.1 Different properties and potential applications of PEG in modern medication and health care.

1.5.2 PEG chain-containing amphiphiles

Since PEG is hydrophilic in nature, it is traditionally coupled with hydrophobic moieties to develop nonionic surfactants. There are a number of well-known nonionic surfactants, such as Tween-20, Triton-X-100, etc., in which PEG acts as a polar head group. New sterically stabilized vesicles were obtained by conjugating PEG with cholesterol. Further,

Lee et al. reported the synthesis and thermal properties of Triton X-based surfactants modified with carboxylic acids [201]. Numerous reports are there describing development and applications of novel nonionic surfactants having PEG as head [202-209]. In 1989, Kabanov et al. first proposed PEG as a hydrophilic part of linear block copolymers for micellization [182]. PEG and poly(methacrylic acid)-containing amphiphilic block copolymers have been developed and their self-assembly behavior has been reported [204]. The PEG-containing block copolymer micelles have been used as drug-delivery carriers by Kwon and Kataoka [183]. A number of micelle-forming polymers containing PEG as polar head have been used for drug delivery applications. Thus coupling of poly(lactic acid) with hydrophilic PEG was performed to enhance the compatibility of the system with protein drugs [209-211]. Custers et al. have reported that modification of nonionic pluronic surfactants, PEG-poly(propylene glycol)-PEG, with carboxylic acids at the terminal exhibits pH-dependent phase separation and micellar behavior for the purpose of the removal of metal ion and organics from waste water [205].

1.6 Origin of the work and outline of the thesis

Inspired by the enormous effects of PEG in drug delivery, everyday products, and also in industrial applications design and development of amphiphilic molecules in which PEG chain replaces hydrocarbon tail was undertaken. The solubility of PEG in organic solvents and its behavior in water at elevated temperatures led this author to consider PEG chain sufficiently hydrophobic. Thus, low-molecular-weight PEG chain could act as hydrophobic tail when covalently linked to a more polar ionic head groups, such as carboxylate ($–COO^–$), sulfonate ($–SO_3^–$) etc. Therefore, considering the hydrophobicity of PEG, it was coupled with more polar moieties. A couple of recent reports from this group, one on cationic and the other on anionic amphiphiles containing PEG tail showed formation of self-assembled microstructures in water [212, 213]. Further, some recent reports have also demonstrated vesicle formation by a few random copolymers constituted by PEG chains and ionic monomers [214-216]. However, there are no reports so far on low-molecular-weight amphiphiles with zwitterionic head group and PEG chain

either as hydrophobic tail or spacer. Therefore, in this work, a detailed investigation is undertaken to study aggregation behavior of this new class of molecules in aqueous solution in order to firmly establish the hydrophilic as well as hydrophobic nature of the PEG chain.

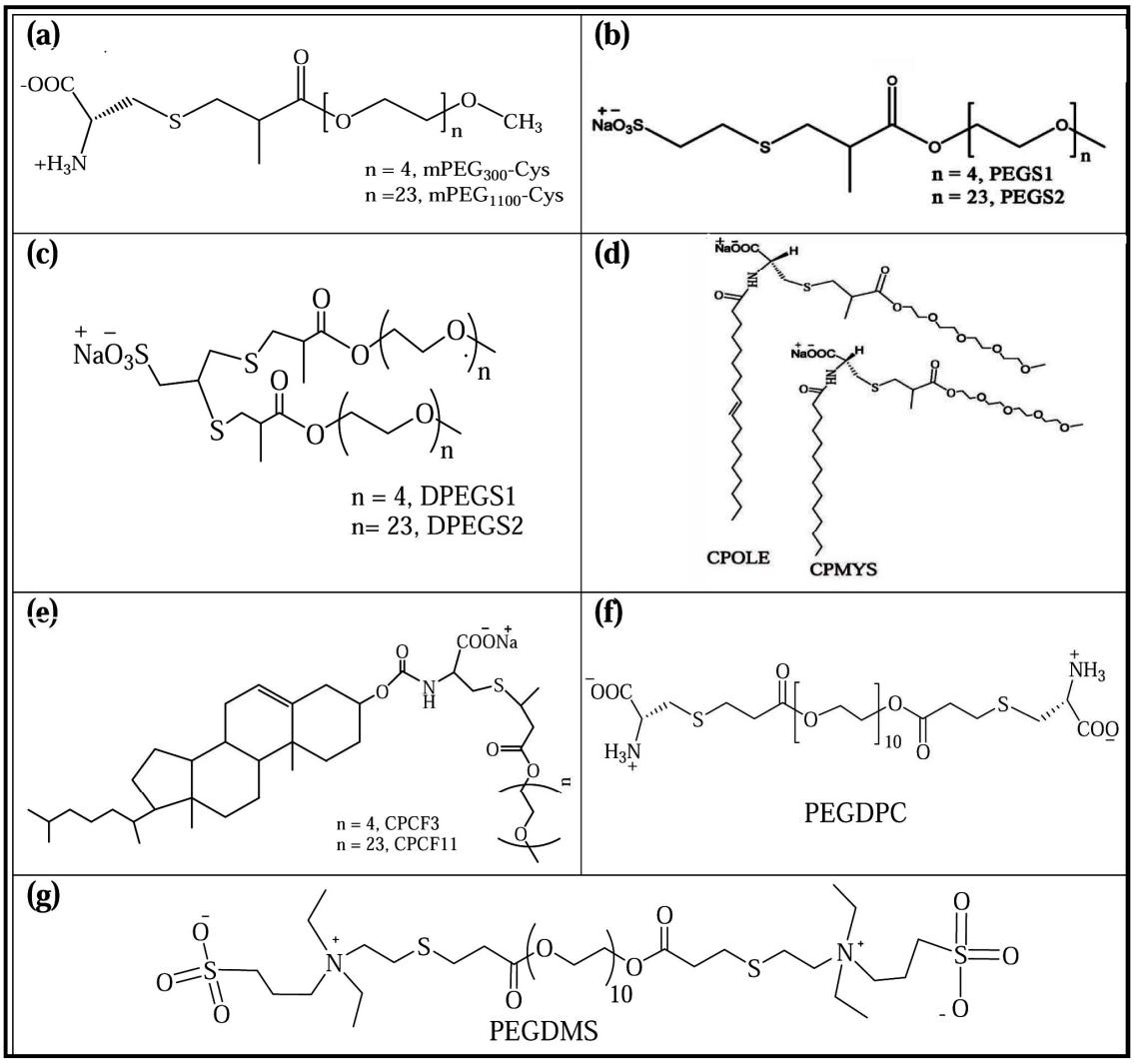

Chart 1.6.1 Chemical structures and abbreviated names of the synthesized amphiphiles.

Thus in the present work the amphiphilic character of molecules bearing PEG as tail(s) and charged group(s) as head has been examined. Consequently, a series of

biocompatible, PEG-based single-tailed, double-tailed, double-headed surfactants including bolaforms have been designed and synthesized. The chemical structures and the abbreviations of the synthesized molecules have been accumulated in **Chart 1.6.1**. The aggregation behavior of the amphiphiles was then thoroughly studied in aqueous solution by a number of techniques, including surface tension, fluorescence and 2D NOESY ^{1}H-NMR spectroscopy, isothermal titration calorimetry, dynamic light scattering, transmission electron microscopy, and atomic force microscopy.

1.7 Objectives of the work

The following objectives were set to understand the self-assembly behavior of this class of molecules:

(a) To study surface activity of the molecules

(b) To study self-assembly behavior of the molecules in aqueous solution in order to answer questions, such as

(i) what is the critical concentration above which the amphiphiles form aggregate?

(ii) what are the shapes and sizes of the aggregates formed in aqueous solution?

(iii) how stable the aggregates are with respect to change of pH, temperature, aging time and additive concentration?

(iv) what is the driving force for aggregate formation?

(v) what is the spatial arrangement of the amphiphiles in the aggregates?

(vi) how does the change of head-group structure affect the self-assembly behavior?

(vii) what happens when both hydrocarbon chain and PEG chains are covalently linked to the same ionic head group?

(viii) how does the change of nature of the hydrophobe from hydrocarbon chain to cholesterol affect the self-assembly behavior?

(ix) what happens when two PEG chains are linked to the same ionic head group?

(x) what happens when the same ionic head group is linked at both ends of the PEG chain?

(c) To demonstrate potential application of these molecules in drug delivery

References

[1] Rosen, M. J. *Surfactants and Interfacial Phenomena*, 4th ed.; Wiley-Interscience: New York, **2004**.

[2] Laughlin, R. G. *The aqueous phase behavior of surfactants*; Academic Press: London, **1994**.

[3] Myers, D. *Surfactant Science and Technology*, 3rd ed.; John Wiley & Sons: New Jersey, **2006**.

[4] Robb, I. D. '*Specialist Surfactants*'; Blackie Academic & Professional: London, **1997**.

[5] Holmberg, K. Ed. '*Novel Surfactants*'; Marcel Dekker: New York, **1998**.

[6] Holmberg, K.; Jönsson, B.; Kronberg B.; Lindman, B. *Surfactants and Polymers in Aqueous Solution.* 2nd ed.; John Wiley & Sons: Chichester, U.K., **2002**; p 227.

[7] Yan. Y.; Xiong, W.; Li, X.; Lu, T.; Huang, J.; Li, Z.; Fu, H. Molecular Packing Parameter in Bolaamphiphile Solutions: Adjustment of Aggregate Morphology by Modifying the Solution Conditions. *J. Phys. Chem. B* **2007**, *111*, 2225–2230.

[8] Dantas, T. N. C.; Moura , E. F.; Junior, H. S.; Neto, A. A. D.; Gurgel, A. Micellization and Adsorption Thermodynamics of Novel Ionic Surfactants at Fluid Interfaces. *Colloids Surf A Physicochem Eng Asp* **2002**, *207*, 243–252.

[9] Whitesides, G. M.; Grzybowski, B. Self-Assembly at All Scales. *Science* **2002**, *295*, 2418–2421.

[10] Whitesides, G.; Boncheva, M. Beyond Molecules: Self-Assembly of Mesoscopic and Macroscopic Components. *Proc. Natl. Acad. Sci. U.S.A* **2002**, *99*, 4769–4774.

[11] Ariga, K.; Nakanishi, T.; Hill, J. P. Self-assembled Microstructures of Functional Molecules. *Curr. Opin. Colloid Interface Sci*. **2007**, *12*, *106*–120.

[12] Tanford, C. *The Hydrophobic Effect: Formation of Micelles and Biological Membranes*; John Wiley & Sons, Inc.: New York, USA, **1973**, p. 200.

[13] Shinoda, K.; Hutchinson, E. Pseudo-Phase Seperation Model for Thermodynamic Calculations on Micellar Solutions. *J. Phys. Chem.*, **1962**, *66* (4), 577–582.

[14] Kamrath, R. F.; Franse, E. I. Thermodynamics of Mixed Micellization. Pseudo-Phase Separation Models. *Ind. Eng. Chem. Fundam.* **1983**, *22 (2)*, 231–235.

[15] Zana, R. Critical Micellization Concentration of Surfactants in Aqueous Solution and Free Energy of Micellization. *Langmuir* **1996**, *12*, 1208–1211.

[16] Kunitake, T.; Okahata, Y.; Shimomura, M.; Yasunami, S.; Takarabe, K. Formation of Stable Bilayer Assemblies in Water from Single-chain Amphiphiles. Relationship between the Amphiphile Structure and the Aggregate Morphology. *J. Am. Chem. Soc.* **1981**, *103*, 5401–5413.

[17] Ray, A. Solvophobic Interactions and Micelle Formation in Structure Forming Nonaqueous Solvents. *Nature* **1971**, *231*, 313–315.

[18] Israelachvili, J. N.; Mitchell, D. J.; Ninham, B. W. Theory of Self-Assembly of Hydrocarbon Amphiphiles into Micelles and Bilayers. *J. Chem. Soc., Faraday Trans. 2* **1976**, *72*, 1525–1568.

[19] Mitchell, D. J.; Ninham, B. W. Micelles, Vesicles and Microemulsions. *J. Chem. Soc., Faraday Trans. 2* **1981**, *77*, 601–629.

[20] Israelachvili, J. *Intermolecular and Surface Forces: With Applications to Colloidal and Biological Systems*, 2nd ed.; Academic Press: San Diego, CA, **1992**.

[21] Miller, D. D.; Bellare, J. R.; Evans, D. F.; Talmon, Y.; Ninham, B. W. Meaning and Structure of Amphiphilic Phases: Inferences from Video-enhanced Microscopy and Cryotransmission Electron Microscopy. *J. Phys. Chem.* **1987**, *91*, 674–685.

[22] Mohanty, A.; Dey, J. Effect of the Headgroup Structure on the Aggregation Behavior and Stability of Self-Assemblies of Sodium N-[4-(n-Dodecyloxy)benzoyl]-L-aminoacidates in Water. *Langmuir* **2007**, *23*, 1033–1040.

[23] Nagarajan, R. Molecular Packing Parameter and Surfactant Self-Assembly: The Neglected Role of the Surfactant Tail. *Langmuir* **2002**, *18*, 31–38.

[24] Taylor, K. M. G.; Farr, S. J. *In Liposomes in Drug Delivery*; Patel, H. M., Ed. vol. *2*; Harwood Academic Publishers: Chur, Switzerland, **1993**, 95–109.

[25] Evans, D. F.; Wennerstrom, H. *The Colloidal Domain: where Physics, Chemistry, Biology, and Technology meet*; Wiley-VCH: New York, **2001**.

[26] Torchilin, V. P.; Weissig, V., Ed. *Liposomes: A Practical Approach*, 2nd ed.; Oxford Univ. Press: USA, **2003**.

[27] Kim, S.; Turker, M. S.; Chi, E. Y.; Sela, S.; Martin, G. M. Preparation of Multivesicular Liposomes. *Biochim. Biophys. Acta* **1983**, *728*, 339–348.

[28] Kim, S.; Jacobs, R. E.; White, S. H. Preparation of Multilamellar Vesicles of Defined Size-distribution by Solventspherule Evaporation. *Biochim. Biophys. Acta* **1985**, *812*, 793–801.

[29] Feitosa, E.; Barreleiro, P. C. A.; Olofsson, G. Phase Transition in Dioctadecyldimethyl Ammonium Bromide and Chloride Vesicles Prepared by Different Methods. *Chem. Phys. Lipids* **2000**, *105*, 201–213.

[30] Mimms L. T.; Zampighi, G.; Nozaki, Y.; Tanford, C.; Reynolds, J. A. Phospholipid Vesicle Formation and Transmembrane Protein Incorporation using Octyl Glucoside. *Biochemistry* **1981**, *20*, 833–840.

[31] Kunitake, T. Synthetic Bilayer Membranes: Molecular Design, Self-Organization, and Application. *Angew. Chem. Int. Ed. Engl*. **1992**, *31*, 709–726.

[32] Mortara, R. A.; Quina, R. H.; Chaimovitch, H. Formation of Closed Vesicles from a Simple Phosphate Diester. Preparation and Some Properties of Vesicles of Dihexadecyl Phosphate. *Biochem. Biophys. Res. Commun*. **1978**, *81*, 1080.

[33] Hoffmann, H.; Kalus, J.; Thrun, H. Small Angle Neutron Scattering Measurements on Micellar Solutions of Perfluor Detergents. *Colloid. Polym. Sci.* **1983**, *261*, 1043-1049.

[34] Kunitake, T.; Okahata, Y.; Tanaki, T.; Kumamaru, F.; Takayangi, M. X-Ray Structural Studies of Bilayers Composed of Monoalkyl-Monocation Type Artificial Amphiphiles. *Chem. Lett*. **1977**, 387-388.

[35] Kunitake, T.; Okahata, Y. A Totally Synthetic Bilayer Membrane. *J. Am. Chem. Soc*. **1977**, *99*, 3860-3862.

[36] Bhattacharya, S.; Dileep, P. V. Synthesis of Novel Dimeric Cationic Lipids Based on an Aromatic Backbone between the Hydrocarbon Chains and Head group. *J. Phys. Chem.* B **2003**, *107*, 3719–3725.

[37] Bhattacharya, S.; Halder, S. Synthesis, Thermotropic Behavior, and Permeability Properties of Vesicular Membranes Composed of Cationic Mixed-Chain Surfactants. *Langmuir* **1995**, *11*, 4748–4757.

[38] Menger, F. M.; Keiper, J. S. Gemini Surfactants. *Angew Chem., Int. Ed. Engl*. **2000**, *39*, 1906–1920.

[39] Rosen, M. J.; Tracy, D. J. Gemini Surfactants *J. Surfactants Deterg.* **1998**, *1*, 547–554.

[40] Zana, R. Gemini (dimeric) Surfactants. *Curr. Opin. Colloid Interface Sci*. **1996**, *1*, 566–571.

[41] Danino, D.; Talmon, Y.; Zana, R.; Alkanediyl-α,ω-Bis(Dimethylalkylammonium Bromide) Surfactants (Dimeric Surfactants). 5. Aggregation and Microstructure in Aqueous Solutions. *Langmuir* **1995**, *11*, 1448–1456.

[42] Fuhrhop, H. J.; David, H. H.; Mathieu, J.; Liman, U.; Winter, J. H.; Boekemat, E. Bolaamphiphiles and Monolayer Lipid Membranes Made from 1,6,19,24-Tetraoxa-3,21-cyclohexatriacontadiene -2,5,20,23–tetrone. *J. Am. Chem. Soc*. **1986**, *108*, 1785–1791.

[43] Bohme, P.; Hicke, H. -G.; Boettcher, C.; Fuhrhop, -H. J. Reactive and Rigid Monolayers of Bisaroyl Azide Diamide Bolaamphiphiles on Polyacrylonitrile Surfaces. *J. Am. Chem. Soc.* **1995**, *117*, 5824–5828.

[44] Escamilla, G. H.; Newkome, G. R. Bolaamphiphiles: From Golf Balls to Fibers. *Angew. Chem. Int. Ed.* **1994**, *33(19)*, 1937–1940.

[45] Kunitake, T.; Okahata, Y. Formation of Stable Monolayer Membranes and Related Structures in Dilute Aqueous Solution from Two-headed Ammonium Amphiphiles. *J. Am. Chem. Soc.* **1979**, *101*, 5231–5234.

[46] Fuhrhop, -H. J.; Fritsch, D. Bolaamphiphiles form Ultrathin, Porous and Unsymmetric Monolayer Lipid Membranes. *Acc Chem Res* **1986**, *19(5)*, 130–137.

[47] Mao, G.; Tsao, Y. H.; Tirrell, M.; Davis, T. H.; Hessel, V.; Van, J. E. Monolayers of Bolaform Amphiphiles: Influence of Alkyl Chain Length and Counterions. *Langmuir* **1994**, *10(11)*, 4174–4184.

[48] Fuhrhop, -H. J.; Wang, T. Bolaamphiphiles. *Chem. Rev.* **2004**, *104*, 2901–2937.

[49] Newkome, R.; Lin, X. F.; Chen, Y. X.; Escamilla, G. H. Two-Directional Cascade Polymer Synthesis: Effects of Core Variation. *J. Org. Chem*. **1993**, *58*, 3123–3129.

[50] Fuhrhop, J. H.; Spiroski, D.; Boettcher, C. Molecular Monolayer Rods and Tubules made of Alpha-(L-lysine),omega-(amino) Bolaamphiphiles. *J. Am. Chem. Soc.* **1993**, *115*, 1600–1601.

[51] Shimizu, T.; Masuda, M. Stereochemical Effect of Even−Odd Connecting Links on Supramolecular Assemblies Made of 1-Glucosamide Bolaamphiphiles. *J. Am. Chem. Soc.* **1997**, *119*, 2812–2818.

[52] Roussel, M.; Lognone, V.; Plusquelleca, D.; Benvegnu, T. Monolayer Lipid Membrane-Forming Dissymmetrical Bolaamphiphiles Derived from Alginate Oligosaccharides. *Chem. Commun*. **2006**, *34*, 3622–3624.

[53] Guilbot, J.; Benvegnu, T.; Legros, N.; Pluspuellec, D. Efficient Synthesis of Unsymmetrical Bolaamphiphiles for Spontaneous Formation of Vesicles and Disks with a Transmembrane Organization. *Langmuir* **2001**, *17*, 613–618.

[54] Shimizu, T.; Iwaura, R.; Masuda, M.; Hanada, T.; Yase, K. Internucleobase-Interaction-Directed Self-Assembly of Nanofibers from Homo- and Heteroditopic 1,ω-Nucleobase Bolaamphiphiles. *J. Am. Chem. Soc.* **2001**, *123*, 5947–5955.

[55] Iwaura, R.; Yoshida, K.; Masuda, M.; Yase, K.; Shimizu, T. Spontaneous Fiber Formation and Hydrogelation of Nucleotide Bolaamphiphiles. *Chem. Mater*. **2002**, *14*, 3047–3053.

[56] Bandyopadhyay, P.; Bharadwaj, P. K. Spontaneous Formation of Vesicles by a Cryptand-Based Bola-Amphiphile. *Langmuir* **1998**, *14*, 7537–7538.

[57] Takakura, K.; Toyota, T.; Sugawara, T. A Novel System of Self-Reproducing Giant Vesicles. *J. Am. Chem. Soc*. **2003**, *125*, 8134.

[58] Kunitake, T. Synthetic Bilayer Membranes: Molecular Design, Self-organization, and Application. *Angew. Chem. Int. Ed. Engl*. **1992**, *31*, 709–726.

[59] Kunitake, T.; Okahata, Y.; Shinomura, M.; Yasunami, S.; Takarabe, K. Formation of Stable Bilayer Assemblies in Water from Single-Chain Amphiphiles. Relationship between the Amphiphile Structure and the Aggregate Morphology. *J. Am. Chem.Soc.***1981**, *103*, 5401–5413.

[60] Menger, F. M.; Yamasaki, Y. Hyperextended Amphiphiles. Bilayer Formation from Single-Tailed Compounds. *J. Am. Chem. Soc*. **1993**, *115*, 3840–3841.

[61] Krafft, M. -P.; Giulieri, F.; Riess, J. G. Supramolecular Assemblies from Single-Chain Perfluoroalkylated Phosphorylated Amphiphiles. *Colloids and Surfaces A: Physicochemical and Engineering Aspects* **1994**, *84*, 113–119.

[62] Adam, C. D.; Durrant, J. A.; Lowry, M. R.; Tiddy, G. J. Gel and Liquid-Crystal Phase Structures of the Trioxyethylene Glycol Monohexadecyl Ether/Water System. *J. Chem. Soc., Faraday Trans.* **1984**, *80*, 789–801.

[63] Vlachy, N.; Merle, C.; Touraud, D.; Schmidt, J.; Talmon, Y.; Heilmann, J.; Kunz, W. Spontaneous Formation of Bilayers and Vesicles in Mixtures of Single-Chain Alkyl Carboxylates: Effect of pH and Aging and Cytotoxicity Studies. *Langmuir* **2008**, *24*, 9983–9988.

[64] Chen, W. J.; Li, G. Z.; Zhou, G. W.; Zhai, L. M.; Li, Z. M. pH-Induced Spontaneous Vesicle Formation from NaDEHP. *Chem. Phys. Lett*. **2003**, *374*, 482–486.

[65] Gebicki, J. M.; Hicks, M. Preparation and Properties of Vesicles Enclosed by Fatty acid Membranes. *Chem. Phys. Lipids* **1976**, *16*, 142–160.

[66] Renoncourt, A.; Bauduin, P.; Nicholl, E.; Touraud, D.; Verbavatz, J. M.; Dubois, M.; Drechsler, M.; Kunz, W. Spontaneous Vesicle Formation of an Industrial Single-chain Surfactant at Acidic pH and at Room-Temperature. *Chem. Phys. Chem.* **2006**, *7*, 1892–1896.

[67] Talmon, Y.; Evans, D. F.; Ninham, B. W. Spontaneous Vesicles Formed from Hydroxide Surfactants: Evidence from Electron Microscopy. *Science* **1983**, *221*, 1047–1048.

[68] Morán, M. C.; Pinazo, A.; Pérez, L.; Clapés, P.; Angelet, M.; García, M. T.; Vinardell, M. P.; Infante, M. R. "Green" Amino Acid-Based Surfactants. *Green Chem.* **2004**, *6*, 233–240.

[69] Pinazo, A.; Pons, R.; Pérez, L.; Infante, M. R. Amino Acids as Raw Material for Biocompatible Surfactants. *Ind. Eng. Chem. Res*. **2011**, *50*, 4805–4817.

[70] Taku, K.; Sasaki, H.; Kimura, S; Imanishi, Y. Synthesis and Structure of a Vesicular Assembly of Dialkylammonium-type Amphiphile Carrying L-3-(3-N-ethylcarbazolyl)alanine. *Amino Acids* **1994**, *7*, 311–316.

[71] Li, Z. C.; Jin, W.; Li, F. M. Synthesis of Cholesterol Derivatives with Amino Acid as Hydrophilic Group and the Vesicles Prepared therefrom. *Chinese Chem. Lett.* **1999**, *10*, 1007−1110.

[72] Marques, E. F.; Brito, R. O.; Silva, S. G.; Rodríguez-Borges, J. E.; Do Vale, M. L.; Gomes, P.; Araújo, M. J.; Söderman, O. Spontaneous Vesicle Formation in Catanionic Mixtures of Amino Acid-Based Surfactants: Chain Length Symmetry Effects. *Langmuir* **2008**, *24*, 11009–11017.

[73] Ghosh, A.; Shrivastava, S.; Dey, J. Concentration and pH-Dependent Aggregation Behavior of an L-Histidine Based Amphiphile in Aqueous Solution. *Chem. Phys. Lipids* **2010**, *163*, 561–568.

[74] Khatua, D.; Dey, J. Fluorescence, Circular Dichroism, Light Scattering, and Microscopic Characterization of Vesicles of Sodium Salts of Three N-Acyl Peptides. *J. Phys. Chem. B* **2007**, *111*, 124–130.

[75] Roy, S.; Khatua, D.; Dey, J. Giant Vesicles of a Single-Tailed Chiral Cationic Surfactant, (1R, 2S)-(–)-N-Dodecyl-N-methylephedrinium Bromide, in Water. *J. Colloid Interface Sci*. **2005**, *292*, 255–264.

[76] Ghosh, A.; Dey, J. Physicochemical Characterization and Tube-Like Structure Formation of a Novel Amino Acid-Based Zwitterionic Amphiphile *N*-(2-Hydroxydodecyl)-L-valine in Water. *J. Phys. Chem. B* **2008**, *112*, 6629–6635.

[77] Tadros, T. F. *Applied Surfactants*: *Principles and Application*, Wiley-VCH: Germany, **2005**.

[78] Palma, S. D.; Maletto, B.; Lo Nostro, P.; Manzo, R. H.; Pistoresi-Palencia, M. C.; Allemandi, D. A. Potential Use of Ascorbic Acid-Based Surfactants as Skin Penetration Enhancers. *Drug Dev. Ind. Pharm.* **2006**, *32*, 821–827.

[79] Zoller, U. Ed. *Handbook of Detergents, Part E: Applications, Surfactant Science Series, vol. 141*; CRC press, Taylor & Francis Group: New York, **2009**.

[80] Mirgorodskaya A. B.; Yatskevich E. I.; Lukashenko, S. S.; Zakharova L. Y.; Konovalov, A. I. Solubilization and Catalytic Behavior of Micellar System Based on Gemini Surfactant with Hydroxyalkylated Head group. *J. Mol. Liq.* **2012**, *169*, 06–109.

[81] Yang, J. Viscoelastic Wormlike Micelles and their Applications. *Curr. Opin. Colloid Interface Sci*. **2002**, *7*, 276–281.

[82] Sinico, C.; Fadda, A. M. Vesicular Carriers for Dermal Drug Delivery. *Expert Opin. Drug Deliv*. **2009**, *6*, 813–825.

[83] Stengel, G.; Zahn, R.; Höök, F. DNA-Induced Programmable Fusion of Phospholipid Vesicles. *J. Am. Chem. Soc*. **2007**, *129*, 9584–9585.

[84] Cazacu, A.; Tong, C.; van der Lee, A.; Fyles, T. M.; Barboiu, M. Columnar Self-Assembled Ureido Crown Ethers: an Example of Ion-Channel Organization in Lipid Bilayers. *J. Am. Chem. Soc.* **2006**, *128*, 9541–9548.

[85] Gust, D.; Moore T. A.; Moore, A. L. Mimicking Photosynthetic Solar Energy Transduction. *Acc. Chem. Res.* **2001**, *34*, 40–48.

[86] Bhosale, S.; Sisson, A. L.; Talukdar, P.; Furstenberg, A.; Banerji, N.; Vauthey, E.; Bollot, G.; Mareda, J.; Roger, C.; Wurthner, F.; Sakai, N.; Matile, S. Photoproduction of Proton Gradients with π-Stacked Fluorophore Scaffolds in Lipid Bilayers. *Science* **2006**, *313*, 84–86.

[87] Villalobos, P.; Chávez, M. I.; Olguín, Y.; Sánchez, E.; Valdés, E.; Galindo, R.; Young, M. E. The Application of Polymerized Lipid Vesicles as Colorimetric Biosensors for Real-time Detection of Pathogens in Drinking Water. *Electron. J. Biotechnol*. **2012**, *15*, 1–12.

[88] Stanish, I.; Lowy, D. A.; Hung, C.-W.; Singh, A. Vesicle-Based Rechargeable Batteries. *Adv*. *Mater*. **2005**, *17*, 1194–1198.

[89] Lundhal, P.; Yang, Q. Liposome Chromatography: Liposomes Immobilized in Gel Beads as a Stationary Phase for Aqueous Column Chromatography. *J. Chromatogr*. **1991**, *544*, 283–304.

[90] Heuschkel, S.; Goebel, A.; Neubert, R. H. H. Microemulsions-Modern Colloidal Carrier for Dermal and Transdermal Drug Delivery. *J. Pharm. Sci*. **2008**, *97*, 603–631.

[91] Drummond, C. J.; Fong, C. Surfactant Self-Assembly Objects as Novel Drug Delivery Vehicles. *Curr. Opin. Colloid Interface Sci.* **2000**, *4*, 449–456.

[92] David, H. H.; Mathieu, J.; Liman, U.; Winter, H. J.; Boekema, E. Bolaamphiphiles and Monolayer Lipid Membranes Made from 1,6,19,24-Tetraoxa-3,21-cyclohexatriacontadiene-2,5,20,23-tetrone. *J. Am. Chem. Soc.*, **1986**, *108*, 1785–1791.

[93] Fuhrhop, J. H.; Bach, R. *Adv. Supramol. Chem.*, **1992**, *2*, 25–63.

[94] Garelli-Calvet, R.; Brisset, F.; Rico, I.; Lattes, A. Buildup of Amphiphilic Molecular Bola from Organic-Inorganic Hybrid Polyoxometalates and their Vesicle-Like Supramolecular Assembly. *Synth. Commun.* **1993**, *23*, 35–44.

[95] Brisset, F.; Garelli-Calvet, R.; Azema, J.; Chebli, C.; Rico-Lattes, I.; Lattes, A. Novel Surfactants: Preparation Applications and Biodegradability. *New J. Chem.*, **1996**, *20*, 595–605.

[96] Madeleine-Dupuich, C.; Guidetti, B.; Rico-Lattes, I.; Lattes, A. Reactions and Synthesis in Surfactant Systems. *New J. Chem.* **1996** *20*, 143–151.

[97] Marr-Leisy, D.; Neumann, R.; Ringsdorf, H. Characterization of Particle Surface and Morphology in Vinyl Acetate-butyl Acrylate Emulsion Copolymers—Influence of the Copolymerization Pathway. *Colloid Polymer Sci*. **1985**, *263*, 791–802.

[98] Zhang, L.; Somasundaran, P.; Maltesh. C. Electrolyte Effects on the Surface Tension and Micellization of n-Dodecyl β-d-Maltoside Solutions. *Langmuir*, **1996**, *12 (10*), 2371–2373.

[99] Seguer, J.; Selve, C.; Allouch, M.; Infante, R. Amino Acids as Raw Material for Biocompatible Surfactants. *J. Am. Oil Chem. Soc.*, **1996**, *73*, 79–86.

[100] Johnsson, M.; Wagenaar, A.; Marc C. A. Stuart, M. C. A.; Engberts, J. B. F. N. Sugar-Based Gemini Surfactants with pH-Dependent Aggregation Behavior: Vesicle-to-Micelle Transition, Critical Micelle Concentration, and Vesicle Surface Charge Reversal. *Langmuir* **2003,** *19*, 4609–4618.

[101] Menger, F. M.; Mbadugha. B. N. A. Gemini Surfactants with a Disaccharide Spacer. *J. Am. Chem. Soc.* **2001,** *123*, 875–885.

[102] Bhattacharya, S.; Acharya, S. N. G. Pronounced Hydrogel Formation by the Self-Assembled Aggregates of *N*-Alkyl Disaccharide Amphiphiles. *Chem. Mater*. **1999,** *11*, 3504–3511.

[103] Holmberg, K., Ed. *Novel Surfactants: Preparation Applications and Biodegradability*, 2nd ed.; CRC Press, Taylor & Francis Group: New York, **2003**.

[104] Rosen, M. J.; Dahanayake, M. *Industrial Utilization of Surfactants: Principles and Practice*; AOCS Press: Champaign IL, **2000**.

[105] Swisher, R. D. *Surfactant Biodegradation, Surfactant Science Series Vol. 18*; Marcel Dekker: New York, **1986**.

[106] Ratner, B. D. The Biocompatibility Manifesto*:* Biocompatibility for the Twenty-First Century. *J Cardiovasc Transl* **2011**, *4*, 523–527.

[107] Tadros, T. F. *Applied Surfactants*: *Principles and Application*, Wiley-VCH: Germany, **2005**.

[108] Kosaric, N. Biosurfactants in Industry. *Pure & Appl. Chem.* **1992**, *64*, 1731–1737.

[109] Castro, M. J. L.; Kovensky, J.; Cirelli, A. F. Ecologically Safe Alkyl Glucoside-Based Gemini Surfactants. *Arkivoc* **2005**, *12*, 253–267.

[110] Alexeeva, M. V.; Churjusova, T. G.; Mokrushina, L. V.; Morachevsky, A. G.; Smirnova, N. A. Influence of the Third Component on the Temperature of the Crystal Surfactant-Micellar Solution Equilibrium. *Langmuir* **1996**, 12, 5263–5270.

[111] Sagnella, S.; Mai-Ngam, K. Chitosan Based Surfactant Polymers Designed to Improve Blood Compatibility on Biomaterials. *Colloids and Surfaces B: Biointerfaces* **2005**, *42*, 147–155.

[112] Dexter, A. F.; Middelberg, A. P. J. Peptides as Functional Surfactants. *Ind*. *Eng*. *Chem*. *Res*. **2008**, *47*, 6391–6398.

[113] Lin, S.; Blankschtein, D. Role of the Bile Salt Surfactant Sodium Cholate in Enhancing the Aqueous Dispersion Stability of Single-Walled Carbon Nanotubes: A Molecular Dynamics Simulation Study. *J. Phys. Chem. B* **2010**, *114*, 15616–15625.

[114] Klein, R.; Touraud, D.; Kunz, W. Choline Carboxylate Surfactants: Biocompatible and Highly Soluble in Water. *Green Chem.* **2008**, *10*, 433–435.

[115] Goñi, F. M.; Requero, M. A.; Alonso, A. Palmitoylcarnitine, a Surface-Active Metabolite. *FEBS Letters* **1996**, *390*, 1–5.

[116] Meissner, D.; Grassert, I.; Oehme, G.; Holzhüter, G.; Vill, V. Preparation and Characterization of New Micelle-Forming Cholesterol Amphiphiles. *Colloid & Polym Sci.* **2000**, *278*, 364–368.

[117] Fong, C.; Wells, D.; Krodkiewska, I.; Weerawardena, A.; Booth, J.; Hartley, P. G.; Drummond, C. J. Diversifying the Solid State and Lyotropic Phase Behavior of Nonionic Urea-Based Surfactants. *J. Phys. Chem. B* **2007**, *111*, 10713–10722.

[118] Anoune, N.; Nouiri, M.; Arnaud, C.; Petit, S.; Lanteri, P. Synthesis and Characterization of New Cationic Surfactants Derived from Lactic Acid. *J. Surfactants Deterg.* **2000**, *3*, 381–386.

[119] Palma, S. D.; Maletto, B.; Lo Nostro, P.; Manzo, R. H.; Pistoresi-Palencia, M. C.; Allemandi, D. A. Potential Use of Ascorbic Acid-Based Surfactants as Skin Penetration Enhancers. *Drug Dev. Ind. Pharm.* **2006**, *32*, 821–827.

[120] Morán, M. C.; Pinazo, A.; Pérez, L.; Clapés, P.; Angelet, M.; García, M. T.; Vinardell, M. P.; Infante, M. R. "Green" Amino Acid-Based Surfactants. *Green Chem.* **2004**, *6*, 233–240.

[121] Pinazo, A.; Pons, R.; Pérez, L.; Infante, M. R. Amino Acids as Raw Material for Biocompatible Surfactants. *Ind. Eng. Chem. Res.* **2011**, *50*, 4805–4817.

[122] Veronese, F. M.; Pasut, G. PEGylation, successful approach to drug delivery. *Drug Discov Today* **2005**, *10*, 1451–1458.

[123] Myers, B. K.; Zhang, B.; Lapucha, J. E. Grayson, S. M. The Characterization of Dendronized Poly(ethylene glycol)s and Poly(ethylene glycol) Multi-arm Stars Using Matrix-assisted Laser Desorption/Iionization Time-of-flight Mass Spectrometry. *Anal Chim Acta* **2014**, *808*, 175–189.

[124] Zhu, M.; Carta, G. Adsorption of Polyethylene-glycolated Bovine Serum Albumin on Macroporous and Polymer-Grafted Anion Exchangers. *J Chromatogr A* **2014**, *1326*, 29–38.

[125] Hutanu, D.; Darie, C. C. Trends in Characterization of PEGylated Proteins by Mass Spectrometry. *Mod Chem Appl.* **2014,** *122*, 526–529.

[126] Veronese, F.; Harris, J. M. Introduction and Overview of Peptide and Protein Pegylation. *Adv. Drug Delivery Rev.* **2002**, *54*, 167–252.

[127] Veronese, F.; Harris, J. M. Pharmacokinetic and Biodistribution Properties of Poly(ethylene glycol)-Protein Conjugates. *Adv. Drug Delivery Rev.* **2003**, *55*, 1259–1350.

[128] Gref, R.; Minamitake, Y.; Peracchia, M. T.; Trubetskoy, V.; Torchilin, V.; Langer, R. Biodegradable Long-circulating Polymeric Nanospheres. *Science* **1994**, *263*, 1600–1603.

[129] Kreuter, J. Nanoparticles--a Historical Pperspective. *Int. J. Pharm.* **2007**, *331*, 1–10.

[130] Torchilin, V. P. Recent Advances with Liposomes as Pharmaceutical Carriers. *Nat. Rev. Drug Discovery* **2005**, *4*, 145–160.

[131] Sheth, S. R.; Leckband, D. Measurements of Attractive Forces between Proteins and End-grafted Poly(ethylene glycol) Chains. *Proc. Natl. Acad. Sci. USA* **1997,** *94*, 8399–8404.

[132] Israelachvili. J. The Different Faces of Poly(ethylene glycol). *Proc. Natl. Acad. Sci. USA*, **1997**, *94*, 8378–8379.

[133] Tadokoro, H.; Chatani, Y.; Yoshihara, T.; Murahashi, S. Structural Studies on Polyethers, $[-(CH_2)_m-O-]_n$ II. Molecular Structure of Polyethylene oxide. *Makromol. Chem.* **1964**, *73*, 109–127.

[134] Connor, T. M.; Mc Lauchlan, K. A. High Resolution Nuclear Resonance Studies of the Chain Conformation of Polyethylene Oxide. *J. Phys. Chem.* **1965**, *69*, 1888−1893.

[135] Liu, K.; Parsons, J. L. Solvent Effects on the Preferred Conformation of Poly(ethylene glycols). *Macromolecules* **1969**, *2*, 529−533.

[136] Blandamer, M. J.; Fox, M. F.; Powell, E.; Stafford, J. W. A Viscometric Study of Poly(ethylene oxide) in t-Butyl Alcohol/Water Mixtures. *Makromol. Chem.* **1969**, *124*, 222−231.

[137] Koenig, J. L.; Angood, A. C. J. Raman Spectra of Poly(ethylene glycols) in Solution. *Polym. Sci. Part A* **1970**, *8*, 1787−1796.

[138] Tasaki, K. Poly(oxyethylene)-Water Interactions: A Molecular Dynamics Study. *J. Am. Chem. Soc.* **1996**, *118*, 8459−8469.

[139] Johnson, W. Final Report on the Safety Assessment of PEG-25 Propylene glycol stearate, PEG-75 Propylene Glycol Stearate, PEG-120 Propylene Glycol Stearate, PEG-

10 Propylene Glycol, PEG-8 Propylene Glycol Cocoate, and PEG-55 Propylene Glycol Oleate. *Int. J. Toxicol.* **2001**, *20*, 13–26.

[140] Le Coz, C. J.; Heid, E. Allergic Contact Dermatitis from Methoxy PEG-17/Dodecyl glycol Copolymer (Elfacos® OW 100) *Contact Dermatitis* **2001**, *44*, 308–319.

[141] Torchilin, V. P.; Trubetskoy, V. S. Targeted Pharmaceutical Nanocarriers for Cancer Therapy and Imaging. *Adv. Drug Delivery Rev.* **1995**, *16*, 141–155.

[142] Mosbah, I. B.; Franco-Go, R.; Abdennebi, H. B.; Hernandez, R.; Escolar, G.; Saidane, D.; Rosello, J. C.; Peralta, C. Effects of Polyethylene Glycol and Hydroxyethyl Starch in University of Wisconsin Preservation Solution on Human Red Blood Cell Aggregation and Viscosity. *Transplant. Proc*. **2006**, *38*, 1229–1235.

[143] Balakrishnana, B.; Kumarb, D.; Yoshidab, Y.; Jayakrishnan, A. Chemical Modification of Poly(vinyl chloride) Resin using Poly(ethylene glycol) to Improve Blood Compatibility. *Biomaterials* **2005**, *26*, 3495–3502.

[144] Rahman, M.; Brazel, C. S. The Plasticizer Market: An Assessment of Traditional Plasticizers and Research Trends to Meet New Challenges. *Prog. Polym. Sci.* **2004**, *29*, 1223–1248.

[145] Gould, S. T.; Matherly, E. E.; Smith, J. N.; Heistad, D. D.; Anseth, K. S. The Role of Valvular Endothelial Cell Paracrine Signaling and Matrix Elasticity on Valvular Interstitial Cell Activation. *Biomaterials* **2014**, *35*, 3596–3606.

[146] Frith, J. E.; Menzies, D. J.; Cameron, A. R.; Ghosh, P.; Whitehead, D. L. Effects of Bound versus Soluble Pentosan Polysulphate in PEG/HA-Based Hydrogels Tailored for Intervertebral Disc Regeneration. *Biomaterials* **2014**, *35*, 1150–1162.

[147] Farooque, T. M.; Camp, C. H.; Tison, C. K.; Kumar, G.; Parekh, S. H. Measuring Stem Cell Dimensionality in Tissue Scaffolds. *Biomaterials* **2014**, *35*, 2558–2567.

[148] Daniele, M. A.; Adams, A. A.; Naciri, J.; North, S. H.; Ligler, F. S. Interpenetrating Networks Based on Gelatin Methacrylamide and PEG Formed Using Concurrent Thiol Click Chemistries for Hydrogel Tissue Engineering Scaffolds. *Biomaterials* **2014**, *35*, 1845–1856.

[149] Dang, L. T.; Feric, N.T.; Laschinger, C. Chang, W. Y.; Zhang, B. Inhibition of Apoptosis in Human Induced Pluripotent Stem Cells During Expansion in a Defined Culture using Angiopoietin-1 Derived Peptide. *Biomaterials* **2014**, *35*, 7786–7799.

[150] Tokuda, E. Y.; Leight, J. L.; Anseth, K. S. Modulation of Matrix Elasticity with PEG Hydrogels to Study Melanoma Drug Responsiveness. *Biomaterials* **2014**, *35*, 4310–4318.

[151] Nguyen, M. K.; Jeon, O.; Krebs, M. D.; Schapira, D.; Alsberg, E. Sustained Localized Presentation of RNA Interfering Molecules from In Situ Forming Hydrogels to Guide Stem Cell Osteogenic Differentiation. *Biomaterials* **2014**, *35*, 6278–6286.

[152] Lin, T. Y.; Ki, C. S.; Lin, C. C.; Manipulating Hepatocellular Carcinoma Cell Fate in Orthogonally Cross Linked Hydrogels. *Biomaterials* **2014**, *35*, 6898–6906.

[153] Jeong, C. G.; Francisco, A. T.; Niu, Z.; Mancino, R. L.; Craig, S. L. Screening of Hyaluronic Acid Poly(ethylene glycol) Composite Hydrogels to Support Intervertebral Disc Cell Biosynthesis Using Artificial Neural Network Analysis. *Acta Biomater* **2014**, *10*, 3421–3430.

[154] Jeon, O.; Samorezov, J. E.; Alsberg, E. Single and Dual Crosslinked Oxidized Methacrylated Alginate/PEG Hydrogels for Bioadhesive Applications. *Acta Biomater* **2014**, *10*, 47–55.

[155] Hoffman, M. D.; Van Hove, A. H.; Benoit, D.S. Degradable Hydrogels for Spatiotemporal Control of Mesenchymal Stem Cells Localized at Decellularized Bone Allografts. *Acta Biomater* **2014**, *10*, 3431–3441.

[156] Zhang, Z.; Loebus, A.; Vicente, G.; Ren, F.; Arafeh, M. Synthesis of Poly(ethylene glycol) based Hydrogels via Amine-Michael Type Addition with Tunable Stiffness and Postgelation Chemical Functionality. *Chem Mater* **2014**, *26*, 3624–3630.

[157] Xu, J.; Feng, E.; Song, J. Bioorthogonally Cross-Linked Hydrogel Network with Precisely Controlled Disintegration Time over a Broad Range. *J Am Chem Soc.* **2014**, *136*, 4105–4108.

[158] Wieduwild, R.; Lin, W.; Boden, A.; Kretschmer, K.; Zhang, Y. A Repertoire of Peptide Tags for Controlled Drug Release from Injectable Noncovalent Hydrogel. *Biomacromolecules* **2014**, *15*, 2058–2066.

[159] McKinnon, D. D.; Brown, T. E.; Kyburz, K. A.; Kiyotake, E.; Anseth, K. S. Design and Characterization of a Synthetically Accessible, Photodegradable Hydrogel for User-directed Formation of Neural Networks. *Biomacromolecules* **2014**, *15*, 2808–2816.

[160] Pasut, G.; Veronese, F. M. Polymer-drug Conjugation, Recent Achievements and General Strategies. *Prog. Polym. Sci*. **2007**, *32*, 933–961.

[161] Morpurgo, M.; Veronese, F. M. Conjugates of Peptides and Proteins to Polyethylene glycols. *Methods Mol Biol.* **2004**, *283*, 45–70.

[162] Pasut, G.; Guiotto, A.; Veronese, F. M. Protein, Peptide and Non-peptide Drug PEGylation for Therapeutic Application. *Expert Opin Ther Patents.* **2004**, *14*, 859–894.

[163] Roberts, M. J.; Bentley, M. D.; Harris, J. M. Chemistry for Peptide and Protein PEGylation. *Adv Drug Deliv Rev.* **2002**, *54(4)*, 459–476.

[164] Harris, J. M. Introduction for Biotechnical and Biomedical Applications of Poly(ethylene glycol). In: Harris JM, ed. *Poly(ethylene glycol) Chemistry Biotechnical and Biomedical Applications.* New York: Plenum Press, **1992**, 1–14.

[165] Zalipsky, S. Functionalized Poly(ethylene glycol) for Preparation of Biologically Relevant Conjugates. *Bioconjug Chem.* **1995**, *6(2)*, 150–165.

[166] Zalipsky, S.; Harris, J. M. Introduction to Chemistry and Biological Applications of Poly(ethylene glycol). In: Harris JM, Zalipsky S, eds. *Poly(ethylene glycol). Chemistry and Biological Applications.* Washington, DC: ACS Symposium series, **1997**, 1–13.

[167] Veronese, F. M.; Boccu, E.; Schiavon, O. Anti-inflammatory and Pharmacokinetic Properties of Superoxide Dismutase Derivatized with Polyethylene glycol via Active Esters. *J Pharm Pharmacol.* **1983**, *35(11)*, 757–758.

[168] Bonora, G.; Drioli, S. *Reactive PEGs for Protein Conjugation.* In: Veronese FM, ed. PEGylated Protein Drugs: Basic Science and Clinical Applications. Basel: Birkh€auser, **2009**, 33–45.

[169] Zalipsky, S.; Lee, C. Use of Functionalized Poly(ethylene glycol)s for Modification of Polypeptides. In: J M H, ed. *Poly(ethylene Glycol) Chemistry Biotechnical and Biomedical Applications.* New York: Plenum, **1992**, 347–370.

[170] Greenwald, R. B.; Choe, Y. H.; McGuire, J.; Conover, C. D. Effective Drug Delivery by PEGylated Drug Conjugates. *Adv Drug Deliv Rev.* **2003**, *55*, 217–250.

[171] Zalipsky, S. Chemistry of Polyethylene glycol Conjugates with Biologically Active Molecules. *Adv Drug Deliv Rev.* **1995**, *16*, 157–182.

[172] Francis, G. E.; Delgado, C.; Fisher, D.; Malik, F.; Agrawal, A. K. Polyethylene glycol Modification: Relevance of Improved Methodology to Tumour Targeting. *J Drug Target.* **1996**, *3*, 321–340.

[173] Veronese, F. M.; Pasut, G. PEGylation, Successful Approach to Drug Delivery. *Drug Discov Today* **2005**, *10(21)*, 1451–1458.

[174] Hermanson, G. T. Discrete PEG Reagents. *Bioconjugate Techniques*. 2nd ed. New York: Academic Press Elsevier, **2008**, 707–742.

[175] Knop, K.; Hoogenboom, R.; Fischer, D.; Schubert, U. S. Poly(ethylene glycol) in Drug Delivery: Pros and Cons as well as Potential Alternatives. *Angew Chem Int Ed Engl.* **2010**, *49(36*), 6288–6308.

[176] Allen, T. M.; Cullis, P. R. Drug Delivery Systems: Entering the Mainstream. *Science* **2004**, *303*, 1818–1822.

[177] Abuchowski, A.; Vanes, T.; Palczuk, N. C.; Davis, F. F. Alteration of Immunological Properties of Bovine Serum Albumin by Covalent Attachment of Polyethylene glycol. *J. Biol. Chem.* **1977**, *252*, 3578– 3581.

[178] Abuchowski, A.; McCoy, J. R.; Palczuk, N. C.; van Es, T.; Davis, F. F. Effect of Covalent Attachment of Polyethylene glycol on Immunogenicity and Circulating Life of Bovine Liver Catalase. *J. Biol. Chem.* **1977**, *252*, 3582–3586.

[179] Klibanov, A. L.; Maruyama, K.; Torchilin, V. P.; Huang, L. Amphipathic Poly(ethylene glycol) Effectively Prolong the Circulation Time of Liposomes. *FEBS Lett.* **1990**, *268*, 235–237.

[180] Blume, G.; Cevc, G. Liposomes for the Sustained Drug Release In Vivo. *Biochim. Biophys. Acta Biomembr.* **1990**, *1029*, 91–97.

[181] Woodle, M. C.; Newman, M.; Collins, L.; Redemann, C.; Martin, F. Prolonged Systemic Delivery of Peptide Drugs by Long-Circulating Liposomes: Illustration with Vasopressin in the Brattleboro Rat. *Proc. Int. Symp. Controlled Release Bioact. Mater.* **1990**, *17*, 77–78.

[182] Kabanov, A. V.; Chekhonin, V. P.; Alakhov, V. Y.; Batrakova, E. V.; Lebedev, A. S.; Melik, N. S.; Nubarov, S. A.; Arzhakov, A. V.; Levashov, G. V. The Neuroleptic Activity of Haloperidol Increases after its Solubilization in Surfactant Micelles: Micelles as Microcontainers for Drug Targeting. *FEBS Lett.* **1989**, *258*, 343–345.

[183] Kwon, G. S.; Kataoka. K. Block Copolymer Micelles as Long-circulating Drug Vehicles. *Adv. Drug Delivery Rev.* **1995**, *16*, 295–309.

[184] Kong, X.; Yu, K.; Yu, M.; Feng, Y.; Wang, J. A Novel Multifunctional Poly(amidoamine) Dendrimeric Delivery System with Superior Encapsulation Capacity for Targeted Delivery of the Chemotherapy Drug 10-hydroxycamptothecin. *Int J Pharm* **2014**, *465*, 378–387.

[185] Oupicky, D.; Ogris, M.; Howard, K. A.; Dash, P. R.; Ulbrich, K.; Seymour, L. W. Importance of Lateral and Steric Stabilization of Polyelectrolyte Gene Delivery Vectors for Extended Systemic Circulation. *Mol. Ther.* **2002**, *5*, 463–472.

[186] Aigner, A.; Fischer, D.; Merdan, T.; Brus, C.; Kissel, T.; Czubayko, F. Delivery of Unmodified Bioactive Ribozymes by an RNA-stabilizing Polyethylenimine (LMW-PEI) Efficiently Down-regulates Gene Expression. *Gene Ther.* **2002**, *9*, 1700–1707.

[187] Nguyen, E. H.; Zanotelli, M. R.; Schwartz, M. P.; Murphy, W. L. Differential Effects of Cell Adhesion, Modulus and VEGFR-2 Inhibition on Capillary Network Formation in Synthetic Hydrogel Arrays. *Biomaterials* **2014**, *35*, 2149–2161.

[188] Moreno, M.; Zurita, E.; Giralt, E. Delivering Wasp Venom for Cancer Therapy. *J Control Release* **2014,** *182*, 13–21.

[189] Pang, H. B.; Braun, G. B.; She, Z. G.; Kotamraju, V. R.; Sugahara, K. N. A Free Cysteine Prolongs the Half-life of a Homing Peptide and Improves its Tumor Penetrating Activity. *J Control Release* **2014,** *175*, 48–53.

[190] Peng, F.; Liu, Y.; Li, X.; Sun, L.; Zhao, D. PEGylation of G-CSF in Organic Solvent Markedly Increase the Efficacy and Reactivity Through Protein Unfolding, Hydrolysis Inhibition and Solvent Effect. *J Biotechnol* **2014**, *170*, 42–49.

[191] Tian, L.; Tadepalli, S.; Hyun Park, S.; Liu, K. K.; Morrissey, J. J. Bioplasmonic Calligraphy for Multiplexed Label-free. *Biodetection. Biosens Bioelectron* **2014**, *59*, 208–215.

[192] Santi, D. V.; Schneider, E. L.; Ashley, G. W. Macromolecular Prodrug that Provides the Irinotecan (CPT-11) Active-metabolite SN-38 with Ultralong Halflife, low C(max), and Low Glucuronide Formation. *J Med Chem* **2014**, *57*, 2303–2314.

[193] An, S.; Kuang, Y.; Shen, T.; Li, J.; Ma, H. Brain-targeting Delivery for RNAi Neuroprotection against Cerebral Ischemia Reperfusion Injury. *Biomaterials* **2013**, *34*, 8949–8959.

[194] Liu, B.; Chen, W.; Evavold, B. D.; Zhu, C. Accumulation of Dynamic Catch Bonds between TCR and aganist Peptide-MHC Triggers T cell Signaling. *Cell* **2014**, *157*, 357–368.

[195] Saville, S. L.; Qi, B.; Baker, J.; Stone, R.; Camley, R. E. The Formation of Linear Aggregates in Magnetic Hyperthermia: Implications on Specific Absorption Rate and Magnetic Anisotropy. *J Colloid Interface Sci* **2014**, *424*, 141–151.

[196] Zhang, Z.; Li, W.; Zhao, Q.; Cheng, M.; Xu, L. Highly Sensitive Visual Detection of Copper (II) Using Water-soluble Azide-functionalized Gold Nanoparticles and Silver Enhancement. *Biosens Bioelectron* **2014**, *59*, 40–44.

[197] Chong, Y.; Ma, Y.; Shen, H.; Tu, X.; Zhou, X. The In Vitro and In Vivo Toxicity of Graphene Quantum Dots. *Biomaterials* **2014**, *35*, 5041–5048.

[198] Chen, J.; Shi, M.; Liu, P.; Ko, A.; Zhong, W. Reducible Polyamidoaminemagnetic Iron Oxide Self-Assembled Nanoparticles for Doxorubicin Delivery. *Biomaterials* **2014**, *35*, 1240–1248.

[199] Tesfay, M. Z.; Kirk, A. C.; Hadac, E. M.; Griesmann, G. E.; Federspiel, M. J. PEGylation of Vesicular Stomatitis Virus Extends Virus Persistence in Blood Circulation of Passively Immunized Mice. *J Virol* **2013**, *87*, 3752–3759.

[200] Gajbhiye, V.; Escalante, L.; Chen, G.; Laperle, A.; Zheng, Q. Drugloaded Nanoparticles Induce Gene Expression in Human Pluripotent Stem Cell Derivatives. *Nanoscale* **2014**, *6*, 521–531.

[201] Lee, D.-I.; Choi, J.-Y.; Lee, E. S.; Ha, C.-S.; Han, M.; Bae, J.-Y. Synthesis and Characterization of TRITON™ X-based Surfactants with Carboxylic or Amino Groups in the Oxyethylene Chain End. *J Appl Polym Sci* **2007**, *104*, 162–170.

[202] Jeong, B.; Bae, Y. H.; Lee, D. S.; Kim, S. W. Biodegradable Block Copolymers as Injectable Drug-Delivery Systems. *Nature* **1997**, *388*, 860–862.

[203] Ruan, G.; Feng, S. -S. Carbonated Calcium Phosphates are Suitable pH-stabilising Fillers for Biodegradable Polyesters. *Biomaterials* **2003**, *24*, 2037–2043.

[204] Govender, T.; Riley, T.; Ehtezazi, T.; Garnett, M. C.; Stolnik, S.; Illum, L.; Davis, S. S. Defining the Drug Incorporation Properties of PLA-PEG Nanoparticles. *Int. J. Pharm.* **2000**, *199*, 95–110.

[205] Custers, J. P. A.; Van den Broeke, L. J. P.; Keurentjes, J. T. F. Phase Behavior and Micellar Properties of Carboxylic Acid End group Modified Pluronic Surfactants. *Langmuir* **2007**, *23*, 12857–12863.

[206] Miller, A. M.; Malker, N. B.; Severynse-Stevens, D.; Yarbrough, K. G.; Bednarcik, M. J.; Dugdell, R. E.; Puskas, M. E.; Krishnan, R.; James, K. D. Amphiphilic Conjugates of Human Brain Natriuretic Peptide Designed for Oral Delivery: In Vitro Activity Screening. *Bioconjugate Chem* **2006**, *17*, 267–274.

[207] Gref, R.; Domb, A.; Quellec, P.; Blunk, T.; Muller, R. H.; Verbavatz, J. M.; Langer, R. The Controlled Intravenous Delivery of Drugs Using PEG-coated Sterically Stabilized Nanospheres. *Adv. Drug Delivery Rev.* **1995**, *16*, 215–233.

[208] Leroux, J. -C.; Allemann, E.; De Jaeghere, F.; Doelker, E.; Gurny, R. Biodegradable Nanoparticles—from Sustained Release Formulations to Improved Site Specific Drug Delivery. *J. Controlled Release* **1996**, *39*, 339–350.

[209] Jeong, B.; Bae, Y. H.; Kim, S. W. Drug Release from Biodegradable Injectable Thermosensitive Hydrogel of PEG-PLGA-PEG Triblock Copolymers. *J. Contolled Release* **2000**, *63*, 155–163.

[210] Lucke, A.; Tessmar, J.; Schnell, E.; Schmeer, G.; Gopferich, A. Biodegradable Poly(d,l-lactic acid)-poly(ethylene glycol)-monomethyl Ether Diblock Copolymers: Structures and Surface Properties Relevant to their Use as Biomaterials. *Biomaterials* **2000**, *21*, 2361–2370.

[211] Breitenbach, A.; Li, Y. X.; Kissel, T. Branched Biodegradable Polyesters for Parenteral Drug Delivery Systems. *J. Controlled Release* **2000**, *64*, 167–178.

[212] Dey, J.; Shrivastava, S. Can Molecules with Anionic Head and Poly(ethylene glycol) Methyl Ether Tail Self-assemble in Water? A Surface tension, Fluorescence Probe, Light Scattering, and Transmission Electron Microscopic Investigation. *Soft Matter* **2012**, *8*, 1305−1308.

[213] Dey, J.; Shrivastava, S. Physicochemical Characterization and Self-Assembly Studies on Cationic Surfactants bearing mPEG Tail. *Langmuir* **2012**, *28*, 17247–17255.

[214] Laskar, P; Dey, J; Ghosh, S. K. Evaluation of Zwitterionic Polymersomes Spontaneously Formed by pH-Sensitive and Biocompatible PEG Based Random Copolymers as Drug Delivery Systems. *Colloids Surf B Biointerfaces* **2016**, *139*, 107–116.

[215] Laskar, P; Dey, J; Ghosh, S. K. Spontaneously Formed Redox- and pH-sensitive Polymersomes by mPEG Based Cytocompatible Random Copolymers. *J. Colloid Interface Sci*. **2017**, *501*, 22–33.

[216] Laskar, P.; Dey, J.; Banik, P.; Mandal, M.; Ghosh, S. K. In Vitro Drug and Gene Delivery using Random Cationic Copolymers Forming Stable and pH-Sensitive Polymersomes. *Macromol. Biosci*. **2017**, *17*, 1600324.

Chapter 2
Materials and Methods

2.1 Materials

Poly(ethylene glycol) methyl ether methacrylate ($mPEG_{300}$, M_n ~ 300 and $mPEG_{1100}$, M_n ~ 1100), poly(ethylene glycol) diacrylate (M_n ~ 575), sodium-2-mercapto ethane sulfonate (mesna, 98%), sodium-2,3-dimercaptopropanesulfonate monohydrate (95%), oleoyl chloride (99%), myristoyl chloride (99%), cholesteryl chloroformate (99%) and cholesterol (Chol, ≥ 99%) were purchased from Sigma-Aldrich (Bangalore, India). L-Cysteine (≥ 99%) was procured from Lab Chem and used without further purification. 1,3-Propane sultone (98%), 1,8-diazabicycloundec-7-ene (DBU, 98%), triethylamine (TEA, 98%), sodium dihydrogen phosphate (≥ 99%), disodium monohydrogen phosphate (≥ 99%), phosphotungstic acid, sodium bicarbonate (99%), sodium carbonate (99%), metallic sodium, sodium hydroxide (97%) and sodium chloride (≥ 99%) were purchased from SRL (Mumbai, India). Solvents such as methanol (MeOH), tetrahydrofuran (THF), chloroform ($CHCl_3$), dichloromethane (DCM), dichloroethane (DCE), ethyl acetate (EA), petroleum ether (PE) and *n*-hexane were obtained from Merck (Mumbai, India). All the solvents were of analytical grade and were dried and distilled following typical procedures before use. All deuterated solvents, such as $CDCl_3$, D_2O and CD_3OD were purchased from Cambridge Isotope Laboratories, Inc (CIL, India). Millipore filter paper was obtained from Merck, India. Milli Q water (18.2 MΩ cm) was obtained from a Millipore water purifier (Elix, Bangalore, India).

The fluorescent probes (see **Figure 2.1.1** for structures) pyrene (Py, 99%), N-phenyl-1-naphthylamine (NPN, 98%), 1,6-diphenyl-1,3,5-hexatriene (DPH, 98%), coumarine-153 (C153, 98%), calcein (CAL, 99%), methylene blue (MB, 99%), curcumin (≥ 95%) , and riboflavin (98%) were obtained from Sigma-Aldrich (Bangalore, India) and were purified by repeated recrystallization from ethanol water mixtures. The purity of the probes was checked by matching fluorescence excitation and absorption spectra.

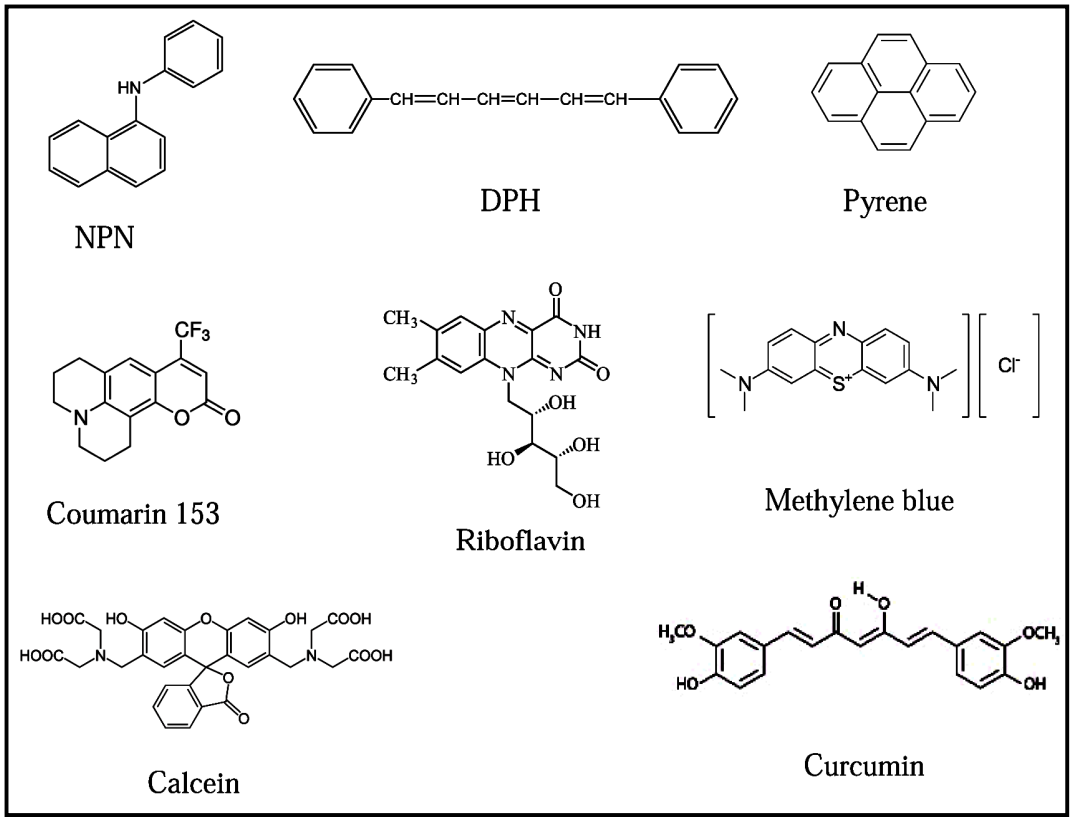

Figure 2.1.1 Chemical structures of fluorescent probes.

2.2 Synthesis of amphiphiles

2.2.1 Synthesis of L-cysteine conjugated $mPEG_{300}$-Cys and $mPEG_{1100}$-Cys

The single-chain zwitterionic amphiphiles were synthesized by the Michael addition reaction of L-cysteine with poly(ethylene glycol) methyl ether methacrylate by thiol−ene "click" chemistry according to the reported method [1,2]. Briefly, $mPEG_{300}$ (2.1 g, 7 mmol) was reacted with L-cysteine (1.275 g, 10.5 mmol) in methanol at room temperature for 6 h in the presence of TEA. The product was obtained as white solid after evaporation of the solvent. To remove unreacted materials, the solid compound was dissolved in water and then reprecipitated by adding dry acetone. The compound was isolated as white solid. The details of the chemical identifications and the representative ^{1}H-NMR (**Figure 2.2.1**) and ^{13}C-NMR (**Figure 2.2.2**) spectra are presented below.

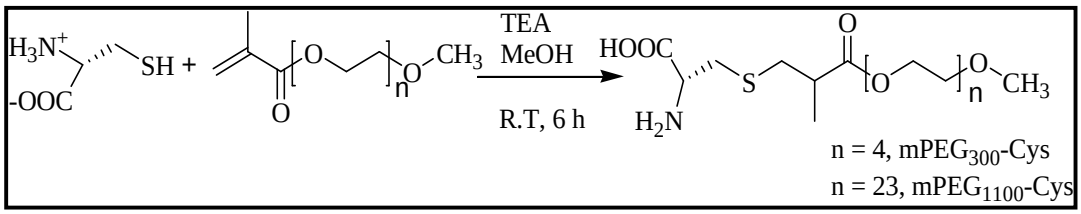

Scheme 2.2.1 Synthetic scheme of $mPEG_{300}$-Cys and $mPEG_{1100}$-Cys.

2.2.1.1 Chemical identification

MW: 421.16 ($mPEG_{300}$-Cys) and 1221.16 ($mPEG_{1100}$-Cys), **State:** white solid, ***mp*** 170 ^{o}C ($mPEG_{300}$-Cys) and 230 ^{o}C ($mPEG_{1100}$-Cys). **Yield** ~ 80%, $[\alpha]_D$ ^{25} (1%, H_2O) = +20, **FTIR (KBr, cm^{-1}):** The broad band centered at 3411 cm^{-1} corresponds to O-H stretching for hydrogen-bonded COOH group. Absence of double bond is confirmed by absence of C-H stretching around 3000 cm^{-1}. Absence of the characteristic band of S-H stretch around 2550 cm^{-1} confirms the absence of S-H. Strong peaks near 1734 cm^{-1} and 1725 cm^{-1} show the presence of C=O stretches of ester and carboxylic acid group, respectively. The absorption peak at 674 cm^{-1} indicates the presence of C-S bond. **^{1}H-NMR ($CDCl_3$, 400 MHz):** δ (ppm) 1.254 (COCH***C*H*$_3$**, t, 3H), 2.868 (COOHCH***C*H*$_2$**, d, 2H), 3.043 (S***C*H*$_2$**-CH, d, 2H), 3.203 (SCH_2***C*H***CO, m, 1H), 3.381 (O***C*H*$_3$**, s, 3H), 3.558 (CO-OCH_2***C*H*$_2$**, t, 2H), 3.661 (long chain glycolic C***H*$_2$**, m, 18H for $mPEG_{300}$-Cys and 104H for $mPEG_{1100}$-Cys), 3.729 (OCH_3 ***C*H*$_2$**CH_2, t, 2H), 3.795(NH_2***C*H***CH_2, t, 1H), 4.351 (CO-O***C*H*$_2$**-CH_2, dd, 2H). **^{13}C-NMR (D_2O, 1% DMSO, 400 MHz):** δ (ppm) 175.1 (***C***$OOCH_2$), 170.2 (***C***OO-), 68.7, 67.3, 66.1, 61.5 (ether ***C*H*$_2$**), 55.7 (O***C***H_3), 51.4(N***C*H***CH_2) 37.7 (SCH_2***C*H***), 32.2 (S***C*H*$_2$** CH), 30.3 (S***C*H*$_2$** CH_2NH_2), 13.9 (***C***H_3). **^{13}C-NMR ($CDCl_3$, 400 MHz):** δ (*ppm*) 175.08 (***C***$OOCH_2$), 172.3 (***C***OOH), 71.8, 70.4, 69.0, 63.7 (ether ***C***H_2), 59.7 (*O***C***H*$_3$**), 53.4(N***C*H***CH_2) 40.0 (SCH_2***C*H***), 35.2 (S***C*H*$_2$**CH), 33.4 (S***C*H*$_2$** CH_2NH_2), 16.9 (***C***H_3). **CHNS Analysis**: Calcd (%) for $C_{16}H_{31}NO_8S$; C: 45.58, H: 7.59, N: 3.32; Found (%): C: 45.74, H: 8.03, N: 3.02.

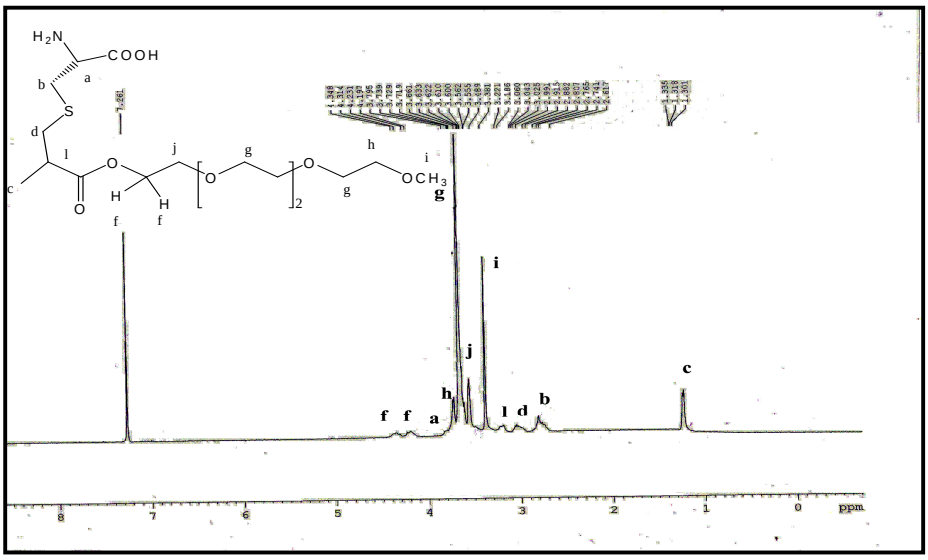

Figure 2.2.1 ^{1}H-NMR spectrum of mPEG$_{300}$-Cys in $CDCl_3$ solvent.

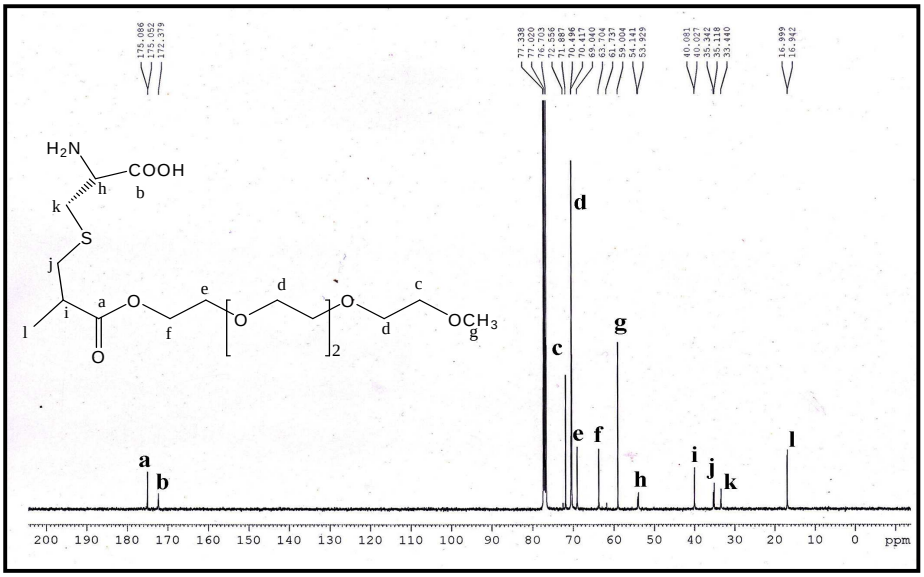

Figure 2.2.2 ^{13}C-NMR spectrum of mPEG$_{300}$-Cys in $CDCl_3$ solvent.

2.2.2 Synthesis of mesna conjugated poly(ethylene glycol) methyl ether methacrylate (PEGS1 and PEGS2)

The compounds PEGS1 and PEGS2 were synthesized by the same procedure described above [1, 2]. The anionic surfactants were synthesized according to the **Scheme 2.2.2**.

Briefly $mPEG_{300}$ (1.06 g, 3.53 mM) and mesna (0.5 g, 3.53 mmol) was stirred in methanol in the presence of TEA (1.0 eq) at room temperature for 6 h. The compound was obtained as a viscous colorless liquid for PEGS1 and as a white solid for PEGS2 after evaporation of the solvent and was purified by column (Al_2O_3) chromatography using 5:1 (v/v) ethyl acetate-petroleum ether mixture. Both PEGS1 and PEGS2 molecules were found to be hygroscopic. The structures of the synthesized molecules were confirmed by FT-IR, ^{1}H-NMR (**Figure 2.2.3**), and ^{13}C-NMR (**Figure 2.2.4**) spectra.

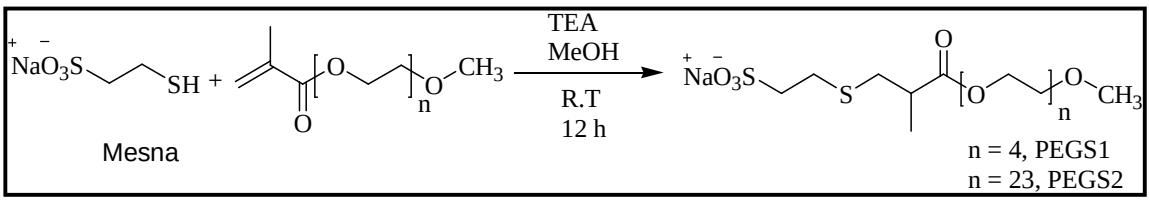

Scheme 2.2.2 General synthetic scheme for PEGS1 and PEGS2.

2.2.2.1 Chemical identification

PEGS1. MW: 464.18, **State**: colorless viscous liquid, **Yield**: 80-85%, **FTIR (KBr, cm^{-1})** Absence of double bond is confirmed by absence of C-H stretching at 3000 cm^{-1} and no band at 2565 cm^{-1} confirms absence of S-H stretching. Peak at 1738 cm^{-1} shows presence of C=O stretching of ester group and peak at 638 cm^{-1} shows presence of C-S stretching. **^{1}H-NMR (CD_3OD, 400 MHz):** δ (ppm) 1.254 (COCHC***H***$_3$, t, 3H), 2.885 (SO_3NaCH***C H***$_2$, d, 2H), 2.895 (S***C H***$_2$-CH, d, 2H), 3.002 (SCH_2***C H***CO, m, 1H), 3.358 (O***C H***$_3$, s, 3H), 3.551 (CO-OCH_2***C H***$_2$, t, 2H), 3.663 (long chain glycolic C***H***$_2$, m, 18H for PS1 and 104H for PS2), 3.729 (SO_3Na ***C H***$_2$, t, 2H), 4.351 (CO-O***C H***$_2$-CH_2, dd, 2H). **^{13}C-NMR (D_2O, 400 MHz):** δ (ppm) 178.5 (***C***OOCH_2), 64.7, 69.5, 70.5, 70.9, 73.6 (ether ***C***H_2), 58.4 (O***C***H_3), 51.4 (S***C***H_2CH), 40.2 (SCH_2***C***H), 34.8 (S***C***H_2 CH_2COOH), 26.4 (SCH_2 ***C***H_2COOH), 16.4 (***C***H_3).

PEGS2. MW: 1264.18, **State:** Hygroscopic white solid, **Yield:** 81%, **FTIR (KBr, cm^{-1}):** Absence of double bond is confirmed by absence of C-H stretching at 3000 cm^{-1} and no band at 2565 cm^{-1} confirms absence of SH stretching. Peak at 1740 cm^{-1} shows presence of C=O stretching of ester group and peak at 635 cm^{-1} shows presence of C-S stretching. **^{1}H-NMR (CD_3OD, 400 MHz):** 1.254 (COCHC***H$_3$***, t, 3H), 2.885

($SO_3NaCHC\boldsymbol{H_2}$, d, 2H), 2.895 ($SC\boldsymbol{H_2}$-CH, d, 2H), 3.002 ($SCH_2C\boldsymbol{H}CO$, m, 1H), 3.358 ($OC\boldsymbol{H_3}$, s, 3H), 3.551 ($CO\text{-}OCH_2C\boldsymbol{H_2}$, t, 2H), 3.663 (long chain glycolic $C\boldsymbol{H_2}$, m, 18H for PS1 and 104H for PS2), 3.729 ($SO_3Na\ C\boldsymbol{H_2}$, t, 2H), 4.351 ($CO\text{-}OC\boldsymbol{H_2}\text{-}CH_2$, dd, 2H). **^{13}C-NMR**. (**D_2O, 400 MHz):** δ (ppm) 178.5 (***C***$OOCH_2$), 64.7, 69.5, 70.5, 70.9, 73.6 (ether ***C***H_2), 58.4 ($O\boldsymbol{C}H_3$), 51.4 ($S\boldsymbol{C}H_2CH$), 40.2 ($SCH_2\boldsymbol{C}H$), 34.8 ($S\boldsymbol{C}H_2\ CH_2COOH$), 26.4 ($SCH_2\ \boldsymbol{C}H_2COOH$), 16.4 ($\boldsymbol{C}H_3$).

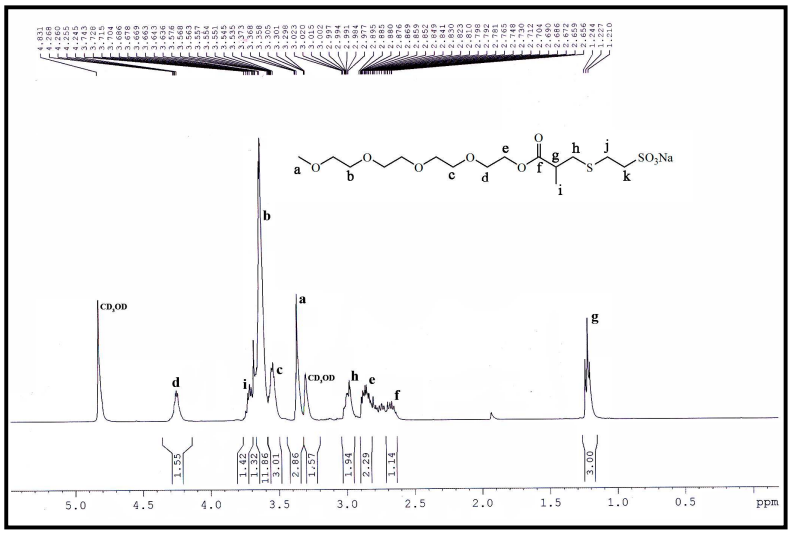

Figure 2.2.3 ^{1}H-NMR spectrum of PEGS1 in CD_3OD solvent.

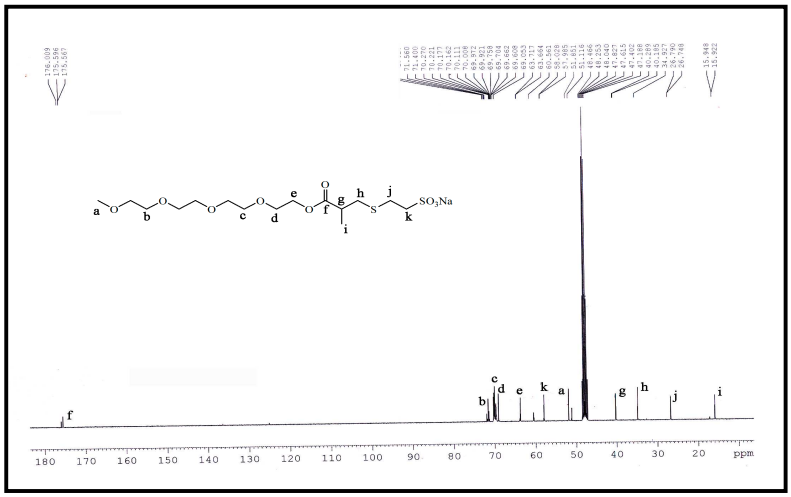

Figure 2.2.4 ^{13}C-NMR spectrum of PEGS1 in CD_3OD solvent.

2.2.3 Synthesis of di-(mercapto propanoyl poly(ethylene glycol)) propane sulfonate (DPEGS1 and DPEGS2)

The amphiphiles with double PEG chains of different lengths (DPEGS1 and DPEGS2) were synthesized by the Michael addition reaction of sodium-2,3-dimercaptopropanesulfonate with poly(ethylene glycol) methyl ether methacrylate by thiol−ene "click" chemistry according to the reported method described earlier following **Scheme 2.2.3**. In brief, sodium-2,3-dimercaptopropanesulfonate (1 eq) was reacted with mPEG (2.2 eq) in methanol at room temperature for 12 h in the presence of TEA (2.2 eq). The solvent was then evaporated and the product was obtained as viscous liquid for DPEGS1 and as white, hygroscopic solid for DPEGS2. The unreacted materials were removed by washing the product repeatedly with *n*-hexane. Then the pure product was air-dried under vacuum. Chemical identifications were performed using ^{1}H- and ^{13}C-NMR NMR spectra shown in **Figure 2.2.5** and **Figure 2.2.6**, respectively.

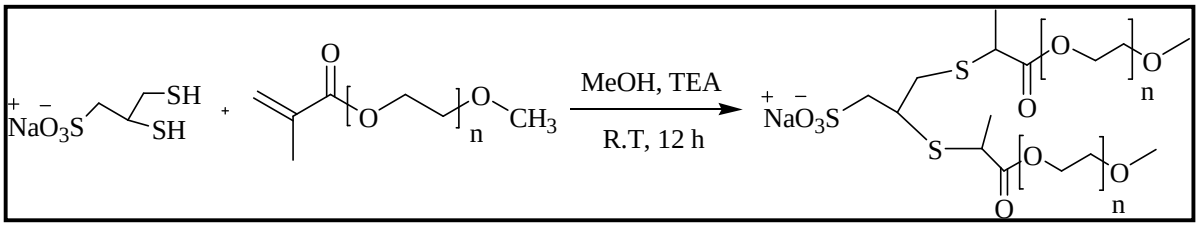

Scheme 2.2.3 General synthetic scheme of the amphiphiles (n = 4, DPEGS1 and n = 23, DPEGS2).

2.2.3.1 Chemical identification of DPEGS1 and DPEGS2

MW: 828.30g (DPEGS1) and 2428.3 (DPEGS2), **State:** colorless semi solid (DPEGS1) and white hygroscopic solid (DPEGS2), **Yield:** ~ 80%, **FTIR (KBr, cm^{-1}):** absence of double bond is confirmed by absence of C-H stretching at 3000 cm^{-1} and no band at 2565 cm^{-1} confirms absence of S-H stretching. Peak at 1738 cm^{-1} shows presence

of C=O stretching of ester group and peak at 638 cm^{-1} shows presence of C-S stretching. **^{1}H-NMR (D_2O, 600 MHz):** δ (ppm) 1.254 (COCH***C*****H**$_3$, t, 3H), 2.885 (SO_3NaCH***C*****H**$_2$, d, 2H), 2.895 (S***C*****H**$_2$-CH, d, 2H), 3.002 (SCH$_2$***C*****H**CO, m, 1H), 3.358 (O***C*****H**$_3$, s, 3H), 3.551 (CO-OCH$_2$***C*****H**$_2$, t, 2H), 3.663 (long chain glycolic C***H***$_2$, m, 36H for DPEGS1 and 208H for DPEGS2), 3.729 (SO_3Na ***C*****H**$_2$, t, 2H), 4.351 (CO-O***C*****H**$_2$-CH$_2$, dd, 2H). **^{13}C-NMR (D_2O, 600 MHz):** δ (ppm) 178.5 (***C***OOCH$_2$), 64.7, 69.5, 70.5, 70.9, 73.6 (ether ***C***H$_2$), 58.4 (O***C***H$_3$), 51.4 (S***C***H$_2$CH), 40.2 (SCH$_2$***C***H), 34.8 (S***C***H$_2$ CH$_2$COOH), 26.4 (SCH$_2$ ***C***H$_2$COOH), 16.4 (***C***H$_3$).

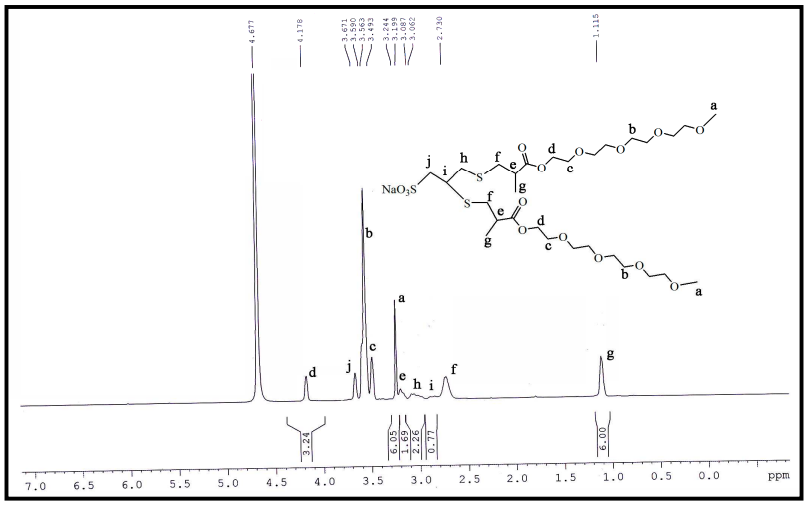

Figure 2.2.5 ^{1}H-NMR spectrum of DPEGS1 in D_2O solvent.

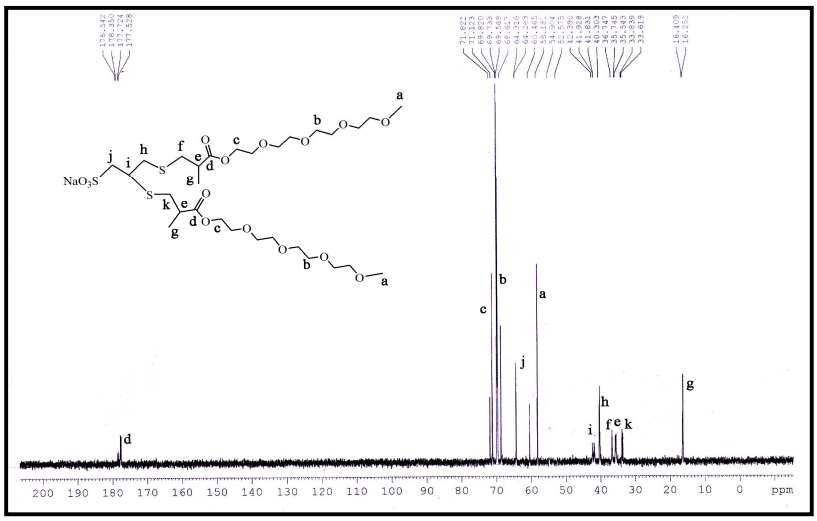

Figure 2.2.6 ^{13}C-NMR spectrum of DPEGS1 in D_2O solvent.

2.2.4 Conjugation of hydrocarbon chain to $mPEG_{300}$-Cys (CPOLE and CPMYS)

The anionic surfactants were synthesized according to the **Scheme 2.2.4**.The starting material, $mPEG_{300}$-Cys was synthesized according to the procedure described earlier. The single-chain amphiphile $mPEG_{300}$-Cys was then reacted with the acid chloride (myristoyl chloride or oleoyl chloride) in super dry DCM in the presence of super dry TEA according to the procedure reported in the literature [3, 4]. In a dry and clean 100 mL round bottom (RB) flask equipped with a magnet, 1eq $mPEG_{300}$-Cys was charged with 2 eq TEA in 20 mL super dry DCM. The mixture was stirred for 2 h. Then the acid chloride (1 eq) in DCM was added drop wise to the reaction mixture in ice-cold condition and the reaction mixture was continued to stir for another more 6h for the complete conversion of the acid chloride to amide. The progress of the reaction was followed by checking TLC from time to time. The solvent was evaporated in a rota-evaporator. The residual white mass (semi-solid) was dissolved in minimum volume of water and the pH of the aqueous mixture was adjusted to 3.0. Then the aqueous phase was solvent extracted by $CHCl_3$ repeatedly to obtain the desired product. $MgSO_4$ was then added to the organic part and was kept for 12 h. The solid $MgSO_4$ was then filtered off and the organic part was concentrated in rota-evaporator. The product thus procured was found to be pure enough and the yield was also very good (~90 %). The compound was identified by FT-IR, ^{1}H-NMR (**Figure 2.2.7**), ^{13}C-NMR (**Figure 2.2.8**) spectra.

The compound thus obtained in the first step was dissolved in THF. An aqueous solution of Na_2CO_3 (1.2 eq.) was then added drop wise dissolved in distilled water for a period of 15 min with continuous stirring at room temperature. The mixture immediately turned turbid, but became clear during the course of reaction. After stirring for 12 h, THF was evaporated, leaving a colorless slurry in the RB flask. The mass was freeze-dried to remove the water and the product was then washed with $CHCl_3$ to remove unreacted Na_2CO_3. The desired pure product was obtained with ~ 80% yield.

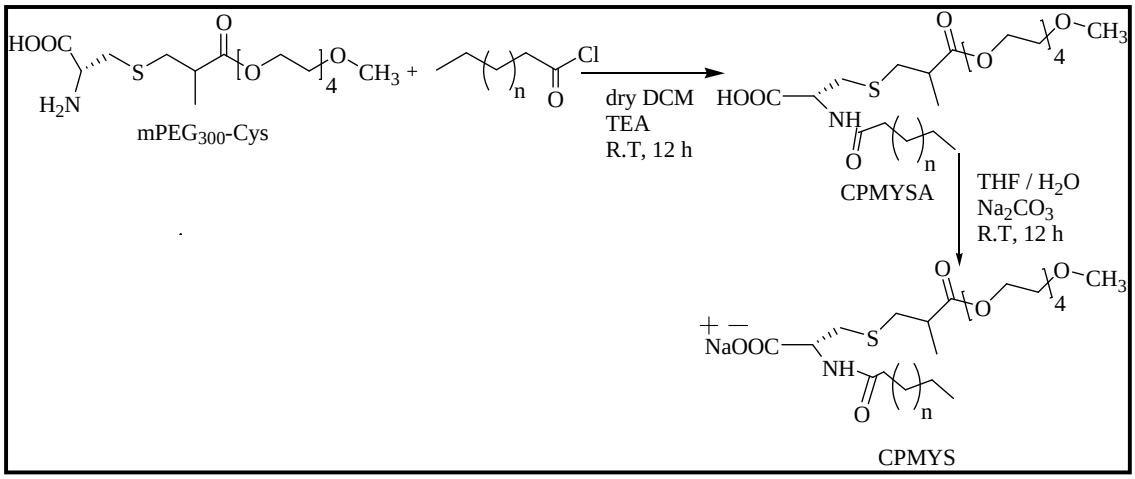

Scheme 2.2.4 General synthetic scheme for CPOLE and CPMYS.

2.2.4.1 Chemical identification of CPOLE and CPMYS

MW: 663.43 g (CPOLEA) and 609.48 g (CPMYSA). **State:** Colorless viscous liquid, **Yield:** ~85%. **FTIR:** (**KBr cm^{-1}**) 3501 cm^{-1} (broad, carboxylic acid O-H stretch), 3337 cm^{-1} (strong, N-H stretch), 1734 cm^{-1} (ester C=O stretch), 1728 (carboxylic acid C=O stretch), 1653 cm^{-1} (amide C=O stretch), 1519 cm^{-1} (N-H bend), 1256, 1218, 1076, and 1038 (C–O stretches). No band at 2565 cm^{-1} confirms absence of S-H stretching and the absorption peak at 772 cm^{-1} indicates the presence of C-S bond. **^{1}H-NMR** (**$CDCl_3$, 600 MHz):** δ (ppm) 1.254 (COCH$C\boldsymbol{H}_3$, t, 3H), 2.868 (COOHCH$C\boldsymbol{H}_2$, d, 2H), 3.043 (S$C\boldsymbol{H}_2$-CH, d, 2H), 3.203 (SCH$_2C\boldsymbol{H}$CO, m, 1H), 3.381 (O$C\boldsymbol{H}_3$, s, 3H), 3.558 (CO-OCH$_2C\boldsymbol{H}_2$, t, 2H), 3.661 (long chain glycolic $C\boldsymbol{H}_2$, m, 18H), 3.729 (OCH$_3$ $C\boldsymbol{H}_2$CH$_2$, t, 2H), 3.795(NH$_2C\boldsymbol{H}$CH$_2$, t, 1H), 4.351 (CO-O$C\boldsymbol{H}_2$-CH$_2$, dd, 2H), 0.886 (CH$_2$-$C\boldsymbol{H}_3$, t, 3H), 1.243 (long chain alkyl $C\boldsymbol{H}2$, m, 20H), 2.024(CH_2-CHCH-$C\boldsymbol{H}_2$, m, 4H), 1.656 (NHCOCH$_2$-$C\boldsymbol{H}_2$, m, 2H), 2.301 (NHCO$C\boldsymbol{H}_2$, t, 2H), 6.530 ($N\boldsymbol{H}$CO, d, 1H) and for the acid form **CPOLE** an extra peak at 5.356 ($\boldsymbol{H}$CC$\boldsymbol{H}$, s, 2H). **^{13}C-NMR** (**$CDCl_3$, 600 MHz):** δ (ppm) 177.1 ($\boldsymbol{C}$OOCH$_2$), 174.3 ($\boldsymbol{C}$OOH), 172.2 ($\boldsymbol{C}$ONH) 68.7, 67.3, 66.1, 61.5 (ether $\boldsymbol{C}$H$_2$), 55.7 (O$\boldsymbol{C}$H$_3$), 51.4 (N$\boldsymbol{C}$H CH$_2$) 37.7 (SCH$_2\boldsymbol{C}$H), 32.2 (S$\boldsymbol{C}$H$_2$CH), 30.3 (S$\boldsymbol{C}$H$_2$CH$_2$NH$_2$), 29 ($\boldsymbol{C}H_2CH_2CH_2CH_2$), 13.9 ($\boldsymbol{C}H_3$), and for **CPOLE** an extra peak at 129.2 ($\boldsymbol{CHCH}$). **HRMS:** Calculated for **CPOLE** acid form is [M+H]$^+$: 662.4300; Found:

662.4326 and Calculated for **CPMYS** acid form is $[M+H]^+$: 608.3800; Found: 608.3918.

MW: 685.43 g (CPOLE) and 632.38 g (CPMYS). **State:** Colorless hygroscopic solid, **Yield:** ~80%. **^{1}H-NMR (D_2O, 600 MHz):** δ (ppm) 1.254 (COCH***C*****H**$_3$, t, 3H), 2.868 (COOHCH***C*****H**$_2$, d, 2H), 3.043 (S***C*****H**$_2$-CH, d, 2H), 3.203 (SCH$_2$***C*****H**CO, m, 1H), 3.381 (O***C*****H**$_3$, s, 3H), 3.558 (CO-OCH$_2$***C*****H**$_2$, t, 2H), 3.661 (long chain glycolic ***C*****H**$_2$, m, 18H), 3.729 (OCH$_3$ ***C*****H**$_2$CH$_2$, t, 2H), 3.795(NH$_2$***C*****H**CH$_2$, t, 1H), 4.351 (CO-O***C*****H**$_2$-CH$_2$, dd, 2H), 0.886 (CH$_2$-***C*****H**$_3$, t, 3H), 1.243 (long chain alkyl ***C*****H**$_2$, m, 20H), 2.024(*CH*$_2$-CHCH-***C*****H**$_2$, m, 4H), 1.656 (NHCOCH$_2$-***C*****H**$_2$, m, 2H), 2.301 (NHCO***C*****H**$_2$, t, 2H), 6.530 (***N*****H**CO, d, 1H) and for **CPOLE** an extra peak at 5.356 (***H***CC***H***, s, 2H). **^{13}C-NMR (D_2O, 600 MHz):** δ (ppm) 177.1 (***C***OOCH$_2$), 171.3 (***C***OO$^-$), 168.2 (***C***ONH) 68.7, 67.3, 66.1, 61.5 (ether ***C***H$_2$), 55.7 (O***C***H$_3$), 51.4 (N***C***H CH$_2$) 37.7 (SCH$_2$***C***H), 32.2 (S***C***H$_2$CH), 30.3 (S***C***H$_2$CH$_2$NH$_2$), 29 (***C****H*$_2$***C****H*$_2$***C****H*$_2$***C****H*$_2$), 13.9 (***C***H$_3$), and for **CPOLE** an extra peak at 129.2 (***C****H****C****H*).

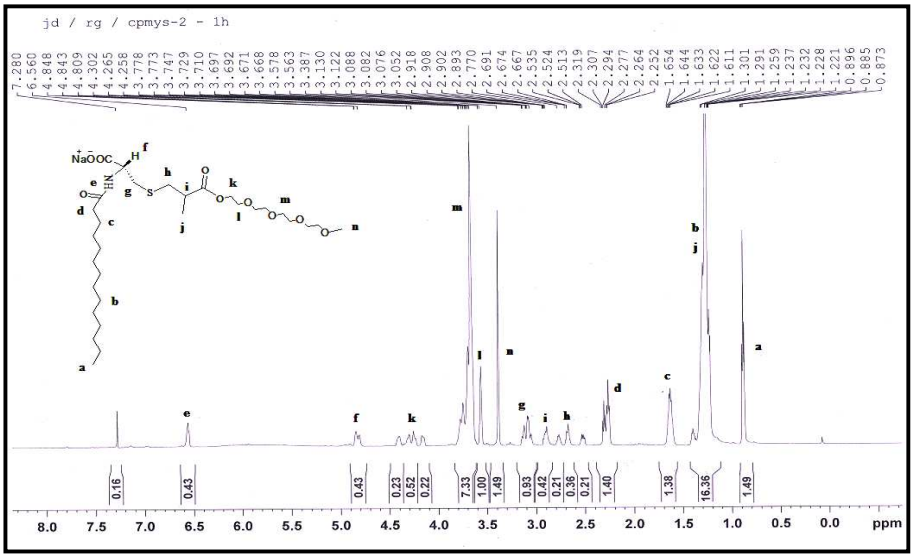

Figure 2.2.7 ^{1}H-NMR spectrum of CPMYS (acid form) in $CDCl_3$ solvent.

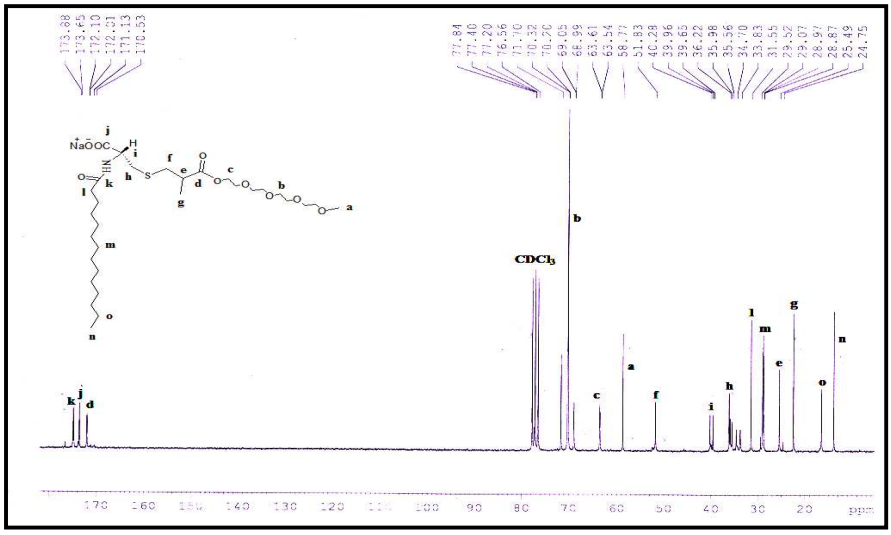

Figure 2.2.8 ^{13}C-NMR spectrum of CPMYS (acid form) in $CDCl_3$ solvent.

2.2.5 Conjugation of Chol to mPEG$_{300}$-Cys (CPCF3 and CPCF11)

In a 100-mL (single-neck) RB flask fitted with a magnetic stirrer, mPEG$_{300}$-Cys (1.0 eq) was dissolved in super dry THF containing 1 eq super dry TEA. But it remained insoluble in THF even after 1 h of stirring. Then some amount of super dry MeOH was added to the RB to dissolve the whole mixture. The reaction mixture was stirred at R.T. for further 30 min. The solution was cooled to 0 ^{o}C in an icebath. To this cold solution, cholesteryl chloroformate (0.9 eq.) dissolved in dry THF was added drop wise with continuous stirring over a period of 2 h. The pH of the reaction mixture was maintained at 8-9 by the addition of TEA at regular intervals. After stirring for 20 h, the solvent was evaporated in a rotavapor, and the residual milky white slurry was transferred into a 50-mL beaker by use of a minimum volume (~ 10 mL) of distilled water. The resulting aqueous milky white dispersion was acidified with aqueous dilute HCl (0.5 M) to pH ~ 2. The compound was then extracted with small portion of $CHCl_3$ from acidified aqueous solution. All the $CHCl_3$ fractions were collected and then the solvent was evaporated out. The product was dried in desiccators overnight under reduced pressure to get colorless semi solid. The product (acid form) was characterized by FT-IR, ^{1}H-NMR, and ^{13}C-NMR

spectra. The ^{1}H-NMR and ^{13}C-NMR spectra have been presented in **Figure 2.2.9** and **Figure 2.2.10**, respectively.

The sodium salt of the acid was prepared by drop wise addition of aqueous $NaHCO_3$ (1.2 eq.) solution to a solution of the acid (1 eq.) in THF over a period of 15 min with continuous stirring at room temperature. The mixture immediately turned turbid, but became clear during the course of the reaction. After stirring for 12 h, THF was evaporated, leaving colorless slurry in the RB flask. The mass was freeze-dried to remove the water and the product was then dissolved in $CHCl_3$ to remove unreacted $NaHCO_3$. The desired pure product was thus obtained with ~ 80% yield.

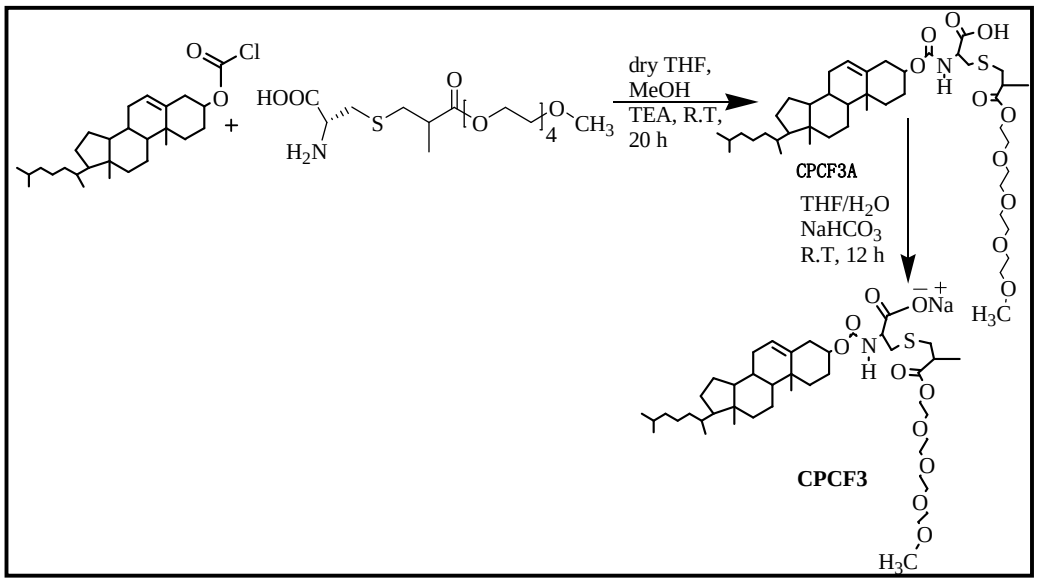

Scheme 2.2.5 General synthetic scheme for CPCF3 and CPCF11 molecules.

2.2.5.1 Chemical identification of CPCF3 and CPCF11

MW: 811.8 (CPCF3A) and 1633.8 (CPCF11A), **State:** colorless viscous semi-solid, **Yield:** 80-85%, **FTIR (KBr, cm^{-1}):** 3501 (broad, carboxylic acid O-H stretch), 3423 (strong, N-H stretch), 2945 (sp2 C-H stretch), 2901 and 2862 (sp3 C-H stretch), 1728 (carboxylic acid C=O stretch), 1695 (NH(C=O) O stretch), 1519 (N-H bend), 1256,

1218, 1076, and 1038 (C-O stretches); **^{1}H-NMR (CDCl3, 400 MHz):** δ (ppm) 5.377 (olefinic ***H*** cholestanyl, d, 1H), 5.170 (N***H***COO, d, 1H), 4.516 (cholestanyl C***H***O(CO), s, 1H), 4.388 (CH_3C***H***COOH, t, 1H), 2.312 (cholestanyl C$\boldsymbol{H}_2$, d, 2H), 1.014 (cholestanyl C$\boldsymbol{H}_3$, s, 3H), 0.916 (cholestanyl C$\boldsymbol{H}_3$, d, 3H), 0.869 (cholestanyl CH(C$\boldsymbol{H}_3$)$_2$, d, 6H), 0.680 (cholestanyl C$\boldsymbol{H}_3$, s, 3H), 1.254 (COCH*C*$\boldsymbol{H}_3$, t, 3H), 2.868 (COOHCH*C*$\boldsymbol{H}_2$, d, 2H), 3.043 (S*C*$\boldsymbol{H}_2$-CH, d, 2H), 3.203 (SCH_2*C*$\boldsymbol{H}$CO, m, 1H), 3.381 (O*C*$\boldsymbol{H}_3$, s, 3H), 3.558 (CO-OCH_2*C*$\boldsymbol{H}_2$, t, 2H), 3.661 (long chain glycolic *C*$\boldsymbol{H}_2$, m, 18H for CPCF3 and 108H for CPCF11), 3.729 (OCH_3 *C*$\boldsymbol{H}_2CH_2$, t, 2H), 3.795(NH_2*C*$\boldsymbol{H}CH_2$, t, 1H), 4.351 (CO-O*C*$\boldsymbol{H}_2$-CH_2, dd, 2H); **^{13}C-NMR (CDCl3, 400 MHz):** δ (ppm) 174.78 (***C***OOCH2), 171.95 (***C***OOH), 155.49 (NH***C***OO), 139.51 (–***C*** =CH), 122.52 (–C=***C***H), 49.90 (***C***H), 68.7, 67.3, 66.1, 61.5 (ether ***C***H_2), 55.7 (O***C***H_3), 51.4 (N***C***H CH_2) 37.7 (SCH_2***C***H), 32.2 (S***C***H_2CH), 30.3 (S***C***$H_2CH_2NH_2$), 29 (***C***$\boldsymbol{H}_2$*C*$\boldsymbol{H}_2$*C*$\boldsymbol{H}_2$*C*$\boldsymbol{H}_2$), 13.9 (***C***H_3).

MW: 833.8 (CPCF3) and 1655.8 (CPCF11), **State:** white sticky solid, **Yield:** 80-85%. **^{1}H-NMR** and **^{13}C-NMR** are as same like the acid form only ***C***OO^{-} comes at 173.23.

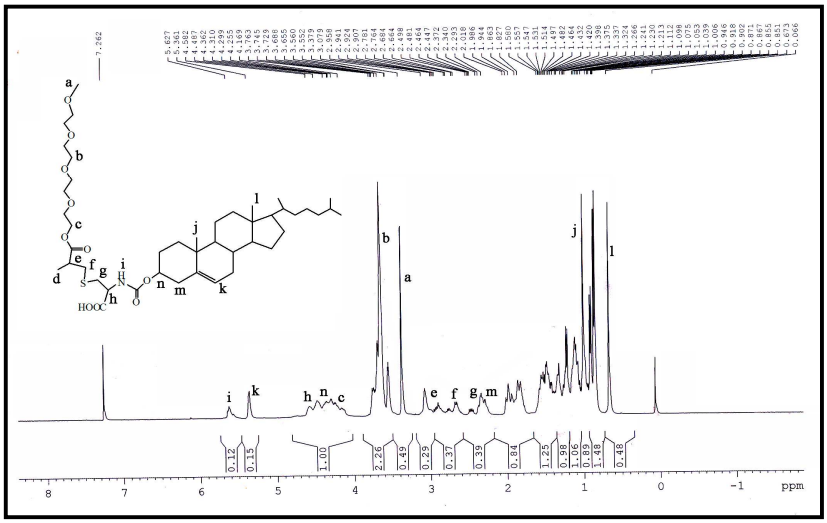

Figure 2.2.9 ^{1}H-NMR spectrum of CPCF3 (acid form) in $CDCl_3$.

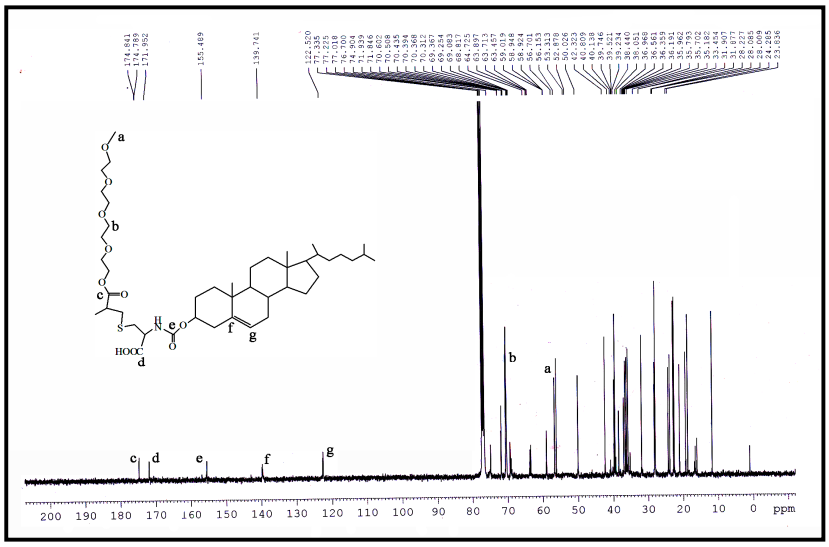

Figure 2.2.10 ^{13}C-NMR spectrum of CPCF3 (acid form) in $CDCl_3$.

2.2.6 Synthesis of poly(ethylene glycol)-di-(propionyl cysteine) (PEGDPC)

The zwitterionic bolaamphiphile PEGDPC was synthesized by the Michael addition reaction of L-cysteine with poly(ethylene glycol) diacrylate according to the method reported earlier by our group following **Scheme 2.2.6**. Briefly, poly(ethylene glycol) diacrylate (1 eq.) was reacted with L-cysteine (2.2 eq.) in methanol at room temperature for 6 h in presence of TEA. The product was obtained as white solid after evaporation of the solvent. To remove unreacted materials, the solid compound was dissolved in water and then reprecipitated by adding dry acetone. Thus the compound was separated as white plate-like solid. The chemical structure of the compound was determined by FTIR, ^{1}H-NMR, and ^{13}C-NMR spectroscopy. Representative ^{1}H-NMR (**Figure 2.2.11**), and ^{13}C-NMR (**Figure 2.2.12**) spectra of PEGDPC are presented below.

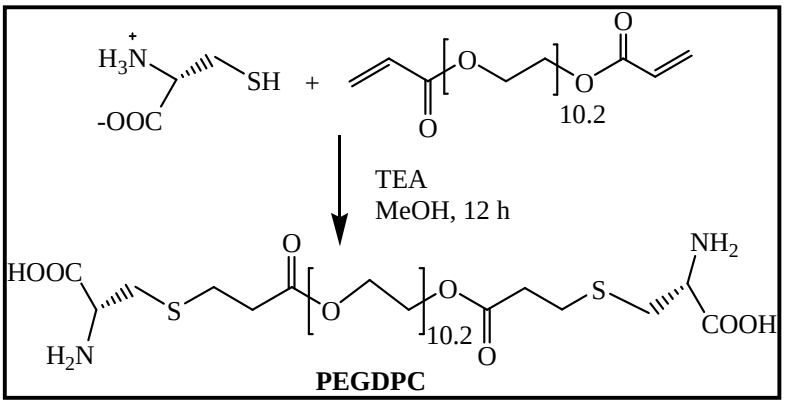

Scheme 2.2.6 Synthetic scheme for PEGDPC molecule.

2.2.6.1 Chemical identification of PEGDPC

MW: 817.32, **State:** white solid (small plate-like structure), ***mp*** 210 ^{o}C, **Yield** ~ 80%, **FTIR (KBr, cm^{-1}):** The broad band centered at 3456 cm^{-1}corresponds to O-H stretching for hydrogen-bonded COOH group. Absence of double bond is confirmed by absence of C-H stretching around 3000 cm^{-1}. Absence of the characteristic band of S-H stretch around 2550 cm^{-1} confirms the absence of S-H. Strong peaks near 1742 cm^{-1} and 1727 cm^{-1} show the presence of C=O stretches of ester and carboxylic acid group, respectively. The absorption peak at 674 cm^{-1} indicates the presence of C-S bond. **^{1}H-NMR (D_2O, 600 MHz):** δ (ppm) 2.689 (SCH_2-C***H$_2$***CO, d, 2H), 2.803 (SC***H$_2$***-CH_2CO, d, 2H), 3.068 (SC***H$_2$***CH, dd, 2H), 3.647 (long chain glycolic C***H$_2$***, m), 3.717 (CO-OCH_2-C***H$_2$***, t, 2H), 3.860 (SCH_2C***H***, d, 1H), 4.235 (CO-OC***H$_2$***-CH_2, dd, 2H). **^{13}C-NMR (D_2O, 1% DMSO, 600 MHz):** δ (ppm) 174.25 (***C***$OOCH_2$), 172.63 (***C***OO^-), 69.55, 68.40, 64.05 (ether ***C***H_2), 61.06 (CO-OCH_2***C***H_2), 60.32 (CO-O***C***H_2CH_2), 52.67 (SCH_2***C***H), 33.87 (SCH_2***C***H_2), 32.06 (S***C***H_2CH), 26.29 (S***C***H_2 CH_2COO).

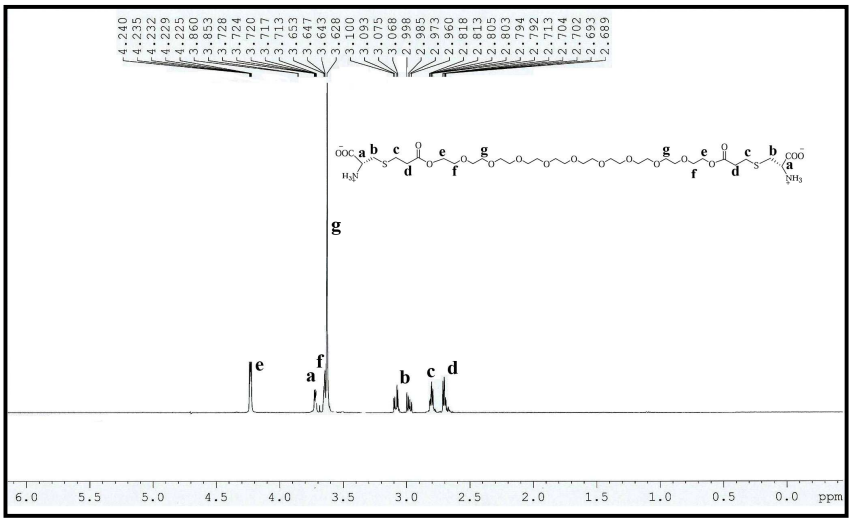

Figure 2.2.11 ^{1}H-NMR spectrum of PEGDPC in D_2O solvent.

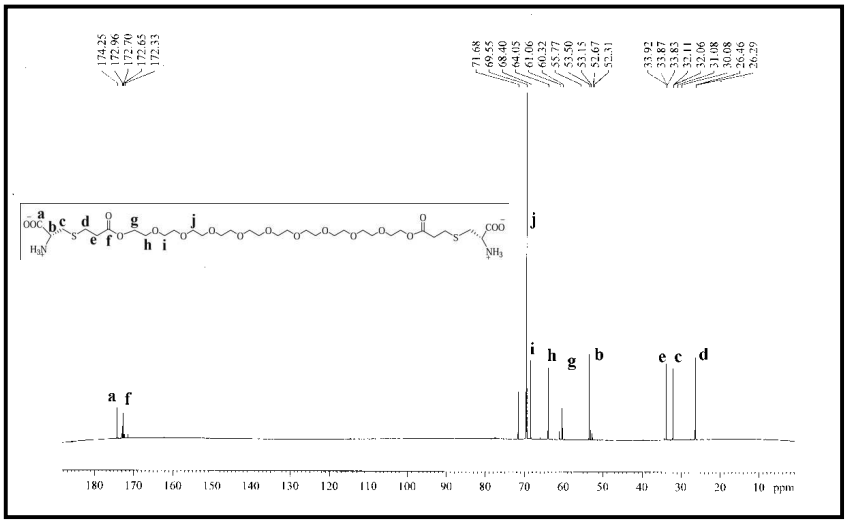

Figure 2.2.12 ^{13}C-NMR spectrum of PEGDPC in D_2O solvent.

2.2.7 Synthesis of poly(ethylene glycol)-di-mercaptoethyl–{N,N-diethyl, (propyl sulfonate)} (PEGDMS)

A mixure of 2-(diethylamino) ethanethiol hydrochloride (2 eq) and DBU (5 eq) dissolved in dry methanol and the mixture was stirred for 30 minutes. Then poly(ethylene glycol) diacrylate (1eq) was added and the mixture was stirred at room temperature for further 24

h under nitrogen atmosphere. After completion of the reaction the solvent was evaporated in a rotavapour. The residue was dissolved in EA and washed with pH = 10.0 buffer solution successively. The organic layer was dried with anhydrous $MgSO_4$ and after removal of $MgSO_4$ evaporated to dryness. The compound thus obtained was dissolved again in DCE. The 1, 3-propane sultone (2 eq) was then added and reaction mixture was stirred for 20 h at 40 °C under nitrogen atmosphere. Next the solvent was evaporated and the residue was washed with PE and was stored in vacuum desiccator. The chemical structure of the resulting compound was identified by ^{1}H- and ^{13}C-NMR spectra as shown in **Figure 2.2.13** and **Figure 2.2.14**, respectively.

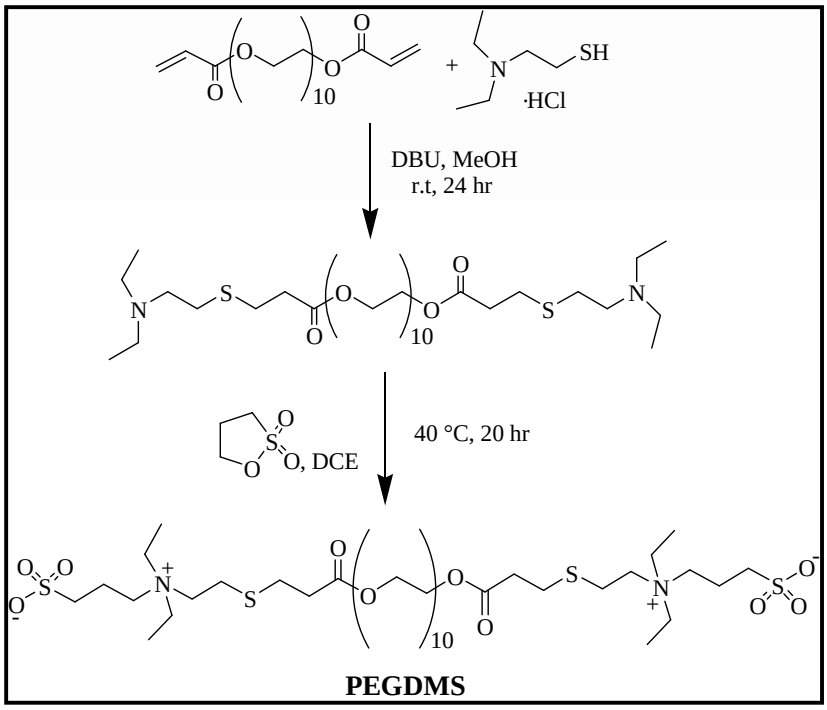

Scheme 2.2.7 Synthetic scheme of PEGDMS.

2.2.7.1 Chemical identification of PEGDMS

PEGDMS (step 1). MW: 783.32, **State:** liquid, **Yield:** 81%, **FTIR (KBr, cm^{-1}):** Absence of double bond is confirmed by absence of C-H stretching at 3000 cm^{-1} and no band at 2565 cm^{-1} confirms absence of SH stretching. Peak at 1740 cm^{-1} shows presence

of C=O stretching of ester group and 635 cm^{-1} show presence of CS stretching. **^{1}H-NMR ($CDCl_3$, 600 MHz):** δ (ppm) 1.20 (NCH_2CH_3, t, 3H), 2.050(NCH_2CH_3, m, 2H), 2.301 (NCH_2CH_2S, t, 2H), 2.532 (SCH_2CH_2CO, d, 2H), 2.677 (NCH_2CH_2S, t, 2H), 2.869 (SCH_2CH_2CO, d, 2H), 3.462 ($COOCH_2CH_2O$, t, 2H), 3.651 (long chain glycolic CH_2, m, 12H), 4.445 ($COOCH_2CH_2O$, t, 2H). **^{13}C-NMR ($CDCl_3$, 600 MHz):** δ (*ppm*) 171.257 ($COOCH_2$), 70.414, 70.556, 70.643, 70.679 (ether CH_2), 61.77 ($COOCH_2CH_2O$), 47.090 (NCH_2CH_3), 46.941 (NCH_2CH_2S), 32.215 ($COCH2CH_2S$), 29.084 (SCH_2CH_2CO), 27.157 (NCH_2CH_2S), 11.8 (NCH_2CH_3).

PEGDMS (step 2). MW: 1027.6, **State:** Viscous liquid, **Yield** 52%, **^{1}H-NMR (CD_3OD, 600 MHz):** δ (ppm) 1.367 (NCH_2CH_3, t, 12H), 2.02 ($NCH_2CH_2CH_2SO_3$, m, 4H), 2.68 (SCH_2CH_2CO, d, 4H), 2.721 (NCH_2CH_2S, t, 4H), 2.82 (SCH_2CH_2CO, t, 4H), 2.926 ($NCH_2CH_2CH_2SO_3$, t, 4H), 2.960 (NCH_2CH_3, m, 8H), 3.408 ($NCH_2CH_2CH_2SO_3$, t, 4H), 3.502 ($COOCH_2CH_2O$, t, 4H),), 3.572 (NCH_2CH_2S, t, 4H), 3.662 (long chain glycolic CH_2, m, 16H), 4.448 ($COOCH_2CH_2O$, t, 4H). **^{13}C-NMR (CD_3OD, 100 MHz):** δ (ppm) 172.65 ($COOCH_2$), 72.27, 70.16, 69.31, 68.76 (ether CH_2), 60.83 (NCH_2CH_2S), 59.16 ($NCH_2CH_2CH_2SO_3$), 56.79 (NCH_2CH_3), 47.17 ($NCH_2CH_2CH_2SO_3$), 34.29 (SCH_2CH_2CO), 27.49 (NCH_2CH_2S), 25.01 (SCH_2CH_2CO), 17.9 ($NCH_2CH_2CH_2SO_3$), 7.8 (NCH_2CH_3).

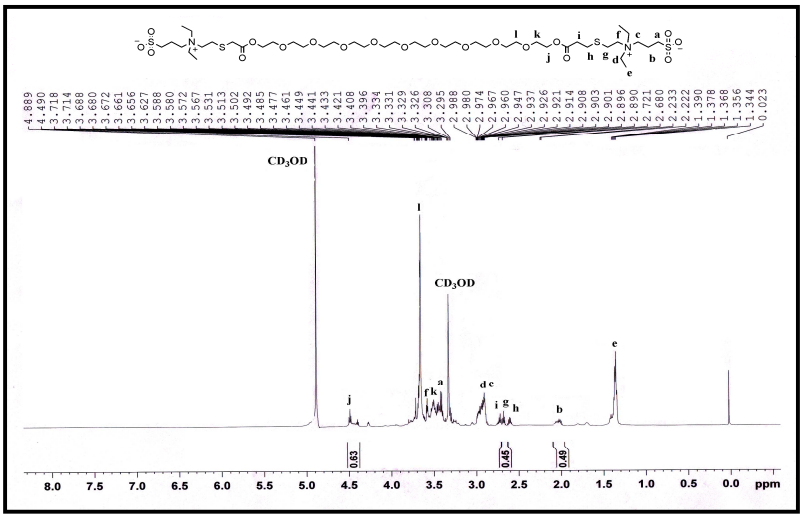

Figure 2.2.13 ^{1}H-NMR spectrum of PEGDMS in CD_3OD solvent.

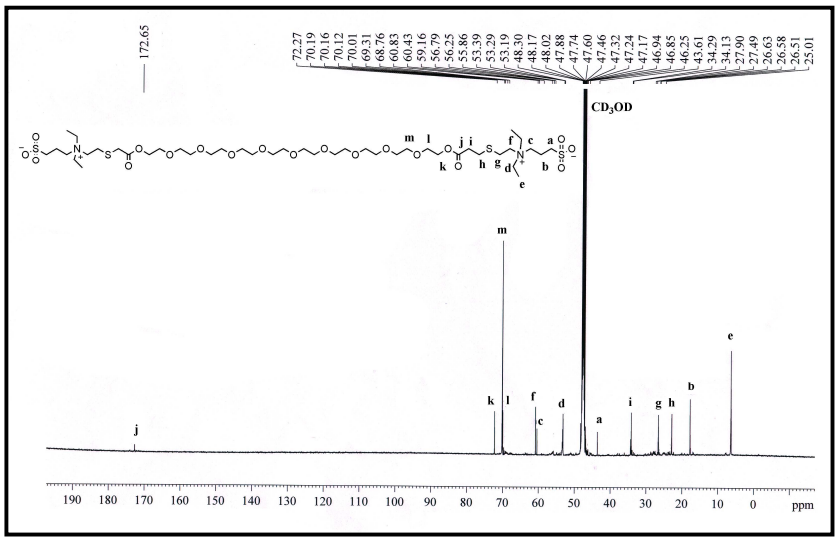

Figure 2.2.14 ^{13}C-NMR spectrum of PEGDMS in CD_3OD solvent.

2.3 Methods

2.3.1 General instrumentation

The elemental analysis was carried out with a Perkin Elmer 2400 Series II CHNS/O analyzer. Melting point was determined by an Instind (Kolkata) melting point apparatus using open capillaries. The measurements of optical rotations were performed with a JASCO (Model P-1020) digital polarimeter. The ^{1}H-NMR and ^{13}C-NMR spectra were recorded on an AVANCE DAX-400 (Bruker, Sweden) 400 MHz and 600 MHz NMR spectrometer using TMS (tetramethyl silane) or acetonitrile as internal standard. Two dimensional (2D NOESY) ^{1}H-NMR spectra were recorded on a Bruker (600 MHz) NMR spectrometer in D_2O solvent. The Fourier transform infrared (FTIR) spectra were recorded with a Perkin-Elmer (model 883 IR) spectrometer. For solid samples, KBr pellet was used as solvent. In case of aqueous solution, a thin layer of solution of the compound was placed between zinc selenide plates. The background spectrum of the pure solvent was subtracted from the raw data using the instrumental software to obtain solvent-corrected

FTIR spectrum. UV-vis absorption spectra were recorded on a Shimadzu (Model UV-2450) UV-vis spectrophotometer using a quartz cell with a path length of 1 cm. Solvent correction was done for all measurements. A digital pH meter (Model pH 5652, EC India Ltd, Kolkata) was used for pH measurements using a glass electrode. All measurements were done at room temperature (~25 ^{o}C) unless otherwise mentioned.

2.3.2 Surface tension (ST) measurements

Surface tension (γ mNm^{-1}) was measured through an automated Surface Tensiometer (model 3S, GBX, France) using the Du Nuöy ring detachment method. A platinum-iridium ring was carefully cleaned with 50% (v/v) ethanol-HCl mixture and finally with distilled water. The ring was burnt in oxidizing flame prior to use for ST measurements. The instrument was calibrated and checked by measuring the ST of distilled water. A stock solution of surfactant was made either in buffer solution or in double distilled water. An aliquot of this solution was transferred to the teflon beaker containing a known volume of buffer solution or (water) and placed within a thermostating vessel holder controlled at 25 ^{o}C by a water circulating bath. The solution was gently stirred and allowed to equilibrate for 5 minutes by setting the timer equipped with the machine. Then γ value was measured by the instrument and recorded through a software (Balance 3S). For each measurement, at least three readings were taken and the mean γ value was recorded.

2.3.3 Steady-state fluorescence measurements

The fluorescence spectra of NPN and DPH probes were recorded on a Perkin Elmer LS-55 luminescence spectrometer equipped with a temperature-controlled cell holder. A SPEX Fluorolog-3 (FL3-11, USA) spectrophotometer was used to measure fluorescence emission spectra of Py. For fluorescence measurements surfactant solutions of required concentrations were prepared in pH 7.0 buffer and were equilibrated for about 30 min prior to measurement. The final probe concentration (Py and DPH) were kept at 1 μM. Py solutions were excited at 335 nm, and emission spectra were recorded in the wavelength range of 350-500 nm using excitation and emission slit widths of 3 and 1 nm, respectively. For fluorescence titration using NPN probe, a saturated solution of NPN in pH 7.0 buffer was used. NPN solutions were excited at 340 nm, and the emission spectra were

measured using excitation slit width of 2.5 nm and emission slit width of 2.5−10 nm, depending on the sample concentration. The temperature of the cuvette holder was controlled by a Thermo Neslab RTE-7 circulating bath. All spectra of Py and NPN were blank subtracted and were corrected for lamp intensity variation during measurement.

2.3.4 Steady-state fluorescence anisotropy measurements

Steady-state fluorescence anisotropy (*r*) of DPH was measured by the Perkin Elmer LS-55luminescence spectrometer equipped with a polarization accessory that uses the L-format instrumental configuration. A Thermo Neslab RTE-7 circulating bath was used for temperature control of the magnetically stirred cuvette holder. The anisotropy was calculated employing the equation: [5]

$$r = (I_{VV} - GI_{VH}) / (I_{VV} + 2GI_{VH}) \quad (2.1)$$

where I_{VV} and I_{VH} are the fluorescence intensities when the emission polarizer is oriented parallel and perpendicular, respectively to the excitation polarizer, and G (= I_{HV}/I_{HH}) is the instrumental grating factor. The software supplied by the manufacturer automatically determined the G factor and *r*. In all measurements, the *r* value was recorded over an integration time of 10 s and an average of five readings was accepted as the *r* value. A stock solution of 1 mM DPH was prepared in super dry methanol. The final concentration of DPH was maintained at 1 μM by addition of an aliquot of the stock solution. Variable temperature anisotropy measurements were performed in the temperature range 25–75 ^{o}C. The sample was excited at 350 nm and the emission intensity was followed at 450 nm using excitation and emission slit width of 2.5 nm and 2.5–10.0 nm, respectively. A 430 nm emission cut-off filter was placed between the emission monochromator and the detector to reduce the effect of scattered and stray radiation. The fluorescence measurements started 30 min after sample preparation.

2.3.5 Time-resolved fluorescence measurements

The fluorescence lifetime (τ_f) of DPH probe was measured by an Optical Building Blocks Corporation Easylife instrument that uses a 380 nm diode laser. The time-resolved decay

curves were analyzed either by single exponential or bi-exponential iterative fitting program provided by the manufacturer. Best fitting was judged by the χ^2 value (0.8–1.2) and by the randomness of the residual plot.

The rigidity (or fluidity) of the microenvironments of self-assemblies is indicated by the microviscosity (η_m) around the probe molecule. The fluorescence lifetimes of DPH probe (τ_f) in the surfactant solution provides useful information about η_m [6,7]. Thus, η_m was calculated from the Debye-Stokes-Einstein relation [7]:

$$\eta_m = kT\tau_R/v_h \qquad (2.2)$$

where v_h is the hydrodynamic volume (313 Å^3) [5] of the DPH molecule and τ_R is its rotational correlation time. The τ_R value was calculated from Perrin's equation [7]:

$$\tau_R = \tau_f (r_o/r - 1)^{-1} \qquad (2.3)$$

where r_o (= 0.362) [8] is the steady-state fluorescence anisotropy of DPH in a highly viscous solvent and τ_f is the measured fluorescence lifetime of DPH in surfactant solution.

2.3.6 Dynamic light scattering measurements

The dynamic light scattering (DLS) measuremens were performed using a Zetasizer Nano ZS (Malvem Instrument Lab, Malvern, U. K.) optical system equipped with a He-Ne laser operated at 4 mW at λ_o = 633 nm, and a digital correlator. The scattering intensity was measured at a 173^o (back scattering) angle to the incident beam. Surfactant solutions were prepared in desired buffer solution. The solution was filtered through a Millipore Millex syringe filter (0.22 μm) directly into the scattering cell. Prior to each measurement, the scattering cell was rinsed several times with the filtered solution. The DLS measurements started 5-10 minutes after the sample solutions were placed in the DLS optical system to allow the sample to equilibrate at the bath temperature. For all light scattering measurements, the temperature was 25 ^{o}C. The average decay rate (Γ) of the electric field autocorrelation function, $g^1(\tau)$, was estimated using the cumulants method [9]. The apparent diffusion coefficient (D_{app}) of the aggregates was obtained from the relation, $\Gamma = D_{app}q^2$ (q being magnitude of the scattering vector given by q =

$[4\pi n\sin(\theta/2)]/\lambda$, where n and λ are the refractive index of the solvent and the wavelength of the laser light, respectively). The corresponding hydrodynamic diameter (d_H), of the particles was calculated using Stokes-Einstein relationship:

$$D_{app} = \frac{k_B T}{3\pi\eta d_H} \tag{2.4}$$

where k_B is the Boltzmann constant, T is the absolute temperature, and η is the viscosity of the solvent.

2.3.7 Transmission electron microscopy (TEM)

High resolution transmission electron micrographs (HRTEM) of the specimens were taken on HRTEM (JEOL-JEM 2100, Japan) operating at 200 kV. For sample preparation, 4 μL of surfactant solution was dropped on to a 400 mesh carbon-coated copper grid and allowed to stand for 1 min. The excess solution was carefully blotted off with a tissue paper and the specimen was air-dried. Further, the specimens were kept in vacuum desiccators until before measurement. Each measurement was repeated at least three times to check the reproducibility of the results.

For cryo-TEM measurements, specimen preparation was done in a controlled environment vitrification system (CEVS). The specimens were prepared in a chamber at 100% relative humidity (Cryoplunge 3) in order to keep surfactant concentration fixed. A 5 μL of the sample solution was applied via the side port of the Vitrobot^{TM} directly onto the carbon-coated side of the formvar carbon-coated perforated polymer film TEM grid held by tweezers inside the chamber by using a pipette. The excess solution was then blotted with a filter paper wrapped on a metal trip to thin the drop into a film the thickness of which was less than 300 nm. The grid was then plunged into liquid ethane at its freezing point (–170°C) cooled by liquid nitrogen. Until imaging, the vitrified specimens were kept under liquid nitrogen and the temperature was maintained at –170°C. Cryo-specimens were imaged in JEM-2100F transmission electron microscope (JEOL, Japan), operated at 200 kV, using a Gatan 655 (Gatan, Pleasanton, CA, USA) cooling holder and

transfer station. Specimens were equilibrated in the microscope below –170°C. To nullify the electron beam radiation damage the specimens were investigated under low-dose intensity. The images were recorded at a nominal under focus to enhance phase-contrast and were acquired digitally by CCD cameras (Gatan, Pleasanton, CA, USA), using the Digital Micrograph software (Gatan UK, Abingdon, UK).

2.3.8 Atomic force microscopy (AFM)

AFM measurements were conducted by a Nanoscope IIIA from Digital Instruments (USA) in tapping mode under ambient conditions. For the sample preparation, one drop of surfactant solution was placed on a freshly cleaved mica surface. The specimen was then dried overnight in air.

2.3.9 Gauss view analysis

To get the energy-minimized monomeric structures of the amphiphile in solution state (water) the theoretical study was performed. All the calculations were done using the Gaussian 09 software package [10]. The geometries were optimized with the spin-unrestricted formalism using B3LYP functional and 3–21G* basis set. The polarized continuum model (PCM) was used to model the solvation effects of water.

2.3.10 Isothermal titration calorimetry (ITC)

A microcalorimeter of Microcal iTC_{200}, (made in U.S.A) was used for thermometric measurements. In a microsyringe of capacity 40 μL, concentrated stock surfactant solution was taken and added in multiple stages to pH 7.0 buffer kept in the calorimeter cell of capacity 200 μL under constant stirring conditions, and the stepwise thermograms of the heats of dilution of the surfactant solution were recorded. The stirring speed was fixed at 400 rpm and Milli-Q water was taken in the reference cell. Each run was duplicated to check reproducibility. Enthalpy calculations were performed with the help of ITC software provided by the manufacturer. All measurements were carried out at 25 ^{o}C.

The standard Gibbs free energy change (ΔG^{o}_{m}) value was calculated from the measured *cmc* value using the following relation: [11, 12]

$$\Delta G^{o}_{m} = (1 + \beta)\, RT \ln(a_{cmc}) \qquad (2.5)$$

where β stands for the degree of counterion binding of the surfactant molecule and is usually taken as 0.8 for anionic surfactants and 0.0 for zwitterionic surfactants [13], and a_{cmc} is the activity of the surfactant solution at *cmc*, which is numerically equal to the value of *cmc* as the solution is very dilute. The standard entropy change (ΔS^{o}_{m}) was evaluated by the Gibbs equation: [13]

$$\Delta S^{o}_{m} = (\Delta H^{o}_{m} - \Delta G^{o}_{m}) / T \qquad (2.6)$$

The spontaneity of vesicle formation is suggested by the very large negative and positive values of ΔG^{o}_{m} and ΔS^{o}_{m}, respectively.

References

[1] Rim, C.; Lahey, L. J.; Zhang, G. P. H.; Son, D. Y. Thiol-ene Reactions of 1,3,5 Triacryloylhexahydro-1,3,5-triazine (TAT): Facile Access to Functional Tripodal Thioethers. *Tetrhedron Lett.* **2009**, *50*, 745−747.

[2] Ghosh, S.; Das Mahapatra, R.; Dey, J. Thermoreversible as Well as Thermoirreversible Organogel Formation by L-Cysteine-Based Amphiphiles with Poly(ethylene glycol) Tail. *Langmuir* **2014**, *30*, 1677−1685.

[3] Roy, S.; Dey, J. Self-Organization and Microstructures of Sodium 11- Acrylamidoundecanoate in Water. *Langmuir* **2003**, *19*, 9625−9629.

[4] Bajani, D.; Dey, J. Spontaneously Formed Robust Steroidal Vesicles: Physicochemical Characterization and Interaction with HSA. *J. Phys. Chem. B.* **2014**, *118*, 4561-4570.

[5] Lakowicz, J. R. *Principles of Fluorescence Spectroscopy*; Plenum Press: New York, **1983**; p 132.

[6] Roy, S.; Mohanty, A.; Dey, J. Microviscosity of Bilayer membranes of some N-Acylamino Acid Surfactants Determined by Fluorescence Probe Method. *Chem. Phys. Lett*. **2005**, *414*, 23-27.

[7] Debye, P. *Polar Molecules*; Dover: New York, **1929**.

[8] Shinitzky, M.; Barenholz, Y. Dynamics of the Hydrocarbon Layer in Liposomes of Lecithin and Sphingomyelin Containing Dicetylphosphate. *J. Biol.Chem.* **1974**, *249*, 2652-2657.

[9] Koppel, D. E. Analysis of Macromolecular Polydispersity in Intensity Correlation Spectroscopy: The Method of Cumulants. *J. Chem. Phys.* **1972**, 57, 4814–4820.

[10] Frisch, M. J.; Trucks, G.W.; Schlegel, H. B.; Scuseria, G. E.; Robb, M. A.; Cheeseman, J. R.; Scalmani, G.; Barone, V.; Mennucci, B.; Petersson, G. A. *Gaussian 09 revision B.01, Gaussian, Inc., Wallingford, CT,* **2010**.

[11] Paula, S.; Siis, W.; Tuchtenhagen, J.; Blume, A. Thermodynamics of Micelle Formation as a Function of Temperature: A High Sensitivity Titration Calorimetry Study. *J. Phys. Chem.* **1995**, *99*, 11742-11751.

[12] Verral, R. E.; Milioto, S.; Zana, R. Ternary Water-in-oil Microemulsions Consisting of Cationic Surfactants and Aromatic Solvents. *J. Phys.Chem.***1988**, *92*, 3939−3943.

[13] Majhi, P.; Moulik, S. Energetics of Micellization: Reassessment by a High-Sensitivity Titration Microcalorimeter. *Langmuir* **1998**, *14*, 3986-3990.

Chapter 3
Vesicle Forming Amphiphiles with PEG Tail

3.1 Spontaneous Vesicle Formation by Amphiphiles with PEG as Tail and L-Cysteine as Head[1]

3.1.1 Scope of the study

PEG has been recognized as one of the most important polymers in drug delivery as it is biocompatible, flexible in nature, water soluble and shows anomalous behavior in water [1-15]. It is well known that PEGs of low molecular weight (M_n<1500) are hydrophilic [16]. The replacement of a $–CH_2–$ by oxygen (–O–) along the hydrocarbon,$–(CH_2)_n–$, chain increases its polarity, thereby favoring its interaction with water. Thus, in general, PEGs are coupled to hydrophobic molecules to develop nonionic surfactants. There are many nonionic surfactants, for example, Tween-20, Triton-X-100, etc. in which the PEG acts as the polar head group are well known [17-24]. However, there are only a couple of report on the surface activity and self-assembly formation of low-molecular-weight amphiphiles consisting of PEG as tail and an ionic group as head [25-26]. But till date there is no report on zwitterionic amphiphile with PEG as hydrophobic tail. Zwitterionic amphiphiles are attractive candidates for delivery vehicles of pharmaceutical formulations and also for industrial applications owing to their ability to form different assemblies at different pH. Additionally, they show better wettability, good biocompatibility, and excellent synergism with other surfactants [27-29].

Therefore, in this work, two zwitterionic molecules, $mPEG_{300}$-Cys and $mPEG_{1100}$-Cys (see **Figure 3.1.1** for structures) bearing mPEG tail of different chain lengths and L-cysteine as the polar head group were synthesized. These zwitterionic amphiphiles with mPEG tail have advantage in that they have pH-sensitive head group. Again, as both mPEG and L-cysteine are biocompatible and eco-friendly, their self-assembled structures in aqueous medium can have potential applications in drug delivery. Moreover, the synthetic procedure is also very easy. The objective of this work is to investigate if this new class of molecules is surface active and exhibits any micellization in water. Thus, a

[1] *Langmuir* **2014**, *30*, 13516−13524.

number of methods including surface tension, fluorescence and NMR spectroscopy, isothermal titration calorimetry (ITC), dynamic light scattering (DLS) and transmission electron microscopy (TEM) were employed to study surface activity and self-assembly properties of these molecules in water at room temperature.

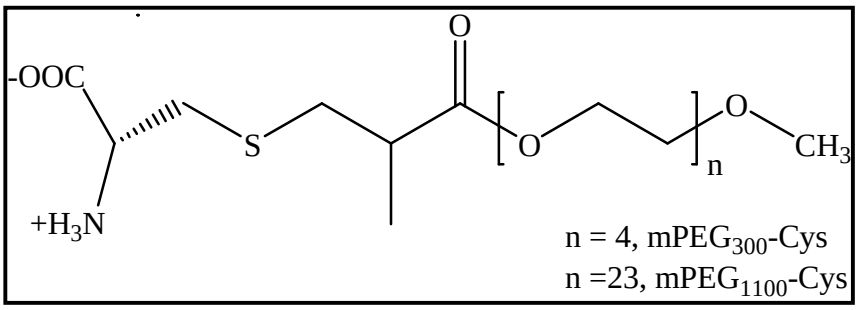

Figure 3.1.1 Molecular structures of $mPEG_{300}$-Cys and $mPEG_{1100}$-Cys.

3.1.2 Surface activity

To determine the surface activity the surface tension (γ mN m^{-1}) of phosphate buffer (pH 7.0) containing different concentrations (C_s) of $mPEG_{300}$-Cys (or $mPEG_{1100}$-Cys) molecules was measured. As shown by the plots of γ versus $\log C_s$ (**Figure 3.1.2**), the γ value of water decreases gradually with the increase of C_s, suggesting spontaneous adsorption of the molecules at the air/water interface. This means that both $mPEG_{300}$-Cys and $mPEG_{1100}$-Cys molecules are amphiphilic in nature. The surface activity of the amphiphiles was found to be quite similar to that of PEG (Mw ~ 300), which exhibits γ_{min} value (52 mN m^{-1}) at about 0.4 w% (~13 mM) [30, 31]. However, the surface activity as measured by pC_{20} (= $-\log C_{20}$, where C_{20} is the molar concentration of the surfactant required to reduce γ of water by 20 units) value, of $mPEG_{300}$-Cys (2.28) and $mPEG_{1100}$-Cys (2.36) is much less in comparison to conventional surfactants with hydrocarbon tail [32-34]. This can be attributed to the hydrophilic nature of the mPEG chain. In fact, the mPEG-containing zwitterionic molecules behave like long chain fatty alcohols in water and have amphiphilic character. The surface behavior of the fatty alcohols in water has been discussed elaborately by Posner et al [35].

Interestingly, unlike conventional surfactants, the ST plots of the molecules do not show any break followed by a plateau in the investigated concentration range. This can be attributed to ionization state of the molecules in phosphate buffer at pH 7.0. In aqueous medium, depending on the pH, both $mPEG_{300}$-Cys and $mPEG_{1100}$-Cys are expected to be present in the zwitterionic, cationic or anionic form. The pK_a values of the cation-zwitterion and zwitterion-anion equilibria obtained from fluorescence probe studies discussed below are respectively 3.9 and 9.3 for $mPEG_{300}$-Cys and 5.1 and 9.1 for $mPEG_{1100}$-Cys. The pI values thus obtained are ~6.6 for $mPEG_{300}$-Cys and ~7.1 for $mPEG_{1100}$-Cys. This means that in pH 7.0 buffer, the molecules exist mainly in the zwitterionic form. Since the mPEG chain is considered to be polar, the polarity difference between the mPEG tail and zwitterionic amino acid head group is small compared to that of hydrocarbon chain-containing surfactants.

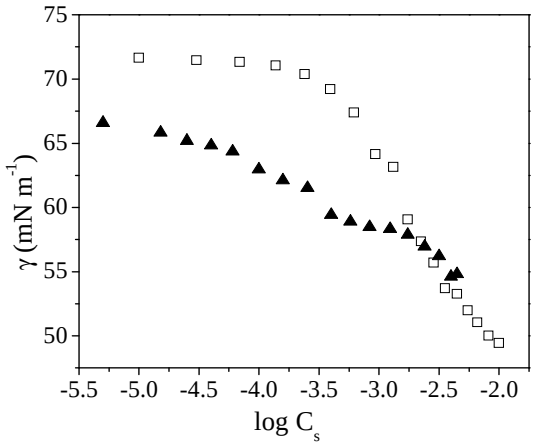

Figure 3.1.2 Plots of surface tension (γ mN m^{-1}) versus log C_s in pH 7.0 at 25 ^oC: (□) $mPEG_{300}$-Cys, (▲) $mPEG_{1100}$-Cys.

3.1.3 Self-assembly behavior

Steady-state fluorescence measurements were performed using different extrinsic probe molecules, such as NPN, C153, Py, and DPH (i) to investigate self-assembly formation, (ii) to determine *cmc* value of the amphiphile, and (iii) to estimate micropolarity and

microviscosity of the aggregates [36]. These probes are non-polar molecules and they preferentially get solubilized in the hydrophobic microdomains of surfactant aggregates. The fluorescence spectra of these probes are sensitive to the microenvironment around them and thus can indicate microstructure formation and provide insight into the surfactant self-assemblies in water.

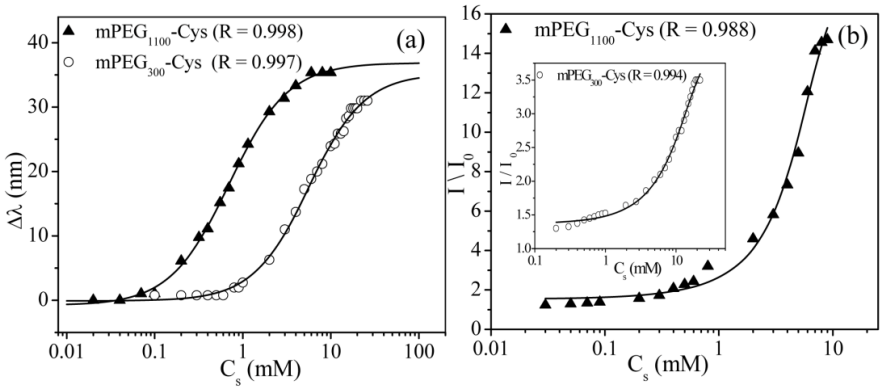

Figure 3.1.3 Plots of (a) spectral shift ($\Delta\lambda$) and (b) relative fluorescence intensity (I/I_o) of NPN as a function of C_s in pH 7.0 at 25 ^oC; inset of figure (b) shows variation of I/I_o with C_s of $mPEG_{300}$–Cys.

NPN has been extensively used as an efficient fluorescence probe as it exhibits a large-spectral shift along with a huge intensity enhancement upon incorporation into the hydrophobic microdomains of surfactant aggregates [37]. In the presence of $mPEG_{300}$-Cys (or $mPEG_{1100}$-Cys) amphiphile the emission maximum (λ_{max}) of NPN exhibits a blue shift of ~30-35 nm and a huge increase of emission intensity relative to that in pH 7.0 buffer. The large blue shift of the emission maxima of NPN suggest its encapsulation within nonpolar environment of the aggregates formed by the amphiphiles in aqueous buffered solution. In addition, the enhancement of the fluorescence intensity indicates that the microenvironment of NPN probe is viscous in nature. The variation of the spectral shift, $\Delta\lambda$ [$\Delta\lambda = \lambda_{max(water)} - \lambda_{max(surfactant)}$] of NPN probe with C_s has been shown in **Figure 3.1.3(a)**. The corresponding plots of relative fluorescence intensity, I/I_o (where I_o and I are the fluorescence intensities at λ = 460 nm in pure buffer and in the presence of

amphiphile, respectively) versus C_s have been depicted in **Figure 3.1.3(b)**. The sigmoid plot corresponding to a two-state transition clearly suggests existence of equilibrium between surfactant monomers and aggregates. The *cmc* values (**Table 3.1.1**) obtained from the onset of rise of the curves (indicated by arrows) are 1.0 mM and 0.2 mM for $mPEG_{300}$-Cys and $mPEG_{1100}$-Cys, respectively. It can be mentioned here that due to the longer mPEG chain the *cmc* value of $mPEG_{1100}$-Cys is less than that of $mPEG_{300}$-Cys [26]. Thus the behavior is very similar to those of surfactants with hydrocarbon (HC) tail.

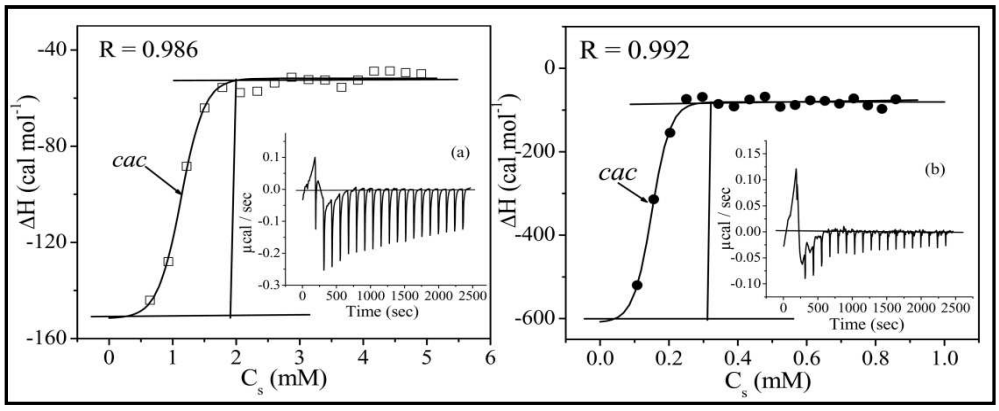

Figure 3.1.4 Plots of variation of change in enthalpy (ΔH) versus C_s at 25 ^oC: (□) $mPEG_{300}$-Cys and (●) $mPEG_{1100}$-Cys; inset: thermogram of the respective titration.

3.1.4 Thermodynamics of self-assembly formation

The self-organization of surfactants in solution is an important and well-studied thermodynamically favorable physicochemical phenomenon [38]. Although there are a number of methods to determine *cmc*, the thermometric titration method has a distinction as it can estimate both *cmc* and energetics of surfactant self-organization from a stepwise addition mode, which provides an excellent process to evaluate all the thermodynamic parameters in a single run. Generally, thermodynamic parameters are calculated to conjecture the mechanism of self-assembly formation. In the present study, the thermodynamic parameters were determined by ITC for both $mPEG_{300}$-Cys and

$mPEG_{1100}$-Cys at 25 ^{o}C using different stock concentrations. However, measurements using lower surfactant stock concentration (5 mM of $mPEG_{300}$-Cys and 2 mM of $mPEG_{1100}$-Cys) failed to give reproducible results. The thermograms obtained by using higher surfactant stock concentration (30 mM of $mPEG_{300}$-Cys and 5 mM of $mPEG_{1100}$-Cys) are presented as insets of **Figure 3.1.4**. The plots show a sigmoid increase of enthalpy with the increase of C_s. The thermodynamic parameters obtained from the plots are included in **Table 3.1.1**. The *cmc* values of $mPEG_{300}$-Cys (~1.1 mM) and $mPEG_{1100}$-Cys (~0.2 mM) were obtained from the inflection point of the respective plot. The *cmc* values thus obtained are close to the corresponding value obtained by fluorometric titration. The *cmc* values thus obtained correspond to the respective zwitterionic form of the amphiphiles.

Table 3.1.1 Critical micelle concentration (*cmc*), standard Gibbs free energy change (ΔG^{o}_{m}), standard enthalpy change (ΔH^{o}_{m}) and standard entropy change (ΔS^{o}_{m}) of the aggregate formation in aqueous buffered solution (pH 7.0) by $mPEG_{300}$-Cys and $mPEG_{1100}$-Cys at 25 ^{o}C.

Surfactant	*cmc* (mM)		ΔG^{o}_{m} (kJ mol^{-1})	ΔH^{o}_{m} (kJ mol^{-1})	ΔS^{o}_{m} (J K^{-1} mol^{-1})	$T\Delta S^{o}_{m}$ (kJ mol^{-1})
	Fluorescence (NPN)	ITC				
$mPEG_{300}$-Cys	1.0 (± 0.07)	1.13 (± 0.02)	−16.81	0.42 (± 0.1)	57.82	17.23
$mPEG_{1100}$-Cys	0.2 (± 0.03)	0.15 (± 0.03)	−21.81	2.20 (± 0.15)	80.57	24.01

The ΔH^{o}_{m} value was obtained by subtracting the initial enthalpy from the final enthalpy indicated by the vertical line in each figure. Basically, enthalpy level between nonmicellar and micellar regions gives a measure of the enthalpy change of micellization [39]. For both the amphiphiles, the self-assembly formation is observed to be endothermic, which is emphasized by the positive ΔH^{o}_{m} values. The spontaneity of

aggregate formation is expressed from the very large negative values of ΔG^{o}_{m} and the very large positive values of ΔS^{o}_{m}. Thus $T\Delta S^{o}_{m}$ value for both the amphiphiles is found to be much larger than that of the corresponding ΔH^{o}_{m} value, which clearly suggests that the spontaneous aggregate formation is an entropy-driven process. The essence of entropy-driven process is the hydrophobic interaction [40, 41]. The release of water molecules around the mPEG tails during aggregation contributes to the entropy rise favoring the process. This means that the aggregation processes of both $mPEG_{300}$-Cys and $mPEG_{1100}$-Cys are similar to most hydrocarbon surfactants. In other words, the mPEG chain behaves like hydrocarbon tail and imparts amphiphilic character to the molecules.

3.1.5 Nuclear Overhauser effect spectroscopy (NOESY)

For further evidence of interaction of mPEG chains and to know the mutual spatial arrangement of surfactant molecules in the aggregated state, two-dimensional (2D) NOESY ^{1}H-NMR measurement was carried out using $mPEG_{300}$-Cys amphiphile as a representative example. Such experiments have been shown to give excellent insights into the nature of interactions in the self-assembly process in a number of aggregated systems [42-45]. Therefore, 2D NOESY spectrum $mPEG_{300}$-Cys in micellar state (**Figure 3.1.5**) was measured taking D_2O as reference solvent. In case of aggregated state (5 mM in D_2O), in addition to diagonal interactions number of cross interactions can be observed. The interactions between d ↔ i, h ↔ e, f and g ↔ e, f protons imply the intermolecular interactions of the head groups of surfactant monomers (**Figure 3.1.5**). Further the interactions among a ↔ c, b, h and b ↔ h, a, i, d protons suggest the strong interactions among the PEG chains of the monomers. That these cross-peaks might originate from intramolecular interactions can be unambiguously ruled out as these key cross-peaks are absent in the 2D NOESY spectrum (not shown) of the non-micellar state of $mPEG_{300}$-Cys (0.5 mM in D_2O). Thus, the intermolecular origin of these key NOE contacts is undisputable. These cross peaks signify the spatial proximity of the surfactant in the self-assembled aggregates. All the above interactions can well be interpreted if the monomers self-organize themselves to form bilayer vesicles.

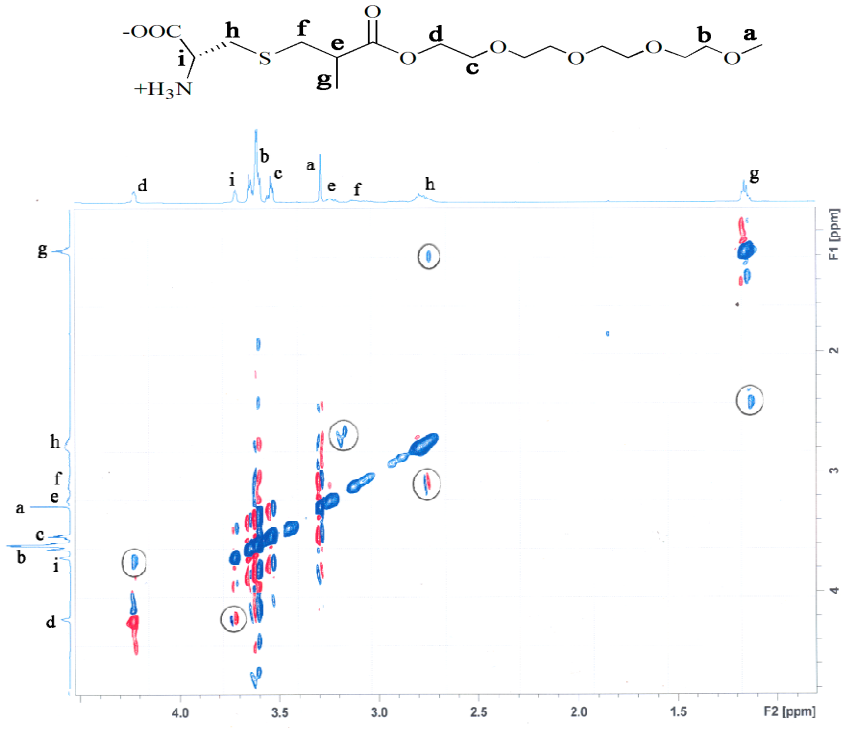

Figure 3.1.5 2D NOESY ^{1}H-NMR spectrum of mPEG$_{300}$-Cys (5 mM) in D_2O solvent.

3.1.6 Micropolarity and microviscosity

The fluorescent probe C153 has been employed to study micropolarity of surfactant aggregates and solvation dynamics in microheterogeneous systems [46]. Thus the microenvironment formed by the mPEG chains of the amphiphiles was investigated by use of C153 probe. C153 is relatively more polar in comparison to NPN and therefore is solubilized in relatively polar environments of the aggregates. Consequently, the variation of $\Delta\lambda$ with the increase in C_s is small compared to that obtained with NPN probe. The fluorescence emission spectra of C153 measured in pH 7.0 buffer in the absence and in the presence of different concentrations of the amphiphiles have been depicted in (**Figure 3.1.6(a)**). The large increase in intensity as well as the spectral shift indicates aggregate formation by both amphiphile in water.

In addition to providing information regarding aggregate formation, the spectral shift of C153 can also correlate the microenvironment of the self-assembly with solvents of different polarity [47]. Micropolarity of the self-assemblies can thus be evaluated by the emission frequency ($\bar{\upsilon}_{em}$) of C153. Micropolarity is expressed in terms of solvent polarity scale (π^*) [45]. The relationship between $\bar{\upsilon}_{em}$ and π^* is given by equation 3.1.

$$\bar{\upsilon}_{em} = 21.217 - 3.505\pi^* \qquad (3.1)$$

The π^* values thus obtained are 0.74 for $mPEG_{300}$-Cys and 0.62 for $mPEG_{1100}$-Cys, which suggest that the polarities of the microenvironments of C153 probe are comparable to those of propionaldehyde ($\pi^* = 0.71$) and acetone ($\pi^* = 0.62$), respectively [47].

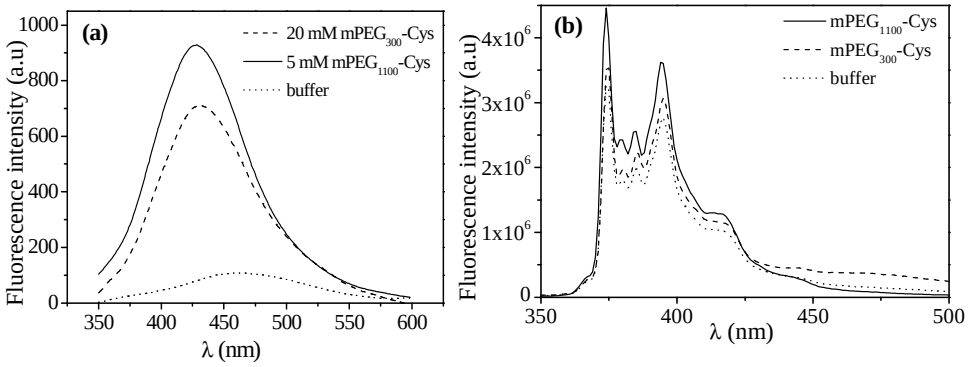

Figure 3.1.6 Representative fluorescence emission spectra of (a) C153 in the presence of 20 mM $mPEG_{300}$-Cys and 5 mM $mPEG_{1100}$-Cys, and (b) Py in pH 7.0 buffer and in the presence of 5 mM $mPEG_{300}$-Cys and 2 mM $mPEG_{1100}$-Cys showing I_1 and I_3 bands.

The microenvironment of the self-assemblies was also investigated by use of Py probe, particularly to evaluate the micropolarity of the aggregates. The solvent dependence of vibronic band intensities in Py fluorescence has captured great attention in the literature. The intensities of the various vibronic bands were found to depend strongly on the solvent polarity [48]. More specifically, the ratio (I_1/I_3) of the intensities of the first (I_1, 372 nm) to the third (I_3, 384 nm) vibronic bands in the fluorescence spectrum of Py is very sensitive to solvent polarity change [49].Therefore, the I_1/I_3 ratio is referred to

as micropolarity index. The polarity ratios for different organic solvents are reported by Kalyansundaram et al [48]. The fluorescence spectra of Py measured in pH 7.0 buffers in the absence and presence of $mPEG_{300}$-Cys or $mPEG_{1100}$-Cys are presented in **Figure 3.1.6(b)**. The I_1/I_3 value was found to be 1.54 for $mPEG_{300}$-Cys and 1.46 for $mPEG_{1100}$-Cys amphiphile. The measured I_1/I_3 values $mPEG_{300}$-Cys and $mPEG_{1100}$-Cys correspond to the polarity of N-Methyl formamide (I_1/I_3 = 1.56) and acetone (I_1/I_3 = 1.46), respectively [48]. This indicates that the microenvironments of the aggregates formed by the amphiphiles are more polar compared to that of long-chain hydrocarbon surfactants [33, 34]. However, the micropolarity index of the self-assemblies as obtained from the probe studies (C153 and Py) shows a good degree of agreement with each other. The results also suggest that the microenvironments of the aggregates are constituted by the mPEG chains, which is consistent with the results of 2D NMR measurements.

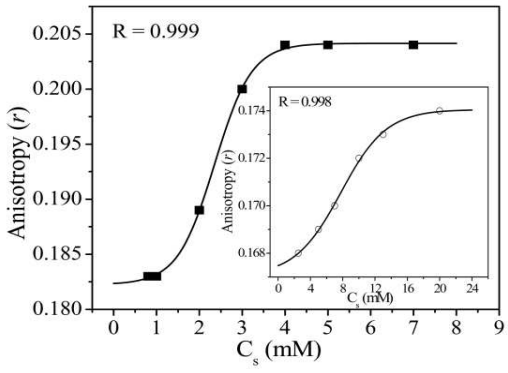

Figure 3.1.7 Plots of fluorescence anisotropy (*r*) of DPH probe versus C_s at 25 ^oC: (○) $mPEG3_{00}$-Cys, and (■) for $mPEG_{1100}$-Cys.

The steady-state fluorescence anisotropy (*r*) measurement was carried out with the help of DPH probe to further investigate the viscosity of the microenvironments of the aggregates constituted by the mPEG chains. DPH is a well-known membrane fluidity probe and its *r* value has been used as an index of membrane rigidity of liposomes (vesicles) [50, 51]. The *r* values in aqueous solutions of $mPEG_{300}$-Cys (5 mM) and $mPEG_{1100}$-Cys (2 mM) were observed to be 0.168 and 0.183, respectively. Such high *r*

values imply tight packing of mPEG chains housing the DPH probe, which is indicative of bilayer formation [52]. The concentration dependence of *r* of DPH was also studied and the results are summarized in **Figure 3.1.7**. As observed, *r* value increases with the increase of concentration of the amphiphiles reaching plateau above a particular concentration, indicating formation of more rigid microenvironments.

The rigidity of the microenvironments of the self-assemblies was also quantified by measuring microviscosity (η_m) value. The η_m value was obtained from the Debye-Stokes-Einstein relation using *r* and fluorescence lifetime (τ_f) data of DPH probe (**Table 3.1.2**). It is reported that the τ_f value of DPH in nonpolar and viscous solvents is usually greater than 4 ns [53]. Therefore, time resolved fluorescence measurements using DPH probe were carried out in solutions containing $mPEG_{300}$-Cys (15 mM) or $mPEG_{1100}$-Cys (5 mM). The experimental time-resolved intensity profiles fit well to biexponential decay function with χ^2 values in fairly accepted range (0.8 − 1.2). It is observed that the τ_f values of DPH in the presence the amphiphiles are greater than the value in pure buffer, indicating rigid microenvironment around DPH molecules. This is also suggested by the η_m values which are larger than those of micelle-forming hydrocarbon surfactants, such as SDS, DTAB, and CTAB [51]. The large η_m value for both amphiphiles is indicative of the existence of microenvironments constituted by tightly packed PEG chains. This is also consistent with the 10 to 20-fold increase in fluorescence intensity of NPN probe upon incorporation into the less polar microenvironments. This is a strong proof of formation of stable and well-packed bilayer aggregates by the amphiphiles at concentrations above *cmc.*

Table 3.1.2 Fluorescence anisotropy (*r*), fluorescence lifetime (τ_f), χ^2 and rotational correlation time (τ_R) of DPH, and microviscosity (η_m) of aggregates at 25 ^oC.

Surfactant	C_s (mM)	*r* (±0.001)	χ^2	τ_f (±0.1ns)	τ_R (ns)	η_m (mPa s)
$mPEG_{300}$-Cys	15	0.173	0.910	5.4	4.95	65
$mPEG_{1100}$-Cys	5	0.205	0.830	4.6	5.60	79

3.1.7 Size and shape of the aggregates

The mean hydrodynamic diameter (d_h) and size distribution of the self-assemblies formed by $mPEG_{300}$-Cys and $mPEG_{1100}$-Cys in pH 7.0 at 25 ^oC were measured by the DLS technique. The size distribution histograms (in % volume) for both the amphiphiles measured at two different concentrations are presented in **Figure 3.1.8**. A bimodal distribution is observed with both amphiphiles. In fact, aggregates of two different sizes with mean d_h value of ~50 nm and ~250 nm coexist in dilute aqueous solutions of both the amphphiles. The histograms also show that the mean d_h increases slightly with C_s, indicating formation of larger aggregates.

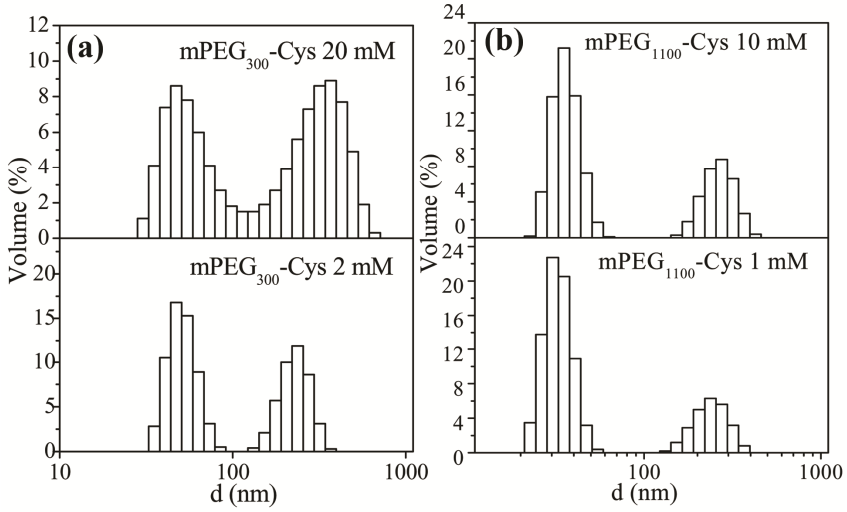

Figure 3.1.8 Size distribution histograms of (a) $mPEG_{300}$-Cys (2 mM and 20 mM) and (b) $mPEG_{1100}$-Cys (1 mM and 10 mM) in phosphate buffer of pH 7.0 at 25 ^oC.

The large bilayer aggregates formed by the amphiphiles are most likely vesicles. To confirm the shape of the aggregates HRTEM images were taken. Representative TEM images of the solutions of both amphiphiles at pH 7.0 buffer have been shown in **Figure 3.1.9(a, d)**. The micrographs clearly reveal the formation of small unilameller vesicles (SUVs) with diameters in the range of 50-300 nm. However, large unilamellar vesicles (LUVs) were also found to form in concentrated solution of the amphiphiles. The

existence of LUVs at higher concentrations as also indicated by the DLS data (**Figure 3.1.8**) can be attributed to the fusion of the SUVs. A close insight into the size and shape of the microstructures show that the vesicles have distorted spherical shape. Thus, the TEM microstructures are consistent with the findings from DLS and fluorescence studies.

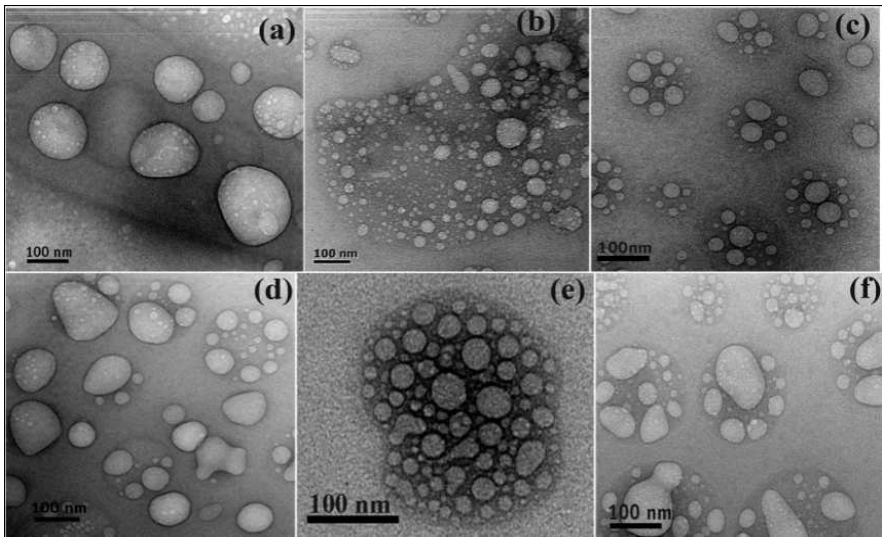

Figure 3.1.9 HRTEM images of 20 mM $mPEG_{300}$-Cys solutions at pH (a) 7.0 (b) 3.0 and (c) 12.0, and 5 mM $mPEG_{1100}$-Cys solutions at pH (d) 7.0 (e) 3.0 and (f) 12.0.

As conventional TEM measurements involve drying of the samples, the vesicular images are often criticized as artifacts. Therefore, in order to show the existence of aqueous core within the large aggregates revealed by the TEM images, encapsulation of a water-soluble dye, such as methylene blue (MB) was attempted. The encapsulation of MB into the aqueous core of vesicles was performed following a method reported elsewhere [54, 55]. For this, 67 mg of $mPEG_{300}$-Cys (to make 80 mM stock solution) with 100 μL of 2 mM MB in methanol was mixed and dried slowly in a round bottomed flask by use of a rotavapor to make a thin film. For complete evaporation of the solvent, the flask was kept overnight in desiccators. The film was then rehydrated overnight with a small amount of buffer. The rehydrated suspension was vortexed for 30 min followed by

dilution with pH 7.0 buffer to attain 0.1 mM MB (λ_{max} = 665 nm). A 2 mL volume of the resulting solution was then loaded onto a column packed with a pre-equilibrated Sephadex G-75 (25 cm height and 1.2 cm diameter) and eluted with pH 7.0 buffer. Vesicular suspension eluted right after the void volume. The filtration was carried out until free MB was gel-filtrated. The eluent was collected in 2 mL fraction each. The absorbance for all the fractions was measured at 665 nm and the data were plotted against the elution volume. The peak with low absorbance at low elution volumes correspond to the vesicle-entrapped dye molecule. It has been found that there is a small initial portion containing vesicles entrapping approximately 2.77% of the total dye followed by a large peak which was due to the unentrapped dye as shown by the chromatogram depicted in **Figure 3.1.10.** The encapsulation of MB is thus confirmed by the characteristic size exclusion chromatogram which in turn confirms existence of aqueous core within the large aggregates formed by the $mPEG_{300}$-Cys and $mPEG_{1100}$-Cys amphiphiles in pH 7 buffer.

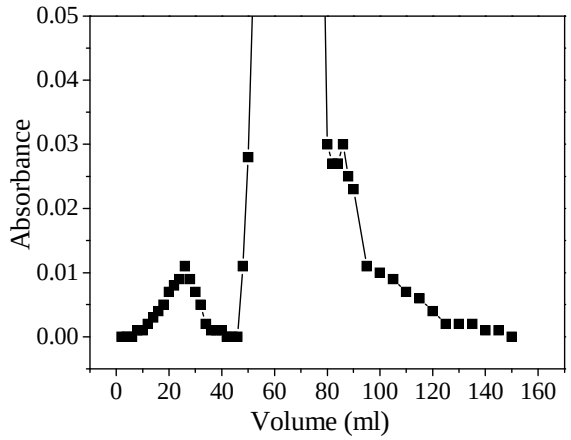

Figure 3.1.10 Gel filtration profile of the separation of the MB entrapped (small peaks) vesicle of $mPEG_{300}$-Cys from the corresponding free dye.

The results of ζ-potential measurements (**Table 3.1.3**) show that the surface charge of the vesicles is almost zero. This can be associated with the fact that the head group of the amphiphiles is zwitterionic in pH 7.0 buffer. As the vesicles are charge

neutral at pH 7.0, they have a tendency to interact with each other leading to fusion thereby increasing the size of the vesicles, especially in concentrated solution. This is supported the fact the vesicles become somewhat larger upon aging as confirmed by the change in turbidity of the surfactant solutions as discussed below.

Table 3.1.3 The ζ-potential values of $mPEG_{300}$-Cys and $mPEG_{1100}$-Cys amphiphiles at different concentrations.

Surfactant	C_S (mM)	ζ-potential (mV)
$mPEG_{300}$-Cys	5	−0.03
	20	−1.86
$mPEG_{1100}$-Cys	2	−0.08
	10	−1.11

3.1.8 Stability of the vesicles

It is well-known that the spontaneously formed surfactant self-assemblies are usually reversible organization of molecules to a higher ordered structure and their physical stability can be altered by external stimuli. The vesicle stability was therefore investigated under various physical conditions, including time, temperature, pH and salt, emphasizing the stability of spontaneously formed vesicles and their ability of encapsulation and release of drugs.

Thermal stability. Temperature is an important factor of self-assembly formation and it also affects the size and shape of aggregates [56-59]. As mentioned above, DPH is a membrane fluidity probe. Thus steady-state fluorescence anisotropy (*r*) of DPH probe was used to study the phase transition of bilayer membrane. The effect of temperature on *r* value of DPH was studied using 15 mM $mPEG_{300}$-Cys and 5 mM $mPEG_{1100}$-Cys in pH 7.0. The plots of variation of *r* as a function of temperature are shown in **Figure**

3.1.11(a). As seen from the plots, *r* value decreases with the increase of temperature, but it still lies in the vesicular range, even at 75 ^{o}C. This suggests that the PEG chains become more fluid at elevated temperatures. This is due to weakening of the hydrophobic interactions caused by the thermal motion among PEG chains. In other words, phase transition from a highly ordered gel-like bilayer state to a slightly less ordered liquid-crystalline state occurs upon increase of temperature. Thus the temperature corresponding to the inflection point of the curves was taken as the melting or phase transition temperature, T_m of the bilayer membrane. The high melting temperatures, 43 ^{o}C and 52 ^{o}C for mPEG$_{300}$-Cys and mPEG$_{1100}$-Cys, respectively, clearly suggest that the vesicles are quite stable at physiological temperature (37 ^{o}C). The existence of ULVs at higher temperatures (75 ^{o}C) is evidenced by the size distribution histogram and TEM picture **(Figure 3.1.11(b))** of 15 mM mPEG$_{300}$-Cys solution. Since the T_m value of the vesicles formed by for mPEG$_{300}$-Cys is ~43 ^{o}C, they can be used in temperature-triggered systemic delivery of drugs.

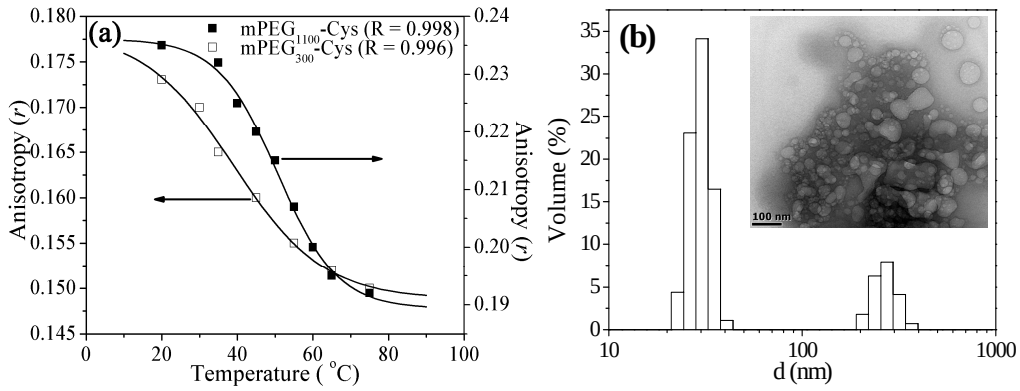

Figure 3.1.11 Plots showing (a) variation of fluorescence anisotropy (*r*) of DPH with temperature; (b) size distribution histogram of mPEG$_{300}$-Cys (15 mM) in pH 7.0 at 75 ^{o}C (inset: TEM micrographs of 15 mM mPEG$_{300}$-Cys solution at 75 ^{o}C).

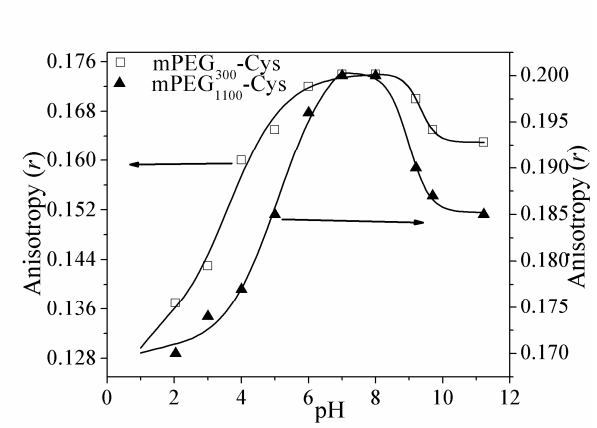

Figure 3.1.12 Plots showing variation of fluorescence anisotropy (*r*) of DPH with pH.

pH effect. The pH-sensitive vesicles have shown potential importance in controlled drug release, as the pH around any damaged tissue differs from that of normal tissue. The variation of solution pH can show a predominant change in the bilayer structure and hence can affect the stability of vesicles formed by amphiphilic molecules with ionizable head group [60-62]. Since the amphiphiles under study are zwitterionic at neutral pH, the stability of the vesicles was studied by varying pH of the medium. The pH-stability measurement was carried out by monitoring the *r* value of DPH probe. The pH of the solution containing fixed concentration of $mPEG_{300}$-Cys (20 mM) and $mPEG_{1100}$-Cys (5 mM) was varied from 2 to 12 at 25 ^{o}C. Each solution was incubated for 30 min prior to the measurement. The plots in **Figure 3.1.12** show the variation of *r* value of DPH with the change in pH of the aqueous solution. It is observed that the *r* value decreases with the decrease in solution pH and the vesicles show maximum stability between pH 6.5 to 8. The bilayer membrane of vesicular aggregates becomes less rigid at lower as well as higher pH as a result of weakening of the packing of the mPEG chains as consequence of electrostatic repulsion between anionic or cationic head groups produced due to ionization of the amphiphiles in water. However, in both lower and higher pH, the *r* value lies in the vesicular range, suggesting existence of cationic and anionic vesicles, respectively. The apparent pK_a values for the proton transfer equilibria were estimated

from the pH variation profiles of *r* and were found to be ~3.9 and ~9.3 for $mPEG_{300}$-Cys, and ~5.1 and ~9.1 for $mPEG_{1100}$-Cys. Thus the pI values calculated from the respective pK_a values are ~6.6 and ~7.1 for $mPEG_{300}$-Cys and $mPEG_{1100}$-Cys, respectively. This clearly indicates that at pH 7.0 both the surfactants remain in the zwitterionic form as shown in **Figure 3.1.1**.

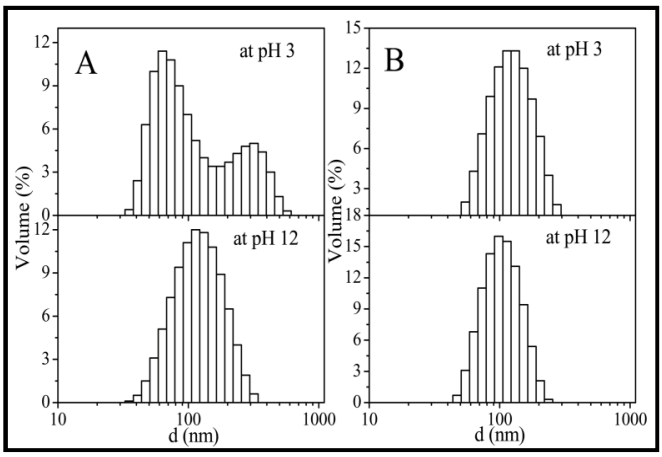

Figure 3.1.13 Hydrodynamic size distributions in aqueous solutions of (A) 20 mM $mPEG_{300}$-Cys and (B) 5 mM $mPEG_{1100}$-Cys at different pH at 25 ^{o}C.

The size distributions (**Figure 3.1.13**) histograms of the vesicles in the acidic and basic pH solution of the amphiphiles were also measured in order to examine if there is any structural change of the vesicles. The mean d_h value of the vesicles formed in acidic (pH 3) and basic (pH 12) pH are observed to be smaller than that of the corresponding zwitterionic vesicles (**Figure 3.1.8**) at neutral pH. However, they are much larger than that of normal micelles which have d_h value usually in the range of 3 to 5 nm [63]. The existence of ULVs in acidic as well as in basic pH is further confirmed by the respective TEM image depicted in **Figure 3.1.9.**

Aging effect. Vesicle stability with respect to time was also monitored by measuring turbidity (τ) of the vesicle solutions of the amphiphiles. The turbidity of a colloidal solution is mainly caused by the scattering of light by the vesicular aggregates

and the scattering intensity depends on the size and population of vesicles. For this turbidity of 6 mM $mPEG_{300}$-Cys and 2.5 mM $mPEG_{1100}$-Cys in pH 7.0 buffer was monitored at 450 nm over a period of 30 days. The plots in **Figure 3.1.14(a)** shows only a slight increase in turbidity for both the vesicle solutions in the initial aging interval and thereafter remains constant at the equilibrium value (~30%) for about 30 days. The formation and growth of the vesicles cause the initial increase of the turbidity while the subsequent constant turbidity indicates high evolution stability with aging time. This is also supported by the size distribution profiles **(Figure 3.1.14(b))**. Thus for both the systems, the vesicles solutions are found to be fairly stable and hence have greater shelf-life. It is important to note that the vesicle solutions of both amphiphiles at pH 3.0 and 12.0 do not exhibit any change of turbidity on storage for a month. This is expected as the vesicles in these solutions are ionic in character they repel each other thus preventing any inter-vesicle interaction that enlarges the vesicle.

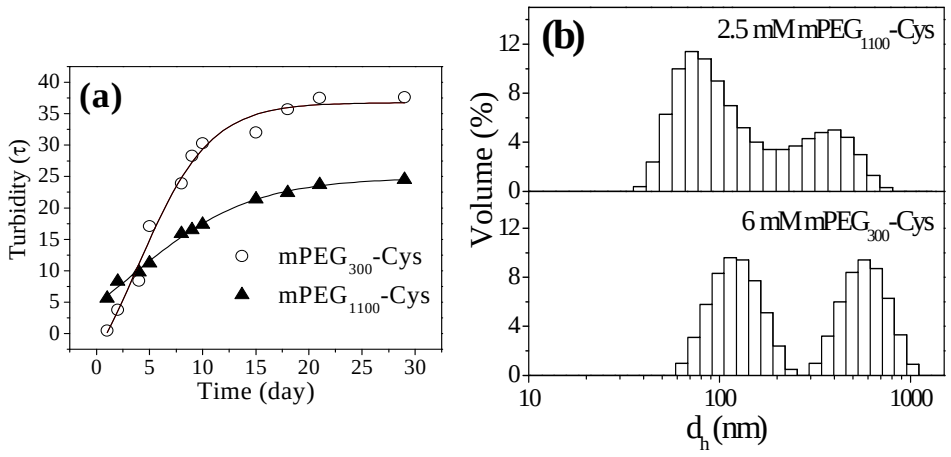

Figure 3.1.14 Plots of (a) turbidity, τ (= 100 − %T) versus aging time, and (b) size distribution histograms of the surfactant solutions at pH 7.0 and 25 ^{o}C after 20 days of sample preparation.

3.1.9 Dye encapsulation and release kinetics

The Cal (λ_{max} = 465 nm) dye was encapsulated within the inner aqueous pool of the vesicles formed by 80 mM $mPEG_{300}$-Cys at pH 7.0 in the same way as described above

for MB dye. The Cal concentration taken was 20 μM. The free unentrapped Cal was separated from the entrapped Cal by using the same gel filtration column chromatography as described for MB. The encapsulation was confirmed by the characteristic fluorescence spectrum of the dye (not shown).

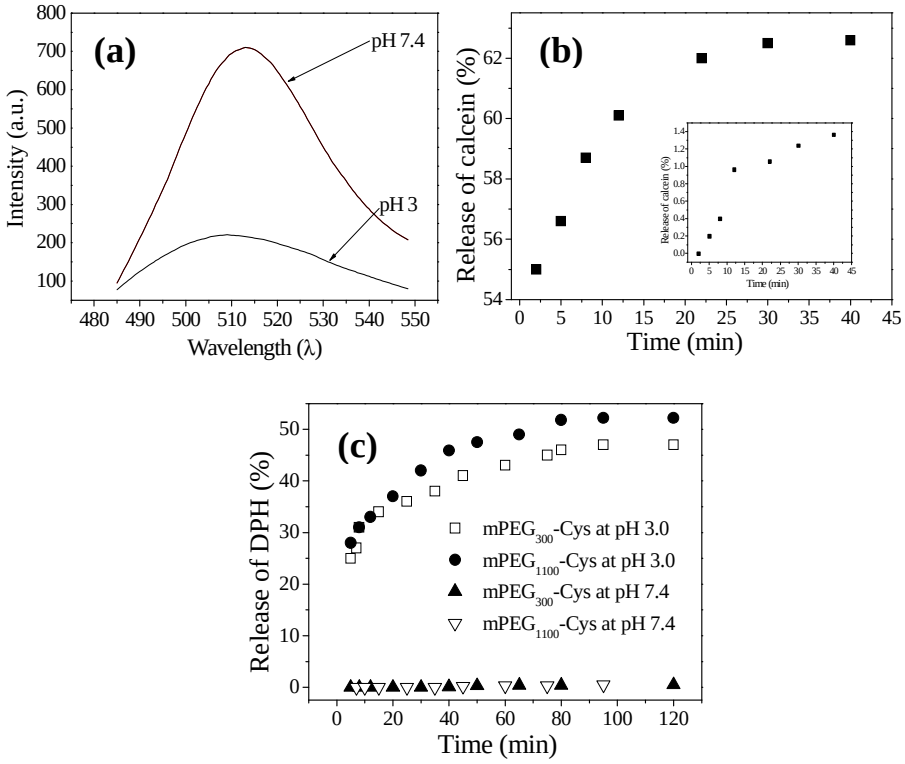

Figure 3.1.15 (a) fluorescence spectra of vesicle-entrapped Cal in 80 mM $mPEG_{300}$-Cys at pH 7.4 and 3.0, (b) plot of % release of Cal as a function of time (min) from vesicles of $mPEG_{300}$-Cys at pH 3.0 and 37 ^{o}C (inset: Cal release profile at pH 7.4), and (c) plots showing variation of % release of DPH with time (min) at 37 ^{o}C in pH 3.0 and pH 7.4.

The pH-triggered release of the Cal from the inner aqueous compartment was performed at pH 3.0 by monitoring its steady-state fluorescence intensity at 514 nm at different time intervals. The % release of the drug was calculated from the relative fluorescence intensity (I/I_o), where I and I_o are the fluorescence intensities of Cal at any

time *t* and at the start of the experiment (i.e. at pH 7.0 buffer), respectively, using equation:

$$\% \text{ Release} = (1 - I/I_o) \times 100\% \qquad (3.2)$$

It can be observed that when an aliquot of dilute HCl solution was added (to attain pH 3.0) to the vesicular solutions containing Cal, the fluorescence intensity of the dye decreased immediately by a large extent (**Figure 3.1.15(a)**). This can be attributed to the burst release (~55%) of the dye molecules due to the large change in permeability of the bilayer membrane as a result of change of ionization behavior of the amphiphile in acidic pH. Another factor which also plays an important role is the acid hydrolysis of the ester linkage which causes the release of dye molecules by disrupting the vesicle membrane. Consequently, after the rapid initial decrease the fluorescence intensity of the dye decreased slowly with time. The fluorescence spectra were therefore recorded at different time intervals following the burst release. From the representative release profile (**Figure 3.1.15(b)**) for $mPEG_{300}$-Cys amphiphile it is obvious that following burst release a slow release occurs reaching plateau at about 62%. The slow release can be attributed to the disruption of the vesicle membrane due to acid catalyzed hydrolysis of the ester linkages. The release of the model drug Cal at pH 7.4 was also carried out as a control study. The release profile is included in **Figure 3.1.15(b)**. It can be observed that there is almost zero percent release of the dye within the experimental time period of 2 h.

Similar experiment using hydrophobic dye DPH was also carried out in both surfactant solutions. The release profiles are shown in **Figure 3.1.15(c)**. In this case also a burst release (35%) followed by a slow release (up to 50%) was observed. Also the control experiment at pH 7.4 did not show any release during the period of experiment. The results of these experiments show that the self-assembled vesicular structures of $mPEG_{300}$-Cys and $mPEG_{1100}$-Cys amphiphiles can be used as efficient sustained release delivery systems in pharmaceutical applications. A schematic of encapsulation of Cal and DPH in the vesicles at pH 7.4 and release of the dyes at lower pH has been shown in **Figure 3.1.16**.

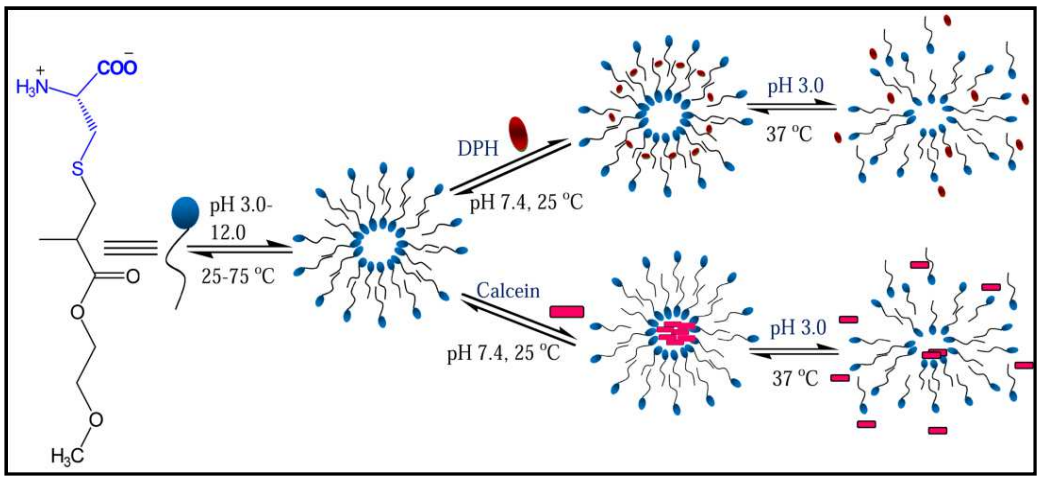

Figure 3.1.16 Schematic representation of encapsulation of drug molecules (DPH and Cal) at pH 7.4 and their release at pH 3.0.

3.1.10 Summary

In summary, two novel L-cysteine-derived zwitterionic amphiphiles with mPEG tail of different chain lengths were developed and characterized. The surface activity and aggregation behavior of the amphiphiles were thoroughly examined in pH 7.0 buffer at 25 ^{o}C. The amphiphiles were found to be weakly surface-active. The results of surface tension, fluorescence, DLS and TEM measurements suggest that the amphiphiles have strong tendency to self-organize spontaneously to form stable ULVs in dilute as well as in concentrated solutions. Unlike amino acid-based hydrocarbon surfactants, a relatively polar but rigid bilayer membrane is observed to form by the mPEG chains. The thermodynamics of vesicle formation was observed to be very similar to conventional hydrocarbon surfactants. The large positive values of ΔS^{o}_{m} indicate that the driving force behind the spontaneous vesicle formation is hydrophobic interaction. The vesicles were observed to be stable in the temperature range 20–75 ^{o}C over a long period of time. The amphiphiles exhibit vesicle formation in acidic as well as in basic pH. The vesicles were found to be capable of encapsulating hydrophilic as well as hydrophobic dyes. However, the vesicles are sensitive to temperature and pH change and therefore can find potential application as efficient sustained drug delivery vehicles in pharmaceutical industry.

3.2 Self-assembly Study of Mesna Based Single PEG-Tailed Anionic Amphiphiles[2]

3.2.1 Scope of the study

In the preceding section, two zwitterionic amphiphiles bearing PEG tail were developed [64]. Herein, the zwitterionic cysteine head group of the amphiphiles has been replaced by mesna (sodium-2-mercapto ethane sulfonate) to introduce the anionic head group. Mesna has been used here as it possesses lots of biological applications. Mesna is a synthetic sulfur compound that produces mucolysis by disrupting the disulfide bonds of the mucous polypeptide chains [65, 66]. It is also used in a variety of disorders, such as a mucolytic agent for pulmonary disorders and as a protective agent against the toxicity of some chemotherapeutic agents. It can also be used during ear surgeries, such as cholesteatoma or atelectatic ears, to make the dissection of tissue layers simpler [67]. As mesna is polar in nature, it prevents its passage out of the vascular bed into cells. This results in efficient renal clearance and avoids any adverse impact on the cytotoxic effects of ifosfamide. As the small molecule has widespread applications in cancer therapy and also in other medicinal field, mesna was chosen as the head group to develop the target amphiphilic molecules.

However, for designing an effective drug delivery vehicle, the major issue is that the system must be biocompatible as well as bioavailable. Considering the chemical and biological uses of PEG in surfactant chemistry, drug delivery systems, it was covalently linked to mesna to synthesize two novel molecules, PEGS1 and PEGS2 (see **Figure 3.2.1** for structures). The PEGS1 and PEGS2 molecules consist of mPEG tail of different lengths and mesna as the anionic head group. The major objective is to examine if there is any micellization by PEGS1 and PEGS2 in water at room temperature. The surface activity and aggregation behavior of these molecules were investigated in phosphate buffer (20 mM, pH 7.0) at 25 ^{o}C. The surface activity of the amphiphiles was determined by measuring surface tension in water. The self-assembly formation was studied by

[2] *J. Colloid Interf. Sci*. **2015**, *451*, 53–62.

fluorescent probe techniques. The thermodynamics of the self-assembly process was also studied by ITC through measurements of the ΔG^{o}_{m}, ΔH^{o}_{m} and ΔS^{o}_{m} of micellization. DLS was used to determine the mean hydrodynamic diameters of the aggregates. The morphology of the aggregates was investigated by use of TEM.

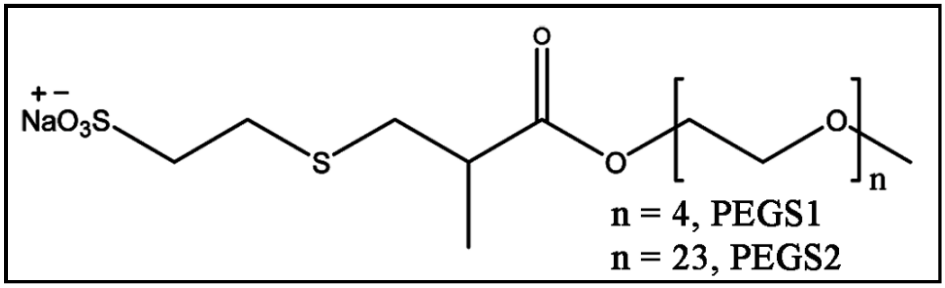

Figure 3.2.1 Chemical structures of the amphiphiles.

3.2.2 Surface activity

The plots of variation of surface tension with the concentration (C_s) of the amphiphiles at room temperature are depicted in **Figure 3.2.2**. As observed the γ value decreases gradually with the increase of concentration, suggesting spontaneous adsorption of the amphiphiles at the air/water interface. The pC_{20} value that measures the adsorption efficiency of PS1 (2.28) and PS2 (2.36) is much less in comparison to conventional hydrocarbon chain surfactants [33, 34]. However, the pC_{20} values are found to be less closely equal to the corresponding zwitterionic amphiphile $mPEG_{300}$-Cys and $mPEG_{1100}$-Cys [64]. That is both PEGS1 and PEGS2 amphiphiles are weakly surface active which can be attributed to the overall polar nature of the molecules.

The features of both plots are similar and no saturation point was found in the ST plot even at the highest concentration (30 mM) employed. However, a small dip in the ST plot (indicated by the downward arrow) at a much lower concentration (~2.0 mM for PEGS1 and ~1.0 mM for PEGS2) is observed with both the amphiphiles. The ST plot in the low concentration region has been separately shown as an inset of the corresponding figure. The concentration corresponding to the dip in the ST plot can be taken as the *cmc*

of the amphihile. Thus these amphiphiles seem to behave like long-chain fatty alcohols in which the polarity difference between the hydrocarbon chain and –OH is quite small. At low concentrations the favorable H-bonding interaction between the PEG chain and water molecules causes the PEG tail to lie flat at the air/water interface, resulting in a small decrease of γ value. Gradual increase of monomer concentration forces the PEG chains to become straight in the interface making more room for other molecules and thus reduces the γ value.

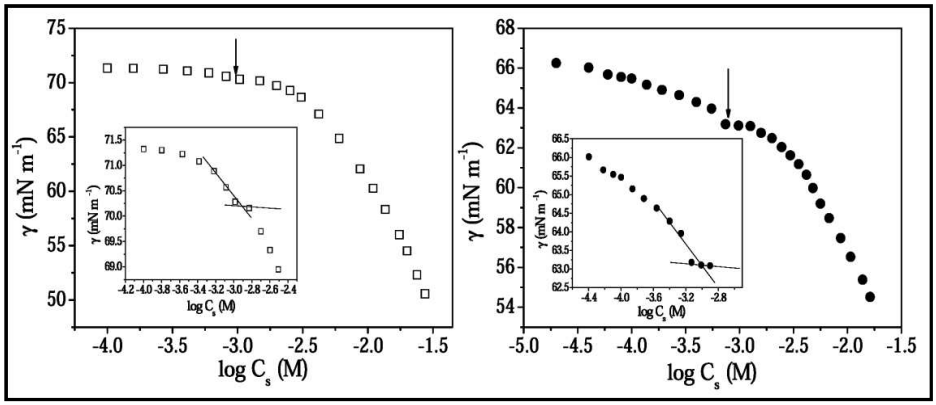

Figure 3.2.2 Plots of variation of surface tension (γ mNm^{-1}) as a function of logC_s in phosphate buffer 20 mM, pH 7.0 at 25 ^{o}C: (□) PEGS1, and (●) PEGS2; inset: γ versus logC_s plot in the lower concentration range of the amphiphiles.

3.2.3 Critical micelle concentration (*cmc*)

To determine *cmc* of the amphiphiles, fluorescence titration using NPN probe was carried out at room temperature. As in the cases of mPEG$_{300}$-Cys and mPEG$_{1100}$-Cys a large spectral blue shift of the emission maximum (λ_{max}) along with a huge rise of fluorescence intensity in presence of amphiphiles above a critical concentration was observed, indicating formation of aggregates with hydrophobic core. The spectral shifts ($\Delta\lambda$) are plotted as a function of C_s as shown in **Figure 3.2.3(a)**. The *cmc* was determined from the onset of rise of the curve as indicated by the arrow. The *cmc* thus obtained are 2.0 and 0.9 mM for PEGS1 and PEGS2, respectively, and are closely similar to those obtained

from ST plots. The lower value of *cmc* of PEGS2 must be due to its longer PEG chain. The higher value of Δλ for PEGS1 can be attributed to the more rigid microenvironment formation by the PEGS1 molecules after reaching *cmc*.

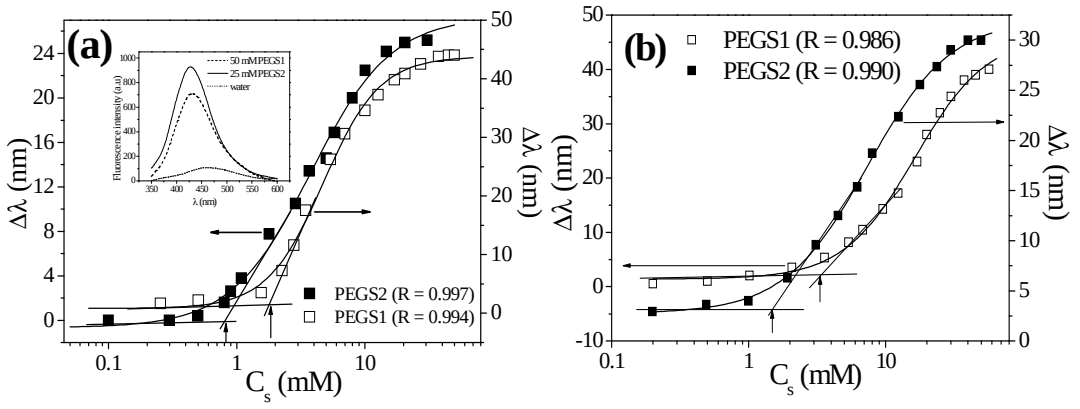

Figure 3.2.3 (a) Plots showing variation of Δλ (= λ_{water} - $\lambda_{surfactant}$) of NPN in phosphate buffer (20 mM, pH 7.0) with the change in C_s at 25 ^oC (inset: representative fluorescence emission spectra of NPN in pH 7.0 buffer containing 0 and 25 mM PEGS2 and 50 mM PEGS1); (b) variation of Δλ of NPN probe with C_s in salt-free water at 25 ^oC: (□) PEGS1 and (■) PEGS2.

The self-assembly formation in salt-free pure water was also studied by fluorescence measurements using NPN probe. The intensity rise along with spectral shift confirmed self-assembly formation in water. The *cmc* values as obtained from the plots in **Figure 3.2.3(b)** are 3.0 and 1.9 mM for PEGS1 and PEGS2, respectively. The *cmc* values, however, are greater than the corresponding value in phosphate buffer (**Table 3.2.2**). This is due to higher ionic strength of the buffer solution that reduces ionic repulsion between head groups decreasing the *cmc* value of the anionic amphiphiles.

3.2.4 Thermodynamics of self-assembly formation

The aggregation behavior of the amphiphiles containing sulfonate head group was further studied by ITC method at 25 ^oC to evaluate the energy of micellization. The *cmc* values and the respective heat of dilution were evaluated from **Figure 3.2.4** and are collected in **Table 3.2.1**. The positive ΔH^o_m values for both PEGS1 and PEGS2 emphasized that the

aggregate formation whether it is micelle or vesicle, is endothermic in nature. The highly negative ΔG^{o}_{m} values, however, imply spontaneity of the aggregate formation process. The data in Table 3.2.1 suggest that the aggregate formation is less favored in the case of PEGS1 which can be attributed to relatively more polar and short PEG chain. The $T\Delta S^{o}_{m}$ value calculated from the respective ΔS^{o}_{m} value is observed to be much higher than that of corresponding ΔH^{o}_{m} value which means aggregate formation by both amphiphiles is an entropy-driven process. In fact, dehydration followed by hydrophobic interaction among HC chains is the sole criterian of entropy-driven processes, such as micelle formation [38]. Thus, as in the case of HC-containing conventional surfactants, the hydrophobic interaction among PEG chains in the micellar interior drives the process of micellization. In other words, the thermodynamics behind aggregate formation are similar for both PEG chain-containing amphiphiles and HC-containing surfactants.

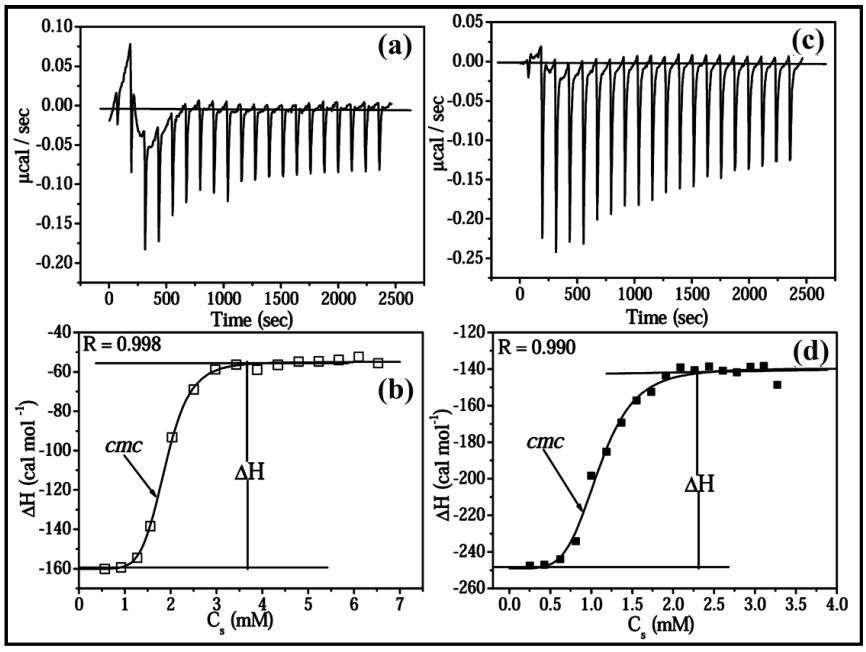

Figure 3.2.4 Calorimetric traces (heat flow against time) for PEGS1 (a) and PEGS2 (c), and variation of enthalpy change with C_s for PEGS1 (b) and PEGS2 (d) in phosphate buffer (20 mM, pH 7.0) at 25 ^{o}C.

Table 3.2.1 Critical micelle concentration (*cmc*), standard Gibbs free energy change (ΔG^o_m), standard enthalpy change (ΔH^o_m) and standard entropy change (ΔS^o_m) of the micelle formation in phosphate buffer (20 mM, pH 7.0) of PEGS1 and PEGS2 at 25 ^oC.

Surfactant	*cmc* (mM)	ΔG^o_m (kJ mol^{-1})	ΔH^o_m (kJ mol^{-1})	ΔS^o_m (J K^{-1} mol^{-1})	$T\Delta S^o_m$ (kJ mol^{-1})
PEGS1	2.6 (± 0.1)	−14.66	0.27 (± 0.06)	50.09	14.93
PEGS2	1.0 (± 0.2)	−16.99	0.43 (± 0.09)	58.50	17.43

3.2.5 2D NOESY ^{1}H-NMR analysis

The 2D NOESY ^{1}H-NMR spectra were measured at both micellar and non-micellar state of the PEGS1 amphiphile, as a representative example. D_2O was used as the reference solvent to search for the key cross-interactions among the amphiphilic molecules. This analysis actually predicts the arrangement of the amphiphilc molecules in the aggregates as described in the previous section. In non-micellar state (0.8 mM PEGS1 in D_2O) mainly diagonal interactions which means only interactions among adjacent H atoms in the PEG chain were observed (not shown here). On the other hand, in addition to the diagonal peaks a number of cross peaks were observed with the micellar aggregates of PEGS1 (8 mM in D_2O). In **Figure 3.2.5** the intense cross peaks d ↔ i, h ↔ e, f and g ↔ e, f protons suggest intermolecular interactions between the head groups of the amphiphile. Again, the close proximity among a ↔ c, b, h and b ↔ h, a, i, d protons features the strong intermolecular interactions among the PEG tails of the monomers. The origin of the intermolecular interactions must be the hydrophobic interaction, which is the driving force of aggregate formation. However, the spatial arrangement of PEGS1 molecules in the aggregated state matching the through-space interactions suggests bilayer formation after reaching *cmc*.

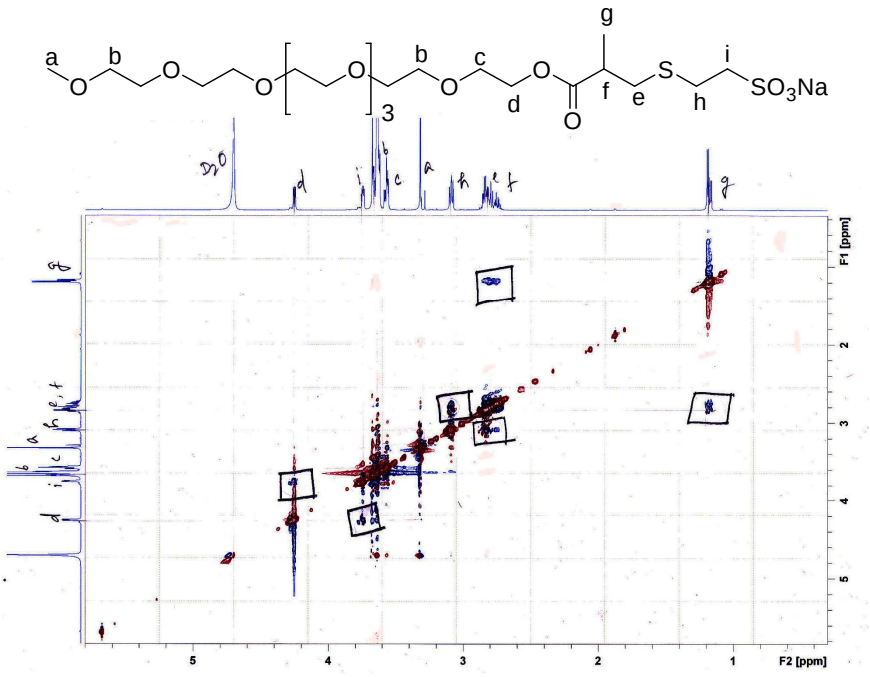

Figure 3.2.5 2D NOESY ^{1}H-NMR spectrum of 8 mM PEGS1 in the aggregated state.

3.2.6 Micropolarity and microviscosity of the self-assemblies

The Py probe was used to determine the micropolarity of the self-assemblies. The fluorescence emission spectra of Py measured in pH 7.0 buffers in the absence and presence of different concentrations of PEGS1 and PEGS2 were measured. The plots showing variation of I_1/I_3 ratio with C_s are depicted in **Figure 3.2.6(a)**. The I_1/I_3 ratio has a value of 1.83 in pH 7.0 buffer in the absence of the surfactant. But the ratio falls off with increasing concentration of the added amphiphile and the limiting values (**Table 3.2.2**) are less than that in water, indicating formation of aggregates with less polar microenvironments [57, 58]. Similar values of I_1/I_3 ratio were also obtained from studies in pure water. However, like $mPEG_{300}$-Cys and $mPEG_{1100}$-Cys amphiphiles, the I_1/I_3 ratio is higher compared to those of conventional surfactants [42, 43].

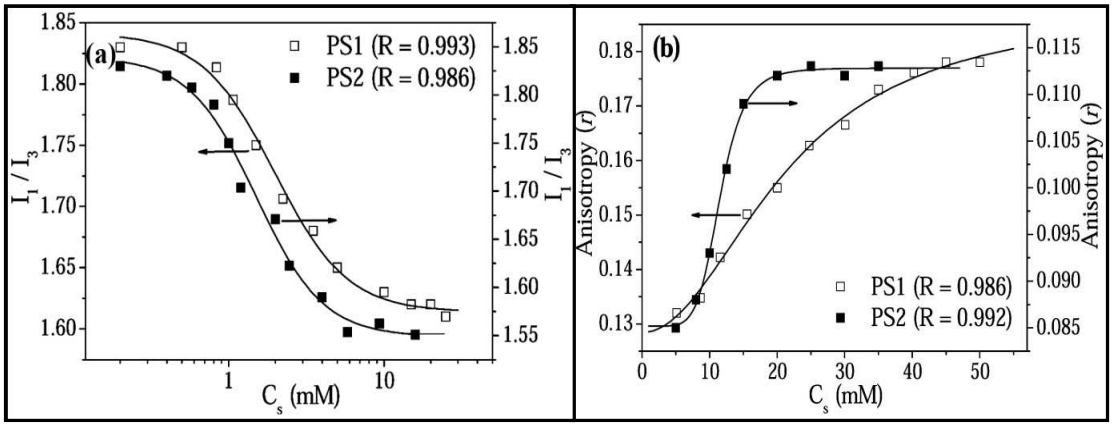

Figure 3.2.6 Plots of (a) variation of micropolarity index (I_1/I_3) with the change of C_s at 25 ^oC, and (b) plots of *r* value of DPH probe versus C_s at 25 ^oC: (□) PEGS1 and (■) PEGS2.

Table 3.2.2 Self-assembly properties of PEGS1 and PEGS2 in phosphate buffer (20 mM, pH 7.0) at 25 ^oC; the values within the parentheses correspond to pure water at 25 ^oC.

Surfactant	pC_{20}	*cmc* (mM)	*r*	η_m (mPa s)	I_1/I_3
PEGS1	2.28	2.0 ± 0.1	0.174 ± 0.04[a]	46.0 ± 3.0[a]	1.61 ± 0.02[a]
		(3.0 ± 0.1)	(0.162 ± 0.09)[a]	(45.0 ± 5.0)[a]	(1.63 ± 0.05)[a]
PEGS2	2.36	0.86 ± 0.11	0.112 ± 0.07[b]	22.0 ± 1.5[b]	1.56 ± 0.03[b]
		(1.9 ± 0.1)	(0.110 ± 0.12)[b]	(30.0 ± 3.0)[b]	(1.61 ± 0.06)[b]

[a] measured in 40 mM of PEGS1; [b] measured in 20 mM of PEGS2.

The *r* value of DPH probe which is used as an index of microrigidity of micelles was measured in the presence of different concentrations of both PEGS1 and PEGS2. **Figure 3.2.6(b)** shows the plots of variation of *r* with C_s. The *r* value of DPH probe in the self-assemblies of PEGS2 is similar to those observed with micellar aggregates of

conventional anionic surfactants (r ~ 0.05). However, interestingly, the r value for self-assemblies of PEGS1 is relatively higher, suggesting more rigid microenvironment. This may be an indication of the formation of bilayer aggregates by PEGS1 and small micellar aggregates by PEGS2. The increase of r with increasing concentration of PEGS1 and PEGS2 can be attributed to the growth of bilayer and micellar aggregates, respectively.

As discussed earlier, the η_m value quantifies the rigidity of the microenvironments of the self-assemblies and can be used as an indirect proof of the nature of aggregate type. Thus, η_m values (**Table 3.2.2**) were calculated using r and τ_f values of DPH probe. For comparison purposes the values of r and η_m obtained from measurements in pure water are also included in **Table 3.2.2**. As observed, the η_m values of the aggregates in water are similar to those in buffer medium. Relatively larger value of η_m in the case of PEGS1 (46 mPa s) indicates formation of larger aggregate. On the other hand, lower value of η_m in case of PEGS2 (22 mPa s) indicates formation of small micelle-like aggregates in buffered solution. A similar observation is also made for aggregates in pure water. It is reported that as the molecular weight of the PEG chain increases (i.e., with the increase in number of ethylene glycol units), helicity of PEG chain increases. Thus PEGS1 having shorter PEG chain spontaneously form larger tightly-packed bilayer aggregates in water as well as in buffered solution, whereas the repulsive interaction among the longer and more helical PEG chain causes the PEGS2 monomers to form loosely-packed smaller aggregates like micelles. The results thus support the mutual spatial arrangement of amphiphilic molecules in the aggregated state as described in section 3.2.5.

3.2.7 Size and shape of the aggregates

The size distribution of the aggregates formed by PEGS1 and PEGS2 in aqueous buffered solution was measured by DLS technique. The histograms in **Figure 3.2.7** represent the volume distribution graphs of the aggregates formed by the amphiphiles at different concentrations. A monomodal size distribution can be observed for PEGS1 at low concentration, but the concentrated solution exhibits bimodal distributions with d_h around 40-80 nm and 250-700 nm, suggesting coexistence of aggregates of different sizes. On

the other hand, a narrow monomodal distribution with d_h of around 3-10 nm is observed with PEGS2, suggesting formation of micellar aggregates in pH 7.0 buffer. The DLS results demonstrate different aggregation behavior in water as well as in aqueous buffered solution despite having identical head group. The results are consistent with the conclusions made from fluorescence anisotropy studies and 2D NOESY NMR analysis. The existence of different types of aggregates in buffered solution of PEGS1 and PEGS2 amphiphiles was further confirmed by the TEM measurements as discussed below.

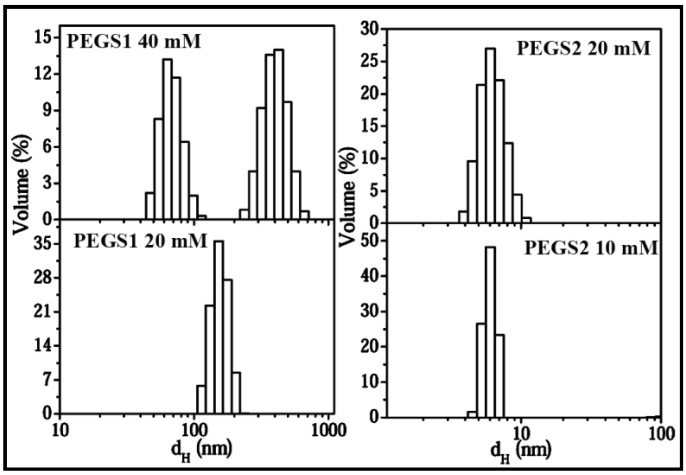

Figure 3.2.7 Size distribution histograms of the aggregates in aqueous buffered solution (20 mM, pH 7.0) of PEGS1 and PEGS2 at different concentrations at 25 ^{o}C.

Surface charge of the aggregates formed by PEGS1 and PEGS2 at different concentrations was estimated by ζ-potential measurements. The ζ-potential values of the aggregates of PEGS1 and PEGS2 amphiphiles are listed in **Table 3.2.3**. As expected, the negative charge density is high for both types of aggregates formed by PEGS1 and PEGS2. Because of intermolecular repulsive interactions among the large sulfonate head groups, the aggregates of PEGS1 are expected to be sufficiently stable. This is manifested by the results of aging effect discussed below.

Table 3.2.3 The ζ-potential values of the self-assembled structures of PEGS1 and PEGS2 in 20 mM phosphate buffer (pH 7.0) at different concentrations.

Surfactant	C_s (mM)	ζ-Potential (mV)
PEGS1	10	−31.1
	20	−29.8
PEGS2	5	−20.0
	10	−15.2

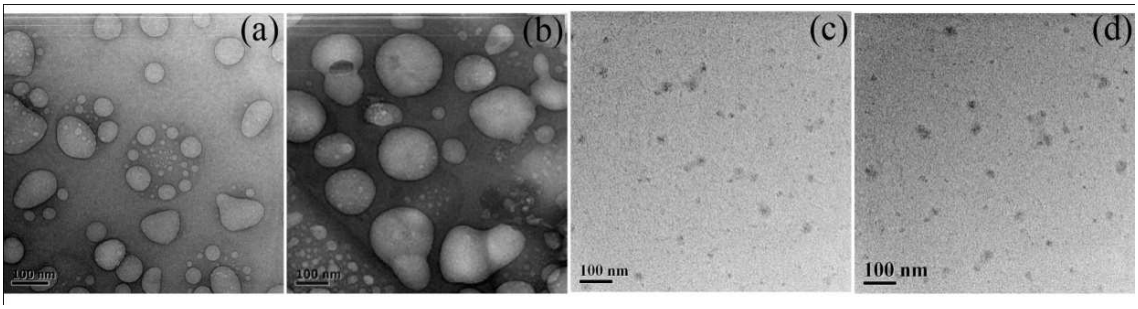

Figure 3.2.8 HRTEM micrographs of the solutions of (a) 10 mM PEGS1, (b) 20 mM PEGS1, (c) 5 mM PEGS2, and (d) 10 mM PEGS2.

The HRTEM images of the aqueous solutions of the amphiphiles were measured to visualize the shape and size of the microstructures. The micrographs (**Figure 3.2.8(a, b)**) of both dilute and concentrated solutions of PEGS1 reveal the existence of ULVs that enclose an aqueous cavity. On the other hand, only small (10 – 15 nm) micellar aggregates are observed in both dilute and concentrated solutions of PEGS2 (**Figure 3.2.8(c, d)**). The diameter of the micelles of PEGS2 is consistent with its long PEG chain. Although TEM images obtained by conventional method are often criticized as the method involves drying of the specimen, the images shown in **Figure 3.2.8** were reproducible. It is clear from the images that in dilute solution of PEGS1, both small (25 – 60 nm) and large vesicles (100 – 200 nm) coexist. However, in concentrated solution

of PEGS1, the population of large vesicles (> 200 nm) increases, which may be due to fusion of the small vesicles with the larger ones. The size of the aggregates of PEGS1 and PEGS2 as seen in the TEM images are, however, smaller than that obtained by DLS measurements. This is expected because the former method involved drying of the sample. Considering the experimental results of fluorescence, 2D NOESY, DLS, and TEM aggregate formation by the amphiphiles can be shown by the schematic (**Figure 3.2.9**), which also features the spatial alignment of the amphiphilc molecules in the aggregate.

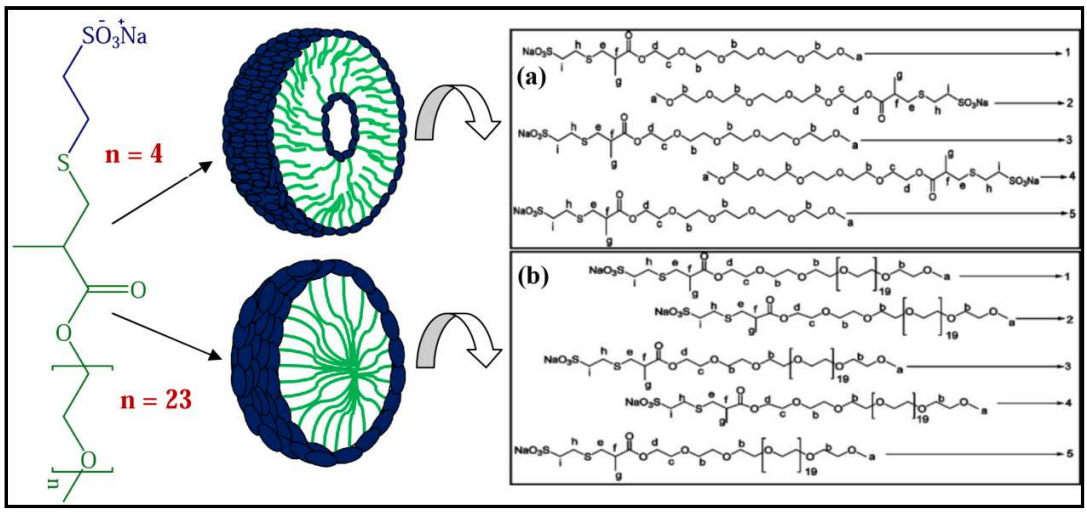

Figure 3.2.9 Schematic representation of the formation of bilayer vesicles by PEGS1 molecules and micelles by PEGS2 molecules; spatial arrangements of (a) PEGS1 molecules in the bilayer state and (b) PEGS2 molecules in the micellar state showing matched through-space interactions as revealed by the 2D NOESY cross-peaks.

3.2.8 Stability of the aggregates

Thermal stability. The effect of temperature on the stability of the aggregates formed by PEGS1 and PEGS2 amphiphiles was studied by use of DPH probe. The fluorescence anisotropy (*r*) of DPH in the presence of both amphiphiles was monitored in the temperature range of 25 ^{o}C to 75 ^{o}C. The plots in **Figure 3.2.10(a)** show the variation of *r* in PEGS1 (40 mM) and PEGS2 (20 mM) solutions with temperature. The magnitude

of *r* is higher at low temperature, but it decreases with the increase of temperature. This is because the viscosity of the microenvironments of the aggregates decreases with the rise in temperature due to weakening of the hydrophobic interaction and other physical forces among PEG chains that are responsible for forming the aggregates. In the case of vesicles of PEGS1, this causes phase transition of the bilayer membrane from more rigid gel state to a more fluid liquid-crystalline state. In the case of PEGS2 amphiphile, the decrease of *r* suggests disruption of the micelles. However, the vesicle structures of PEGS1 still remain at 75 ^{o}C which is indicated by the higher *r* value (0.155). The existence of vesicles at 75 ^{o}C was confirmed by the size distribution histogram as well as by the TEM image as shown in **Figure 3.2.10(b, c)**. The temperature corresponding to the inflection point of the sigmoidal curves in **Figure 3.2.10(a)** can be taken as the phase transition temperature, T_m. The higher value of T_m (44 ^{o}C) is consistent with the stronger interactions among PEG chains in the vesicle bilayer of PEGS1. On the other hand, in the case of PEGS2, the interaction among PEG chains being weak the micelles get disrupted as a result of increase of temperature above 49 ^{o}C. Thus the vesicles of PEGS1 are quite stable at the physiological temperature (37 ^{o}C) and therefore can be used for drug delivery purposes.

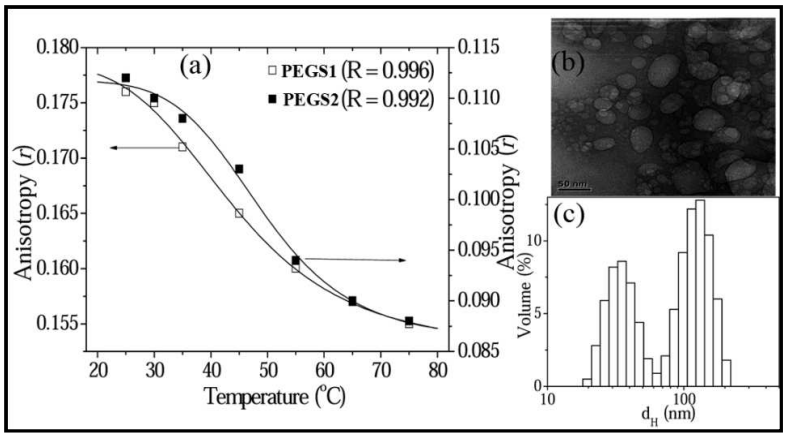

Figure 3.2.10 (a) Plots showing variation of *r* of DPH probe in 40 mM PEGS1 and in 20 mM PEGS2 solutions with temperature (^{o}C); representative TEM micrograph (b), and size distribution histogram (c) of 40 mM PEGS1 solution at 75 ^{o}C.

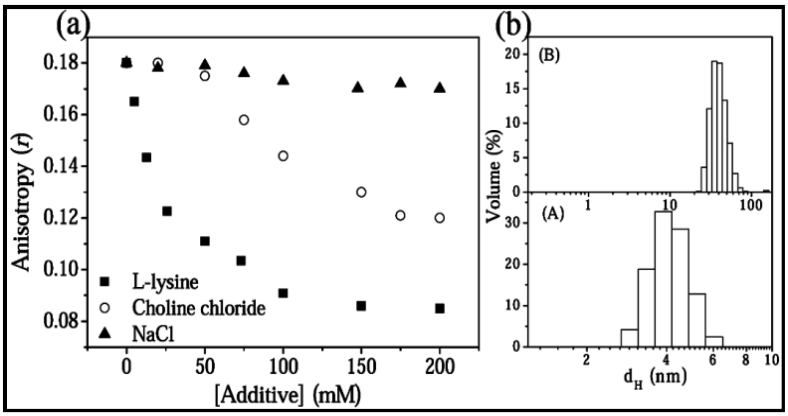

Figure 3.2.11 (a) Variation of *r* of DPH probe in 40 mM PEGS1 with the concentration of NaCl (▲), L-lysine hydrochloride (■) and choline chloride (○); (b) size distribution histograms of 40 mM PEGS1 solution in the presence of 150 mM L-lysine hydrochloride (A) and 200 mM choline chloride (B).

Effect of additives. The effect of salt concentration on the aggregation behavior of PEGS1 and PEGS2 was also examined. It is commonly observed that the increase of counterion concentration or even an increase of ionic strength of ionic surfactant solution induces transition of bilayer vesicles to form spherical micelles and rod-like micelles tubular structure or from small vesicles to giant vesicles [68-70]. In order to examine this, the *r* value of DPH probe in 40 mM PEGS1 and 20 mM PEGS2 was monitored with the variation of the concentration of three types of salts, including NaCl, choline chloride, and L-lysine hydrochloride having different cations. But the additives were found to have no significant effect on the *r* value of DPH in solution of PEGS2 (**Figure 3.2.11(a)**), suggesting either micellar structures remain unchanged or undergo transition to form larger micelles. Addition of salt causes a reduction of electrostatic repulsion among the anionic head-groups which results in a growth of aggregates. But, as there was no change of microviscosity, the possibility of formation of large rod-like aggregates can be ruled out.

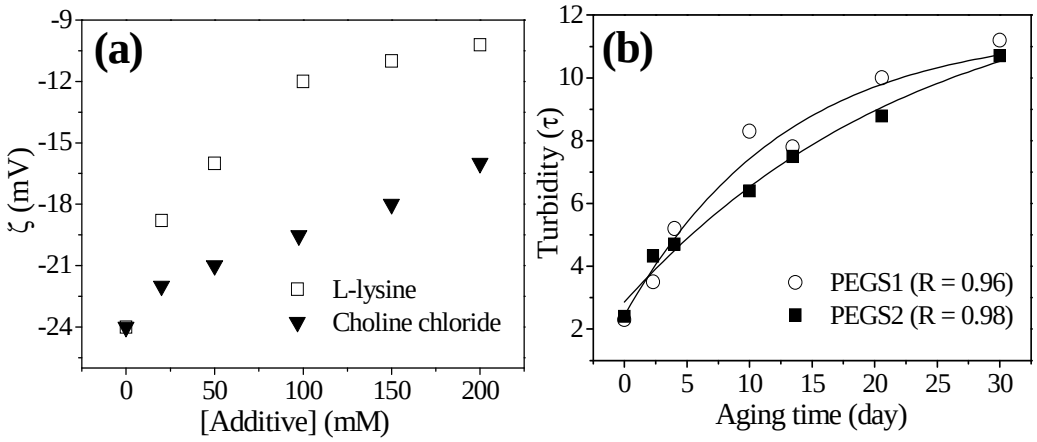

Figure 3.2.12 (a) Variation of ζ-potential with the increase in concentration of L-lysine hydrochloride and choline chloride; (b) plots of turbidity (τ = 100 − % T) versus aging time.

As with PEGS2, addition of NaCl to the solution of PEGS1 did not also show any significant change in the *r* value of DPH. Interestingly, addition of organic salts, such as choline chloride and L-lysine hydrochloride was observed to have a significant effect on the stability of the vesicles of PEGS1. The plots of *r* of DPH as a function of [L-lysine] or [choline chloride] have been shown in **Figure 3.2.11(a)**. For both L-lysine hydrochloride and choline chloride, the plot shows a sharp decrease of *r* with the increase of additive concentration, suggesting transformation of bilayer structure to some other morphology. The transformation of the vesicles to small vesicles in the presence of choline chloride is shown by the corresponding size distribution histogram in **Figure 3.2.11(b)**. However, upon addition of L-lysine hydrochloride to the solution of PEGS1 transformed vesicles into small micelles having d_h of ~4 nm. The increased salt concentration, however, reduces the surface charge density of the aggregates as indicated by the reduction of ζ-potential (**Figure 3.2.12(a)**). The different effects of L-lysine hydrochloride and choline chloride on the vesicular structures of PEGS1 can be attributed to the difference in charge of the organic counter ions. Thus relatively weaker

electrostatic interaction of singly charged choline chloride with the $-SO_3^-$ head group causes partial disruption of the vesicles, leading to the formation of smaller vesicles. On the other hand, relatively strong interaction of the cationic L-lysine with the $-SO_3^-$ head group results in a complete destruction of PEGS1vesicles to small micellar aggregates. This is demonstrated by the size distribution histograms in **Figure 3.2.11(b)**.

Aging effect. The turbidity (τ) of the solutions of the amphiphile was measured at different time intervals in order to investigate shelf-life of the aggregates. The turbidity of 10 mM PEGS1 and 5 mM PEGS2 in pH 7.0 (20 mM) buffer was monitored at 450 nm at different time intervals over 30 days. The experimental results are presented in **Figure 3.2.12(b)**. The plot reveals that the turbidity initially increases only slightly with time, and reaches almost to a steady value. The initial increase in turbidity could be attributed to the formation and growth of vesicles (PEGS1) or micelles (PEGS2) upon aging, while the subsequent plateau refers to the storage life of the aggregates.

3.2.9 Summary

In conclusion, two novel amphiphiles consisting of PEG as tail and mesna as head were designed and synthesized. The surface activity and intriguing self-assembly properties of the amphiphiles in buffer (pH 7.0) were investigated. Unlike conventional surfactants with hydrocarbon tail, these amphiphiles were found to have weak surface activity. However, the *cmc* of these amphiphiles was relatively low. On the basis of the experimental results of fluorescence, DLS and TEM measurements PEGS1 with shorter PEG chain have strong tendency to self-organize spontaneously to form stable ULVs in dilute as well as in concentrated solutions, whereas small micellar aggregates were observed to form in both dilute and concentrated solutions of PEGS2 bearing longer PEG chain. This difference in aggregation behavior of the PEG based amphiphiles having same head group can be attributed to the difference in conformation of the PEG chains. The longer PEG chain has higher helicity which controls here the microstructure of the aggregates. The thermodynamics of self-assembly formation, however, was observed to be quite similar to conventional surfactants. The large positive values of ΔS^o_m indicated

that the driving force behind the spontaneous aggregate formation is hydrophobic interaction. The vesicles as well as the micelles formed by the PEGS1 and PEGS2 surfactants were also observed to be sufficiently stable at the physiological temperature for a longer period of time which suggests that they can have potential use in drug delivery applications. The addition of choline chloride caused transformation of the large vesicles of PEGS1 into smaller vesicles. Interestingly, the vesicular aggregates transformed into small micellar aggregates upon addition of relatively low concentration of L-lysine hydrochloride salt.

3.3 Vesicle Formation by Anionic Amphiphiles with Double PEG Tails

3.3.1 Scope of the study

There are numerous reports on double-tailed amphiphiles bearing hydrophobic tails, such as alkyl chain, aromatic moiety, pyrolle, steroid etc. [71-85]. There are also reports on bilayer membrane formation by nonionic double-tailed surfactants which contain polyglyceryl as head group [86]. In the preceding sections, however, spontaneous and stable vesicle formation by unconventional, single PEG-tailed amphiphiles with zwitterionic or anionic head group has been demonstrated [64, 87]. This led to the present investigation to study self-assembly behavior of double PEG-tailed amphiphiles keeping the PEG chain lengths and head group (sulfonate) same. Thus in this work, two novel double PEG-tailed molecules, sodium di-(mercaptopropanoyl poly(ethylene glycol))-propane sulfonate having PEG chains of length M_n ~ 300 (DPEGS1) and M_n ~1100 (DPEGS2) were developed and characterized. The introduction of a second PEG chain is expected to increase polarity of the molecule. Therefore, it will be really very interesting to see whether such molecules undergo self-organization in aqueous solution or not. The solution behavior of the newly developed amphiphiles was thoroughly investigated in aqueous buffer (pH 7.0) at 25 ^{o}C. The self-assembly behavior in aqueous solution was studied by steady-state fluorescence probe techniques. The size and shape of the aggregate form were measured by DLS, TEM and AFM measurements. 2D ^{1}H-NMR spectra of the aqueous solutions of the surfactants were measured to study the interactions between PEG chains. The stability of the aggregates with the change of temperature and concentration of additives was also investigated.

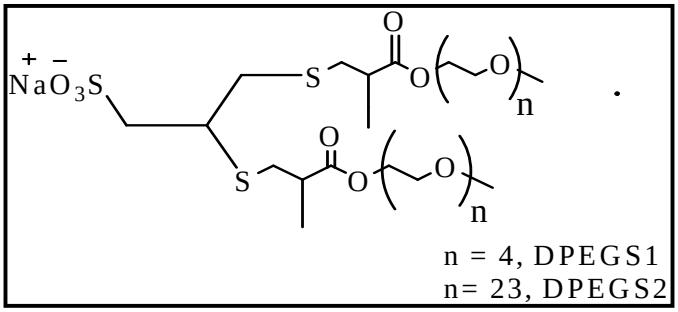

Figure 3.3.1 Chemical structures of the amphiphiles sodium di-(mercapto propanoyl poly(ethylene glycol)) propane sulfonate (n = 4, DPEGS1 and n = 23, DPEGS2).

3.3.2 Self-assembly behavior

To demonstrate self-assembly formation the steady-state fluorescence spectra of NPN probe was measured in aqueous solutions containing different concentrations of DPEGS1 and DPEGS2 molecules. Surprisingly, the fluorescence spectrum of NPN in the presence of both DPEGS1 and DPEGS2 exhibits a large blue shift with a concomitant rise of intensity (**Figure 3.3.2(a)**), indicating formation of microdomains of polarity much less than that of bulk water [46]. In other words, they behave like conventional HC tail surfactants in water at room temperature. This shows the amphiphilic nature of both DPEGS1 and DPEGS2 molecules.

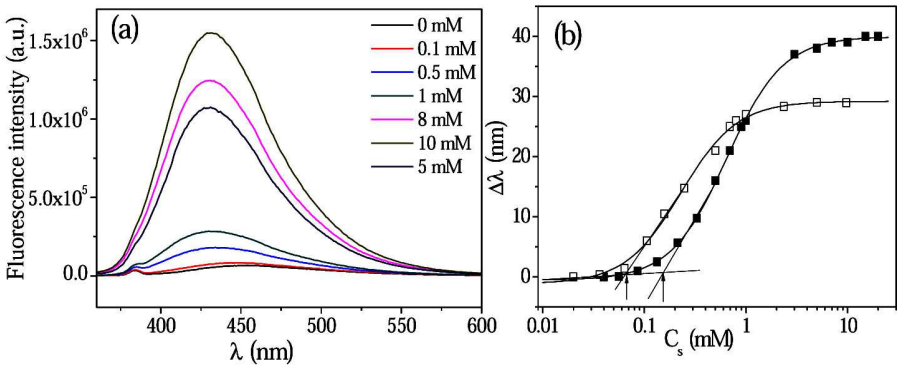

Figure 3.3.2 Plots of (a) representative fluorescence emission spectra of NPN in pH 7.0 buffer containing different concentrations of DPEGS2, and b) plots of spectral shift ($\Delta\lambda$) of NPN as a function of C_s in pH 7.0 buffer at 25 ^{o}C: DPEGS1 (■) and DPEGS2 (□).

The plots of variation of spectral shift, $\Delta\lambda$ [= $\lambda_{max(water)} - \lambda_{max(surfactant)}$] as a function of concentration (C_s) of DPEGS1 and DPEGS2 are shown in **Figure 3.3.2(b)**. It is observed that the $\Delta\lambda$ value increases with C_s until a limiting value is reached corresponding to the plateau region. The C_s value corresponding to the inflection point (indicated by arrows) was taken as the *cmc* value of the amphiphile. The *cac* values thus obtained from the onset rise of the curves are collected in **Table 3.3.1**.

Table 3.3.1 The self-association properties of DPEGS1 and DPEGS2 in phosphate buffer (20 mM, pH 7.0) and fluorescence properties of DPH probe in solutions of DPEGS1 and DPEGS2 at 25 ^oC.

Surfactant	*cac* (mM)	I_1/I_3	$\Delta\lambda$ (nm) (NPN)	*r*	τ_f (ns)	η_m (mPa s)
DPEGS1	0.15 ±0.02	1.65 ± 0.03[a]	40	0.165[a]	5.06[a]	48.1 ± 5.0[a]
DPEGS2	0.07 ± 0.03	1.70 ± 0.04[b]	30	0.135[b]	4.79[b]	39.2 ± 3.0[b]

*a and b corresponds to 5 mM DPEGS1 and 5 mM DPEGS2

3.3.3 Microenvironment study

To examine the micropolarity of the microenvironments formed by the double-tailed amphiphiles steady-state fluorescence spectra using Py in presence of different concentrations of DPEGS1 or DPEGS2 were measured and the corresponding value of the polarity parameter I_1 / I_3 was determined. For both amphiphiles, the I_1/I_3 ratio continues to fall with the increase of concentration. The lowest I_1/I_3 value was noted for DPEGS1 and DPEGS2 and is included in **Table 3.3.1**. The I_1/I_3 values of both amphiphiles observed to be higher and are greater than those of corresponding single-chain amphiphiles PEGS1 and PEGS2. This shows that the polarity of the microenvironment Py probe is very polar like alcohols [40, 41]. This means either the probe molecules are solubilized near the aggregate surface or the PEG chains are so tightly packed that the Py molecules cannot penetrate into the core, or the degree of water penetration into the micelle core is large. In contrast, the large blue shift of the emission

spectrum of NPN suggests nonpolar environment around the probe molecules. In order to address this, the steady-state fluorescence spectra of DPH probe were measured.

The rise emission intensity (not shown) indicates solubilization of the probe molecules within the hydrophobic microdomains formed by the amphiphilic molecules. The *r* value of DPH probe is also known to change when encapsulated into the hydrophobic microdomains formed by surfactant aggregates [59-62]. Thus the *r* value of DPH probe was measured in the presence of DPEGS1 and DPEGS2 amphiphiles at different concentrations above their *cmc* values and the data are presented in **Figure 3.3.3**. The *r* value is observed to increase nonlinearly in the concentration range employed. The *r* value corresponding to 10 mM DPEGS1 or DPEGS2 was noted and the data are listed in **Table 3.3.1**. The *r* values are much higher than that of SDS micelles (*r* = 0.045), but are comparable to many vesicle- or liposome-forming amphiphiles [42, 43]. This suggests that the DPH molecules are solubilized within very rigid microenvironments and the self-assembled microstructures formed by the amphiphilic molecules are most likely bilayer type aggregates.

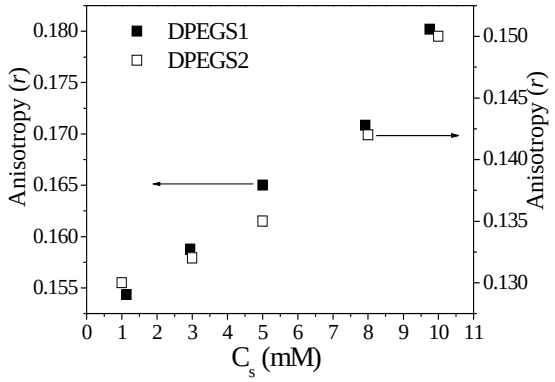

Figure 3.3.3 Plots of fluorescence anisotropy (*r*) of DPH as a function of C_s at 25 ^oC.

The above experimental findings were further enriched by the measurements of fluorescence lifetime (τ_f) the DPH probe which enabled estimation of η_m of the bilayer aggregates. The τ_f values obtained from the analysis of fluorescence intensity decays of DPH probe are listed in **Table 3.3.1**. The η_m values calculated using *r* and τ_f values of

DPH are also included in the table. The higher values of η_m indicate rigid microenvironments around the probe molecules and suggest formation of vesicular structures. It can also be concluded that the bilayer membrane is constituted by the PEG chains of the amphiphiles. This is also suggested by the results of NMR measurements.

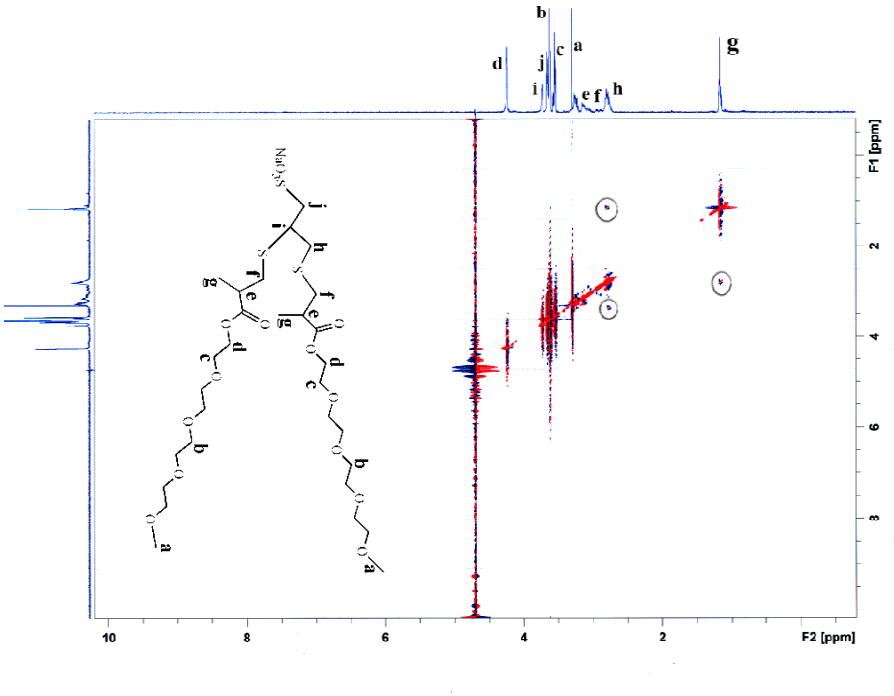

Figure 3.3.4 2D NOESY ^{1}H-NMR spectrum of 2 mM DPEGS1 in D_2O solvent.

3.3.4 Alignment of PEG chains in the aggregates

In order to determine the spatial interactions among the amphiphilic molecules in the aggregated state, 2D NOESY ^{1}H-NMR experiment was performed at a C_s > *cmc* value. The representative 2D NOESY spectrum of 2 mM DPEGS1 has been shown in **Figure 3.3.4**, together with the molecular chain labeling. In addition to the diagonal peaks there are also some key cross peaks. The key cross-peaks reveal the proximity of some essential proton pairs. The interactions among g ↔ f; f ↔ e, h; i ↔ (d, j, b, c, a, h, e, f); a ↔ (b, c, i, j, d, e, f, h) and b ↔ (a, c, i, j, d, e, f, h) protons imply the intermolecular

interactions among the PEG chains. Thus, all these 2D cross-peak patterns evidence that the surfactant molecules are arranged in at least two layers with the PEG as inner layer. The key intermolecular NOE contacts are indicated with circles. The existence of these primary interactions leads to the conclusion that the sulfonate groups form the corona and PEG chains constitute the bilayer membrane of the aggregates which is consistent with the results of fluorescence probe studies.

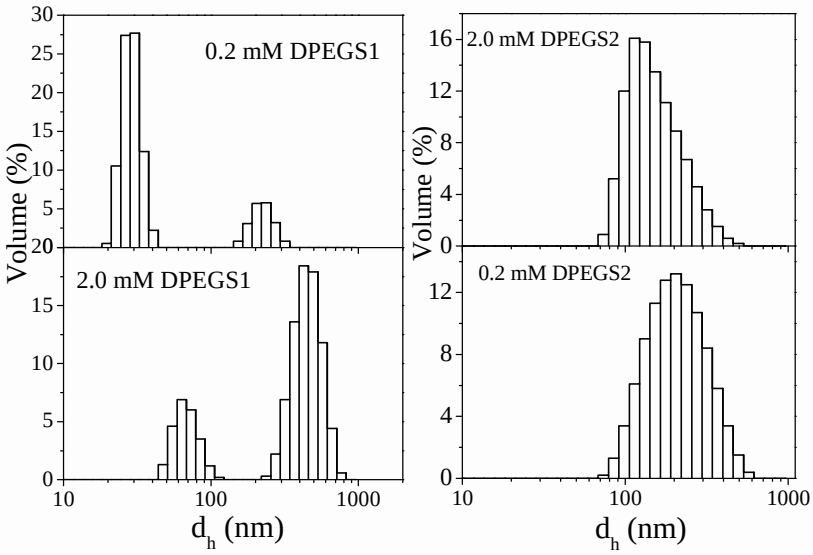

Figure 3.3.5 Size distribution histograms of DPEGS1 and DPEGS2 at different concentrations in pH 7.0 at 25 ^{o}C.

3.3.5 Size and shape of the aggregates

The mean d_h of the aggregates formed at different concentrations were determined by DLS measurements in pH 7.0 at 25 ^{o}C. The histograms in **Figure 3.3.5** represent the size distribution (expressed in percentage volume) profiles for the amphiphiles at different concentrations. A bimodal distribution, one at around 40-100 nm and the other around 300-600 nm for DPEGS1 implies formation of large aggregates. But in the case of DPEGS2 a monomodal size distribution with d_h ranging between 100 nm and 400 nm is observed.

To further visualize the actual morphology of the aggregates TEM images of the surfactant solutions were taken. The representative TEM images of the unstained specimens prepared from dilute as well as concentrated surfactant solutions are shown in **Figure 3.3.6(a, b)**. The micrographs reveal formation of vesicles of d_h in the range of 150-200 nm in case of DPEGS1. However relatively smaller sized vesicles of d_h in the range of 60-120 nm can be observed for DPEGS2 at concentrations above the *cmc* value. It should be noted that the size of the vesicles is slightly smaller than that obtained by DLS measurements. This must be due to the drying of the samples required for conventional HRTEM technique which often criticized as artifacts. However, the vesicle formation was confirmed by the corresponding cryo-TEM images shown in **Figure 3.3.6(c, d)** also exhibit ULVs having diameters in the range of 100 to 300 nm.

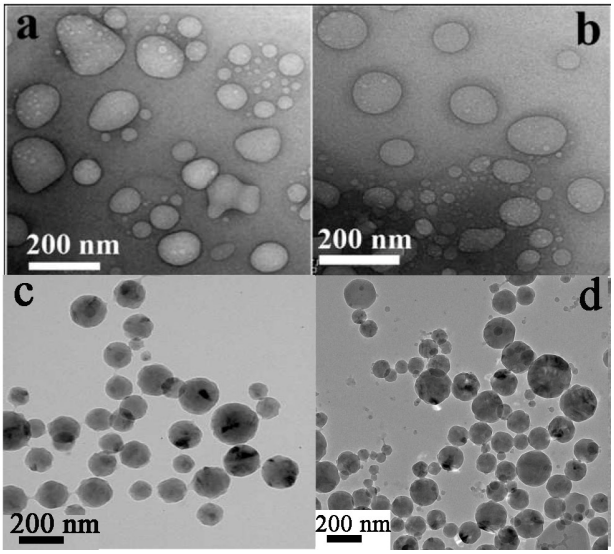

Figure 3.3.6 HRTEM images of the solutions (pH 7) of (a) 2 mM DPEGS1 and (b) 2 mM DPEGS2; cryo-TEM images of the solutions (pH 7) (c) 2 mM DPEGS1 and (d) 2 mM DPEGS2.

That the vesicle membrane is constituted by the PEG chains is evidenced by the surface charge of the aggregates which is measured by the ζ-potential value. The ζ-potential values were measured at different concentrations of the amphiphiles in pH 7.0

buffer at 25 ^{o}C and the data are collected in **Table 3.3.2**. A significant negative ζ-potential value of the vesicles confirms that the sulfonate groups make the outer surface of the vesicles negative. In other words, the mPEG chains constitute the bilayer membrane of the vesicles.

Table 3.3.2 The ζ-potential values of the vesicles of DPEGS1 and DPEGS2 amphiphiles at different concentrations.

Surfactant	C_s (mM)	ζ-potential (mV)
DPEGS1	0.2	−6.93
	2	−16.00
DPEGS2	0.1	−6.28
	2	−7.61

The shape of the aggregates can also be observed in the AFM images as shown in **Figure 3.3.7**. In both images, well-defined spherical structures can be detected and the d_h ranges from 50-250 nm for DPEGS1 and 80-150 nm for DPEGS2 agree well with the results obtained using cryo-TEM. The height profile obtained using AFM is representative of the thickness of two closely stacked membranes tilted together after drying and collapse of the vesicles. Thus, half of the thickness can be considered as the membrane thickness of the vesicle and the height of ~ 8 nm corresponds to a membrane thickness of 4 nm **(Figure 3.3.7)**. From the Chem Draw energy minimized structue analysis the length of the PEG tails of DPEGS1 molecule is found to be ~ 1.9 nm, which is about half of the membrane thickness confirming bilayer vesicle formation by the DPEGS1 molecules. The same explanation is also applicable for DPEGS2 amphiphile. For DPEGS2, however, the height obtained is equal to ~ 1.7 nm. The energy minimization of DPEGS2 molecule using MM2 software of Chem Draw reveals the length of the PEG chains is ~ 8.5 nm. Therefore, AFM data clearly suggest that the bilayer thickness of the vesicle membranes is ~ 16.5 – 17 nm, which is close to twice the

fully-extended length (~8.5 nm) of PEG chain. Considering all the above results a schematic representation (**Figure 3.3.8**) showing vesicle formation including bilayer structure can be proposed.

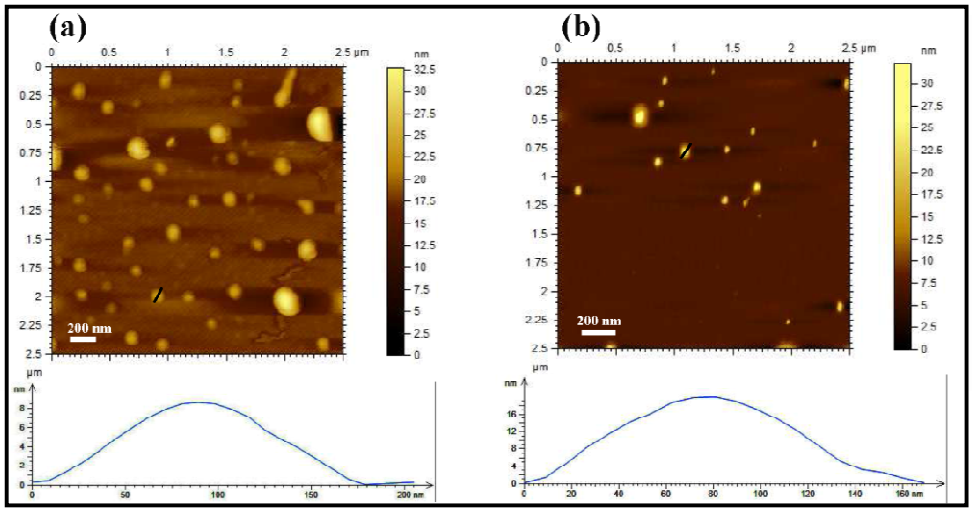

Figure 3.3.7 AFM height images with scale-bar of (a) 2 mM DPEGS1 and (b) 2 mM DPEGS2 in pH 7.0 on freshly cleaved mica.

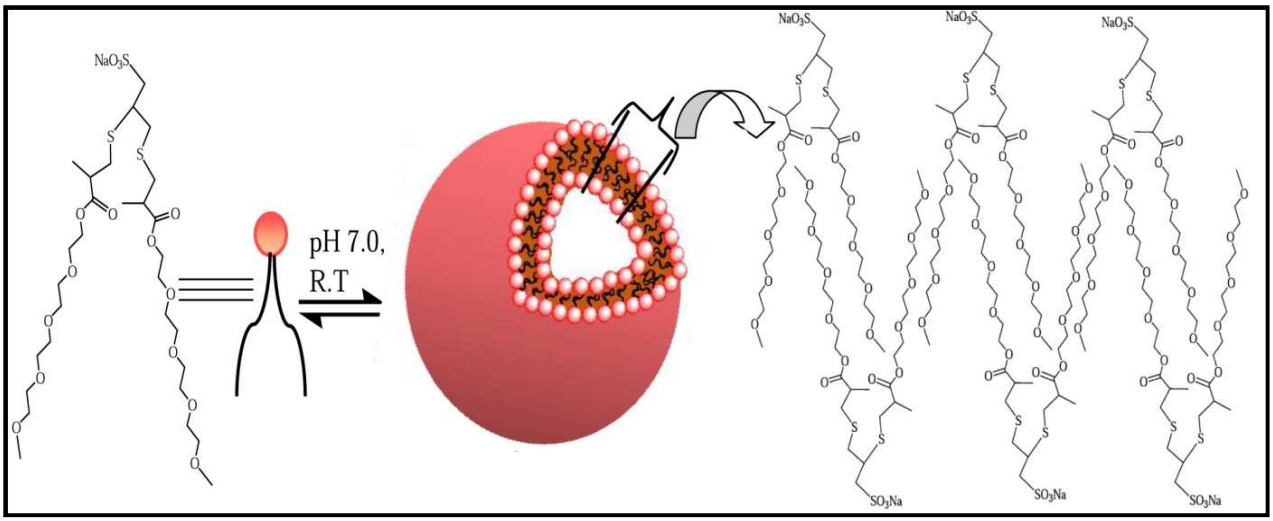

Figure 3.3.8 Schematic representation of bilayer vesicle formation by the DPEGS1 molecules.

3.3.6 Stability of the vesicles

Effect of temperature. Determination of physical stability of the vesicles at higher temperatures is necessary for their practical applications and therefore, the effect of temperature on their stability was studied. As discussed earlier, the *r* value of DPH when solubilized within aggregates is sensitive to temperature change. Therefore the *r* value of DPH in the presence of DPEGS1or DPEGS2 amphiphile was measured in the temperature range of 25 ^{o}C to 75 ^{o}C. The plots in **Figure 3.3.9(a)** show the variation of *r* in solution (5 mM) of DPEGS1 or DPEGS2 with temperature. The magnitude of *r* is higher at lower temperature, but it decreases with the increase in temperature. This is because the viscosity of the microenvironment decreases with the rise in temperature due to weakening of the hydrophobic interaction and other physical forces among PEG chains that are responsible for forming the aggregates. In the case of vesicles of DPEGS1, this causes phase transition of the bilayer membrane from more rigid gel state to a more fluid liquid-crystalline state. Thus the temperature corresponding to the inflection point of the sigmoidal curves can be taken as the phase transition temperature, T_m. The higher value of T_m (52 ^{o}C for DPEGS1 and 50 ^{o}C for DPEGS2) is consistent with the stronger interactions among PEG chains in the vesicle bilayer. It is important to note that no turbidity appeared even at 75 ^{o}C, suggesting very good vesicles stablity at the physiological temperature (37 ^{o}C) which makes them good candidates for use in drug delivery applications.

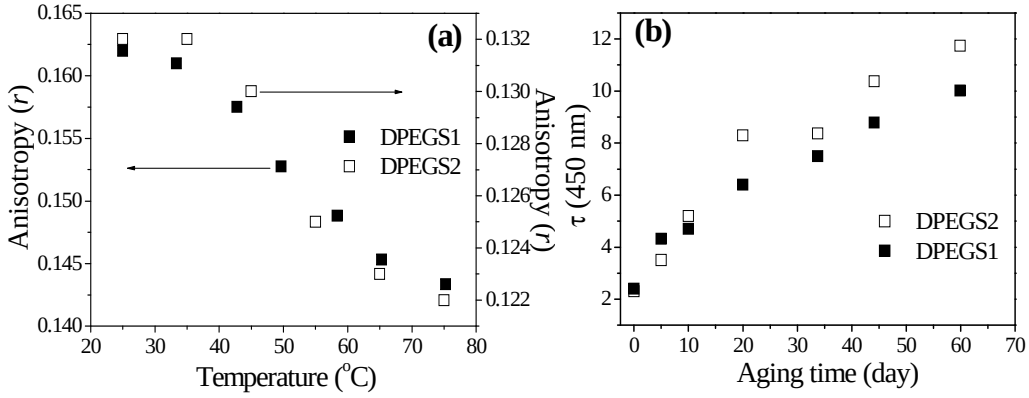

Figure 3.3.9 (a) Variation of *r* value of DPH in the presence of DPEGS1 (5 mM) and DPEGS2 (5 mM) with temperature (^{o}C), and (b) plots of τ versus aging time at 25 ^{o}C.

Effect of aging. In order to investigate the shelf-life of the vesicles, the turbidity (τ) of the solutions (1 mM) of DPEGS1 and DPEGS2 at pH 7.0 (20 mM) was monitored at 25 ^{o}C at different time intervals during 60 days. The experimental results are presented in **Figure 3.3.9(b)**. The plots reveal that the turbidity initially increases only slightly with time, and reaches almost a steady value after 60 days. The initial increase in turbidity is due to the formation and growth of the vesicles, while the subsequent plateau refers to the storage life of the aggregates. Thus the bilayer vesicles obtained from both the double PEG-tailed surfactants exhibit excellent stability at physiological temperature (37 ^{o}C) over months.

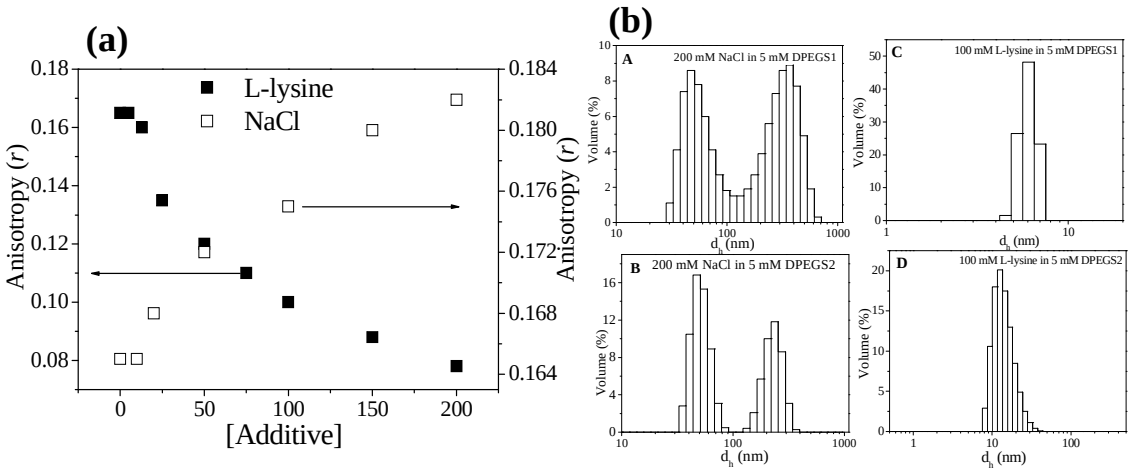

Figure 3.3.10 (a) Variation of *r* in 5 mM DPEGS1 with concentration of NaCl (□) and L-lysine hydrochloride (■); (b) size distribution histograms of solutions of (A) 5 mM DPEGS1 containing 200 mM NaCl, (B) 5 mM DPEGS2 containing 200 mM NaCl, (C) 5 mM DPEGS1 containing 100 mM L-lysine hydrochloride, and (D) 5 mM DPEGS2 containing 100 mM L-lysine hydrochloride.

Effect of additives. As the surfactants are anionic in nature there might be significant effect of salt concentration on the aggregation behavior of the surfactants. As discussed earlier, the addition of counter ion usually induces transition of bilayer vesicle to other structures [88-92]. To investigate the influence of salt concentration on aggregate morphology, the *r* value of DPH probe was measured in solution of DPEGS1 in the

presence of varying concentration of NaCl. The plot of variation of *r* with [NaCl] can be found in **Figure 3.3.10 (a)**. The plot shows a slight increase of *r* value with the rise of NaCl concentration, suggesting transformation of ULVs to MLVs, tubules or rod-like aggregates. The DLS measurements with solutions of 5 mM DPEGS1 and DPEGS1 both containing 200 mM NaCl were performed and the data are presented in **Figure 3.3.10(b)**. It is observed that the mean d_h value is higher than the value obtained in the absence of salt, indicating growth of aggregates. Since no significant increase of solution viscosity was observed, this can be associated with the transformation of ULVs to large MLVs or tubules or disk-like aggregates. Indeed the TEM micrograph of the 5 mM surfactant solution containing 200 mM NaCl shows formation tubular aggregates (**Figure 3.3.11(a)**) in the case of DPEGS1 and large disk-like micelles in the case of DPEGS2 (**Figure 3.3.11(c)**). The tube-like aggregates have length of ~700 nm and inner diameter of ~80-100 nm. This can be linked to the tight packing of the PEG chains caused by the removal of ionic repulsion upon addition of salt.

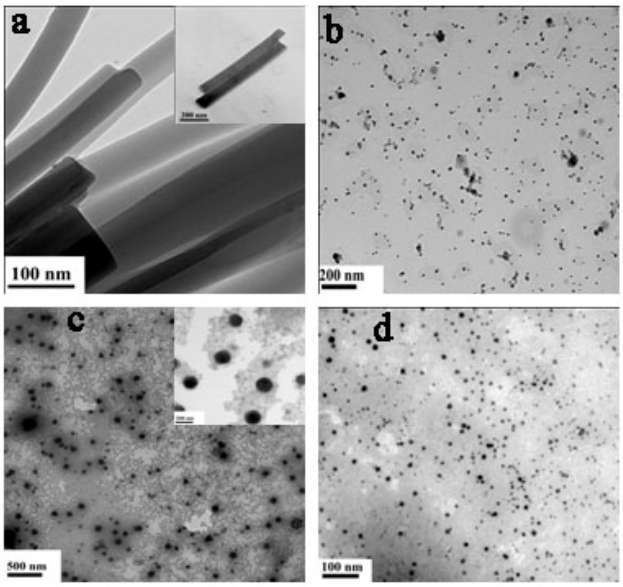

Figure 3.3.11 HRTEM images of (a) 5 mM DPEGS1 containing 200 mM NaCl, (b) 5 mM DPEGS1 containing 100 mM L-lysine hydrochloride, (c) 5 mM DPEGS2 containing 200 mM NaCl, and (d) 5 mM DPEGS2 containing 100 mM L-lysine hydrochloride; inset (a): one section analysis; inset (c): one section analysis.

Surprisingly, addition of L-lysine hydrochloride was observed to have significant effect on the stability of the vesicles formed by both the surfactants. The plot of *r* of DPH in 5 mM DPEGS1 as a function of [L-lysine hydrochloride] is presented in **Figure 3.3.10(a)** which shows a sharp decrease of *r* with the increase of [L-lysine hydrochloride], indicating transformation of bilayer structure to some other morphology. The size distribution histograms of 5 mM DPEGS1 and DPEGS2 in presence of 100 mM L-lysine hydrochloride show aggregates of mean d_h<10 nm (**Figure 3.3.10(b)**). The corresponding TEM images (**Figure 3.3.11(b, d)**) also exhibit very small micelles–like aggregates for both the amphiphiles. The transformation of bilayer vesicles to small micelles with the increase of L-lysine hydrochloride concentration can be attributed to the strong electrostatic attraction among the negatively charged $–SO_3^-$ head group of the surfactant molecules and large, positively charged L-lysine cations. Strong electrostatic interaction of the L-lysine cation with the $–SO_3^-$ head group results in a complete destruction of vesicles forming small micellar aggregates. This kind of behavior has also been observed with single-tailed amphiphiles having sulfonate head. The vesicle-to-micelle transition is consistent with the decrease of membrane rigidity (*r* value) at higher concentrations of L-lysine hydrochloride. The results of this experiment suggest that L-lysine can be used to induce release of drug molecules encapsulated by the vesicles of DPEGS1 and DPEGS2 amphiphiles.

3.3.7 Summary

In summary, two novel double PEG-tailed surfactants with sulfonate head group were developed and characterized. The solution behavior of the amphiphiles was investigated in pH 7.0 at 25 ^oC. The interesting result is that despite having two polar PEG chains both DPEGS1 and DPEGS2 were found to have strong tendency to self-assemble in aqueous buffered solution above a very low critical concentration. The results of fluorescence, DLS, TEM and AFM measurements showed spontaneous formation of bilayer vesicles in dilute as well as in concentrated solutions of both the double-tailed surfactants without the requirement of any external stimuli. This is the first report on vesicle formation by double PEG-tailed amphiphiles the polar PEG chains of which behave like hydrocarbon

tails of conventional double-tail surfactants. It appears that the driving force behind the vesicle formation is the hydrophobic interaction among the PEG chains. The alignment of the amphiphilic molecules in bilayer vesicles has also been shown by 2D NOESY NMR analysis. The vesicles were found to be stable at body temperature (37 ^{o}C) over months. However, in the presence of NaCl the vesicles of both amphiphiles are transformed into either tubules or disk-like aggregates. On the other hand, in the presence of L-lysine hydrochloride salt the vesicles produce small micelles. The vesicle-to-micelle transition can find application in L-lysine cation-triggered delivery of drug molecules in the pharmaceutical industry.

References

[1] Davis, F. F. The Origin of Pegnology. *Adv. Drug Delivery Rev.* **2002**, *54*, 457-458.

[2] Bhadra, D.; Bhadra, S.; Jain, P.; Jain, N. K. Pegnology: A Review of PEG-ylated Systems. *Die Pharmazie* **2002**, *57*, 5-29.

[3] Storm, G.; Belliot, S. O.; Daemen, T.; Lasic, D. D. Surface Modification of Nanoparticles to Oppose Uptake by the Mononuclear Phagocyte System. *Adv. Drug Delivery Rev.* **1995**, *17*, 31-48.

[4] Duncan, R. Polymer Conjugates as Anticancer Nanomedicines. *Nat. Rev. Cancer* **2006**, *6*, 688-701.

[5] Howard, M. D.; Jay, M.; Dziubla, T. D.; Lu, X. PEGylation of Nanocarrier Drug Delivery Systems: State of the Art. *J. Biomed. Nanotechnol.* **2008**, *4*, 133-148.

[6] Ringsdorf, H. Structure and Properties of Pharmacologically Active Polymers. *J. Polym. Sci.: Pol. Sym.* **1975**, *51*, 135-153.

[7] Torchilin, V. P. PEG-based Micelles as Carriers of Contrast Agents for Different Imaging Modalities. *Adv. Drug Delivery Rev.* **2002**, *54*, 235-252.

[8] Yokoyama, M.; Fukushima, S.; Uehara, R.; Okamoto, K.; Kataoka, K.; Sakurai, Y.; Okano, T. Characterization of Physical Entrapment and Chemical Conjugation of Adriamycin in Polymeric Micelles and Their Design for in vivo Delivery to a Solid Tumor. *J. Control. Release* **1998**, *50*, 79-92.

[9] Morpurgo, M.; Veronese, F. M. Conjugates of Peptides and Proteins to Polyethylene glycols. *Methods Mol Biol.* **2004**, *283*, 45–70.

[10] Pasut, G.; Guiotto, A.; Veronese, F. M. Protein, Peptide and Non-peptide Drug PEGylation for Therapeutic Application. *Expert Opin Ther Patents.* **2004**, *14*, 859–894.

[11] Roberts, M. J.; Bentley, M. D.; Harris, J. M. Chemistry for Peptide and Protein PEGylation. *Adv Drug Deliv Rev.* **2002**, *54*, 459–476.

[12] Harris, J. M. Introduction for Biotechnical and Biomedical Applications of Poly(ethylene glycol). In: Harris JM, ed. *Poly(ethylene glycol) Chemistry Biotechnical and Biomedical Applications.* New York: Plenum Press, **1992**, 1–14.

[13] Zalipsky, S. Functionalized Poly(ethylene glycol) for Preparation of Biologically Relevant Conjugates. *Bioconjug Chem.* **1995**, *6(2)*, 150–165.

[14] Zalipsky, S.; Harris, J. M. Introduction to Chemistry and Biological Applications of Poly(ethylene glycol). In: Harris JM, Zalipsky S, eds. *Poly(ethylene glycol). Chemistry and Biological Applications.* Washington, DC: ACS Symposium series, **1997**, 1–13.

[15] Veronese, F. M.; Boccu, E.; Schiavon, O. Anti-inflammatory and Pharmacokinetic Properties of Superoxide Dismutase Derivatized with Polyethylene glycol via Active Esters. *J Pharm Pharmacol.* **1983**, *35*, 757–758.

[16] Zaslavsky, B. Y.; Baevskii, A. V.; Rogozhin, S. V.; Gedrovich, A. V.; Shishkov, A. V.; Gasanov A. A.; and Masimov, A. A. Relative Hydrophobicity of Synthetic Macromolecules : I. Polyethylene glycol, Polyacrylamide and Polyvinylpyrrolidone. *J. Chromatogr.* **1984**, *285*, 63- 68.

[17] Carstens, M. G.; van Nostrum, C. F.; Ramji, A.; Meeldijk, J. D.; Verrijk, R.; de Leede, L. L.; Crommelin, J. A.; Hennink, W. E. Poly(ethylene glycol)−oigolactates with Monodisperse Hydrophobic Blocks: Preparation, Characterization, and Behavior in Water. *Langmuir* **2005**, *21*, 11446−11454.

[18] Park, M. -J.; Chung, Y. -C.; Chun, C. B. PEG-based Surfactants that Show High Selectivity in Disrupting Vesicular Membrane with or without Cholesterol. *Colloids Surf. B* **2003**, *32*, 11−18.

[19] Salonen, A.; Knyazev, N.; von Bandel, N.; Degrouard, J.; Langevin, D.; Drenckhan, W. A Novel Pyrene-based Fluorescing Amphiphile with Unusual Bulk and Interfacial Properties. *ChemPhysChem* **2011**, *12*, 150−160.

[20] Mandal, A. B.; Ray, S.; Biswas, A. M.; Moulik, S. P. Physicochemical Studies on the Characterization of Triton X 100 Micelles in an Aqueous Environment and in the Presence of Additives. *J. Phys. Chem.* **1980**, *84*, 856−859.

[21] Ito, K.; Tanaka, K.; Tanaka, H.; Imai, G.; Kawagachi, S.; Itsuno, S. Poly(ethylene oxide) Macromonomers. 7. Micellar Polymerization in Water. *Macromolecules* **1991**, *24*, 2348−2354.

[22] Geetha, B.; Mandal, A. B.; Ramasami, T. Synthesis, Characterization, and Micelle Formation in an Aqueous Solution of Methoxypolyethylene glycol Macromonomer, Homopolymer, and Graft Copolymer. *Macromolecules* **1993**, *26*, 4083−4088.

[23] Geetha, B.; Mandal, A. B. Self-diffusion Studies on .Omega.-methoxy Polyethylene glycol Macromonomer Micelles by using Cyclic Voltammetric and Fourier Transform Pulsed Gradient Spin-echo Nuclear Magnetic Resonance Techniques. *Langmuir* **1995**, *11*, 1464−1467.

[24] Geetha, B.; Mandal, A. B. Determination of the Critical Micelle Concentration of the Methoxy Polyethylene glycol Based Macromonomer and Partition coefficient of a New Electrochemical Probe using a Cyclic Voltammetric Technique. *Langmuir* **1997**, *13*, 2410−2413.

[25] Dey, J.; Shrivastava, S. Can Molecules with Anionic Head and Poly(ethylene glycol) methyl ether Tail Self-assemble in Water? A Surface tension, Fluorescence probe, Light scattering, and Transmission Electron Mmicroscopic Investigation. *Soft Matter* **2012**, *8*, 1305−1308.

[26] Dey, J.; Shrivastava, S. Physicochemical Characterization and Self-Assembly Studies on Cationic Surfactants bearing mPEG Tail. *Langmuir* **2012**, *28*, 17247-17255.

[27] Yoshimura, T.; Nyuta, K.; Esumi, K. Zwitterionic Heterogemini Surfactants Containing Ammonium and Carboxylate Headgroups. 1. Adsorption and Micellization. *Langmuir* **2005**, *21*, 2682-2688.

[28] Lomax, E. G. In *Amphoteric surfactants*. Ed.; Surfactant Science Series, Vol 59, 2nd edn. Marcel Dekker, New York, **1996**, 75–190.

[29] Domingo, X. In *Amphoteric Surfactants*; Lomax, E. G., Ed.; Surfactant Science Series; Marcel Dekker: New York, **1996**; Vol. 59, Chapter 3.

[30] Amooey, A. A.; Fazlollahnejad, M. Study of Surface Tension of Binary Mixtures of Poly (Ethylene Glycol) in Water and Poly (Propylene Glycol) in Ethanol and its Modeling Using Neural Network. *Iranian Journal of Chemical Engineering*, **2014**, *11*, 19-29.

[31] Kim, M. W.; Cao, B. H. Additional Reduction of Surface Tension of Aqueous Polyethylene Oxide (PEO) Solution at High Polymer Concentration. *Europhys. Lett.*, **1993**, *24*, 229-234.

[32] Ghosh, A.; Shrivastava, S.; Dey, J. Concentration and pH-Dependent Aggregation Behavior of an L-Histidine Based Amphiphile in Aqueous Solution. *Chem. Phys. Lipids* **2010**, *163*, 561-568.

[33] Mohanty, A.; Dey, J. Spontaneous Formation of Vesicles and Chiral Self-Assemblies of Sodium N-(4-Dodecyloxybenzoyl)-L-Valinate in Water. *Langmuir* **2004**, *20*, 8452-8459.

[34] Patra, T.; Ghosh, S.; Dey, J. Spontaneous Formation of pH-sensitive, Stable Vesicles in Aqueous Solution of *N*-[4-n-octyloxybenzoyl]-L-histidine. *Soft Matter* **2010,** *6***,** 3669-3679.

[35] Posner, A. M.; Anderson, J.R.; Alexander, A. E. The Surface Tension and Surface Potential of Aqueous Solutions of Normal Aliphatic Alcohols. *J. Colloid Sci*. **1952**, *7*, 623-644

[36] Ananthapadmanabhan, K. P.; Goddard, E. D.; Turro, N. J.; Kuo, P. L. Fluorescence Probes for Critical Micelle Concentration. *Langmuir* **1985**, *1*, 352-355.

[37] Saitoh, T.; Taguchi, K.; Hiraide, M. Evaluation of Hydrophobic Properties of Sodium Dodecylsulfate/γ-Alumina Admicelles Based on Fluorescence Spectra of N-Phenyl-1-Naphthylamine. *Analytica Chimica Acta*. **2002**, *454*, 203–208.

[38] Clint, J. H. *Surfactant Aggregation*; J. Blackie: London, Published in USA by Chapman and Hall: New York, **1991**.

[39] Paula, S.; Siis, W.; Tuchtenhagen, J.; Blume, A. Thermodynamics of Micelle Formation as a Function of Temperature: A High Sensitivity Titration Calorimetry Study. *J. Phys. Chem.* **1995**, *99*, 11742-11751.

[40] Verral, R. E.; Milioto, S.; Zana, R. Ternary Water-in-oil Microemulsions Consisting of Cationic Surfactants and Aromatic Solvents. *J. Phys.Chem.***1988**, *92*, 3939−3943.

[41] Majhi, P.; Moulik, S. Energetics of Micellization: Reassessment by a High-Sensitivity Titration Microcalorimeter. *Langmuir* **1998**, *14*, 3986-3990.

[42] Neuhaus, D.; Williamson, M. The Nuclear Overhauser Effect in Structural and Conformational Analysis; Wiley-VCH: New York, **2000**.

[43] Yuan, H.; Cheng, G.; Zhao, S.; Miao, X.; Yu, J.; Shen, L.; Du, Y. Conformational Dependence of Triton X-100 on Environment Studied by 2D NOESY and ^{1}H NMR Relaxation. *Langmuir* **2000**, *16*, 3030-3035.

[44] Emin, S. M.; Denkova, P. S.; Papazova, K. I.; Dushkin, C. D.; Adachi, E. Study of Reverse Micelles of Di-isobutyl phenoxy ethoxy ethyl dimethyl benzyl ammonium Methacrylate in Benzene by Nuclear Magnetic Resonance Spectroscopy. *J. Colloid Interface Sci*. **2007**, *305*, 133-141.

[45] Denkova, S. P.; Lokeren, V. L.; Verbruggen, I.; Willem, R. Self-Aggregation and Supramolecular Structure Investigations of Triton X-100 and SDP2S by NOESY and Diffusion Ordered NMR Spectroscopy. *J. Phys. Chem. B* **2008**, *112*, 10935–10941.

[46] Chapman, C. F.; Fee, R. *S.*; Maroncelli, M. Measurements of the Solute Dependence of Solvation Dynamics in 1-Propanol: The Role of Specific Hydrogen-Bonding Interactions. *J. Phys. Chem.* **1995**, *99*, 4811-4819.

[47] Horng, M. L.; Gardecki, J. A.; Papazyan, A.; Maroncelli, M. Subpicosecond Measurements of Polar Solvation Dynamics: Coumarin 153 Revisited. *J. Phys. Chem.* **1995**, *99*, 17311-17337.

[48] Kalyanasundaram, K.; Thomas, J. K. Environmental Effects on Vibronic Band Intensities in Pyrene Monomer Fluorescence and Their Application in Studies of Micellar Systems. *J. Am. Chem. Soc.* **1977**, *99*, 2039-2044.

[49] Kalyansundaram, K. *Photophysics of Microheterogeneous Systems*; Academic Press: New York, 1988.

[50] Shinitzky, M.; Barenholz, Y. Dynamics of the Hydrocarbon Layer in Liposomes of Lecithin and Sphingomyelin Containing Dicetylphosphate. *J. Biol.Chem.* **1974**, *249*, 2652-2657.

[51] Roy, S.; Mohanty, A.; Dey, J. Microviscosity of Bilayer membranes of some N-Acylamino Acid Surfactants determined by Fluorescence Probe Method. *Chem. Phys. Lett.* **2005**, *414*, 23-27.

[52] Lakowicz, J. R. *Principles of Fluorescence Spectroscopy*; Plenum Press: New York, 1983; p 132.

[53] Cehelnik, E. D.; Cundall, R. B.; Lockwood, J. R.; Palmer, T. F. Solvent and Temperature Effects on the Fluorescence of all-trans-1,6-diphenyl-1,3,5-hexatriene. *J. Phys. Chem*. **1975**, *79*, 1369-1376.

[54] Bhattacharya, S.; Biswas, J. Vesicle and Stable Monolayer Formation from Simple "Click" Chemistry Adducts in Water. *Langmuir* **2011**, *27*, 1581-1591.

[55] Bhattacharya, S.; Ghanashyam Acharya, N. S. Vesicle and Tubular Microstructure Formation from Synthetic Sugar-linked Amphiphiles. Evidence of Vesicle Formation from Single-chain Amphiphiles Bearing a Disaccharide Headgroup. *Langmuir* **2000**, *16*, 87−97.

[56] Ranck, J. L.; Mateu, L.; Sadler, D. M.; Tardieu, A.; Gulik-Krzywicki, T.; Luzzati, V. Order-Disorder Conformational Transitions of the Hydrocarbon Chains of Lipids. *J. Mol. Biol*.**1974**, *85*, 249-260.

[57] Mansilla, M. C.; Cybulski, L. E.; Albanesi, D.; de Mendoza, D. Control of Membrane Lipid Fluidity by Molecular Thermosensors. *J. Bacteriol*. **2004**, *186*, 6681-6688.

[58] Valério, J.; Lameiro, M. H.; Funari, S. S.; Moreno, M. J.; Melo, E. Temperature Effect on the Bilayer Stacking in Multilamellar Lipid Vesicles. *J. Phys. Chem. B* **2012**, *116*, 168-178.

[59] Yan, Y.; Huang, J.; Li, Z.; Ma, J.; Fu, H.; Ye, J. Vesicles with Superior Stability at High Temperature. *J. Phys. Chem. B* **2003**, *107*, 1479-1482.

[60] Jaeger, D. A.; Brown, E. L. G. Double-Chain Surfactants with Two Carboxylate Head Groups That Form Vesicles. *Langmuir* **1996**, *12*, 1976–1980.

[61] Lehn, J. M. Toward Self-Organization and Complex Matter. *Science* **2002**, *295***,** 2400–2403.

[62] Morigaki, K.; Walde, P. Fatty Acid Vesicles. *Curr. Opin. Colloid Interface Sci.* **2007**, *12*, 75–80.

[63] Jusufi, A.; Antti-Pekka Hynninen, A. P.; Haataja, M.; Panagiotopoulos, A. Z. Electrostatic Screening and Charge Correlation Effects in Micellization of Ionic Surfactants. *J. Phys. Chem. B* **2009**, *113*, 6314−6320.

[64] Ghosh, R.; Dey, J. Vesicle Formation by L-Cysteine-Derived Unconventional Single- Tailed Amphiphiles in Water: A Fluorescence, Microscopy, and Calorimetric Investigation. *Langmuir* **2014**, *30*, 13516-13524.

[65] Clarke, S.W.; Lopez-Vidriero, M. T.; Pavia, D. The Effect of Sodium 2-Mercapto-Ethane Sulphonate and Hypertonic Saline Aerosols on Bronchial Clearance in Chronic Bronchitis. Br *J Clin Pharmacol*. **1979**, *7*, 39–44.

[66] Berrigan, M.; Marinello, A.; Pavelic, Z. Protective Role of Thiols in Cyclophosphamide Induced Urotoxicity and Depression of Hepatic Drug Metabolism. *Cancer Res.* **1982**, *42*, 3688–3695

[67] Yilmaz, M.; Goksu, N.; Bayramoglu, I.; Practical Use of MESNA in Atelectatic Ears and Adhesive Otitis Media. *J Otorhinolaryngol Relat Spec*. **2006**, *68*, 195–198.

[68] Mohanty, A.; Patra, T.; Dey, J. Salt-Induced Vesicle to Micelle Transition in Aqueous Solution of Sodium *N*-(4-*n*-Octyloxybenzoyl)-L-valinate. *J. Phys. Chem. B* **2007,** *111*, 7155-7159.

[69] Lu, T.; Han, F.; Li, Z.; Huang, J. Transitions of Organized Assemblies in Mixed Systems of Cationic Bolaamphiphile and Anionic Conventional Surfactants. *Langmuir* **2006,** *22*, 2045-2049.

[70] Grillo, I.; Kats, E. I.; Muratov, A. R. Formation and Growth of Anionic Vesicles Followed by Small-Angle Neutron Scattering. *Langmuir* **2003,** *19*, 4573-4581.

[71] Legrand, F.; Breyton, C.; Guillet, P.; Ebel, C.; Durand, G. Hybrid Fluorinated and Hydrogenated Double-Chain Surfactants for Handling Membrane Proteins. *J. Org. Chem.* **2016**, *81*, 681−688.

[72] Biswal, N. R.; Paria, S. Wetting of PTFE and Glass Surfaces by Aqueous Solutions of Cationic and Anionic Double-Chain Surfactants. *Ind. Eng. Chem. Res.* **2012**, *51*, 10172−10178.

[73] Jaeger, D. A.; Russell, S. G. G.; Shinozaki, H. Double-Chain Surfactants with Two Quaternary Ammonium Head Groups. *J. Org. Chem.* **1994**, *59*, 7544-7548.

[74] Jaeger, D. A.; Brown, E. L. G. Double-Chain Surfactants with Two Carboxylate Head Groups That Form Vesicles. *Langmuir* **1996**, *12*, 1976-1980.

[75] Dubois, M.; Zemb, T. Phase Behavior and Scattering of Double-Chain Surfactants in Diluted Aqueous Solutions. *Langmuir* **1991**, *7*, 1352-1360.

[76] Bai, G.; Wang, J.; Yan, H.; Li, Z.; Thomas, R. K. Thermodynamics of Molecular Self-Assembly of Cationic Gemini and Related Double Chain Surfactants in Aqueous Solution. *J. Phys. Chem. B* **2001**, *105*, 3105-3108.

[77] Menger, F. M.; Littau, C. A. Gemini Surfactants: A New Class of Self-assembling Molecules. *J. Am. Chem. Soc.* **1993**, *115*, 10083- 10090.

[78] Zana, R.; Talmon,Y. Dependence of Aggregate Morphology on Structure of Dimeric Surfactants. *Nature* **1993**, *362*, 228-230.

[79] Karaborni, S.; Esselink, K.; Hilbers, P. A. J.; Smit, B.; Kartha¨user, J.; van Os, N. M.; Zana, R. Simulating the Self-Assembly of Gemini (Dimeric) Surfactants. *Science* **1994**, *266*, 254-256.

[80] Bhattacharya, S.; De, S. Vesicle Formation from Dimeric Surfactants through Ion-pairing. Adjustment of Polar Headgroup Separation leads to Control over Vesicular Thermotropic Properties. *J. Chem. Soc., Chem. Comm.* **1995**, *0*, 651- 652.

[81] Zana, R. Cur. Opin. Solution Properties of Gemini Surfactant of Decanediyl-1-10-bis (dimethyltetradecylammonium bromide) in Aqueous Medium. *Colloid Interface Sci.* **1996**, *1*, 566-571.

[82] Fletcher, P. DI Self-assembly of Micelles and Microemulsions. *Cur. Opin. Colloid Interface Sci.* **1996**, *1*, 101- 106.

[83] Kevelam, J.; Engberts, J. B. F. N. Formation and Stability of Micelles and Vesicles. *Cur. Opin. Colloid Interface Sci*. **1996**, *1*, 779-789.

[84] Kim, S. S.; Zhang, W. Z.; Pinnavaia, T. J. Ultrastable Mesostructured Silica Vesicles. *Science* **1998**, *282*, 1302- 1305.

[85] Regev, O.; Zana, R. Aggregation Behavior of Tyloxapol, a Nonionic Surfactant Oligomer, in Aqueous Solution. *J. Colloid Interface Sci.* **1999**, *210*, 8-17.

[86] Aramaki, K.; Yamada, J.; Tsukijima, Y.; Maehara, T.; Aburano, D.; Sakanishi, Y.; Kitao, K. Formation of Bilayer Membrane and Niosomes by Double-Tailed Polyglyceryl-Type Nonionic Surfactant. *Langmuir* **2015**, *31*, 10664−10671.

[87] Ghosh, R.; Dey, J. Aggregation Behavior of Poly(ethylene glycol) Chain-Containing Anionic Amphiphiles: Thermodynamic, Spectroscopic and Microscopic Studies. *Journal of Colloid and Interface Science* **2015**, *451*, 53-62.

[88] Aswal, V. K.; Goyal, P. S. Dependence of the Size of Micelles on the Salt Effect in Ionic Micellar Solutions. *Chem. Phys. Lett.* **2002**, *364*, 44–50.

[89] Yu, D.; Huang, X.; Deng, M.; Lin, Y.; Jiang, L.; Huang, J.; Wang, Y. Effects of Inorganic and Organic Salts on Aggregation Behavior of Cationic Gemini Surfactants. *J. Phys. Chem. B* **2010**, *114*, 14955–14964.

[90] Wang, X.; Zhu, J.; Wang, J.; Zeng, G. Micelle Formation and Aggregate Morphology Transition from Vesicle to Rod Micelle for Allyl Alkyldimethylammonium Bromide Cationic Surfactant. *J. Dispersion Sci. Technol.* **2008**, *29*, 83-88.

[91] Yan, Y.; Xiong, W.; Li, X.; Lu, T.; Huang, J.; Li, Z.; Fu, H. Molecular Packing Parameter in Bolaamphiphile Solutions: Adjustment of Aggregate Morphology by Modifying the Solution Conditions. *J. Phys. Chem. B* **2007**, *111*, 2225-2230.

[92] Ryhänen, S. J.; Säily, V. M. J.; Parry, M. J.; Luciani, P.; Mancini, G.; Alakoskela, J. M. I.; Kinnunen, P. K. J. A Mesoscale Lipid Phase Transition from Small Submicroscopic Vesicles to Cytomimetic Membrane Assemblies. *J. Am. Chem. Soc.* **2006**, *128*, 8659–8663.

Chapter 4
pH-Responsive Self-Assembly Formation

4.1 Vesicle-to-Micelle Transition in Aqueous solutions of Hydrocarbon and PEG Chain-Containing Amphiphiles[1]

4.1.1 Scope of the study

As PEG is hydrophilic in nature, it is generally coupled with hydrophobic moiety for developing amphiphilic molecules [1-4]. Thus a number of amphiphilic molecules have been developed by coupling PEG chain with hydrophobic units, such as proteins [5-7], cholesterol [8, 9] etc. However, there are also some reports on hydrophobicity of PEG chain, where the PEG chain has been shown to act like the hydrocarbon (HC) tail of conventional surfactants [10-13]. In previous chapter, vesicle formation by amphiphiles having PEG as hydrophobic tail has been explored in detail. Therefore, it was thought that when both hydrocarbon and PEG chains are covalently linked to a polar carboxylate ($-COO^-$) group, the resulting amphiphilic molecule might behave like a double-tail surfactant. In order to examine this, two amphiphilic molecules, CPOLE and CPMYS (see **Chart 4.1.1**) were designed and synthesized. Both amphiphiles comprised of PEG and HC chains of different lengths which are covalently linked to L-cysteine amino acid. These types of amphiphiles may act either like a single-chain or double-chain surfactant depending upon (i) how the PEG chain behaves and (ii) what molecular conformation is adopted in aqueous medium. Therefore, aggregation behavior of these amphiphiles was investigated thoroughly in pH 7.0 buffer at 25 ^oC. Theoretical calculations were also performed to obtain the stable molecular conformation of the amphiphiles in aqueous solution. Surface activity and *cmc* of the amphiphiles were analyzed by ST method. The self-assembly behavior, and micropolarity and microviscosity of the aggregates were measured through fluorescence probe technique. DLS was used to determine mean d_h value of the aggregates. The morphology of the aggregates was confirmed by use of TEM. The thermodynamics of self-assembly process was studied by ITC. The stability of the aggregates with respect to surfactant concentration (C_s), solution pH, temperature,

[1] *Langmuir* **2017**, *33*, 543−552.

and ageing time was studied. The effect of cholesterol on the physical stability of the self-assembled structures formed by these amphiphiles was also investigated.

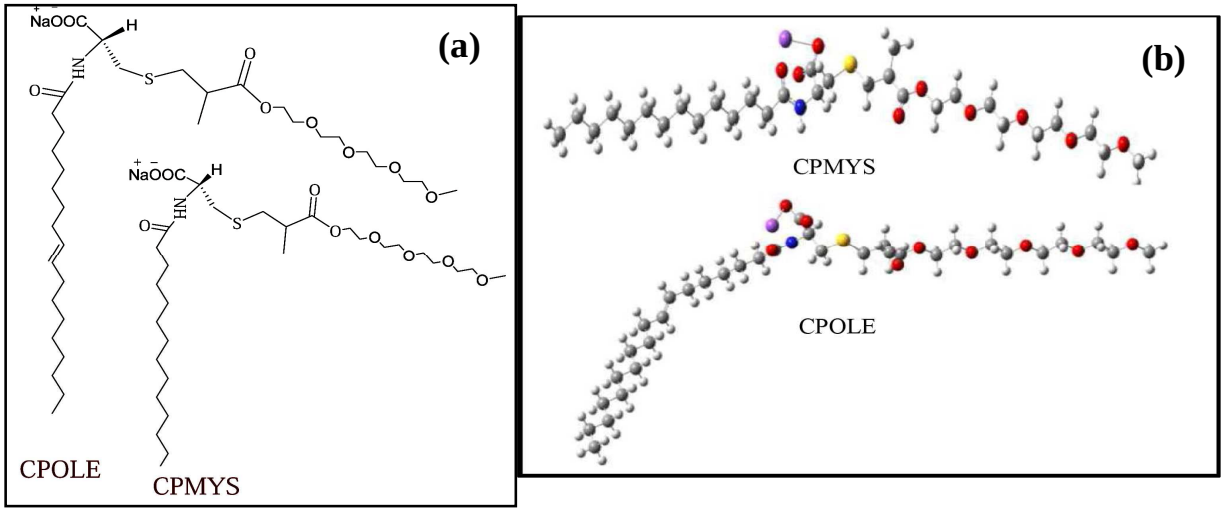

Figure 4.1.1 (a) Chemical structures of CPOLE and CPMYS, and (b) energy-minimized structure of CPOLE and CPMYS in solution phase (water); grey: C, white: H, red: O, blue: N, yellow: S.

4.1.2 Interfacial properties

Surface activity of CPOLE and CPMYS was studied by ST measurements in pH 7.0 buffer at 25 ^{o}C. **Figure 4.1.2** shows the plots of γ versus logC_s, which exhibits two breakpoints, suggesting change of morphology of the aggregates with the increase of surfactant concentration above *cmc*. The surface activity of the amphiphiles can be compared by the minimum surface tension (γ_{min}) and pC_{20} values. For both CPOLE and CPMYS, the γ_{min} value is ca. 30 mN m^{-1} and is similar to those of conventional HC chain surfactants. Also, the pC_{20} values of CPOLE (5.25) and CPMYS (4.84) are higher than conventional anionic surfactants, suggesting higher surface activity. Further, the *cmc* values obtained from the corresponding breakpoints are very low and are similar to those of neutral surfactants [14]. This means that, the HC chain acts as the tail and PEG chain acts as a head group of the amphiphile.

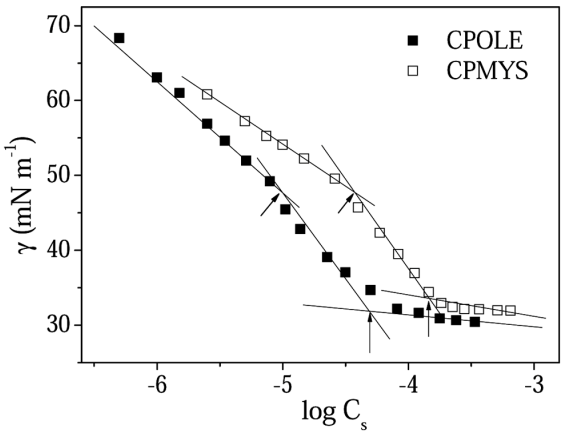

Figure 4.1.2 Plots showing variation of surface tension (γ) as a function of log C_s.

4.1.3 Fluorescence probe studies

As the fluorescence emission spectra of NPN are sensitive to solvent polarity and viscosity change [15], it was employed as a probe to study the self-assembly behavior of CPOLE and CPMYS in aqueous buffer. The representative spectra recorded in the presence of varying concentrations of CPMYS are shown in **Figure 4.1.3(a)**. It can be observed that the fluorescence emission spectrum of NPN not only shifts toward shorter wavelength relative to that in water, but also exhibit an intensity rise with the increase of C_s. The plots of spectral shift ($\Delta\lambda$) of the emission maximum relative to water [$\Delta\lambda = \lambda_{water} - \lambda_{surfactant}$] as a function of C_s are shown in **Figure 4.1.3(b)**. The large blue shift of the fluorescence spectrum suggests that the NPN molecules are solubilized within some hydrocarbon-like environment. The feature of the plots of CPOLE and CPMYS shows two distinct inflections in the sigmoid curve, indicating existence of two overlapping equilibrium processes in the concentration range employed. This is consistent with the existence of two breakpoints in the ST plots and suggests existence of two types of aggregates in buffered solution of the surfactants above a critical concentration. Similar observations have also been reported for many hydrocarbon chain surfactants [16,17].The concentrations corresponding to the inflection points were taken as the *cmc* values and

are included in **Table 4.1.1**. It is observed that the *cmc* values obtained by fluorescence titration are closer to the respective value obtained by ST measurements.

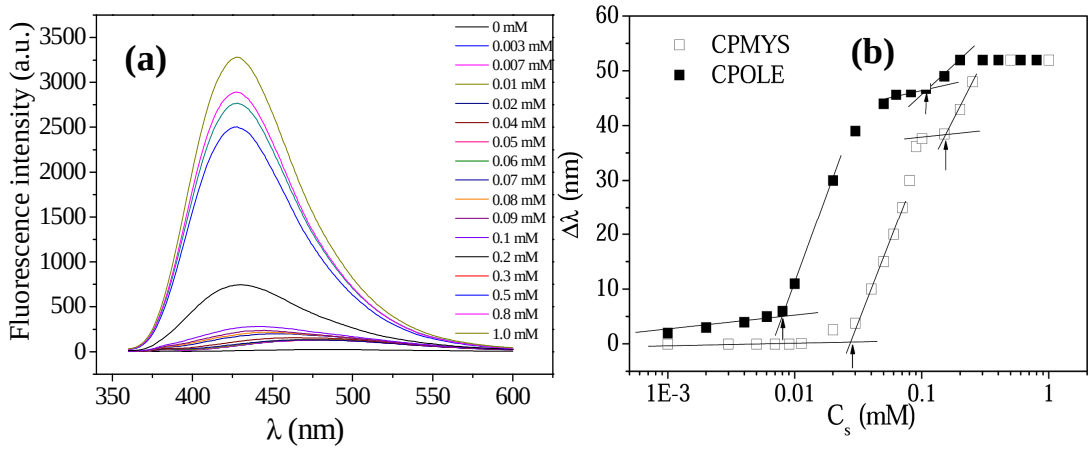

Figure 4.1.3 (a) Representative fluorescence emission spectra of NPN in pH 7.0 buffer and different concentrations of CPMYS (b) spectral shift (Δλ) of NPN as a function of C_s in pH 7.0 at 25 ^{o}C: (■) CPOLE, and (□) CPMYS.

Table 4.1.1 Self-assembly properties of CPOLE and CPMYS surfactants in aqueous solutions of pH 7.0 and 3.0 at 25 ^{o}C.

pH	Surfactant	*cmc* (μM)		I_1/I_3	η_m	d_h (nm)
		ST	Fluorescence			
7.0	CPOLE	10 ± 10	10 ± 10	1.02 ± 0.02[a]	22.3 ± 3.0[a]	5.5[a]
		100 ± 30	110 ± 15			
	CPMYS	37 ± 10	28 ± 10	1.02 ± 0.03[b]	25.8 ± 5.0[b]	10.5[b]
		150 ± 50	160 ± 30			
3.0	CPOLE	_	4 ± 2	1.05 ± 0.01[a]	45.2 ± 4[a]	30[a]
	CPMYS	_	8 ± 2	1.06 ± 0.01[b]	56.3 ± 5[b]	40[b]

[a][CPOLE] = 2 mM; [b][CPMYS] = 2 mM.

4.1.4 Thermodynamics of self-assembly formation

To conjecture the mechanism of self-assembly formation the ITC method was employed to determine all the thermodynamic parameters associated with the process. In the present study, the thermodynamic parameters were determined by ITC at 25 ^{o}C using 0.5 mM or 3 mM stock solution of CPOLE, and 1 mM or 4 mM stock solution of CPMYS. The ITC thermograms of the amphiphiles obtained by use of lower and higher stock concentrations are depicted in **Figure 4.1.4**. The plots show a sigmoid increase of enthalpy with the increase of C_s. The feature ITC titration curves also suggest existence of two aggregation processes for both CPOLE and CPMYS in the concentration range employed. The *cmc* values of the amphiphiles obtained from the inflection point of the respective plot are close to the corresponding value obtained by ST measurements and fluorimetric titrations.

The thermodynamic parameters obtained from the respective plots are summarized in **Table 4.1.2**. The spontaneity of aggregate formation is suggested by the very large negative and positive values of ΔG^{o}_{m} and ΔS^{o}_{m}, respectively [18, 19]. The very large negative values of ΔG^{o}_{m} also indicate that the transition between two types of aggregates at high surfactant concentrations is spontaneous, but less favored in comparison to the aggregate formation in dilute solution. Further, the $T\Delta S^{o}_{m}$ value of both the surfactants is found to be much larger than that of the ΔH^{o}_{m} value, which means spontaneous aggregate formation is an entropy-driven process. This means that the driving force for aggregation is hydrophobic interaction [20]. The release of water molecules around the hydrocarbon tails contributes to the large entropy rise facilitating the self-assembly process. This suggests that the aggregation process of the two surfactant systems is similar to most hydrocarbon tail surfactants. The thermodynamic parameters of the surfactants demonstrate that the aggregate formation is much more feasible and spontaneous compared to not only conventional ionic surfactants with hydrocarbon tail, but also to those with only PEG-tail [12-13]. This must be due to the reduction of ionic repulsion among $-COO^{-}$ groups due to the stealth properties of the PEG chains on the surface.

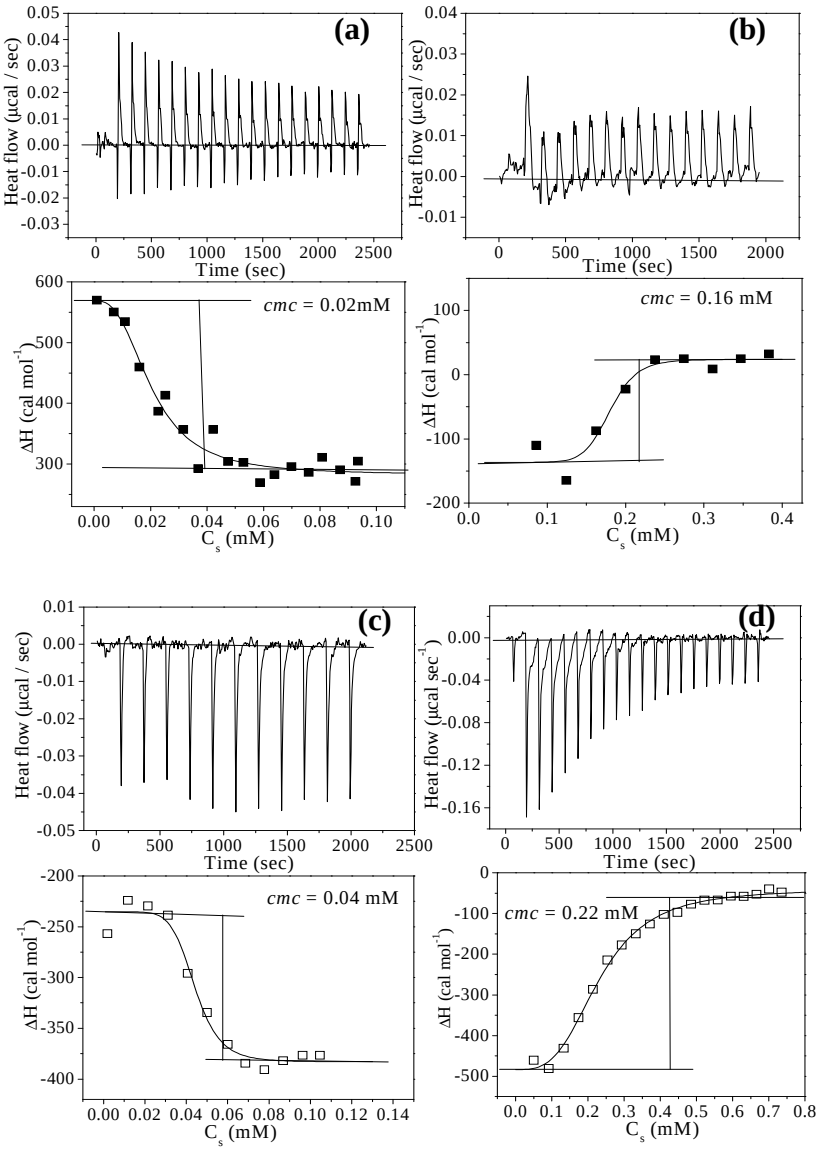

Figure 4.1.4 ITC profiles of the stock concentrations (a) 0.5 mM CPOLE, (b) 3 mM CPOLE, (c) 1 mM CPMYS, and (d) 4 mM CPMYS.

Table 4.1.2 Critical micelle concentration (*cmc*), standard Gibbs energy change (ΔG^{o}_{m}), standard enthalpy change (ΔH^{o}_{m}) and standard entropy change (ΔS^{o}_{m}) of micelle formation in aqueous buffered solution (pH 7.0) by CPOLE, and CPMYS at 25 ^{o}C.

Surfactant	cmc_1 (μM)	cmc_2 (μM)	ΔH_1 (kJ/mol)	ΔH_2 (kJ/mol)	ΔG_1 (kJ/mol)	ΔG_2 (kJ/mol)	ΔS_1 (J K^{-1}/ mol)	ΔS_2 (J K^{-1}/ mol)
CPOLE	20 (± 10)	160 (± 40)	–1.13 (± 0.10)	+0.42 (± 0.06)	–48.25	–38.98	+158	+132
CPMYS	37 (± 20)	200 (± 40)	–0.61 (± 0.09)	+1.78 (± 0.07)	–44.74	–37.56	+149	+131

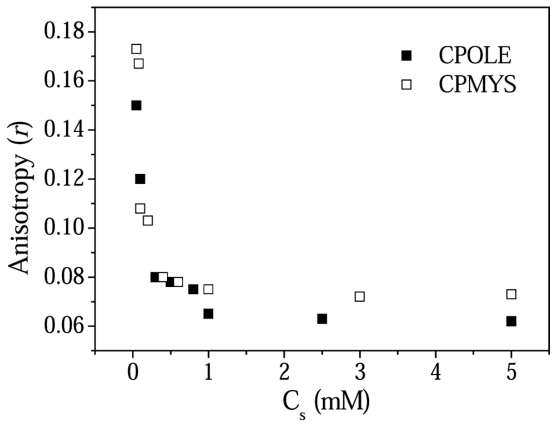

Figure 4.1.5 Plots of fluorescence anisotropy (*r*) of DPH versus surfactant concentration (C_s) at 25 ^{o}C: (■) CPOLE, (□) CPMYS.

4.1.5 Microenvironment of the aggregates

The micropolarity of the self-assemblies both amphiphiles was estimated by use of Py as the fluorescent probe. The I_1/I_3 values (**Table 4.1.1**) of Py probe in the presence of

CPOLE (2 mM) and CPMYS (2 mM) amphiphiles are very low compared to that in water (1.82). This means that Py is solubilized within the hydrophobic micro domains of self-assemblies consisted of only HC tails [21, 22]. The I_1/I_3 values, within the limit of experimental error, are almost equal for CPOLE and CPMYS. This is because Py is solubilized deep into the hydrocarbon region of the aggregates. It is interesting to note that the I_1/I_3 values of CPOLE and CPMYS are much less than those of conventional HC tail surfactants. This means that the HC tails of the surfactant molecules in the aggregates are tightly packed and as a result, the degree of water penetration is very low.

Thus the value of *r* which is an index of microviscosity (or microfluidity) was measured using DPH probe [23, 24]. The plots in **Figure 4.1.5** show the variation of *r* with the change of C_s of CPOLE and CPMYS. As observed the *r* value is very high at low concentrations, but decreases upon increase of C_s. The higher value of *r* in low concentration is indicative of ordered environment around the DPH probe and suggests the existence of bilayer vesicles in dilute solution of the amphiphiles. However, smaller *r* value at high C_s values suggests existence of loosely-packed self-assemblies, such as micelles [25]. The decrease of steady-state *r* value of DPH probe clearly indicates that the vesicles with rigid bilayer membrane are transformed into small micelles with the increase in concentration of the amphiphile.

Table 4.1.3 Fluorescence anisotropy (*r*), lifetime (τ_f), and rotational correlation time (τ_R) of DPH, and microviscosity (η_m) of the surfactant self-assemblies at pH 7.0 at 25 ^oC at different concentrations; the quantities within parenthesis presents corresponding χ^2 values.

Surfactant	C_s (mM)	*r* (±0.001)	τ_f (±0.1ns)	τ_R (ns)	η_m (mPa s)
CPOLE	0.08	0.162	3.9 (1.14)	3.17	49.6
	1	0.067	5.8 (1.09)	1.48	22.3
CPMYS	0.05	0.175	3.67 (1.1)	3.43	55.8
	1	0.073	6.7 (1.07)	1.69	25.8

In order to quantify the rigidity of the microenvironments of the aggregates, microviscosity (η_m) was also determined using corresponding r and τ_f values (**Table 4.1.3**). The η_m-values of concentrated (2 mM) CPOLE and CPMYS is 22.3 mPa s^{-1} and 25.8 mPa s^{-1}, that are similar to those of micellar aggregates of SDS and DTAB surfactants [26]. However, at low surfactant concentrations, for example, in 0.08 mM CPOLE (49.6 mPa s^{-1}) and 0.1 mM CPMYS (55.8 mPa s^{-1}) the η_m values of the self-assemblies are relatively higher, which is indicative of formation of closed bilayer vesicles as also suggested by the TEM pictures as shown below.

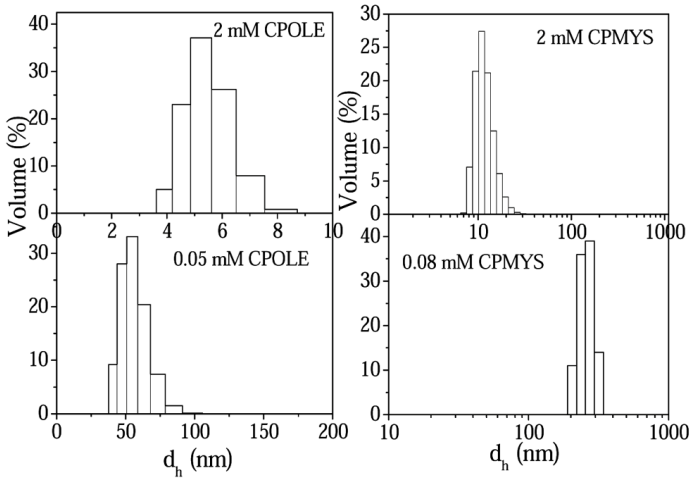

Figure 4.1.6 Size distribution histograms of CPOLE in solutions of pH 7.0 with C_s = 0.05 and 2.0 mM, and of CPMYS with C_s = 0.08 and 2.0 mM at 25 ^oC.

4.1.6 Hydrodynamic size and morphology of aggregates

To investigate the structural transition in solutions of CPOLE and CPMYS, DLS measurements were carried out and the mean d_h value of the aggregates was measured at different concentrations. The size distribution histograms of the aggregates are shown in **Figure 4.1.6**. In dilute solution, a monomodal distribution with large mean d_h value of ~ 60 nm for CPOLE and ~ 250 nm for CPMYS is observed, suggesting existence of large aggregates. On the other hand, the monomodal size distribution with a much smaller

mean d_h value of ~ 5 nm for CPOLE and ~ 10 nm for CPMYS in moderately concentrated solutions clearly indicates existence of small micelles. This means both CPOLE and CPMYS produce larger aggregates at lower concentrations, which transform into a much smaller micelle-like aggregates upon increase of concentration.

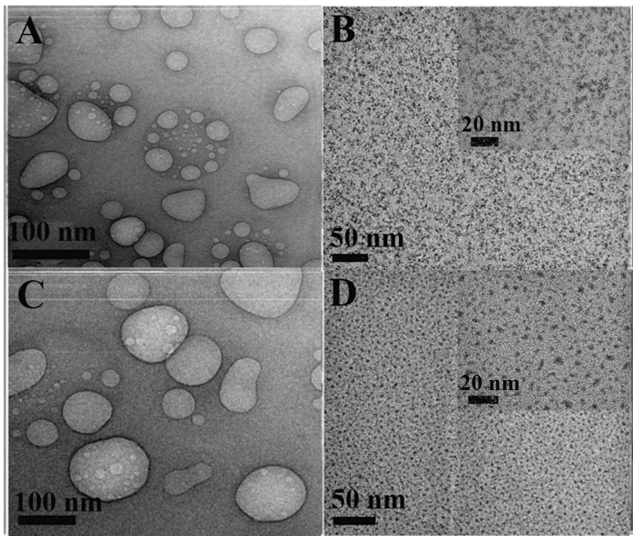

Figure 4.1.7 HRTEM micrographs of (A) 0.05 mM CPOLE, (B) 3 mM CPOLE (inset: enlarged image), (C) 0.08 mM CPMYS, (D) 3 mM CPMYS (inset: enlarged image) in pH 7.0 buffer.

In order to determine morphology of the aggregates, TEM measurements were carried out using both dilute and concentrated solutions of CPOLE and CPMYS. The unstained HRTEM micrographs of the specimens are shown in **Figure 4.1.7**. Large closed spherical vesicles can be observed in dilute aqueous solutions of both amphiphiles. However, at higher concentrations, only small micelle-like microstructures are found with both CPOLE and CPMYS. It should be noted that though the sample preparation involved drying, the results were reproducible. Although because of low resolution, it is difficult to comment on the exact number of lamella of the vesicles, they appear to have a thin boundary corresponding to ULVs. The deformation observed in the vesicular

structure could be due to fusion of smaller vesicles facilitated by the exchange of amphiphiles between two interacting vesicles. As a result, the vesicles are polydisperse (which is normal with spontaneously formed vesicles) in size with d_h value in the range of 50 to 200 nm. However, the results are consistent with those of DLS measurements. The existence of small aggregates (micrographs B and D) in concentrated surfactant solutions is also consistent with the results of DLS measurements.

The ζ-potential value which is a measure of surface charge and determines the stability of colloid particles was measured in solution of CPOLE and CPMYS at different concentrations and pH. The data are accumulated in **Table 4.1.4**. Relatively low ζ-potential values are expected for the carboxylate surfactants, as the salts hydrolyze in dilute solution to produce corresponding acid form, facilitating formation of acid-soap dimer. Consequently, in dilute solution, the stronger intermolecular attraction induces the amphiphilic molecules to pack tightly thereby producing large vesicular aggregates. On the other hand, higher ζ-potential value in concentrated solution means greater repulsion among head groups and hence formation of smaller aggregates. The very low ζ-potential values for the aggregates of both surfactants at pH 3.0 suggest formation of uncharged micelles due to conversion of soap to acid form of the amphiphile as discussed below.

Table 4.1.4 ζ-potential (mV) values of CPOLE and CPMYS surfactant solutions of different concentrations at pH 7.0 and 3.0.

Surfactant	C_s (mM)	ζ-values at pH 7.0(mV)	ζ-values at pH 3.0(mV)
CPOLE	0.05	–11.5	
	1	–18.5	–0.8
CPMYS	0.08	–10.0	
	1	–13.5	–0.4

4.1.7 Vesicle-to-micelle transition

From the above discussion it can be concluded that the first *cmc* (cmc_1) corresponds to vesicle formation and therefore it can be referred to as critical vesicle concentration (*cvc*). On the other hand, the second *cmc* (cmc_2) is actually the critical concentration for the vesicle-to-micelle phase transition. Several mechanisms of vesicle-to-micelle transition, including monomer diffusion and fusion of vesicles have been suggested [27, 28]. The vesicles have a dynamic structure between monomers and vesicles. Actually in dilute solutions of the amphiphiles in pH 7.0, hydrolysis of the salt form of the surfactant produces its acid form. When their concentrations are equal they interact through H-bonding and thus produce acid-soap dimers. Since the electrostatic repulsion between head groups is eliminated, the acid-soap dimers self-organize to produce large aggregates, such as bilayer vesicles. Such behavior of the amphiphiles is quite similar to that of medium and long chain fatty acid salts [29-32]. However, at higher concentrations, due to the decrease of degree of hydrolysis the carboxylate form predominates, resulting in an increase of electrostatic repulsion among amphiphiles and thereby triggering reorganization of bilayer vesicles to form small spherical micelles.

According to the results of fluorescence probe studies the HC chain of the amphiphiles constitute the bilayer membrane of vesicles at low concentrations and the core of micelles at higher concentrations. The spatial arrangement of the surfactant molecules in the aggregated state was further inferred from the 2D NOESY ^{1}H-NMR spectra (**Figure 4.1.8**) of CPOLE**,** as a representative example. As the *cvc* values of the amphiphiles are very low, it was difficult to record NOESY spectra in the vesicular state of the surfactant. Therefore, NOESY spectrum was recorded in D_2O at the micellar state of CPOLE at C_s = 2 mM. From the NOESY analysis it is clear that there are mainly diagonal interactions along with some key cross interactions, which imply that the only interactions between adjacent H atoms in the PEG chain and hydrocarbon chain were observed. In other words, only intra- and intermolecular interactions among PEG chains and HC chains were observed for CPOLE in their aggregated state. Thus the spatial interactions of the H atoms indicate micelle-like aggregate formation by CPOLE at higher concentrations.

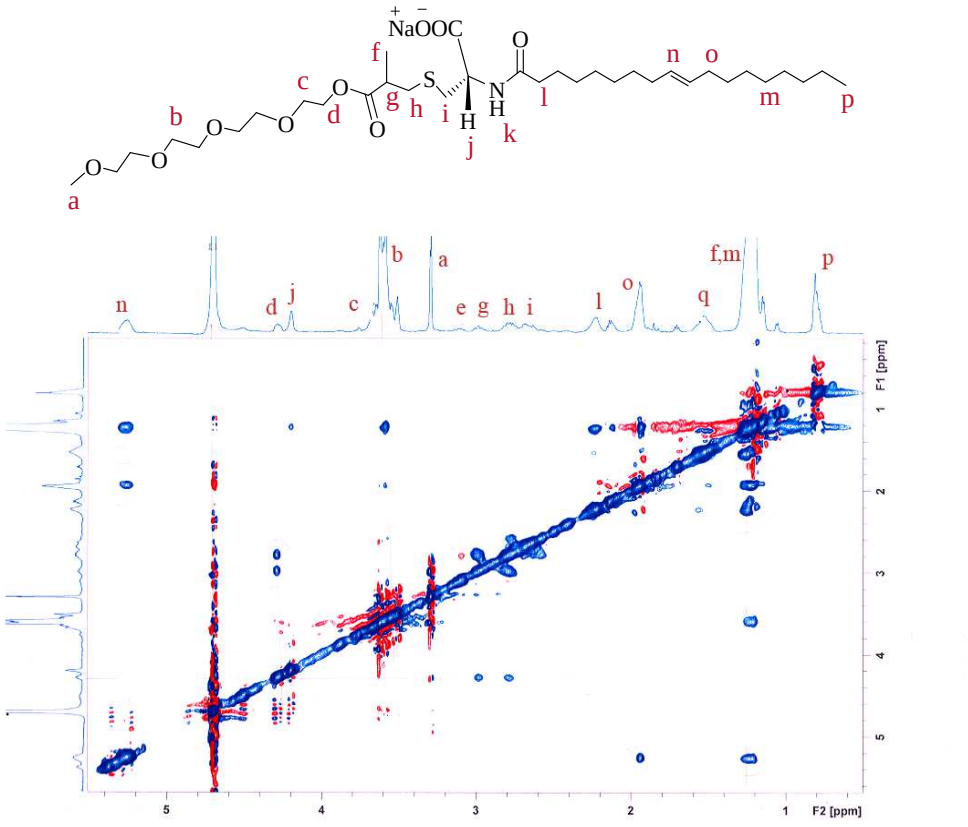

Figure 4.1.8 The 2D NOESY ^{1}H-NMR spectrum of 2mM CPOLE in D_2O solvent.

4.1.8 Effect of pH on aggregate morphology

The surfactants CPOLE and CPMYS being sodium salts of carboxylic acids, it is expected that change of pH will have an effect on the aggregation behavior of the amphiphiles [33-38]. This is because the pH-induced protonation of the $-COO^-$ group affects the hydrophilic interaction between the head groups of the ionic amphiphile and hence will have a defining effect on *cvc* value as well as on the shape and size of the aggregates formed by the surfactant molecules. The *cmc* values (4 μM for CPLOLE and 8 μM for CPMYS) of the surfactants were therefore measured at pH 3.0 using NPN as a fluorescent probe. The fluorescence titration curves are shown in **Figure 4.1.9(a)**. It is

interesting to note that the plots exhibit only one inflection point. The *cmc* values obtained from the concentration corresponding to the inflection point are found to be much less than the *cvc* value obtained at neutral pH. This is expected because at pH 3.0 the $-COO^-$ group being protonated, the surfactant molecule exists mainly in the neutral form. Thus as a result of elimination of charge repulsion among head groups, the *cmc* value decreased for both surfactants (**Table 4.1.1**). As can be seen from the fluorescence titration curves the fluorescence spectrum of NPN is highly blue shifted relative to that in water, suggesting that the micelles have hydrocarbon-like micellar core. The effect of the pH on the microenvironment is also indicated by the I_1/I_3 ratio of Py probe. The data in **Table 4.1.1** show that the micelles in pH 3.0 have micropolarity like hydrocarbon solvents.

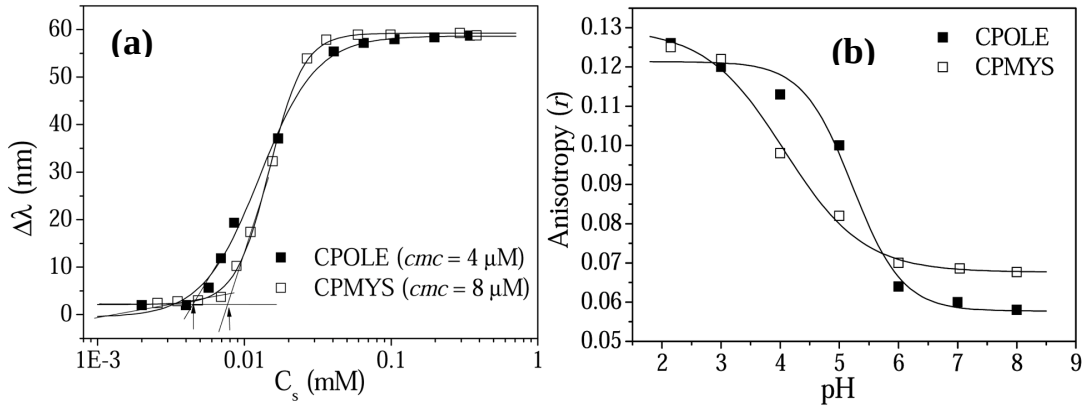

Figure 4.1.9 Plots of (a) spectral shift ($\Delta\lambda$) of NPN as a function of surfactant concentration (C_s) in pH 3.0, and (b) variation of anisotropy (r) of DPH with in 2 mM CPOLE and 2 mM CPMYS at 25 ^oC.

The rigidity of the microenvironment was monitored by fluorescence anisotropy of DPH probe. The variation of r as a function of pH has been depicted in **Figure 4.1.9(b)**. The sigmoidal plots clearly indicate existence of a two-state equilibrium between the $-COO^-$, and –COOH forms of the amphiphilic molecules. The pK_a values thus obtained from the inflection points of the plots are ~5.5 and ~4.5 for CPOLE and

CPMYS, respectively. This suggests that at pH 3.0, both the amphiphilic molecules are present mostly in the neutral carboxylic acid form. This means a reduction of the electrostatic repulsion between head groups and hence a tighter packing of the monomers in the aggregates at pH ≤ 3, as indicated by the higher η_m value (**Table 4.1.1**) of the micelles.

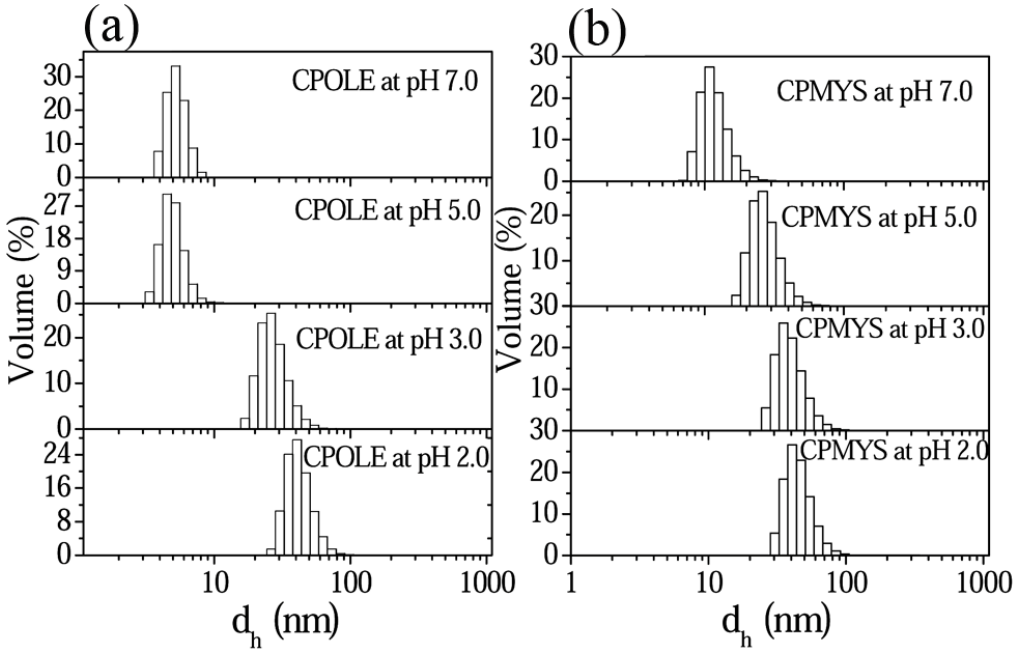

Figure 4.1.10 Size distribution histograms of (a) 2 mM CPOLE, and (b) 2 mM CPMYS at different pHs.

The tight packing of the charge neutral surfactant monomers in the aggregates as discussed above will result in a growth of micelles at low pH. Therefore, the mean d_h value of the micelles was measured for both CPOLE and CPMYS molecules at different pH. The size distribution histograms have been shown in **Figure 4.1.10**. It is observed that the mean d_h value increased relative to that in neutral pH. This suggests formation of larger micelles in acidic pH, which is confirmed by the HRTEM images of the surfactant solutions at pH 3.0. Indeed, both micrographs (E) and (F) in **Figure 4.1.11(a)** exhibit large disk-like micelles for CPOLE and CPMYS molecules.

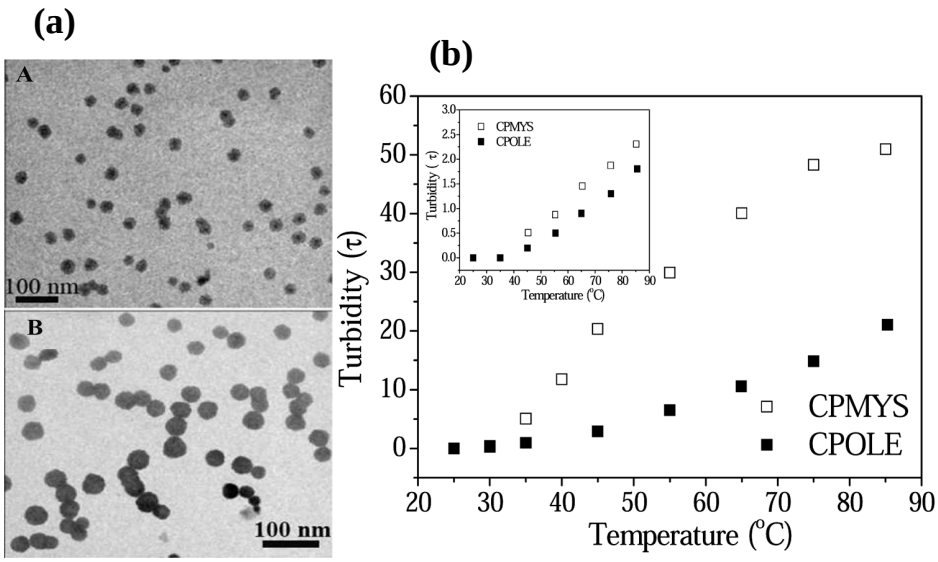

Figure 4.1.11 (a) HRTEM images of (A) 2 mM CPOLE and (B) 2 mM CPMYS at pH 3.0; (b) plots of turbidity (τ) as a function of temperature (^{o}C) of the surfactant solutions (0.5 mM) at pH 3.0: (■) CPOLE, and (□) CPMYS (inset: turbidity plots at pH 7.0).

4.1.9 Effect of temperature on vesicle stability

As PEG chain-containing neutral surfactants and polymers are known to undergo dehydration at higher temperatures and fall out of solution showing appearance of turbidity [39], the temperature variation of turbidity of the solutions of CPOLE and CPMYS amphiphiles was measured in the temperature range of 20 to 80 ^{o}C at different concentrations. However, the surfactant solutions at pH 7.0 did not exhibit any significant turbidity in the concentration rage (0.05 to 2 mM) studied as evident from the plots in the inset of **Figure 4.1.11(b)**. This means that the aggregates of CPOLE and CPMYS are stable at the physiological pH (7.4) and temperature (37 ^{o}C). In contrast, surfactant solutions (0.05 mM) of both surfactants at pH 3.0 exhibit clouding of the solution. The temperature dependence of turbidity (τ = 100 − %T) has been shown in **Figure 4.1.11(b)**. As can be seen CPMYS exhibits ~50% turbidity upon elevation of temperature to 85 ^{o}C. The cloud point (T_c) appears to be ~43 ^{o}C. The T_c value, however, is found to be less at

higher concentrations of CPMYS molecule. On the other hand, for CPOLE, the turbidity of 0.05 mM solution was found to be less (< 20 %) even at the highest achievable temperature (85 ^{o}C) in water and the T_c value is observed to be ~ 55 ^{o}C. This suggests that nonionic CPMYS (at pH 3.0) may have potential application in the field of drug delivery for hydrophobic therapeutic agents.

4.1.10 Shelf-life of the aggregates

It should be noted that the PEG chain covalently attached to the surfactant head group contains a hydrolysable ester linkage. The hydrolysis of the surfactant could destabilize the vesicles or micelles at room temperature even at neutral pH. Therefore, it is important to determine the shelf-life of the vesicles/micelles formed by these amphiphiles in neutral pH at room temperature. In order to determine the stability of colloidal formulation, the turbidity of the solutions of CPOLE and CPMYS was measured at different time intervals. Turbidity, generally, arises from the scattering of light by the aggregates, and depends on their sizes and populations. The turbidity of 0.05 mM and 0.5 mM CPOLE, and 0.08 mM and 0.5 mM CPMYS solutions in pH 7.0 buffer was monitored at 450 nm at different time intervals during 30 days. The results are summarized in **Figure 4.1.12(b)**. It is important to note that in the concentration range employed, the turbidity remains almost constant at ≤10 % throughout the aging period, showing good storage life of the vesicles as well as of the micelles.

4.1.11 Effect of cholesterol on stability of bilayer membrane

As mentioned earlier, the ULVs get deformed as a result of fusion with each other due to exchange of amphiphilic molecules. Therefore, in order to enhance the stability of vesicles in dilute solution, Chol was added to the surfactant solution. It is a well-known and major component of biological membrane lipids which controls the fluidity, diffusional mobility and permeability of membrane [40, 41]. Usually, there is an upper limit to Chol incorporation within the aggregate, above which Chol seems to precipitate as crystals of pure Chol either in the monohydrate or in the anhydrous form. Indeed, the solubility of Chol in the vesicle bilayer was found to be only ~ 2 mol% in 0.08 mM

solution of CPOLE and CPMYS. In the presence of 2% Chol, the *r* value of DPH probe was observed to increase from 0.162 to 0.263 for CPOLE and from 0.175 to 0.282 for CPMYS (**Figure 4.1.12(a)**), indicating increase of bilayer rigidity and hence physical stability of the vesicles.

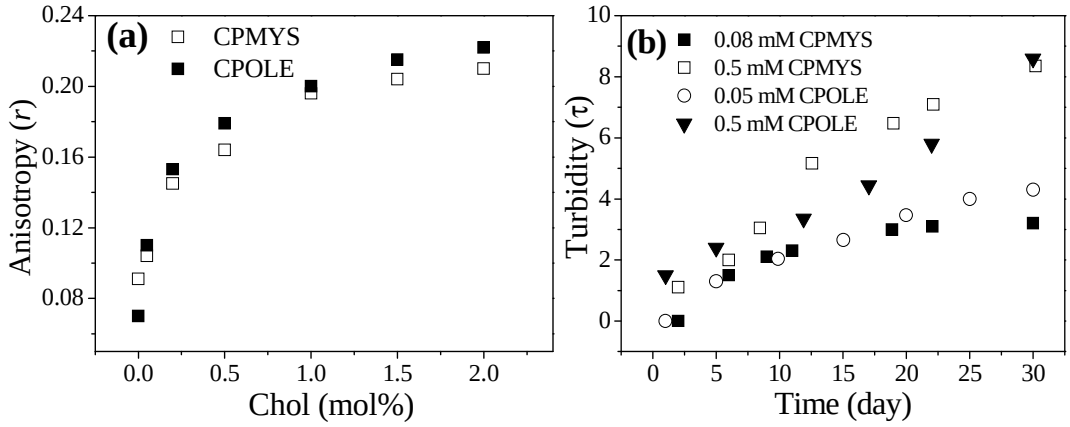

Figure 4.1.12 Plots of (a) variation of *r* value of DPH in 0.08 mM CPMYS with the variation of Chol (mol %), and (b) change in turbidity with the variation of time.

4.1.12 Encapsulation of curcumin

The results of solubility of Chol in the vesicle solutions of CPOLE and CPMYS led to the conclusion that hydrophobic compounds can be solubilized within the non-polar microenvironments of their vesicles. Therefore, the solubility of curcumin was measured in micellar solutions of both surfactants. Surprisingly, encapsulation efficiency was found to be ~ 80 % for CPMYS, and ~ 50 % for CPOLE. As a result of incorporation into the surfactant micelles, the rate of hydrolytic degradation of curcumin was observed to be drastically suppressed. The degradation rate of curcumin was monitored by recording the UV-Vis spectra after certain intervals. It is reported that, after 1 h interval, 80% of curcumin is degraded in an aqueous buffer solution of pH 7.4 [42]. In the present work, the extent of curcumin degradation inside the micelles was determined by monitoring the time dependent absorption spectra, as shown in **Figure 4.1.13(a)**. Inside CPMYS

micelles, the degradation rate is observed to be 10% and for CPOLE micelles it is 12% after 1 day of incubation. The fluorescence emission spectra were also taken at different time intervals (**Figure 4.1.13(b)**). The large blue shift (45 nm) of the spectrum along with a huge amount of intensity enhancement upon encapsulation into the micelles even after 1 day reveals high curcumin encapsulation efficiency and very low degradation rate of the curcumin in the CPOLE and CPMYS micelles. This means the surfactant micelles could act as a good stabilizer for curcumin. A plausible explanation for higher stability of curcumin inside CPOLE and CPMYS micelles is the ability to form hydrogen bonds with the enol form of the β-diketone linker of curcumin with the amide and/or ester linkages. Similar degradation rates are also reported for curcumin on binding with hydrophobic cavities present in cyclodextrins and proteins [43]. Qian et al. recently established that the stability of curcumin increased drastically upon encapsulation into polymeric micelles [44]. Moreover, it was also demonstrated that the efficiency of intravenous application of curcumin-loaded micelles is higher than that of free curcumin. Thus it can be concluded that the CPOLE and CPMYS micelles can be potentially good carriers of curcumin.

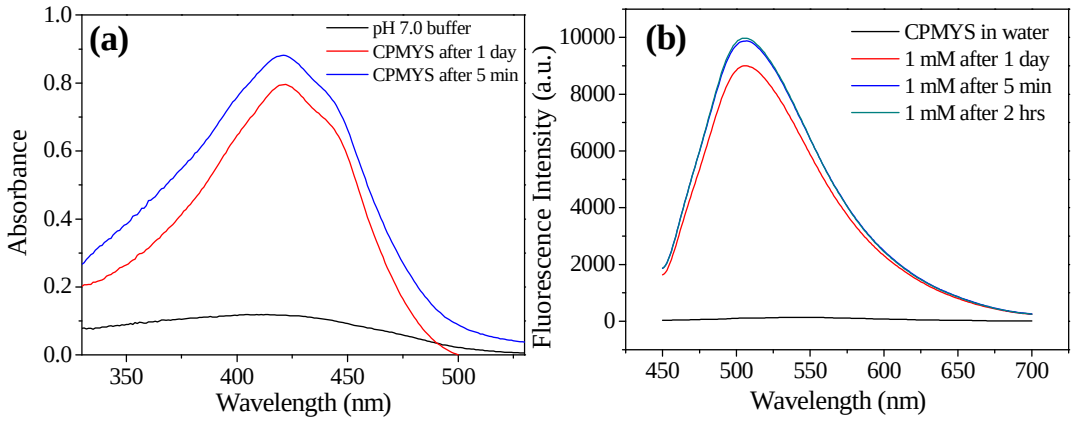

Figure 4.1.13 (a) Absorption and (b) emission spectra of curcumin in buffer (pH 7.0) and 1 mM CPMYS micelles at different time intervals after encapsulation.

4.1.13 Summary

In summary, two anionic surfactants CPOLE and CPMYS containing both PEG and hydrocarbon chain have been developed, and characterized. Both surfactants exhibit very good surface activity in pH 7.0 buffer at 25 ^{o}C. The surfactants were observed to self-organize spontaneously to form unilamellar vesicles (ULVs) in very dilute solution. However, the vesicles are transformed into micelles upon increase in concentration of the amphiphile. The *cmc* values for vesicle and micelle formation are relatively low. The thermodynamic data suggest that both vesicles and micelles are formed spontaneously in solution above a relatively low *cmc* value. The large positive values of ΔS^{o}_{m} indicate that the driving force behind the spontaneous vesicle/micelle formation is hydrophobic interaction. The micropolarity of both vesicles and micelles were observed to be much less compared to bulk water, suggesting that the vesicle bilayer and the micelle core are constituted by the hydrocarbon chains of the CPOLE and CPMYS molecules. This means the PEG chains are directed either toward aqueous core of the bilayer vesicles or to toward bulk water. At a pH below their pK_a value, both amphiphiles form large disk-like micelles above a very low critical concentration (*cmc* $\approx$ 5 μM). The vesicles as well as micelles were observed to be stable in the temperature range 20–75 ^{o}C at pH 7.0 over a long period of time. However, at pH 3.0, micelles of CPMYS surfactants exhibit clouding at a temperature of about 43 ^{o}C as a result of temperature-induced dehydration of the PEG chains. The ULVs formed in dilute solutions of CPOLE and CPMYS become more stable upon addition of cholesterol as additive. Despite having ester linkage in the molecular structure of the surfactants, the ULVs of both surfactants were found to be stable at pH 7.0 for more than 30 days. Thus, the ULVs formed by CPOLE and CPMYS can have potential applications in drug delivery.

4.2 Self-assembly Behavior of Cholesterol and PEG Chain-Containing Amphiphiles at Room Temperature

4.2.1 Scope of the study

In the preceding section, spontaneous and stable vesicle formation followed by vesicle-to-micelle transition by a couple of amphiphiles having different amount of hydrophobe has been demonstrated [45]. The excellent surface properties, versatile self-assembly behavior and drug solubilization capacity of both hydrocarbon and PEG chain-containing amphiphiles (CPOLE and CPMYS) led to this study to investigate the surface properties and self-assembly behavior of two structurally similar amphiphiles bearing Chol as hydrophobe. The self-assembled nanostructures produced by the amphiphiles containing Chol were expected to increase the solubilization capacity of drug molecules and shelf-life of the aggregates. Also, Chol is a fundamental structural and functional component of animal cell membrane, whereby it controls membrane fluidity and permeability [46-48]. It also works as a precursor for the biosyntheses of steroid hormones, bile acids, and vitamin D [49]. Moreover, it involves many membrane related bioprocesses, such as intracellular transport, signal transduction, and cell trafficking within the cell membrane [50-52]. Thus it was thought that incorporation of Chol in the amphiphile structure might be helpful making more biocompatible and more rigid drug delivery system. PEG was taken as the hydrophile because of its good water solubility, biocompatibility, and reduced uptake by the RES [49-51], which result in a prolonged blood circulation time in comparison to non-PEG derivatives. The versatile applications of PEG and PEGylation towards various fields of research have already been discussed in the Chapter 1 [53-58].

There are also numerous reports on PEG-Chol conjugates. Due to relatively good biocompatibility with the host, as well as low toxicity profiles [59], PEG-Chol conjugates are used to obtain PEGylated drug delivery system (DDS), such as micelles [60], liposomes [61], nanoparticles [62], hydrogels etc. When combined with the oral or injectable administration of PEG-Chol based therapeutic agents, PEGylated DDS are now used to treat many infectious diseases, central nervous system diseases, augmentation of cancer chemotherapies, enhance imaging efficiency in vivo, and to optimize numerous in

vivo gene therapy applications [63]. Furthermore, biodegradable PEG-Chol conjugates can effectively prolong circulation half-life time of liposomes or vesicles [64].

Therefore, in this work, two carboxylate surfactants (CPCF3 and CPCF11) were developed by conjugating both Chol and PEG chain with L-cysteine amino acid. The chemical structures of CPCF3 and CPCF11 are depicted in **Figure 4.2.1.** The structures of molecules differ only in their PEG chain lengths. The aim of this work is to (i) physicochemically characterize the pH-sensitive nanoaggregates using different experimental conditions and (ii) compare the results between themselves as well as with those of CPOLE and CPMYS surfactants.

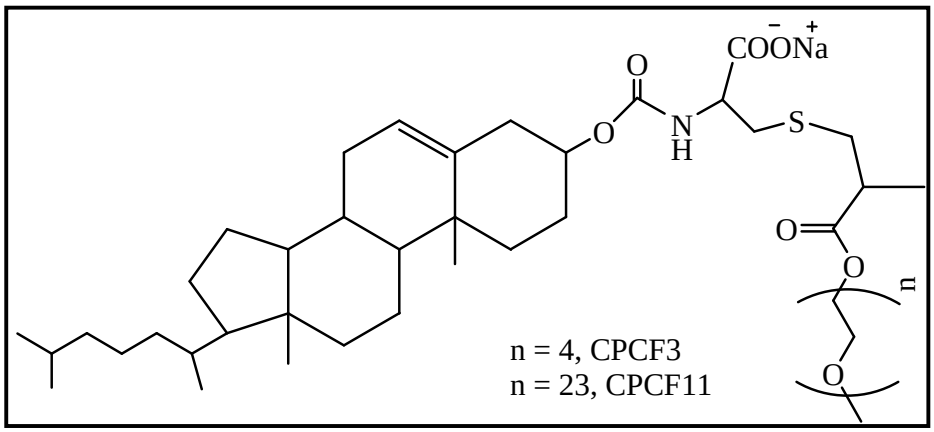

Figure 4.2.1 Molecular structure of CPCF3 and CPCF11.

4.2.2 Surface activity

As CPCF3 and CPCF11molecules are consisted of both hydrophobic and hydrophilic groups, they are expected to reduce surface tension (γ) of water. Therefore, surface tension of pH 7 buffer was measured in the presence of different concentrations (C_s) of the amphiphiles at room temperature. The data are presented in **Figure 4.2.2.** The reduction of γ value of water with increasing C_s suggests that the amphiphiles are surface

active. The pC_{20} values of the molecules were observed to be 4.45 for CPCF3 and 4.67 for CPCF11 which suggest that they are highly surface active. However, the surface activities of CPCF3 and CPCF11 are less than those of CPOLE and CPMYS surfactants which can be attributed to the bent structure of the Chol unit preventing tight packing of the molecules at the air/water interface. Since the γ value decreased over a large concentration range and there was no sharp break in the surface tension plot, it was difficult to determine *cmc* from these plots. Therefore, fluorescence probe technique was used to determine *cmc* of the surfactants as described below.

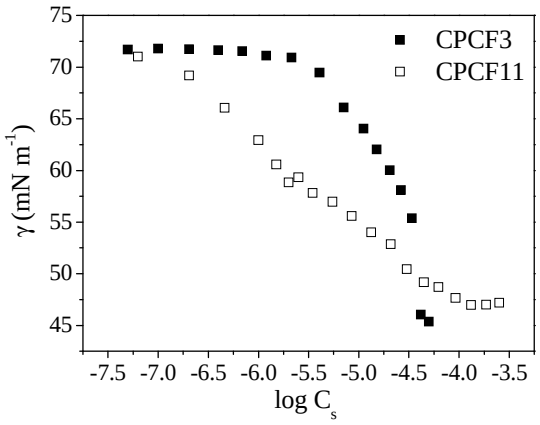

Figure 4.2.2 Plots showing variation of surface tension (γ mN m^{-1}) of water with log C_s of CPCF3 and CPCF11 in pH 7.0 buffer at 25 ^oC.

4.2.3 Self-assembly formation

In order to study the self-association behavior of the surfactants, the steady-state fluorescence titration experiments were performed using NPN as probe molecule. As a representative example, the fluorescence spectra of NPN measured in the presence of different concentrations of CPCF3 surfactant are depicted in **Figure 4.2.3 (a)**. A ~ 70 nm blue shift of the λ_{max} along with a 35 to 40-fold intensity rise of NPN fluorescence spectrum can be observed in presence of CPCF3 surfactant. The variation of spectral shift (Δλ) with C_s has been shown in **Figure 4.2.3(b)**. The *cmc* value as obtained from the

concentration of the onset of rise of the plot is 0.4 μM and 0.9 μM for CPCF3 and CPCF11, respectively. The *cmc* values are much less than those of CPOLE and CPMYS surfactants. This is due to the greater hydrophobicity of the Chol unit in comparison to HC chains.

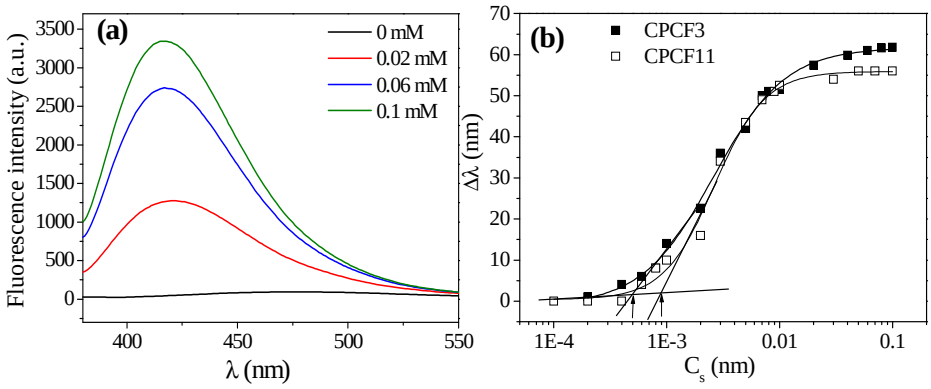

Figure 4.2.3 (a) Fluorescence spectra of NPN in pH 7.0 buffer at different concentrations (C_s) of CPCF3, and (b) variation of spectral shift ($\Delta\lambda$) of NPN as a function of C_s in pH 7.0 at 25 ^oC: (■) CPCF3 and (□) CPCF11.

4.2.4 Thermodynamics of self-assembly formation

The ITC measurements were performed in pH 7.0 at 25 ^oC taking a stock solution of 0.1 mM CPCF3 and 0.2 mM CPCF11. The corresponding thermograms and the respective plot of enthalpy change with the variation of C_s have been presented in **Figure 4.2.4** and the relevant data are listed in **Table 4.2.1**. The *cmc* values of CPCF3 (~2 μM) and CPCF11 (~4 μM) were obtained from the inflection point of the respective plot. It should be noted that for both surfactants, the *cmc* value obtained from ITC titration is almost ten times higher than the corresponding value obtained by fluorometric titration (**Table 4.2.2**). The relatively smaller value of *cmc* obtained by fluorescence measurements can be associated with the fact that fluorescence being a highly sensitive technique could small change in intensity due to formation small aggregates, such as dimer, trimer, etc. at

a very low surfactant concentration. The energy change involved in this concentration region is so small that it could not be detected by ITC measurements.

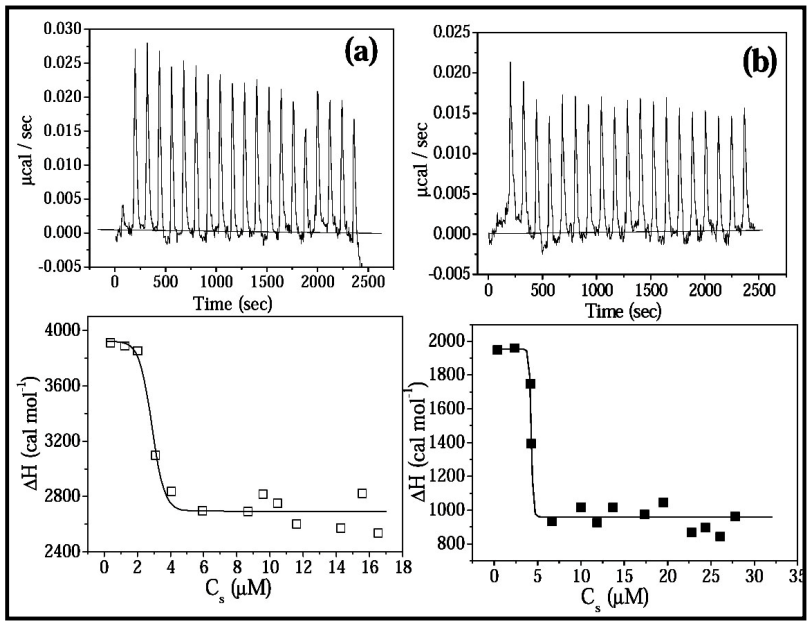

Figure 4.2.4 ITC profiles of (a) 0.1 mM CPCF3 (b) 0.2 mM CPCF11 solutions in pH 7.0 buffer at 25 ^{o}C.

Table 4.2.1 Critical aggregation concentration (*cmc*), standard Gibbs energy (ΔG^{o}_{m}), standard enthalpy (ΔH^{o}_{m}) and standard entropy (ΔS^{o}_{m}) changes of aggregate formation in aqueous buffered solution (pH 7.0) by CPCF3 and CPCF11 at 25 ^{o}C.

Surfactant	*cmc* (µM)	ΔG^{o}_{m} (kJ mol^{-1})	ΔH^{o}_{m} (kJ mol^{-1})	ΔS^{o}_{m} (J K^{-1} mol^{-1})	$T\Delta S^{o}_{m}$ (kJ mol^{-1})
CPCF3	2.2 (± 0.02)	–56.73	–4.49 (± 0.1)	175	52.24
CPCF11	4.8 (± 0.03)	–21.81	–4.17 (± 0.13)	80.57	24.01

The ΔH^{o}_{m} value was obtained by subtracting the initial enthalpy from the final enthalpy as indicated by the vertical arrow in each plot of **Figure 4.2.4**. The spontaneity of aggregate formation is shown by the very large negative values of ΔG^{o}_{m} and also by the very large positive values of ΔS^{o}_{m} (**Table 4.2.1**). Thus $T\Delta S^{o}_{m}$ values for both the surfactants are found to be much larger than that of the ΔH^{o}_{m} values, suggesting that the spontaneous aggregate formation is an entropy-driven process and hence favored by the hydrophobic interactions among the Chol units.

4.2.5 Micropolarity and microviscosity

The microenvironment of the aggregates formed by the surfactants was studied using Py and DPH as fluorescent probes. The I_1/I_3 values of 1 mM CPCF3 and 1 mM CPCF11 were found to be very low (see **Table 4.2.2**) relative to that in pH 7.0 buffer (1.82), which implies that Py is solubilized within the hydrophobic microdomain of the self-assemblies composed of hydrophobic cholesterol units. These results are consistent with those obtained from the fluorescence titration using NPN probe and thus confirm the accuracy of the methods. The very low micropolarity of the self-assembled structures might be very useful for solubilization of highly hydrophobic drugs.

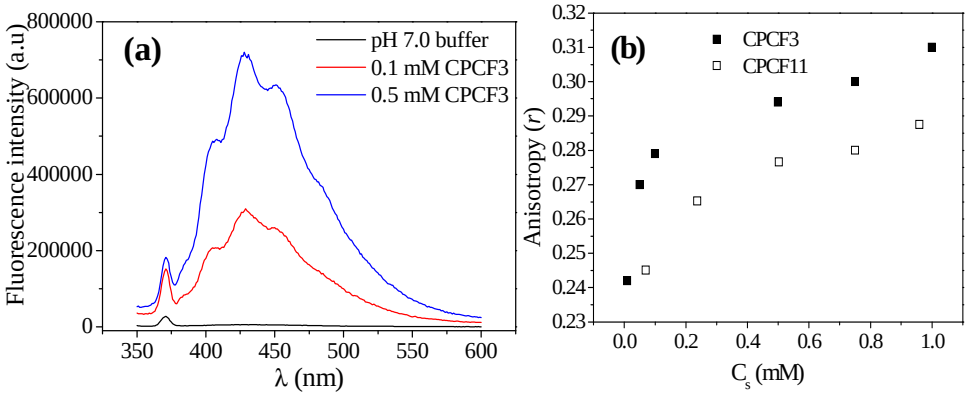

Figure 4.2.5 (a) Representative fluorescence emission spectra of DPH in pH 7.0 buffer and in the presence of 0.1 mM and 0.5 mM CPCF3 and (b) concentration (C_s) variation fluorescence anisotropy (r).

Further, the steady-state fluorescence anisotropy of DPH probe was measured in the presence of different concentrations of the surfactants. The partitioning of DPH molecules into the microenvironments of the aggregates is shown by the enhancement of fluorescence intensity in the presence of surfactants (**Figure 4.2.5(a)**). The variation of *r* with C_s is shown by the plots in **Figure 4.2.5(b)**. The higher *r* values (**Table 4.2.2**) suggest that the microdomains formed by the surfactants are very rigid. Indeed the η_m-values obtained from the corresponding *r* and τ_f values (**Table 4.2.2**) suggest that the microenvironments of the aggregates formed by both CPCF3 and CPCF11 are very rigid. The highly ordered microenvironment of the aggregates of both surfactants clearly indicates existence of bilayer vesicles in solution.

Table 4.2.2 Critical micelle concentration (*cmc*), fluorescence anisotropy (*r*), fluorescence lifetime (τ_R), microviscosity (η_m) and I_1/I_3 of Py in aqueous buffered solution (pH 7.0) by CPCF3 and CPCF11 at 25 ^oC.

Surfactant	*cmc* (μM)	*r*	τ_f (ns)	η_m (mPa s)	I_1/I_3
CPCF3	0.4 ± 0.3	0.32 ± 0.02[a]	8.52[a]	540 ± 20[a]	0.93 ± .04[a]
CPCF11	0.9 ± 0.2	0.29 ± 0.02[b]	7.45[b]	485± 30[b]	1.00 ± .03[b]

*a and b designates 1.0 mM of respective surfactant concentration.

4.2.6 Hydrodynamic diameter and morphology of the aggregates

DLS was used to measure size distributions of the aggregates in aqueous buffer (pH 7.0). The size distribution profiles **(Figure 4.2.6)** thus obtained are narrow and monomodal in nature for both the surfactants. As can be seen aggregates having sizes in the range of ~ 20-40 nm are formed by both the surfactants at the lower concentrations. However, larger aggregates of d_h in the range of 100-200 nm is found in concentrated surfactant solutions. For CPCF3, small size aggregates with mean d_h ~ 25 nm is observed in dilute solution,

whereas in concentrated surfactant solution the size increased to ~150 nm. CPCF11 also self-assembled to give aggregates with average d_h ~ 30 nm in dilute solutions and 200 nm in concentrated solutions. The presence of large aggregates indicates formation vesicles in concentrated solutions of both surfactants.

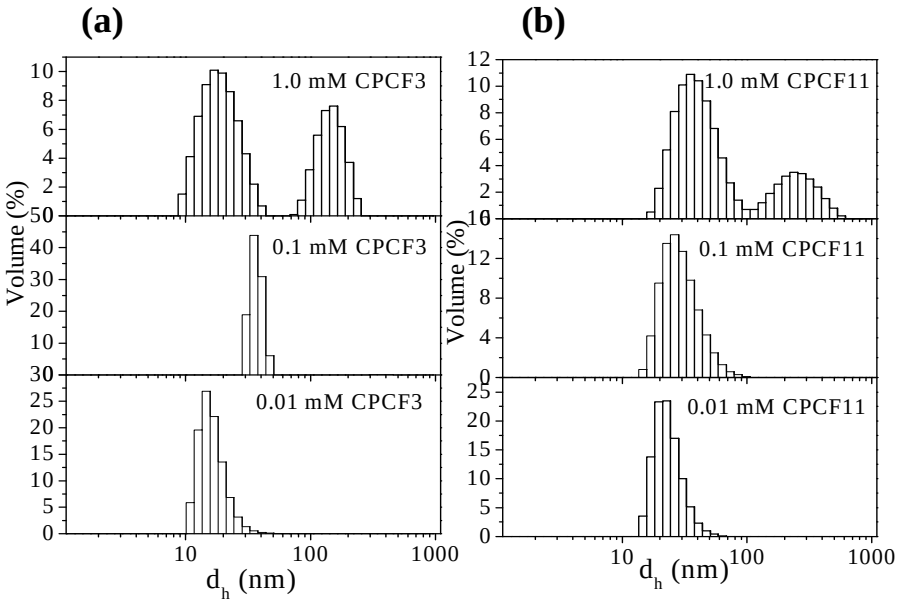

Figure 4.2.6 Concentration dependent size distribution profiles of the aggregates formed by (a) CPCF3 and (b) CPCF11 in pH 7.0 buffer at 25 ^{o}C.

The existence of large size aggregates can also be seen in the HRTEM images (**Figure 4.2.7**) of surfactant solutions of different concentrations. Interestingly, very small unilamellar vesicles (SUVs) can be found to form in dilute surfactant solutions. Also clusters of SUVs having size ~20 nm are found to form in pH 7.0 buffer for both the surfactants. However, the size of the SUVs increases to some extent with the increase of surfactant concentration. Consequently, vesicles of diameter ~100 nm can be found in concentrated surfactant solutions (1.0 mM). The growth of vesicle in concentrated surfactant solutions can be ascribed to strong intermolecular H-bonding interactions among the carbamate groups which facilitates tight packing of the aggregates.

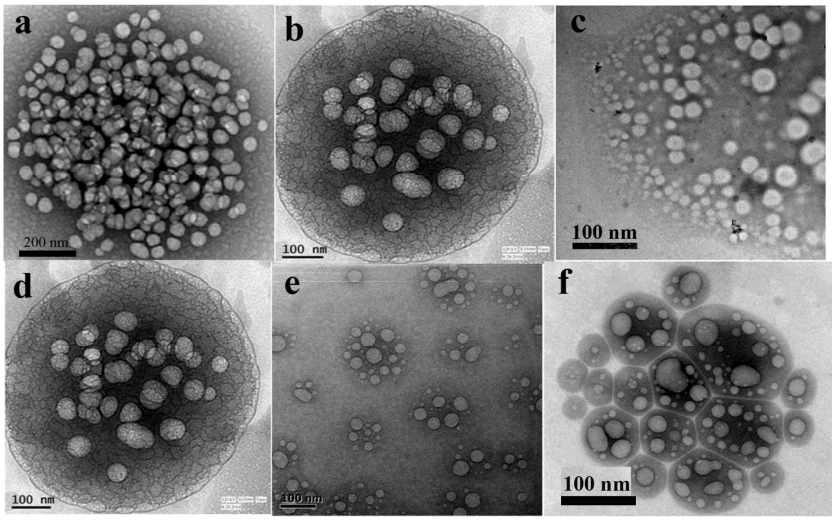

Figure 4.2.7 Unstained HRTEM micrographs in pH 7.0 of CPCF3 solutions of (a) 0.01 mM (b) 0.1 mM (c) 1.0 mM and CPCF11 solutions of (d) 0.01 mM (e) 0.1 mM and (f) 1.0 mM.

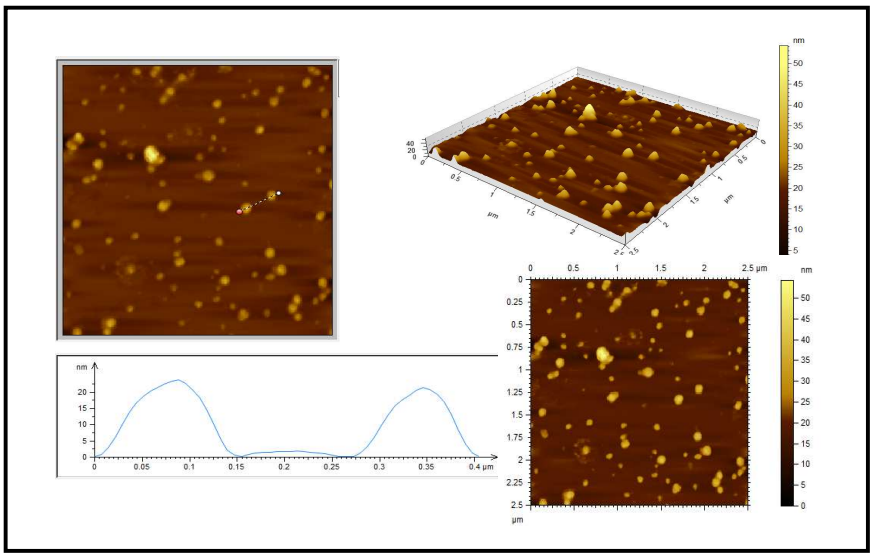

Figure 4.2.8 AFM height image with scale-bar, 3D sectional analysis of CPCF3 solution (1.0 mM, pH 7.0), and on mica.

As a representative example, the aggregates in the surfactant solutions of CPCF3 were further characterized by AFM in the dehydrated state. **Figure 4.2.8** shows the tapping-mode AFM image of 1.0 mM CPCF3 in pH 7.0 buffer which reveals spherical aggregates with diameters of ~200 nm. This is in good agreement with the results obtained by DLS and TEM measurements. The section analysis profile of a selected aggregate is also shown in **Figure 4.2.8**. The collapsed aggregate height was observed to be ~ 20 nm. This means the average wall thickness of the hollow sphere is about 10 nm which is equal to the thickness of the bilayer constituted by the Chol units. This means formation of only ULVs by the surfactants.

In order to rule out any artifacts in the HRTEM and AFM images and to show the existence of aqueous core within the vesicular aggregates, an experiment involving entrapment of **Cal**, a hydrophilic fluorescent dye, was performed. The entrapment of the dye, in the aqueous core of the vesicles was confirmed by the quenching of fluorescence intensity of the probe (**Figure 4.2.9**) in comparison to the fluorescence of absorbance matched solution of the probe in the absence of surfactant. The fluorescence quenching is due to the confinement of the probe molecules within the aqueous core of small volume. However, fluorescent microscopic images could not be visualized because of small size (<300 nm) the vesicles.

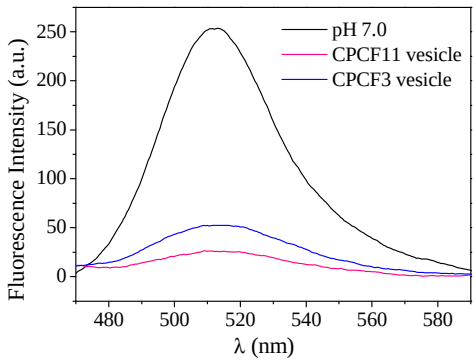

Figure 4.2.9 Plots of fluorescence spectra of free **Cal** and **Cal**-entrapped vesicles of CPCF3 and CPCF11 surfactants (0.1 mM) in pH 7.0 buffer.

The surface charge of the vesicles formed by the surfactants was determined by ζ-potential measurements. The relevant data presented in **Table 4.2.3** show that the vesicles are negatively charged. As expected, the monomers being negatively charged when assembled to produce vesicles the total surface charge is also negative. However, at lower pH (pH 3.0) the surface charge of the surfactants become almost zero, and the surfactants become nonionic in nature. Consequently, in acidic pH, the SUVs become uncharged.

Table 4.2.3 The ζ-potential values of differently concentrated CPCF3 and CPCF11 solutions at different pHs.

Surfactant	C_s (mM)	ζ –potential at pH 7.0 (mV)	ζ –potential at pH 3.0 (mV)
CPCF3	0.01	-13.8	
	0.1	-9.3	-0.9
CPCF11	0.01	-18.2	
	0.1	-13.5	-1.3

4.2.7 Constitution of vesicle bilayer

The supramolecular arrangement of the amphiphiles in the aggregates can be explained by the hydrophilic/lipophilic, electrostatic, van der Waals and H-bonding interactions among the surfactant monomers. As discussed before, though the major driving force for aggregation is hydrophobic effect, the slightly negative ΔH^o_m value suggests that there is a significant interaction among head groups. Since both CPCF3 and CPCF11 contain a carbamate (–OCONH–) and a carboxylate ($–COO^–$) group at the head, it is highly likely that there will be intermolecular H-bonding interactions among the head groups. This is indicated by the low micropolarity sensed by both NPN and Py probes (**Table 4.2.2**) in surfactant solutions. The low value of I_1/I_3 ratio suggests bilayer formation by the Chol units involves expulsion of water molecules from the interfacial region of the self-

assemblies which means disruption of the carbamate-water H-bonds. That is, the solvation of the hydrophilic carbamate group near the surfactant head group is lost during aggregation and consequently, the intermolecular carbamate-carbamate H-bonding interaction is established.

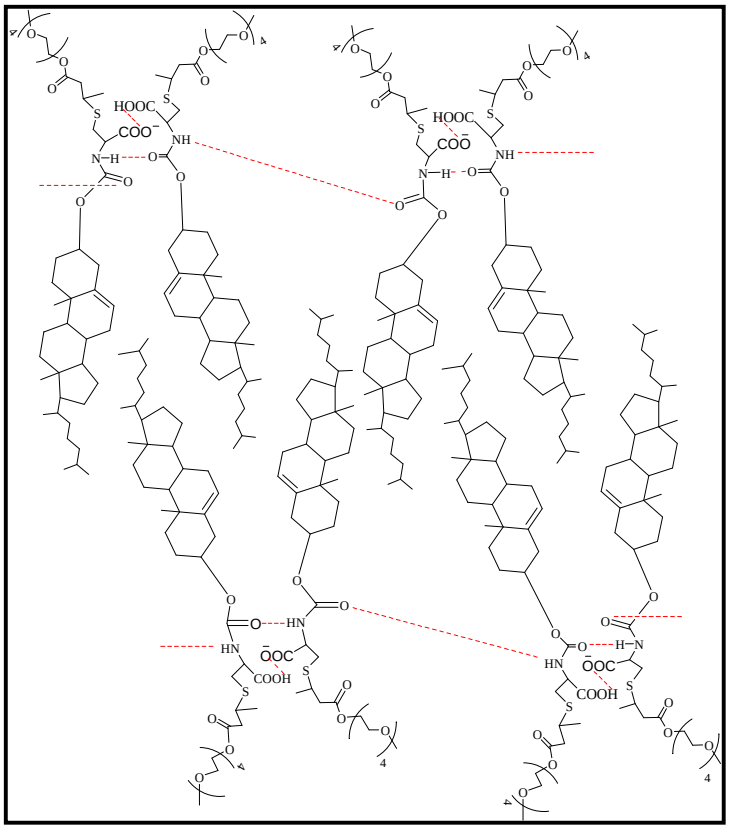

Figure 4.2.10 Schematic representation of the bilayer structure formed by CPCF3 molecules in aqueous solution.

In order to confirm the existence of intermolecular H-bonding among the surfactant molecules through the carbamate groups, FT-IR spectra (not shown) of CPCF3, as a representative example, were recorded (i) in pure aqueous sample (0.1 mM) as well as (ii) in dry chloroform ($CHCl_3$) solvent. The appearance of the N–H stretching

frequency (3430 cm^{-1}) and the amide-I band (1645 cm^{-1}) of the aqueous solutions of the amphiphiles indicates the existence of carbamate group. Though the amide-I band in aqueous sample (1645 cm^{-1}) resembles the corresponding stretching frequency measured in $CHCl_3$ solution, the amide-II band in aqueous solution is shifted to higher frequency (1593 cm^{-1}) relative to that of the unassociated state in $CHCl_3$ solvent (1580 cm^{-1}). This shows the existence of intermolecular H-bonding between adjacent molecules. The intermolecular H-bonding interactions of the carbamate groups induce tighter packing of the molecules leading to the formation of bilayer vesicles. These H-bonding interactions at the head-group region minimize the repulsive interactions among the $–COO^-$ groups and thus favor bilayer formation as shown in **Figure 4.2.10**. The two-layer arrays of the intermolecular H-bonding interactions through the amide bonds of the neighboring surfactant molecules result in a parallel arrangement of the corresponding hydrophobic tails such that the surfactant molecules self-assembled into bilayer structures in aqueous buffer.

4.2.8 Effect of pH on vesicle stability

As the amphiphiles contain $–COO^-$ as one of the head groups, it is important to investigate the pH-dependence of solution behavior [33-38]. To explore the pH-dependent change of the microenvironment of the self-assemblies formed by the amphiphiles, fluorescence probe studies using DPH were performed at different pH. With the decrease in solution pH the *r* value of DPH was found to increase for both the amphiphiles. It may be attributed to protonation of the $–COO^-$ group that reduces ionic repulsions as well as promotes intermolecular H-bonding interaction between the –COOH groups or between –COOH and –OCONH groups at the interface. The ordering at the aggregate interface should also result in compact packing in the interior of the bilayer aggregates as manifested by the increase of *r* value. The intermolecular H-bonding as a result of protonation of the $–COO^-$ group increases the curvature of the bilayer aggregates to produce large unilameller vesicles (LUVs). The pH adjustment provides a way for the bilayer surface charge density to be varied precisely through changing the degree of protonation of the $–COO^-$ head-group. As a result, the concomitant electrostatic and H-bonding interactions force the bilayers to adopt LUV structure. The polarity of the

hydrophobic domain depends upon microstructure of the self-assemblies and the solubilization of the dye. The I_1/I_3 values for both the amphiphiles at pH 3.0 were found to much lower (0.85 for 1 mM CPCF3 nd 0.91 for 1 mM CPCF11) than that of buffer at pH 7.0. The decrease of ionic character at lower pH results in a decrease of charge repulsion and hence tighter packing of the cholesterol units thereby preventing water penetration. The hydrophobic domain formation must result from pH-induced conformational change of the amphiphiles.

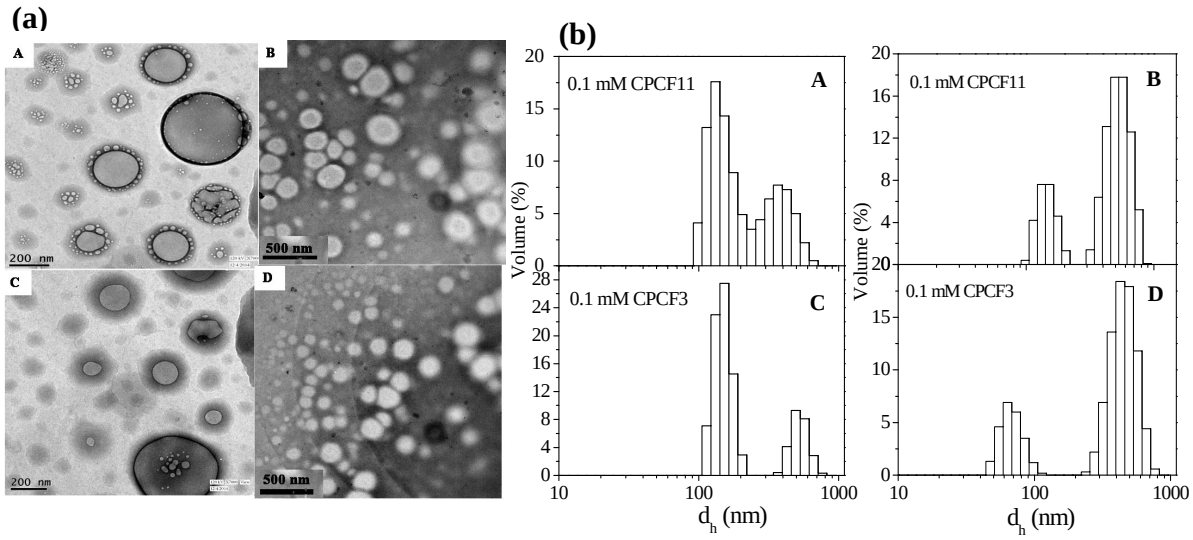

Figure 4.2.11 (a) HRTEM images of (A) 0.1 mM CPCF3 solution at pH 3.0 (B) 0.1 mM CPCF3 solution at pH 5.0 (C) 0.1 mM CPCF11 solution at pH 3.0 and (D) 0.1 mM CPCF11 solution at pH 5.0; (b) size distribution histograms (A) 0.1 mM CPCF11 solution at pH 3.0 (B) 0.1 mM CPCF11 solution at pH 5.0 (C) 0.1 mM CPCF3 solution at pH 3.0 and (D) 0.1 mM CPCF3 solution at pH 5.0.

The change in size of the aggregates with lowering of pH is also evident from the results of DLS and TEM measurements (see **Figure 4.2.11**). From **Figure 4.2.11(a)** it is evident that ~250 nm sized vesicles were found for 0.1 mM CPCF3 in pH 3.0, whereas ~350 nm sized vesicles were found in pH 5.0. This is also supported by the results of DLS measurements summarized in **Figure 4.2.11(b).** The change in size of the

aggregates at different pH can be explained by the protonation of the $–COO^-$ group. At pH 5.0, some of the $–COO^-$ ions are converted to –COOH which leads to strong H-bonding interaction between the head groups. This results in a decrease of the effective area of head group (A_o) and hence an increase of packing parameter (P) value which means formation of LUVs at pH 5.0. On the other hand, at pH 3.0 all the $–COO^-$ groups are converted to the neutral form (–COOH), which also form intermolecular H-bonds with the nearby –COOH groups. But interaction between –COOH groups is much weaker than that between –COOH and $–COO^-$ groups. Consequently, the SUVs are formed in pH 3.

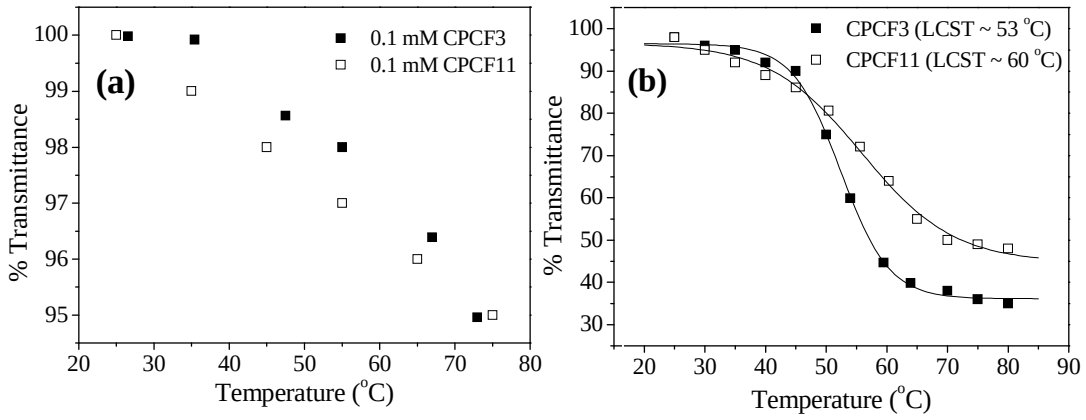

Figure 4.2.12 Plot of percent transmittance (%T at λ = 450 nm) of surfactant solution (0.1 mM) as a function of temperature (T /°C) at (a) pH 7.0 buffer and (b) pH 3.0 buffer.

4.2.9 Thermal stability of the aggregates

For drug delivery applications, the vesicles should be stable under physiological conditions (pH 7.4, 37 °C). It should be noted that at neutral pH the aqueous solutions of both the surfactants do not exhibit any cloudiness even at 80 °C as indicated by the plots of transmittance (% T) versus temperature (**Figure 4.2.12 (a)**). This means the SUVs are highly stable at physiological temperature at neutral pH. However, a sharp fall of transmittance can be observed with both the surfactants at pH 3.0 above a critical temperature which can be taken as the cloud point (T_c). The T_c values thus obtained are

53 ^{o}C and 60 ^{o}C for CPCF3 and CPCF11, respectively. As reported for PEG-containing copolymers, this is due to temperature-induced dehydration of the PEG chains which makes polymer chain more hydrophobic [57, 58]. The slightly higher value of the cloud point and hence higher stability of CPCF11 vesicles is due to its longer PEG chains. The size distributions histograms (not shown here) at pH 3.0 at 80 ^{o}C also showed a large shift toward larger d_h values, suggesting good thermal stability of the vesicles at physiological temperature.

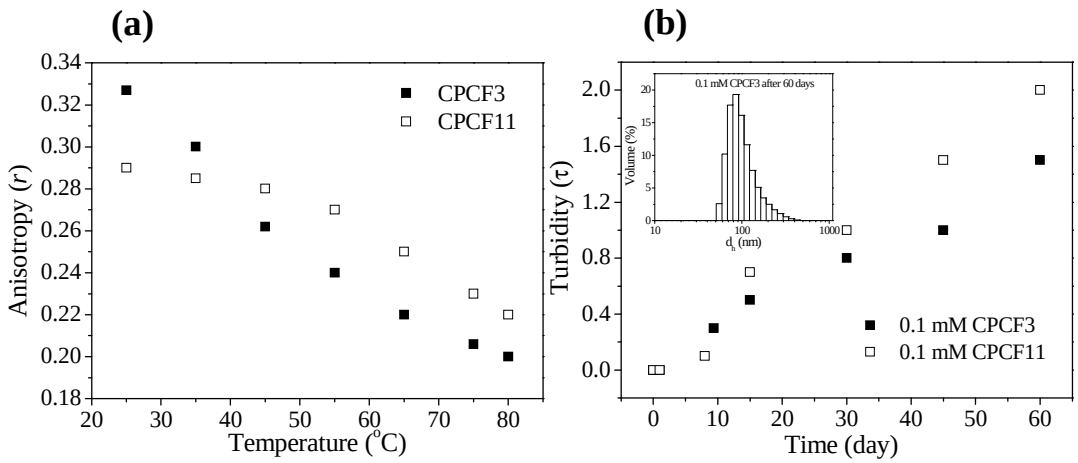

Figure 4.2.13 (a) Variation of fluorescence anisotropy (*r*) of DPH at λ = 430 nm with temperature (T /^{o}C) in the presence of 0.1 mM CPCF3 and CPCF11 in pH 3.0, and (b) variation of turbidity (100 – %T) of CPCF3 and CPCF11solutions (0.1 mM each) with aging at pH 7.0 (inset: size distribution profile of 0.1 mM CPCF3 after 60 days of sample preparation).

The thermal stability of the vesicles was also studied by fluorescence probe method using DPH as a probe molecule at pH 3.0. The fluorescence spectra of DPH were measured at different temperatures in the range 25–80 ^{o}C in pH 3.0. As observed from the plots in **Figure 4.2.13(a)**, the *r* value of DPH probe decreases with the increase of temperature, indicating increase of internal fluidity of the vesicles. The increase in the internal fluidity of the vesicles facilitates DPH molecules to diffuse out as manifested by the decrease of fluorescence intensity (not shown). However, the temperature-induced release of DPH molecules is less at 37 ^{o}C, suggesting sufficient thermal stability of the

micelles even at pH 3.0. In support of this conclusion the hydrodynamic size distributions (not shown here) of the vesicles was also measured at 37 ^{o}C (310 K). However, only a very small shift toward larger d_h value, showing partial disruption of the bilayers above physiological temperature was observed.

4.2.10 Shelf-life of vesicles

Vesicle stability was also studied by measuring turbidity (τ) of the surfactant solutions (0.1 mM) at pH 7.0 buffer over a period of 60 days. The results are presented in **Figure 4.2.13(b)**. It is evident that there is only a small increase in τ value after 60 days of vesicle preparation. Actually the formation and growth of the vesicles cause a small increase of the turbidity. The size distribution profile (inset of **Figure 4.2.13(b)**) also does not exhibit any change in d_h value. This means SUVs formed at room temperature are highly stable over several months and therefore they can have potential applications in drug delivery.

4.2.11 Summary

In summary, two novel amphiphilic molecules CPCF3 and CPCF11 were designed and synthesized using biocompatible PEG and Chol. The amphiphiles were characterized by surface tension and various spectroscopic methods. Both the amphiphiles were found to self-assemble at a very low concentration. The thermodynamics of aggregate formation was also studied using ITC technique. The thermodynamic parameters suggest that the hydrophobic interaction among the Chol units is the main driving force for aggregate formation. However, the intermolecular H-bonding among the amphiphiles also plays a vital role for vesicle formation. The amphiphiles were observed to form stable SUVs with mean d_h of ~20 nm in very dilute surfactant solutions at pH 7.0. However, the vesicle size increases to ca. 80 nm in concentrated surfactant solution. The microenvironments of the SUVs were found to be highly viscous as well as much less polar compared to bulk water due to having Chol-like steroidal moiety as hydrophobe. The interesting observation was that the SUVs transform into LUVs at lower pH. Though surfactant solutions at pH 7.0 remained transparent over a large temperature range, both amphphiles showed clouding

phenomenon at pH 3.0. Indeed, the SUVs formed in neutral pH were found to have extremely good stability over several months under the physiological conditions.

References

[1] Carstens, M. G.; Nostrum, C. F.; Ramji, A.; Meeldijk, J. D.; Verrijk, R.; Leede, L. L.; Crommelin, J. A.; Hennink, W. E. Poly(ethylene glycol)−oigolactates with Monodisperse Hydrophobic Blocks: Preparation, Characterization, and Behavior in Water. *Langmuir* **2005**, *21*, 11446−11454.

[2] Park, M.-J.; Chung, Y.-C.; Chun, C. B. PEG-Based Surfactants That Show High Selectivity in Disrupting Vesicular Membrane with or without Cholesterol. *Colloids Surf. B* **2003**, *32*, 11−18.

[3] Salonen, A.; Knyazev, N.; Bandel, N.; Degrouard, J.; Langevin, D.; Drenckhan, W. A Novel Pyrene-Based Fluorescing Amphiphile with Unusual Bulk and Interfacial Properties. *ChemPhysChem* **2011**, *12*, 150−160.

[4] Mandal, A. B.; Ray, S.; Biswas, A. M.; Moulik, S. P. Physicochemical Studies on the Characterization of Triton X 100 Micelles in an Aqueous Environment and in the Presence of Additives. *J. Phys. Chem*. **1980**, *84*, 856−859.

[5] Zalipsky, S. Chemistry of Polyethylene-Glycol Conjugates with Biologically-Active Molecules. *Adv. Drug Delivery Rev.* **1995**, *16*, 157− 182.

[6] Veronese, F. M. Peptide and Protein PEGylation: A Review of Problems and Solutions. *Biomaterials* **2001**, *22*, 405−417.

[7] Caliceti, P.; Veronese, F. M. Pharmacokinetic and Biodistribution Properties of Poly(ethylene glycol)−Protein Conjugates. *Adv. Drug Delivery Rev.* **2003**, *55*, 1261−1277.

[8] Li, J.M.; He, Z.Y.; Yu, S.; Li, S.Z.; Ma, Q.; Yu, Y.Y.; Zhang, J.L.; Li, R.; Zheng, Y.; He, G.; Song, X.R. Micelles Based on Methoxy Poly(ethylene glycol) Cholesterol Conjugate for Controlled and Targeted Drug Delivery of a Poorly Water Soluble Drug. *Journal of Biomedical Nanotechnology* **2012**, *8*, 809–817.

[9] Xu, H., Wang, K.Q., Deng, Y.H., Chen, D.W. Effects of Cleavable PEG-Cholesterol Derivatives on the Accelerated Blood Clearance of PEGylated Liposomes. *Biomaterials* **2010**, *31*, 4757–4763.

[10] Dey, J.; Shrivastava, S. Can Molecules with Anionic Head and Poly(ethylene glycol) methyl ether Tail Self-assemble in Water? A Surface tension, Fluorescence probe, Light scattering, and Transmission Electron Microscopic Investigation. *Soft Matter* **2012**, *8*, 1305−1308.

[11] Dey, J.; Shrivastava, S. Physicochemical Characterization and Self-Assembly Studies on Cationic Surfactants bearing mPEG Tail. *Langmuir* **2012**, *28*, 17247-17255.

[12] Ghosh, R.; Dey, J. Vesicle Formation by L-Cysteine-Derived Unconventional Single-Tailed Amphiphiles in Water: A Fluorescence, Microscopy, and Calorimetric Investigation. *Langmuir* **2014**, *30*, 13516-13524.

[13] Ghosh, R.; Dey, J. Aggregation Behavior of Poly(ethylene glycol) Chain-Containing Anionic Amphiphiles: Thermodynamic, Spectroscopic and Microscopic Studies. *Journal of Colloid and Interface Science* **2015**, *451*, 53-62.

[14] Mittal, K. L. Determination of CMC of Polysorbate 20 in Aqueous Solution by Surface Tension Method. *Journal of Pharmaceutical Science* **1972**, *61*, 1334-1335.

[15] Saitoh, T.; Taguchi, K.; Hiraide, M. Evaluation of Hydrophobic Properties of Sodium Dodecylsulfate/γ-Alumina Admicelles Based on Fluorescence Spectra of N-Phenyl-1 Naphthylamine. *Anal. Chim. Acta* **2002**, *454*, 203−208.

[16] Roy, S.; Dey, J. Spontaneously Formed Vesicles of Sodium N-(11 Acrylamidoundecanoyl)-Glycinate and L-Alaninate in Water. *Langmuir* **2005,** *21*, 10362-10369.

[17] Ghosh, A.; Shrivastava, S.; Dey, J. Concentration and pH-dependent Aggregation Behavior of an l-Histidine Based Amphiphile in Aqueous Solution. *Chemistry and Physics of Lipids* **2010**, *163*, 561–568.

[18] Paula, S.; Siis, W.; Tuchtenhagen, J.; Blume, A. Thermodynamics of Micelle Formation as a Function of Temperature: A High Sensitivity Titration Calorimetry Study. *J. Phys. Chem.* **1995**, *99*, 11742-11751.

[19] Verral, R. E.; Milioto, S.; Zana, R. Ternary Water-in-oil Microemulsions Consisting of Cationic Surfactants and Aromatic Solvents. *J. Phys.Chem.***1988**, *92*, 3939−3943.

[20] Majhi, P.; Moulik, S. Energetics of Micellization: Reassessment by a High-Sensitivity Titration Microcalorimeter. *Langmuir* **1998**, *14*, 3986-3990.

[21] Kalyanasundaram, K.; Thomas, J. K. Environmental Effects on Vibronic Band Intensities in Pyrene Monomer Fluorescence and Their Application in Studies of Micellar Systems. *J. Am. Chem. Soc.* **1977**, *99*, 2039-2044.

[22] Kalyansundaram, K. *Photophysics of Microheterogeneous Systems*; Academic Press: New York, **1988**.

[23] Shinitzky, M.; Dianoux, A.-C.; Gitler, C.; Weberil, G. Microviscosity and Order in the Hydrocarbon Region of Micelles and Membranes Determined with Fluorescent Probes. I. Synthetic Micelles. *Biochemistry* **1971**, *10*, 2106−2113.

[24] Shinitzky, M.; Yuli, I. Lipid Fluidity at the Submacroscopic Level: Determination by Fluorescence Polarization. *Chem. Phys. Lipids* **1982**, *30*, 261−282.

[25] Zana, R.; Martin, I.; Lévy, H. Alkanediyl-α,ω-bis- (dimethylalkylammonium bromide). 7. Fluorescence Probing Studies of Micelle Micropolarity and Microviscosity. *Langmuir* **1997**, *13*, 21-27.

[26] Roy, S.; Mohanty, A.; Dey, J. Microviscosity of Bilayer Membranes of Some N-Acylamino Acid Surfactants determined by Fluorescence Probe Method. *Chem. Phys. Lett*. **2005**, *414*, 23-27.

[27] Zhdanov, V.P.; Kasemo, B. Lipid-Diffusion-Limited Kinetics of Vesicle Growth. *Langmuir* **2000**, *16*, 7352.

[28] Ohta, A.; Danev, R.; Nagayama, K.; Mita, T,; Asakawa, T.; Miyagishi, S. Transition from Nanotubes to Micelles with Increasing Concentration in Dilute Aqueous Solution of Potassium *N*-Acyl Phenylalaninate**.** *Langmuir* **2006**, *22*, 8472-8477.

[29] Gebicki, J.M.; Hicks, M. Ufasomes are Stable Particles Surrounded by Unsaturated Fatty Acid Membranes. *Nature* **1973**, *243*, 232–234.

[30] Namani, T.; Walde, P. From Decanoate Micelles to Decanoic Acid/ Dodecylbenzenesulfonate Vesicles. *Langmuir* **2005,** *21*, 6210-6219.

[31] Cistola, D. P.; Hamilton, J. A.; Jackson, D.; Small, D. M. Ionization and Phase Behavior of Fatty Acids in Water: Application of the Gibbs Phase Rules. *Biochemistry* **1988**, *27*, 1881-1888.

[32] Hargreaves, W. R.; Deamer, D. W. Liposomes from Ionic, Single-Chain Amphiphiles. *Biochemistry* **1978**, *17*, 1978-1987.

[33] Di Marzio, L.; Marianecci, C.; Cinque, B.; Nazzarri, M.; Cimini, A. M.; Cristiano, L.; Cifone, M. G.; Alhaique, F.; Carafa, M. pH-Sensitive Non-Phospholipid Vesicle and Macrophage-Like Cells: Binding, Uptake and Endocytotic Pathway. *Biochim. Biophys. Acta, Biomembr.* **2008**, *1778*, 2749–2756.

[34] Carafa, M.; Di Marzio, L.; Marianecci, C.; Cinque, B.; Lucania, G.; Kajiwara, K.; Cifone, M. G.; Santucci, E. Designing Novel pH-Sensitive Non-phospholipid Vesicle: Characterization and Cell Interaction. *Eur. J. Pharm. Sci.* **2006**, *28*, 385–393.

[35] Karanth, H.; Murthy, R. S. pH-Sensitive Liposomes-Principle and Application in Cancer Therapy. *J. Pharm. Pharmacol.* **2007**, *59*, 469-483.

[36] Sumida, Y.; Masuyama, A.; Takasu, M.; Kida, T.; Nakatsuji, Y.; Ikeda, I.; Nojima, M. New pH-Sensitive Vesicles. Release Control of Trapped Materials from the Inner Aqueous Phase of Vesicles Made from Triple-Chain Amphiphiles Bearing Two Carboxylate Groups. *Langmuir* **2001**, *17*, 609–612.

[37] Jiang, L.; Wang, K.; Ke, F.; Liang, D.; Huang, J. Endowing Catanionic Surfactant Vesicles with Dual Responsive Abilities via a Noncovalent Strategy: Introduction of a Responser, Sodium Cholate. *Soft Matter* **2009**, *5*, 599–606.

[38] Johnsson, M.; Wagenaar, A.; Engberts, J. B. F. N. Sugar-Based Gemini Surfactant with a Vesicle-to-Micelle Transition at Acidic pH and a Reversible Vesicle Flocculation near Neutral pH. *J. Am. Chem. Soc.* **2003**, *125*, 757–760.

[39] Cui, Q.; Wu, F.; Wang, E. Thermosensitive Behavior of Poly(ethylene Glycol)-Based Block Copolymer (PEG-b-PADMO) Controlled via Self-Assembled Microstructure. *J. Phys. Chem. B* **2011**, *115*, 5913–5922.

[40] Yeagle, P. L. Cholesterol and the Cell Membrane. *Biochim. Biophys. Acta* **1985**, *822*, 267–287.

[41] Raffy, S.; Teissie, J. Control of Lipid Membrane Stability by Cholesterol content. *Biophys. J.* **1999**, *76*, 2072-2080.

[42] Harada, T.; Pham, D. T.; Leung, M. H. M.; Ngo, H. T.; Lincoln, S. F.; Easton, C. J.; Kee, T. W. Cooperative Binding and Stabilization of the Medicinal Pigment Curcumin by

Diamide Linked γ-Cyclodextrin Dimers: A Spectroscopic Characterization. *J. Phys. Chem. B* **2011**, *115*, 1268−1274.

[43] Leung, M. H. M.; Kee, T. W. Effective Stabilization of Curcumin by Association to Plasma Proteins: Human Serum Albumin and Fibrinogen. *Langmuir* **2009**, *25*, 5773−5777.

[44] Gou, M.; Men, K.; Shi, S. H.; Xiang, L. M.; Zhang, J.; Song, J.; Long, L. J.; Wan, Y.; Luo, F.; Zhao, X.; Qian, Y. Z. Curcumin-Loaded Biodegradable Polymeric Micelles for Colon Cancer Therapy in Vitro and in Vivo. *Nanoscale* **2011**, *3*, 1558−1567.

[45] Ghosh, R.; Dey, J. Vesicle-to-Micelle Transition in Aqueous Solutions of L-Cysteine-Derived Carboxylate Surfactants Containing Both Hydrocarbon and Poly(ethylene glycol) Tails. *Langmuir* **2017**, *33*, 543−552.

[46] Yeagle, P. L. Modulation of Membrane Function by Cholesterol. *Biochimie* **1991**, *73*, 1303−1310.

[47] Yeagle, P. L. Cholesterol and the Cell Membrane. *Biochim. Biophys. Acta* **1985**, *822*, 267−287.

[48] Bloch, K. E. Sterol. Structure and Membrane Function. *Crit. Rev. Biochem. Mol. Biol.* **1983**, *14*, 47−92.

[49] Hanukoglu, I. Steroidogenic Enzymes: Structure, Function, and Role in Regulation of Steroid Hormone Biosynthesis. *J. Steroid Biochem. Mol. Biol*. **1992**, *43*, 779−804.

[50] Incardona, J. P.; Eaton, S. Cholesterol in Signal Transduction. *Curr. Opin. Cell Biol.* **2000**, *12*, 193−203.

[51] Maxfield, F. R.; Tabas, I. Role of Cholesterol and Lipid Organization in Disease. *Nature* **2005**, *438*, 612−621.

[52] Simons, K.; Ikonen, E. How Cells Handle Cholesterol. *Science* **2000**, *290*, 1721−1726.

[53] Davis, F. F. The Origin of Pegnology. *Adv. Drug Delivery Rev.* **2002**, *54*, 457-458.

[54] Bhadra, D.; Bhadra, S.; Jain, P.; Jain, N. K. Pegnology: A Review of PEGylated Systems. *Die Pharmazie* **2002**, *57*, 5-29.

[55] Storm, G.; Belliot, S. O.; Daemen, T.; Lasic, D. D. Surface Modification of Nanoparticles to Oppose Uptake by the Mononuclear Phagocyte System. *Adv. Drug Delivery Rev.* **1995**, *17*, 31-48.

[56] Duncan, R. Polymer Conjugates as Anticancer Nanomedicines. *Nat. Rev. Cancer* **2006**, *6*, 688-701.

[57] Howard, M. D.; Jay, M.; Dziubla, T. D.; Lu, X. PEGylation of Nanocarrier Drug Delivery Systems: State of the Art. *J. Biomed. Nanotechnol.* **2008**, *4*, 133-148.

[58] Torchilin, V. P. PEG-based Micelles as Carriers of Contrast Agents for Different Imaging Modalities. *Adv. Drug Delivery Rev.* **2002**, *54*, 235-252.

[59] Hullin-Matsuda, F.; Ishitsuka, R.; Takahashi, M.; Kobayashi, T. Imaging Lipid Membrane Domains with Lipid-specific Probes. *Methods in Molecular Biology* **2009**, *580*, 203–220.

[60] Li, S. Z.; Ma, Q.; Yu, Y. Y.; Zhang, J. L.; Li, R.; Zheng, Y.; He, G.; Song, X. R. Micelles Based on Methoxy Poly(ethylene glycol) Cholesterol Conjugate for Controlled and Targeted Drug Delivery of a Poorly Water Soluble Drug. *Journal of Biomedical Nanotechnology* **2012**, *8*, 809–817.

[61] Xu, H.; Deng, Y.; Chen, D.; Hong, W.; Lu, Y.; Dong, X. Esterase-catalyzed de PEGylation of pH-sensitive Vesicles Modified with Cleavable PEG-lipid Derivatives. *Journal of Controlled Release* **2008**, *130*, 238–245.

[62] Lingwood, D.; Simons, K. Lipid Rafts as a Membrane-organizing Principle. *Science* **2010**, *327*, 46–50.

[63] He, Z. –Y.; Chu, B. –Y.; Wei, X. –W.; Li, J.; Carl K., E.; Song, X. –R.; He, G.; Xie, Y. –M.; Wei, Y. –Q.; Qi, Z. –Y. Recent Development of Poly(ethylene glycol)-cholesterol Conjugates as Drug Delivery Systems. *International Journal of Pharmaceutics* **2014**, *469*, 168–178.

[64] Xu, H.; Wang, K. Q.; Deng, Y. H.; Chen, D. W. Effects of Cleavable PEG-cholesterol Derivatives on the Accelerated Blood Cearance of PEGylated Liposomes. *Biomaterials* **2010**, *31*, 4757–4763.

Chapter 5
Monolayer Vesicle Forming Bolaamphiphile

5.1 Monolayer Vesicle Formation by Zwitterionic Bolaamphiphile with L-Cysteine as Head Groups[1]

5.1.1 Scope of the study

Bolaamphiphiles have been used in formulating stable nano-carrier systems and have already demonstrated to hold enough potential in effective drug as well as gene delivery [1-11]. There are many reports describing chemical properties of bolaamphiphiles and their effects on self-assembly pattern and applications in drug and gene delivery [12-22]. Indeed, bolaamphiphiles have demonstrated their ability to serve as important structural blocks of vesicles and/or micelles for drug delivery as depicted by archaeosomes. After three decades of initial development, bolaamphiphiles have presented a new area of research to formulation scientists. Therefore, extensive research should now be focused on assessing their safety profile to establish them as safe excipients for drug delivery applications.

In previous chapters, the self-assembly behavior of amphiphiles with anionic or zwitterionic head group and PEG tail have been described [23, 24]. The results have suggested that the so-called polar PEG chain can also act like hydrocarbon chain of conventional surfactants. Thus it becomes obvious in the next step to develop bolaamphiphile bearing PEG as spacer chain. It will be very interesting to see whether such bolaamphiphiles can form aggregates in solution. Despite a large number of reports on the aggregation behavior and biomedical applications of bolaamphiphiles containing hydrocarbon chains, steroids, porphyrenes etc., till now there is not a single report on bolaamphiphile bearing PEG as spacer. Therefore, in this work, a first-in-class bolaamphiphile containing PEG backbone as the spacer has been developed. Since unilamellar vesicle formation by $mPEG_{300}$-Cys and $mPEG_{1100}$-Cys amphiphiles bearing zwitterionic L-cysteine head has been demonstrated in **chapter 3**, another L-cysteine head was covalently linked to the other end of PEG chain to obtain a bolaamphiphile,

[1] *Langmuir* **2017**, 33, 7741−7750.

PEGDPC (**Figure 5.1.1**). Since both PEG and L-cysteine are biocompatible and eco-friendly, their self-assembled structures in aqueous medium can have potential applications in drug delivery. Therefore, aggregation behavior of this amphiphile was thoroughly investigated in pH 7.0 buffer at 25 ^{o}C by use of a number of techniques, including surface tension, fluorescence probe, ITC, DLS, and TEM. Encapsulation and pH-triggered release of model hydrophobic as well as hydrophilic drugs have also been demonstrated.

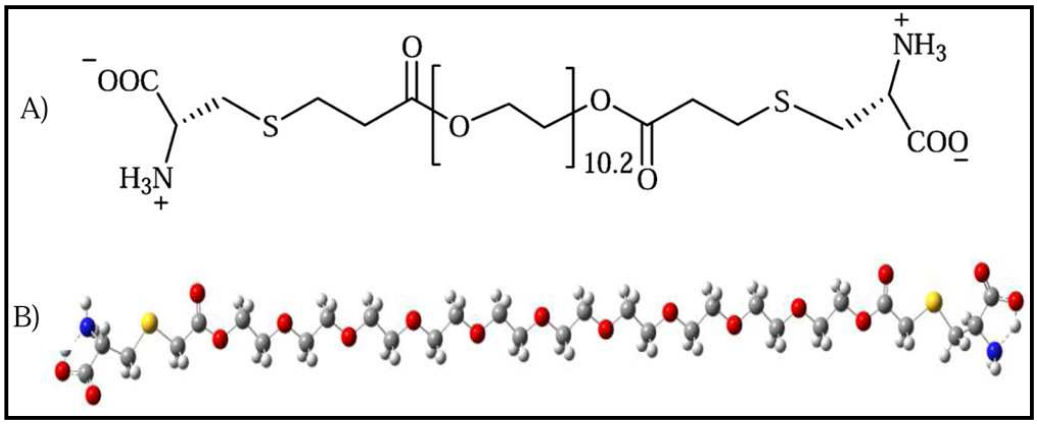

Figure 5.1.1 A) Chemical structure of the amphiphile (PEGDPC) and B) energy-minimized structure of the amphiphile in solution phase (water) (grey: C, white: H, red: O, blue: N, yellow: S).

5.1.2 Surface activity

The surface tension of the aqueous solutions (pH 7.0) of PEGDPC at different concentrations was measured at 25 ^{o}C. As shown by the plot in **Figure 5.1.2** γ value decreases with the increase of PEGDPC concentration (C_s), indicating its amphiphilic character and spontaneous adsorption of the molecules at the air/water interface. The pC_{20} value of PEGDPC as obtained from the ST plot is ~ 2.3, which is less than those of conventional surfactants ($pC_{20} \geq 3.0$) [25, 26] and therefore can be considered as a moderately surface-active amphiphile. Interestingly, unlike conventional bolaforms, the plot does not show any break followed by a plateau in the investigated concentration range. However, a dent in the curve is observed at a C_s value of about 0.5 mM which can

be considered as the *cmc* value. Further reduction of γ value with increasing concentration of PEGDPC can be attributed to formation of larger aggregates above its *cmc*. Similar behavior has already been reported in the literature for other surfactants [23, 24].

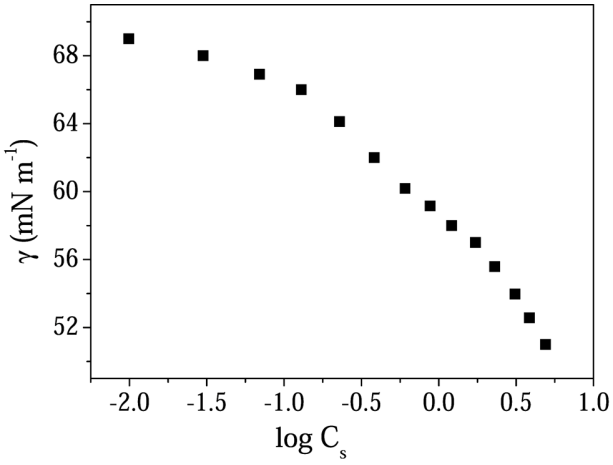

Figure 5.1.2 Plot of variation of γ (mNm^{-1}) with logC_s of PEGDPC (mM) in pH 7.0 buffer at 25 ^{o}C.

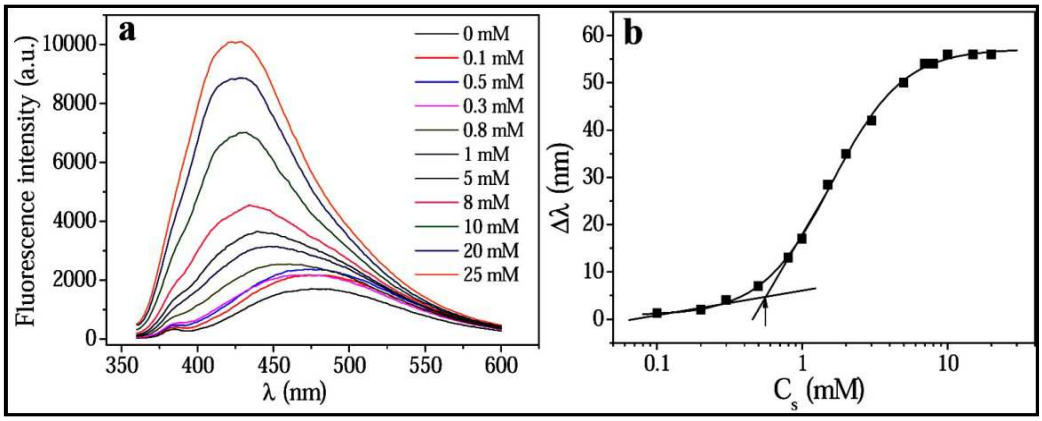

Figure 5.1.3 (a) Representative fluorescence emission spectra of NPN in presence of different surfactant concentration in pH 7.0 buffer (b) Variation of spectral shift (Δλ) of NPN probe in phosphate buffer (20 mM, pH 7.0) with the change in C_s at 25 ^{o}C.

5.1.3 Self-assembly formation

As in the cases of single-headed amphiphiles the self-assembly behavior of PEGDPC in pH 7 buffer was studied by use of NPN probe. In the presence of PEGDPC the intensity of fluorescence emission spectrum of NPN (**Figure 5.1.3(a)**) is not only enhanced the emission maximum also exhibits a blue shift relative to that in pH 7.0 buffer. The plot showing variation of the shift ($\Delta\lambda$) of emission maximum of NPN probe with PEGDPC concentration (C_s) is depicted in **Figure 5.1.3(b)**. The sigmoid plot corresponding to a two-state process clearly suggests existence of equilibrium between surfactant monomers and self-assembled aggregates. The *cmc* value (0.60± 0.04 mM) obtained from the onset of rise of $\Delta\lambda$ is closely equal to the value obtained from ST plot.

5.1.4 Driving force for self-assembly formation

The results of fluorescence probe studies spontaneous self-assembly formation by PEGDPC molecules which means the process is accompanied by a negative ΔG^o value. In order to determine the driving force for the self-assembly process, ITC method was employed to estimate other thermodynamic parameters such as ΔH^o_m and ΔS^o_m associated with the aggregate formation. The thermogram along with the titration curve is displayed in **Figure 5.1.4**. From this calorimetric titration curve, the *cmc* and ΔH^o_m values were directly obtained from the plot and ΔG^o_m and ΔS^o_m values were calculated by the procedure described in chapter 2. The values of *cmc* and thermodynamic parameters are listed in **Table 5.1.1**. The *cmc* value obtained from the onset of rise of ΔH is consistent with the values obtained from fluorescence titrations. The aggregate formation is spontaneous as confirmed by the large negative value of ΔG^o_m as well as by the large positive values of ΔS^o_m. Since the $T\Delta S^o_m$ value for the self-assembly of PEGDPC molecules is greater than that of the ΔH^o_m value, the spontaneous aggregate formation is an entropy-driven process [27-30]. The large increase of entropy can be associated with the dehydration of the PEG chains during self-assembly formation. That is, the PEG spacer of the bolaamphiphile behaves like hydrocarbon chain of conventional surfactants. However, when the thermodynamic data for the vesicle formation by PEGDPC are compared with those of the corresponding single-headed zwitterionic amphiphile (see

Table 3.1.2, chapter 3), it is found that the aggregate formation is more favorable in the case of latter molecule [23].

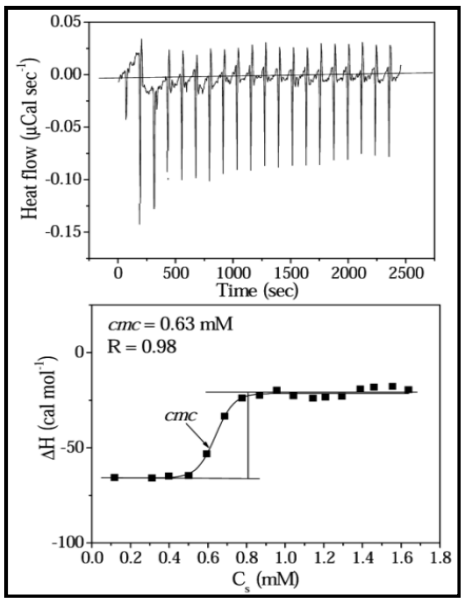

Figure 5.1.4 Thermogram (upper panel) and plot of variation of enthalpy change (ΔH) with PEGDPC concentration (C_s) at 25 ^oC; stock concentration of PEGDPC solution was 5 mM.

Table 5.1.1 Critical micelle concentration (*cmc*), standard Gibbs free energy change (ΔG^o_m), standard enthalpy change (ΔH^o_m) and standard entropy change (ΔS^o_m) for the self-assembly formation by PEGDPC in aqueous buffered solution (pH 7.0) at 25 ^oC.

cmc (mM)		ΔG^o_m	ΔH^o_m	ΔS^o_m	$T\Delta S^o_m$
Flu	ITC	(kJ mol^{-1})	(kJ mol^{-1})	(J K^{-1} mol^{-1})	(kJ mol^{-1})
0.60 (± 0.04)	0.63 (± 0.02)	−18.26	0.19 (± 0.1)	61.91	18.45

5.1.5 2D NOESY analysis

As indicated by the results of ITC measurement, the hydrophobic interaction between the PEG spacers of PEGDPC molecules is responsible for aggregate formation. The results of fluorescence probe study also indicated formation of less polar microdomains, possibly, by the PEG chains. Since the PEGDPC molecule has two polar head groups at the two ends of PEG chain, the only possible arrangement of PEGDPC molecules in the self-assembly is monolayer as shown in **Figure 5.1.5**. The constitution of monolayer membrane was confirmed by 2D NOESY ^{1}H-NMR analysis. The NOESY spectrum of 1 mM PEGDPC solution (in D_2O) as depicted in **Figure 5.1.6** shows mostly diagonal peaks that arise from the interactions of the nearby H atoms in the same molecule. In addition to diagonal interactions a number of key cross interactions can also be observed in **Figure 5.1.6**. The interactions among g ↔ a, b, c, d, e, f protons imply the intermolecular interactions among the PEG chains. Further the interactions among a ↔ b, c, d and b ↔ c, d protons suggest the strong intermolecular interactions among the head groups. As already discussed earlier the cross peaks signify the spatial proximity of the surfactant in the self-assembled aggregates [31-33]. In other words, the monolayer is constituted by the PEG spacer of the bolaamphiphile. Based on the above results of fluorescence probe studies and 2D NOESY analysis it can be concluded that the bolaamphiphile forms monolayer vesicles as shown in the cartoon pictures depicted in **Figure 5.1.5**.

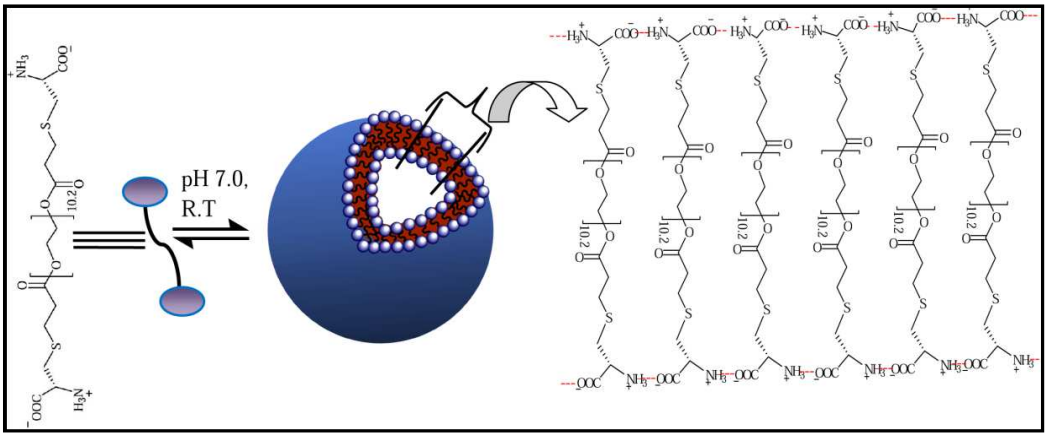

Figure 5.1.5 Schematic representation of monolayer vesicle structure formed by the monomers.

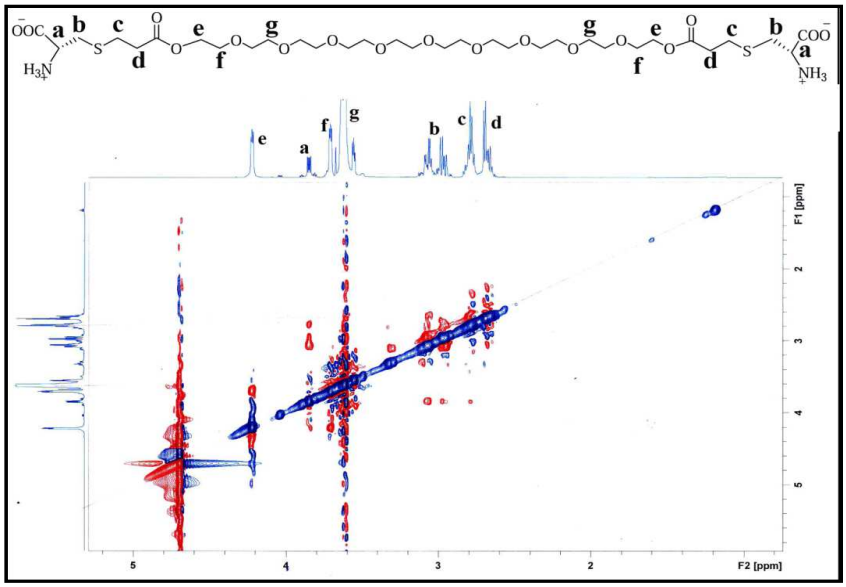

Figure 5.1.6 2D NOESY spectrum of 1 mM PEGDPC in D_2O (aggregated state).

5.1.6 Nature of microenvironment of aggregates

As discussed in chapter 3, the nature of microenvironment of the aggregates can give an idea about the molecular arrangement in the aggregates. Therefore, the micropolarity and microviscosity of the aggregates were determined by use of Py and DPH probes, respectively. In pure buffer medium, the micropolarity index (I_1/I_3) has a value of 1.81. But the ratio falls off with increasing C_s and the limiting value reaches to 1.48 ± 0.03 at C_s = 20 mM. Thus, I_1/I_3 value corresponds to the polarity of ethylene glycol [34-36]. This suggests that the Py molecules are solubilized within the microenvironment constituted by the PEG chains as already inferred from the results of NMR measurements. However, the polarity of the microenvironment of the self-assemblies of PEGDPC amphiphile is higher compared to those of L-cysteine-derived amphiphile with a single PEG tail [23]. This can be attributed to the increase of overall polarity of the amphiphile due to the presence of a second large L-cysteine head group. In pH 3.0 buffer, however, the I_1/I_3 ratio is less (1.38 ± 0.04) which is comparable to those of conventional single-tailed ionic surfactants. This is because in pH 3.0 buffer, both $–COO^-$ and $–NH_2$ groups of L-cysteine

head get protonated, thus converting the head groups to cationic (ammonium). Consequently, a reduction of hydration of the head group occurs, which favors tight packing of the PEG chains. This means less penetration of water molecules inside the monolayer membrane and hence a reduction in polarity of the microenvironment of the Py molecule. The fluorescence probe study thus confirms monolayer formation by the PEG spacer chain of the amphiphile.

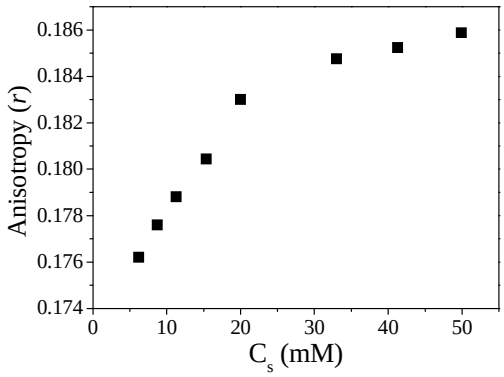

Figure 5.1.7 Plots of fluorescence anisotropy (*r*) of DPH probe versus surfactant concentration (C_s) at 25 ^oC.

Further, the steady-state fluorescence anisotropy (*r*) value of DPH probe at different concentrations above its *cmc* value of the amphiphile was measured. The plot of variation of *r* with C_s is shown in **Figure 5.1.7.** High *r* value (> 0.14) of the DPH probe indicates viscous microenvironment constituted by tight packing of PEG chains [37-40]. The feature of the plot suggests increase of η_m value of the aggregates with the increase of C_s above the *cmc* and may be attributed to the formation of larger aggregates with more rigid microenvironment which is consistent with the feature of ST plot (**Figure 5.1.2**). The η_m value was calculated using the limiting value or *r* (0.185 ± 0.003) and fluorescence lifetime of DPH corresponding to 20 mM PEGDPC solution. The η_m value (~70.14 mPa s) thus obtained is greater than that of conventional surfactant micelles, but similar to those of vesicles [41-44]. The high η_m value is consistent with the formation of monolayer membrane by the PEGDPC molecules.

5.1.7 Hydrodynamic diameter and size distribution of aggregates

The mean d_h value of the aggregates formed at different concentrations and pH were determined by DLS measurements. The histograms in **Figure 5.1.8** represent the number distribution profiles of the aggregates formed at different concentrations. It is observed that the aggregates formed in pH 7.0 have narrow and bimodal size distributions. The aggregates are found to be much larger in size than small spherical micelles. Considering the η_m value of the aggregates, the size distribution histograms presented in **Figure 5.1.8** can be associated with small vesicles having mean d_h value in the range of 100-250 nm.

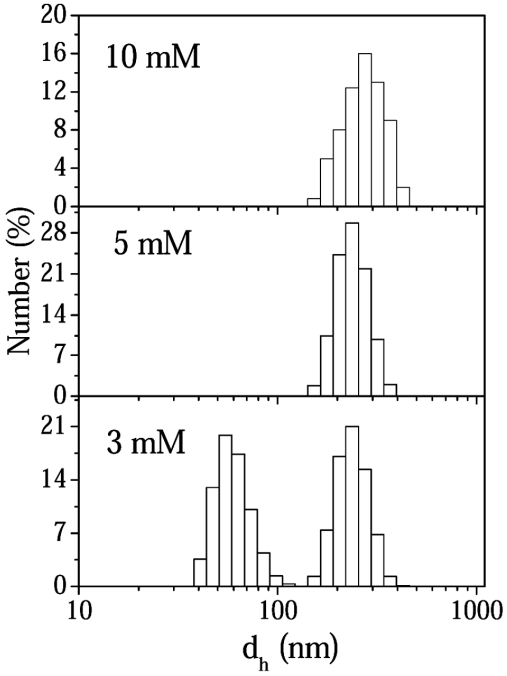

Figure 5.1.8 Concentration dependent size distribution profiles of the aggregates formed by PEGDPC in pH 7.0 buffer at 25 ^{o}C.

The surface potential of the vesicles in 3 mM PEGDPC solution was also measured and the data are collected in **Table 5.1.2**. Slightly negative ζ-potential value (−5.2 mV) of the vesicles at around neutral pH (~6.0–7.0) clearly suggests that the L-cysteine head group of the bolaamphiphile is exposed to the bulk water. In other words, the PEG spacer constitutes the monolayer membrane of the vesicles.

Table 5.1.2 The ζ-potential values of 3 mM PEGDPC at different pHs.

pH	ζ-values (mV)
7.0	– 5.2
2.0	+14.3
10.0	–34.8
Pure water	–2.5

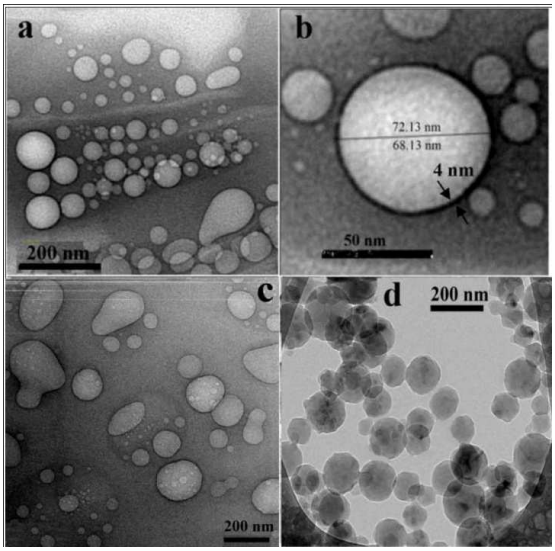

Figure 5.1.9 Unstained HRTEM images of PEGDPC in pH 7.0 buffer: (a, b) 3 mM and (c) 5 mM; Cryo-TEM image of (d) 3 mM PEGDPC in pH 7.0 buffer.

5.1.8 Microscopic study

The HRTEM images of surfactant solutions of different concentrations were taken to visualize the shape of the microstructures formed in aqueous solution. The TEM micrographs (**Figure 5.1.9**) reveal existence of spherical vesicles with aqueous core. The vesicle diameters (150-200 nm) in dilute solution of PEGDPC as seen in the micrographs

are in close agreement with the results of DLS measurements. A very careful look at the vesicular pictures reveals that the thickness of the vesicle wall is ~ 4 nm which is almost equal to the length of the spacer PEG chain (40.51 Å) as obtained from the Gaussview model of the molecule. The microscopic investigations thus confirm existence of small unilamellar vesicles (SUVs) in both dilute and concentrated solutions of PEGDPC. Since the PEG chain is relatively short, monolayer lipid membrane (MLM) formation as shown in **Figure 5.1.5** is much more favorable than bilayer lipid membrane (BLM). This is because for BLM formation, the molecule has to be bent in U-shape, which is energetically less favorable.

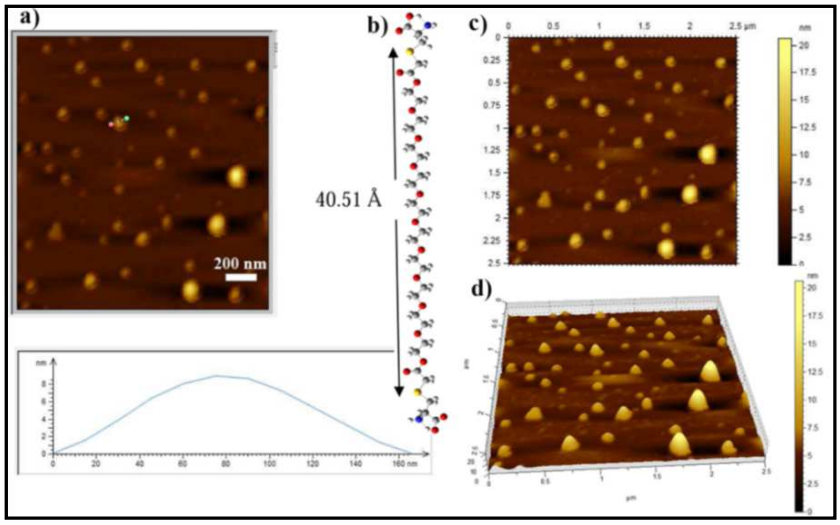

Figure 5.1.10 (a) AFM height image (b) the energy-minimized structure of PEGDPC in solution phase (water) showing the spacer length (c) AFM image with scale bar, and (d) 3D sectional analysis of PEGDPC solution (10 mM, pH 7.0) on mica.

The aggregates of PEGDPC were also characterized by AFM in a dehydrated state. **Figure 5.1.10** shows the tapping-mode AFM image of a 10 mM PEGDPC solution which clearly reveals existence of spherical aggregates with diameters in the range of 80 to 220 nm. This is in good agreement with the results obtained from TEM and DLS measurements. The section analysis profile of a selected aggregate is shown in **Figure**

5.1.10(c). The collapsed aggregate height was observed to be ~ 8 nm. This means the average wall thickness of the hollow sphere is about 4 nm, which is almost equal to the spacer length (40.51Å) of PEGDPC molecule. This implies that the vesicle wall is composed of only a monolayer of PEGDPC molecules. Considering its similarity to a symmetric bolaamphiphile with short chain, PEGDPC could not adopt a U-bent shape, but span the wall to form a monolayer vesicle.

As the HRTEM and AFM methods are associated with the drying of the sample, the images might appear as artefacts. Therefore, in order to rule out the possibility of any artefact in the HRTEM and AFM images, Cryo-TEM measurements were performed. The Cryo-TEM image of the 3 mM PEGDPC solution is shown in **Figure 5.1.9 (d)**. The image clearly reveals existence of vesicles having outer diameters in the range of 120 to 180 nm. Thus the results are consistent with the results of DLS, HRTEM and AFM measurements.

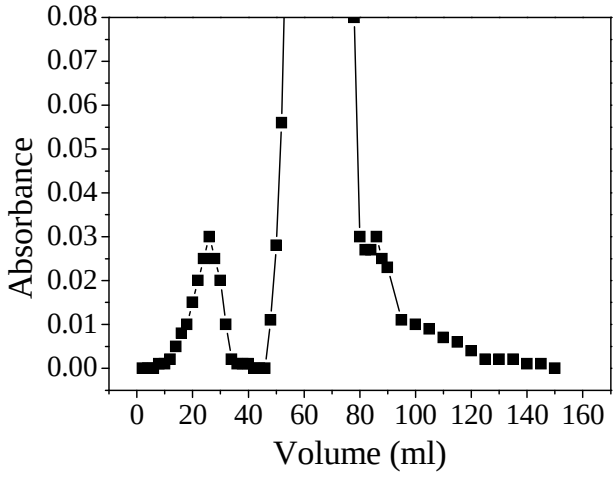

Figure 5.1.11 Gel filtration profile of the separation of the dye-entrapped vesicles (small peak) of PEGDPC from the free dye (MB).

Further to demonstrate the presence of aqueous core in the vesicular aggregate, encapsulation of a hydrophilic dye, methylene blue (MB) was attempted following similar procedure described in chapter 3. The vesicular suspension that eluted right after the void volume (**Figure 5.1.11)** was collected. The encapsulation was confirmed by the

characteristic UV spectrum of MB in water. Thus approximately 1.75% of the total dye could be encapsulated within the vesicles. This study clearly demonstrates that the vesicles contain inner aqueous pool.

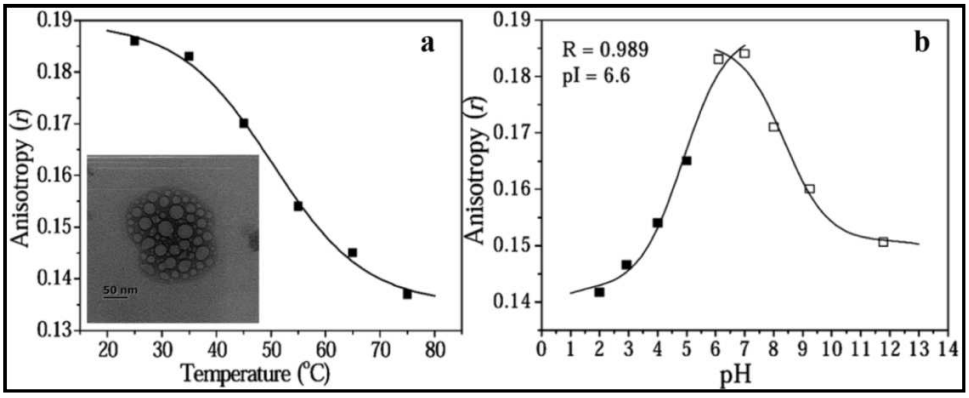

Figure 5.1.12 Plots of variation of fluorescence anisotropy (*r*) of DPH as a function of (a) temperature (inset: TEM image at 80 ^{o}C), and (b) pH.

5.1.9 Stability of the vesicles

As the microenvironment of the vesicle membrane formed by the PEG spacer is slightly polar in character, it can be concluded that the PEG chains in the membrane are partially hydrated. Thus heating of the PEGDPC solution is expected to cause dehydration of the PEG chains and hence change the membrane rigidity. Thus *r* value of DPH probe was measured at different temperatures to observe the phase transition, if any, of the vesicle membrane. **Figure 5.1.12(a)** depicts the variation of *r* as a function of temperature. As seen the *r* value of DPH decreases with the increase of temperature, but it still lies in the vesicular range, even at 80 ^{o}C. The existence of vesicle phase at 80 ^{o}C was confirmed by the TEM image depicted in the inset of **Figure 5.1.12(a).** This suggests that the PEG chains become more fluid and hence leaky at elevated temperatures. This is due to weakening of the hydrophobic interactions among PEG chains caused by the thermal motion. The temperature corresponding to the inflection points of the curves can be taken as the melting or phase transition temperature, T_m of the membrane. The high melting

temperature (48 ^{o}C) for PEGDPC, clearly suggests higher thermal stability of the vesicles at physiological temperature (37 ^{o}C). Interestingly, no clouding of the solution occurred at higher temperatures.

Since the surfactant head group is zwitterionic in nature at ~ pH 6.0-7.0, the stability of the vesicles was also studied by varying pH of the medium. The pH-stability measurement was carried out using 20 mM PEGDPC by monitoring the fluorescence anisotropy of DPH probe. **Figure 5.1.12(b)** shows the variation of *r* with the change in pH of the surfactant solution. It is observed that the *r* value decreases with the decrease as well as with the increase of solution pH, showing a maximum at pH around 7.0. This suggests that the MLM becomes less rigid both at lower and higher pHs as a result of ionization of –COOH or $–NH_3^+$ groups which as discussed above weakens the packing of the PEG chains in the MLM. The weak packing of the PEG units results from increased electrostatic repulsion between anionic or cationic head groups of the amphiphiles at the surface. The pK_a values for the proton transfer equilibria were evaluated from the pH value corresponding to the inflection point of the respective titration curves. The pK_a values thus obtained are 4.8 and 8.4 for the cation-zwitterion and zwitterion-anion equilibria, respectively. The pI value of the head group calculated from the respective pK_a value is ~6.6 at which the amphiphile remains in the zwitterionic form and the aggregates exist either as uncharged or weakly charged entities.

In order to investigate the change in vesicle structure with pH, DLS measurements were performed with the PEGDPC solutions of varying pH. The existence of large aggregates at higher as well as at lower pH is confirmed by the size distribution histograms (**Figure 5.1.13**) of the corresponding solution. The size distribution histograms show that with increase or decrease in pH from 7.0, the aggregate size decreases. The aggregate size is largest in pH 7.0 and is consistent with the zwitterionic head group of the amphiphile in pH 7.0. The existence of vesicles at both lower and higher pH is demonstrated by the TEM picture (**Figure 5.1.14**) of the respective solution. Indeed, vesicle structures can be found in pH 3.0 as well as in 10.0. However, the vesicles shrink upon increase or decrease of pH which supports the results of DLS measurements (**Figure 5.1.13**). This is due to the cationic and anionic character of the

amphiphile head group in acidic and basic medium, respectively. The ionic character of the amphiphile actually causes electrostatic repulsion among the ionic head groups leading to the formation of smaller vesicles.

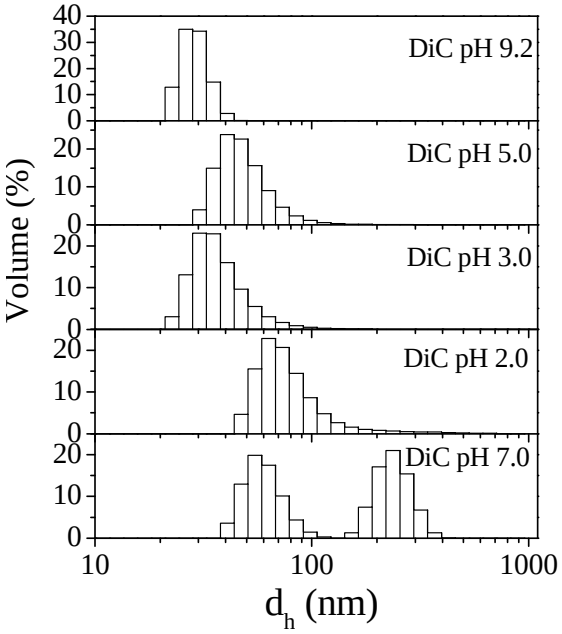

Figure 5.1.13 Hydrodynamic size distribution profiles of vesicles in 3 mM PEGDPC at different pHs.

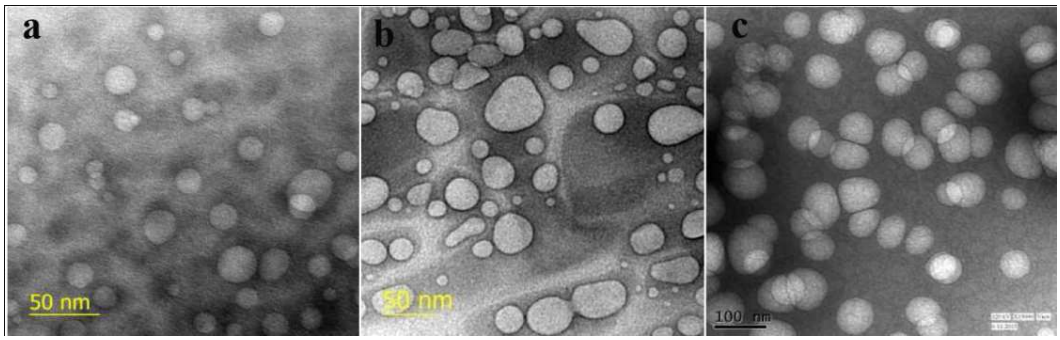

Figure 5.1.14 Unstained HRTEM images of 3 mM PEGDPC at (a) pH 2.0 (b) pH 3.0, and (c) pH 10.0.

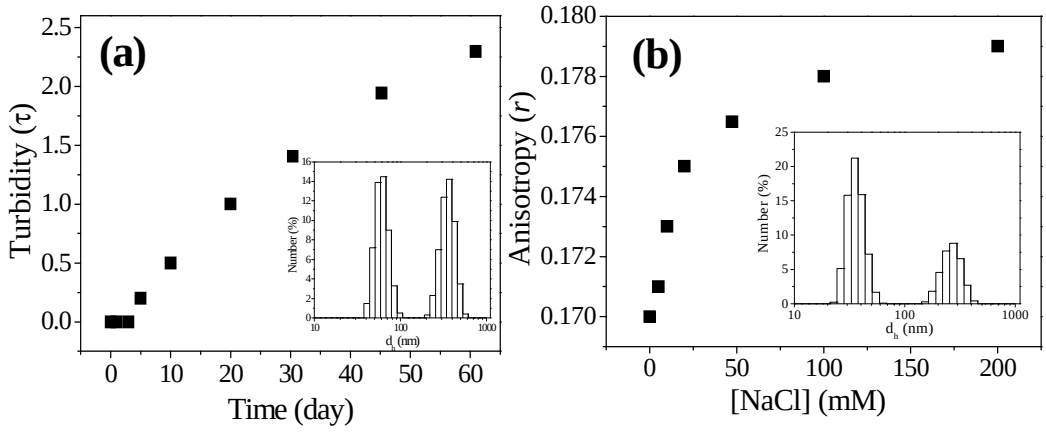

Figure 5.1.15 (a) Variation of turbidity of the vesicles with aging time in neutral pH at room temperature (inset: Size distribution histograms of 2 mM PEGDPC after 60 days of sample preparation) (b) Plot of variation of anisotropy (*r*) of DPH versus NaCl concentration (mM) using 5 mM PEGDPC solution at 25 ^{o}C (inset: size distribution histogram of 5 mM PEGDPC in the presence of 200 mM NaCl).

The vesicles prepared in acidic, neutral, and basic pH were also found to be stable enough with respect to aging time. This is because of surface charge (ζ-potential) of the vesicles. The ζ-values of the vesicles in 3 mM PEGDPC were measured at different pHs and the data are listed in **Table 5.1.2**. The results clearly indicate that the surface charge of the vesicles is positive and negative at pH 3.0 and 10, respectively. However, at around pH 6–7 the surface charge is slightly negative. Since the zwitterionic vesicles at around neutral pH have tendencies to either grow in size or coagulate producing precipitates, turbidity (τ) measurement of the surfactant solution (3 mM, pH 7) was monitored over a period of two months at 400 nm to assure vesicle stability and the results are presented in **Figure 5.1.15(a)** which shows only a slight increase in turbidity for the vesicle solution and can be attributed to the growth of vesicles. This is supported by the size distribution histograms (inset of **Figure 5.1.15(a)**) of the vesicle solution measured at different time intervals. In fact, the monolayer vesicles in 3 mM PEGDPC solution are found to be highly stable even after two months of sample preparation. The excellent stability of the vesicles makes them suitable for applications in drug delivery.

Bilayer vesicles sometimes get destructed in presence of external additives like NaCl, KCl etc. [47, 48] The monolayer vesicle stability was then investigated in the presence of NaCl salt by the measurement of *r* value of DPH probe in pH 7.0 buffer. In the presence of increasing NaCl concentration the *r* value of DPH increases only slightly. The plot showing variation of *r* with [NaCl] is depicted in **Figure 5.1.15(b).** The slight increase of *r* value of DPH at [NaCl] = 200 mM suggests that the monolayer vesicles remain unaffected even in the presence of high salt concentration. The size distribution histogram of 5 mM PEGDPC in the presence of 200 mM NaCl is shown as an inset of **Figure 5.1.15(b)**. As seen the d_h value of the monolayer vesicles remains almost unaltered at this high NaCl concentration.

5.1.10 Dye entrapment and release kinetics

The encapsulation and release of entrapped guest molecules from vesicles is an important issue in drug delivery. As the monolayer membrane of the vesicles consists of biocompatible PEG chains and there is an aqueous pool inside the monolayer vesicles, hydrophilic guest molecules can be encapsulated in the vesicles. Thus, **Cal** was entrapped within the aqueous core of the vesicles at pH 7 according to the method described elsewhere [45-46]. The free, unentrapped dye was separated by dialysis. As the vesicle surface is consisted of zwitterionic L-cysteine head groups, the stability of the membrane is expected to be sensitive to acid-base ionization process. Thus in order to demonstrate pH-triggered release of the encapsulated **Cal** dye from the vesicles, the fluorescence spectra of the **Cal**-loaded vesicles was measured at different pHs. As evident from the **Figure 5.1.16(a)** the fluorescence intensity of **Cal** dye decreased both upon decrease as well as upon increase of solution pH. In fact, the fluorescence intensity of **Cal** in water is known to decrease with the decrease in pH. In both acidic and basic pH, the monolayer vesicles become either positively or negatively charged due to ionization of the head group which increases repulsion among head groups making vesicle membrane unstable and leaky thus releasing the hydrophilic guest to the bulk water having pH higher or lower than pH 7.0. It is also clear from **Figure 5.1.16(b)** that almost 55% of the guest

was released from the vesicles within 45 min of acidification of the vesicle solution (pH $\leq$ 4) as a result of burst release which is highly desirable for drug delivery to solid tumors.

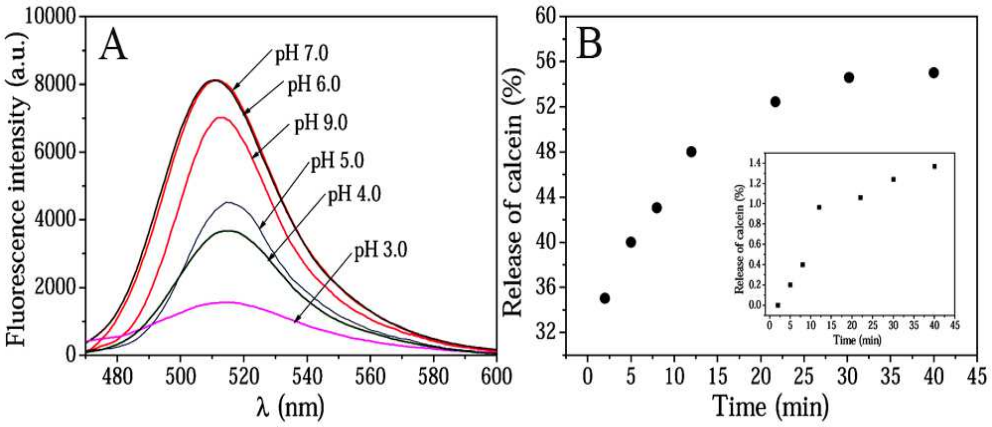

Figure 5.1.16 (A) Change of fluorescent intensity of **Cal** dye showing release of **Cal** from vesicles of DPEGDMS (60 mM) at different pHs after 45 min of incubation at 25 ^{o}C, and (B) % release of **Cal** with the variation of time (min) from the vesicles at pH 4.0 and 37 ^{o}C; inset: **Cal** release profile at pH 7.4 and 37 ^{o}C.

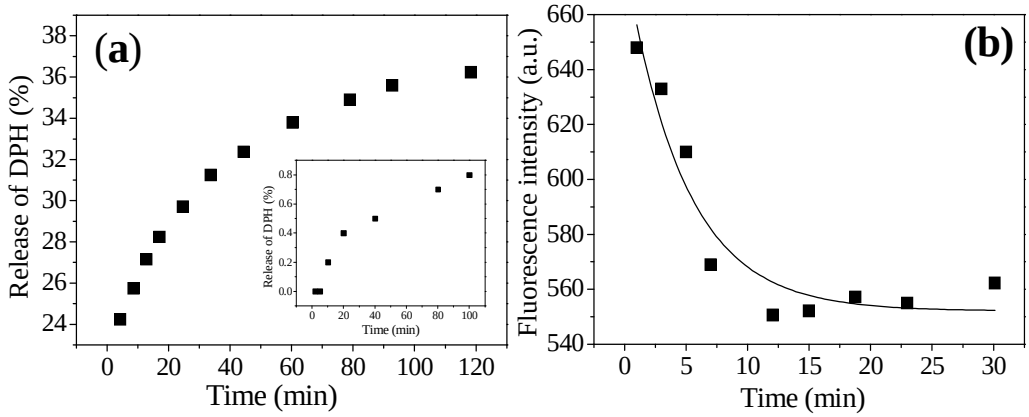

Figure 5.1.17 (a) Plots of release (%) of DPH with time (min) at 37 ^{o}C in pH 4.0 (inset: pH 7.0), and (b) OH- permeability profile of riboflavin entrapped vesicles.

Similar experiment using hydrophobic dye DPH was also carried out. The release profile is shown in **Figure 5.1.17(a)**. In this case also at pH 4.0 a release (25%) followed by a slow release (up to 30%) was observed. The control experiment at pH 7.4 did not show any release during the period of experiment. Thus the monolayer vesicles might be used as efficient hydrophilic as well as hydrophobic drug carrier.

5.1.11 Kinetics of transmembrane permeation

Usually, closed vesicles have the capacity to hold hydrophilic molecules or ions inside their inner aqueous cavity. In the entrapped situation, these solutes cannot permeate across the monolayer membrane freely. The membrane permeability can be measured with a suitable water soluble marker. Thus, riboflavin, a neutral water-soluble molecule which is strongly fluorescent in its neutral form, but becomes nonfluorescent upon deprotonation (pK_a ~ 10.2) was employed for this study [49, 50]. The fluorescence emission intensity (*I*) of the riboflavin-containing PEGDPC vesicular solution (60 mM) in pH 6.8 measured at λ_{flu} = 514 nm (λ_{ex} = 374 nm) was observed to be 1250 a.u, which arises from the contribution of the dye molecules that are adsorbed on the outer membrane surface and also those entrapped within the inner aqueous core of vesicles. When the pH of the vesicular solution was adjusted to 10.2, the fluorescence intensity "instantaneously" decreased to 650 a.u. That is a reduction of ~ 50% intensity is observed. This immediate loss in *I* results from the deprotonation of riboflavin bound on the outer surface of the vesicles. The residual *I*, however, gradually decreased with time (*t*) (**Figure 5.1.17(b)**) and can be attributed to the deprotonation of riboflavin enclosed within the inner aqueous core of the vesicles. The result of this experiment demonstrates that the monolayer membrane formed by the PEGDPC molecules is permeable to ions (OH^- in this case), and that a pH gradient across the membrane can be developed and maintained for some time owing to the existence of the permeability barrier provided by the membrane. Time-dependent loss of the fluorescence intensity due to the conversion of neutral riboflavin into its deprotonated form upon pH adjustment further demonstrates that the monolayer vesicles contain an internal aqueous compartment.

5.1.12 Summary

In this work, a novel L-cysteine-derived bolaamphiphile (PEGDPC) with PEG as spacer was developed and was thoroughly characterized. The solution behavior of the amphiphile at different pHs and temperatures was investigated. Despite having so-called polar PEG spacer the molecule exhibits a reasonably good surface activity in water. Different techniques, including fluorescence spectroscopy, DLS, TEM, and AFM confirmed spontaneous formation of monolayer vesicles by the amphiphilic molecule in neutral, acidic and basic pH. The surfactant monomers organize themselves to form small monolayer vesicle in very dilute as well as in concentrated solution. To the best of knowledge of this author, this is the first report on vesicle formation by a bolaamphiphile containing PEG as spacer chain. The thermodynamic data suggest that the driving force for vesicle formation is hydrophobic effect. The monolayers were observed to be fairly stable with respect to increase of surfactant concentration and temperature. However, the hydrodynamic size of the monolayer vesicles was found to decrease with both decrease and increase of solution pH. The vesicle membrane was also observed to be permeable to OH^- ions. The vesicle stability under physiological condition also suggests that they can have potential applications in drug delivery.

5.2 Monolayer Vesicle Formation by Zwitterionic Bolaamphiphile with Sulfobetaine as Head Groups

5.2.1 Scope of the study

In the preceding section, monolayer vesicle formation by a zwitterionic bolaamphiphile, PEGDPC, having pH-sensitive L-cysteine head groups has been demonstrated. The monolayer vesicles of PEGDPC shows variation in microenvironment and size with the change in pH, which in turn was observed to affect the drug encapsulation and drug release properties of the vesicles [51]. Thus it becomes an obvious choice to evaluate the solution behavior of a pH-silent zwitterionic bolaamphiphile containing the same PEG spacer. Thus, it is intended to establish formation of highly stable vesicles which will be silent to solution pH and other stimuli. In other words, the objective of this study is to investigate the effects of head group change on the aggregation behavior of the PEGDPC bolaamphiphile. Therefore, a zwitterionic bolaamphiphile, (poly(ethylene glycol)-di-(mercaptoethyl sulfobetaine)) (PEGDMS, **Figure 5.2.1**) bearing PEG as spacer and sulfobetaine ($–N^+(C_2H_5)_2SO_3^-$) as head groups was synthesized. As the sulfobetaine group is larger than the zwitterionic L-cysteine group, the solution behavior of PEGDMS molecule is expected to be different from that of PEGDPC amphiphile. This led to the study of surface activity and self-assembly behavior of the molecule in aqueous solution at room temperature. Therefore, the eperimental results have been compared with those of PEGDPC amphiphile.

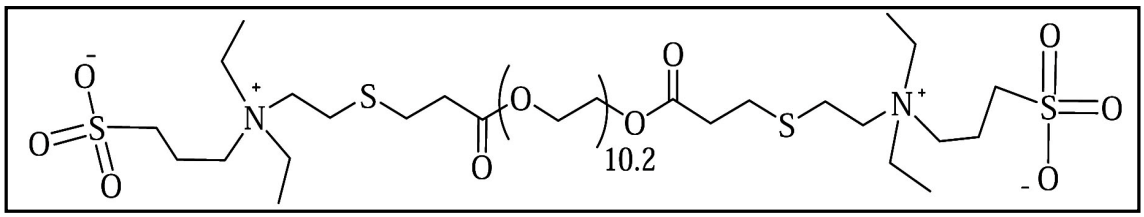

Figure 5.2.1 Chemical structure of PEGDMS molecule.

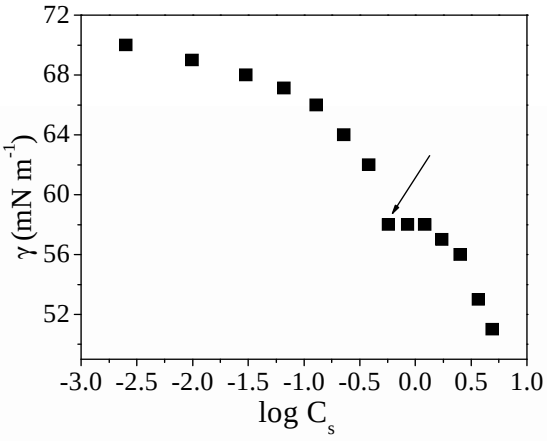

Figure 5.2.2 Plot of surface tension (γ) of phosphate buffer (20 mM, pH 7.0) as a function of concentration (log C_s) of PEGDMS at 25 ^oC.

5.2.2 Surface activity

The variation of surface tension (γ / mN m^{-1}) of phosphate buffer (pH 7.0) at 25 ^oC with the concentration (C_s) of PEGDMS is shown in **Figure 5.2.2**. The γ value decreases gradually with the increase of C_s, indicating spontaneous adsorption of the PEGDMS molecules at the air/water interface which shows amphiphilic character of the molecule. The reduction of γ value is almost same for both PEGDMS and PEGDPC bolaamphphile. Indeed the pC_{20} value of the former (~2.3) amphiphile is also same as the latter (~2.4). This means both the amphiphiles are almost equally surface-active. However, the feature of the ST plot showing a sharp dent (indicated by arrow) is similar to that of PEGDPC amphiphile. The concentration corresponding to the dent (C_s = 0.55 mM) can be taken as the *cmc* value of PEGDMS. The *cmc* value of PEGDMS being less than that of PEGDPC the aggregate formation by the former is more favored. The fall of γ value with increasing concentration above the *cmc* value can be associated with the growth of the aggregates.

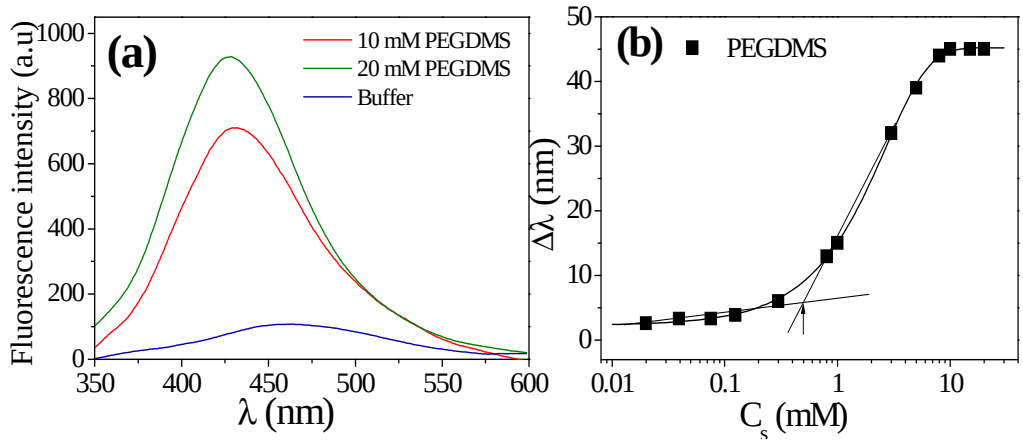

Figure 5.2.3 (a) Representative fluorescence emission spectra of NPN in presence of different concentrations of PEGDMS in pH 7.0, and (b) plot of spectral shift (Δλ) of NPN versus C_s of PEGDMS in pH 7.0 at 25 ^oC.

5.2.3 Self-assembly formation

The self-assembly of PEGDMS in phosphate buffer of pH 7.0 was investigated by use of NPN probe at 25 ^oC. As in the case of PEGDPC, the fluorescence spectrum (**Figure 5.2.3(a)**) in the presence of PEGDMS exhibits an enhancement of intensity and a large blue shift with respect to that in pure buffer. This indicates aggregate formation with a less polar and more viscous microenvironment. The variation of the shift (Δλ) of emission maximum of NPN probe with C_s is shown by the plot in **Figure 5.2.3(b)**. The *cmc* value (0.53 ± 0.02 mM) obtained from the onset of rise of the curve is surprisingly equal to the value obtained by ST measurement. This confirms accuracy of the measurements.

5.2.4 Thermodynamics of aggregate formation

The spontaneous self-assembly formation by PEGDMS molecules is also suggested by the thermodynamic data (see **Table 5.2.1**) obtained by ITC measurements. The titration process of 10 mM PEGDMS in pH 7.0 buffer is featured in **Figure 5.2.4** which shows a

sigmoid increase of enthalpy with the increase of C_s. The *cmc* value of PEGDMS (~0.53 mM) obtained from the inflection point of the plot is consistent with values obtained from ST and fluorescence titration. The data in **Table 5.2.1** show that ΔG^o_m (-18.69 kJ mol^{-1}) is negative and the ΔS^o_m (63.39 J K^{-1} mol^{-1}) is positive which confirm spontaneity of the self-assembly process. Further $T\Delta S^o_m$ value for PEGDMS is found to be much larger than that of the ΔH^o_m, suggesting that the spontaneous aggregate formation is an entropy-driven process [52-54]. This means hydrophobic interaction (as a consequence of dehydration of the PEG spacer) of the PEG spacer chains is the driving force for aggregation. Thus the behavior of PEGDMS is similar to that of PEGDPC.

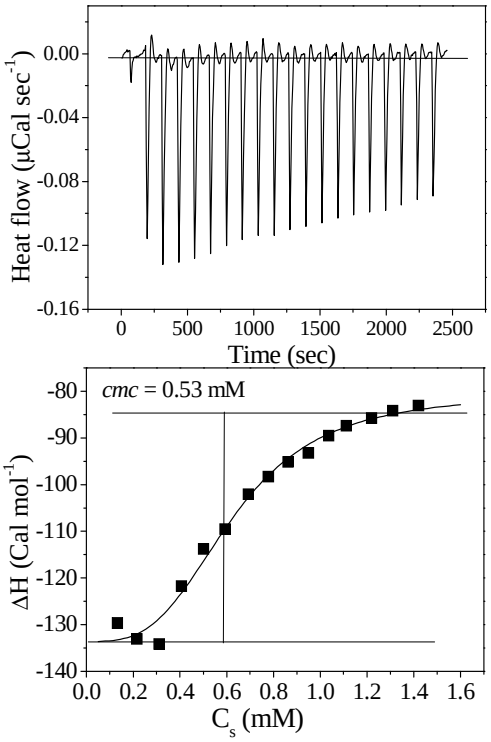

Figure 5.2.4 The upper panel shows a record of heat flow versus time during the titration; the lower panel shows the variation of the change in enthalpy (ΔH) with the final concentrations (C_s) of PEGDMS amphiphile.

Table 5.2.1 Critical micelle concentration (*cmc*), standard Gibbs free energy change (ΔG^{o}_{m}), standard enthalpy change (ΔH^{o}_{m}) and standard entropy change (ΔS^{o}_{m}) for the aggregate formation in aqueous buffered solution (pH 7.0) by PEGDMS at 25 ^{o}C.

cmc (mM)		ΔG^{o}_{m}	ΔH^{o}_{m}	ΔS^{o}_{m}	$T\Delta S^{o}_{m}$
Flu	ITC	(kJ mol^{-1})	(kJ mol^{-1})	(J K^{-1} mol^{-1})	(kJ mol^{-1})
0.53 (± 0.02)	0.53 (± 0.03)	−18.69	0.20 (± 0.1)	63.39	18.89

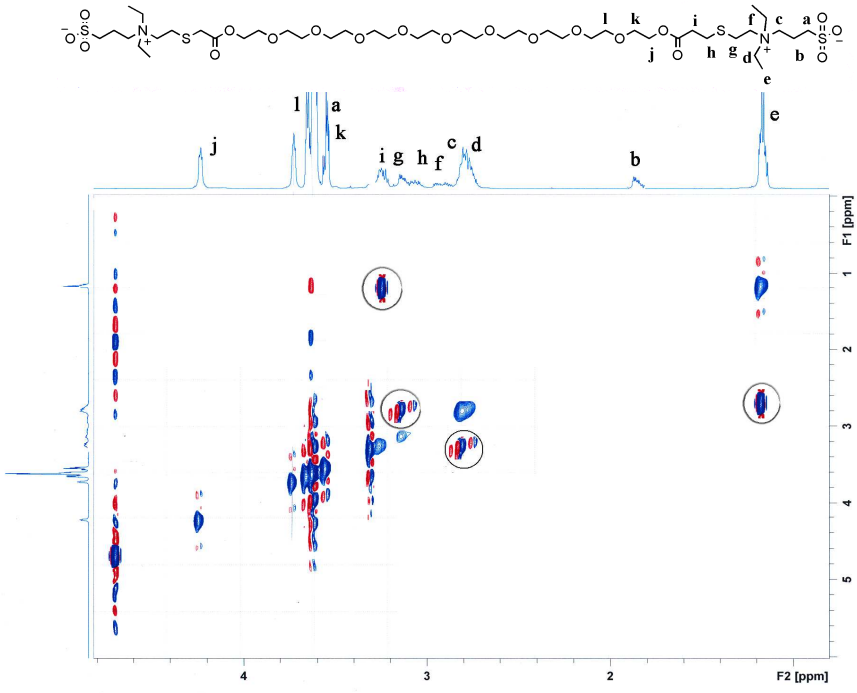

Figure 5.2.5 2D NOESY ^{1}H-NMR spectrum of 2 mM PEGDMS in D_2O.

5.2.5 Molecular alignment of the amphiphile in the aggregate

That the hydrophobic interactions among the PEG chains are responsible for aggregate formation by the PEGDMS molecules is substantiated by the results of 2D NOESY ^{1}H-NMR spectrum (**Figure 5.2.5)** of the molecule in D_2O solvent. The interactions between l

↔ i, g, h, f, k, a, j imply intermolecular interactions among the PEG chains. Further, the key cross peaks reveal strong interactions among e ↔ i, g, h; c ↔ i, g, f and l ↔ i, g, h, f which suggest interactions mainly among the head groups. Thus, it can be concluded that the PEGDMS molecules arrange themselves in the same way as the PEGDPC molecules (**Figure 5.1.5**) do to form the monolayer membrane. This conclusion also substantiated by the zeta-potential value of the aggregates. Indeed, ζ-value of 5 mM PEGDMS solution in pH 7.0 was found to be negative (–5.02 mV). The small negative ζ-value indicates that the aggregate surface is slightly negatively charged and is therefore composed of the zwitterionic $-N^{+}(C_2H_5)_2SO_3^{-}$ head group of the PEGDMS molecules.

Table 5.2.2 Critical micelle concentration (*cmc*), fluorescence anisotropy (*r*) and lifetime of DPH probe (τ_f), micropolarity index (I_1/I_3), and microviscosity (η_m) of PEGDMS molecule.

cmc (mM)		I_1 / I_3	*r*	τ_f (ns)	η_m (mPa s)
Flu	ITC				
0.52	0.53	1.36 ± 0.04	0.172*	4.20	48.9 ± 5.0

*measured in 20 mM PEGDMS

5.2.6 Micropolarity and microviscosity

The micropolarity index (I_1/I_3) of the aggregates formed by the PEGDMS molecules is included in **Table 5.2.2**. The I_1 / I_3 ratio in 20 mM solution of PEGDMS in pH 7.0 buffer was observed to be 1.36, which corresponds to the polarity of dichloromethane solvent (I_1/I_3 =1.37) [34, 35]. This means that the microenvironment of the Py probe is constituted by the PEG chains as observed with the PEGDPC amphiphile. This is consistent with the results of NMR measurements which suggest interaction PEG chains. The micropolarity of PEGDMS monolayer, however, is less than that of PEGDPC amphiphile.

In order to determine rigidity of the monolayer membrane constituted by the PEG chains, the *r* and τ_f values of DPH probe were measured in 20 mM PEGDMS solution.

The microviscosity (η_m) value calculated from the Debye-Stokes-Einstein using fluorescence data is included in **Table 5.2.2**. Although the η_m value (ca. 48.9 ± 5.0 mPa s) is slightly less than that of PEGDPC vesicles, it indicates rigid microenvironment of the DPH probe. This means that PEGDMS also forms similar type of aggregates like PEGDPC amphiphiles. This conclusion is further supported by the results of DLS and TEM measurements as discussed below.

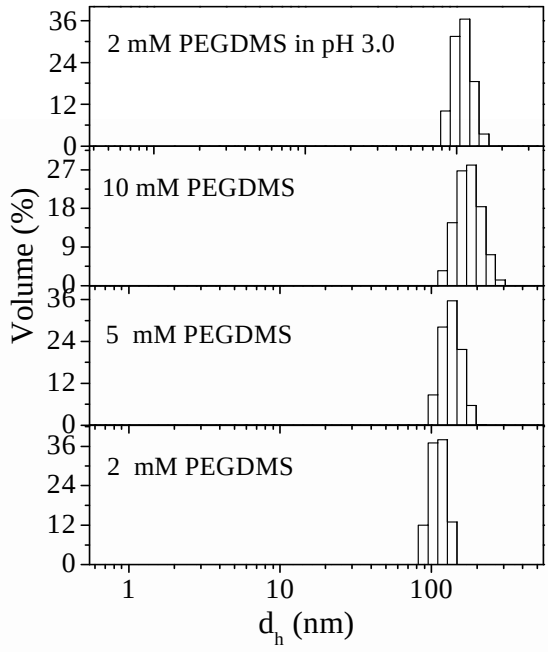

Figure 5.2.6 Concentration dependent size distribution histograms of PEGDMS in pH 7.0 at 25 ^{o}C (upper panel: histogram of 2 mM PEGDMS in pH 3.0).

5.2.7 Size and shape of the aggregates

The size distribution histograms of the aggregates formed by the PEGDMS amphiphile in solutions of different concentrations are presented in **Figure 5.2.6**. The mean d_h value of the aggregates of PEGDMS in the investigated concentration region ranges between 80 nm and 250nm. The presence of large aggregates at all concentrations is consistent with vesicular aggregates as indicated by the fluorescence data. The existence of vesicles is further evidenced by the results of TEM measurements. Representative HRTEM images

of unstained specimens prepared from dilute as well as concentrated solutions of PEGDMS are depicted in **Figure 5.2.7**. The micrographs clearly reveal the existence of spherical vesicles with an aqueous cavity in all the micrographs of PEGDMS. The vesicles have diameter in the range 60-150 nm is also consistent with the results of cryo-TEM measurements (**Figure 5.2.7(d)**). Thus it can be concluded that as in the case of PEGDPC, PEGDMS amphiphiles also form unilamellar vesicles.

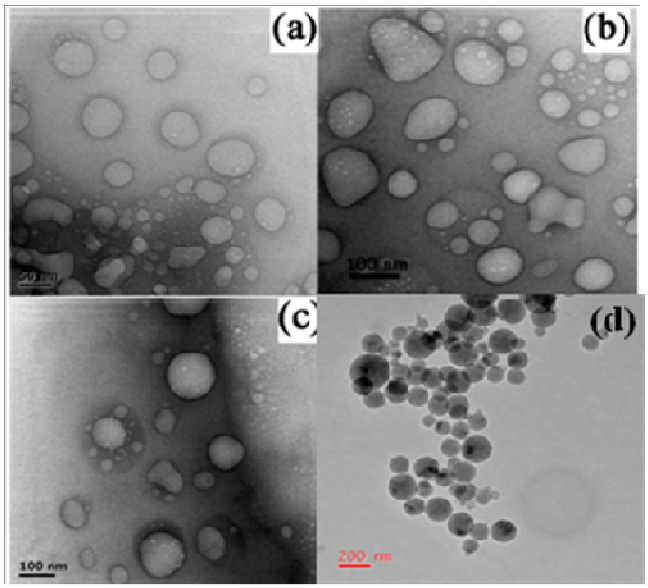

Figure 5.2.7 HRTEM images of (a) 2 mM (b) 10 mM PEGDMS in pH 7.0 (c) 2 mM PEGDMS in pure water and cryo-TEM image of (d) 2 mM PEGDMS in pH 7.0 buffer.

In support to the results of DLS and TEM studies AFM measurements were carried out with the same PEGDMS solutions at room temperature. As shown in **Figure 5.2.8** spherical aggregates having diameters in the range of 50 to 120 nm can be found in 2 mM PEGDMS solution. This is in good agreement with the result obtained from TEM and DLS measurements. The 3D section analysis profile has also been shown in **Figure 5.2.8**. The collapsed aggregate height is observed to be ~ 8 nm. Thus the average wall thickness of the sphere is about 4 nm which is equal to the spacer length of PEGDMS

bolaamphiphile. This means that the aggregates formed are monolayer vesicles as also observed with PEGDPC bolaamphiphile. Considering the results obtained from all the above measurements a schematic of monolayer vesicles formation by the PEGDMS molecules have been shown in **Figure 5.2.9**.

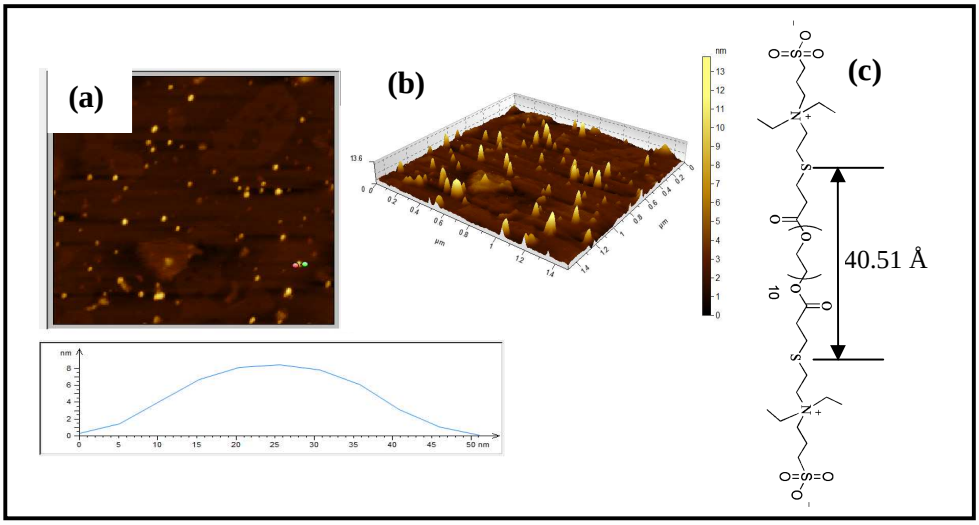

Figure 5.2.8 (a) AFM height image of 2 mM PEGDMS (b) 3D sectional analysis and (c) fully stretched structure of PEGDMS showing the spacer chain length.

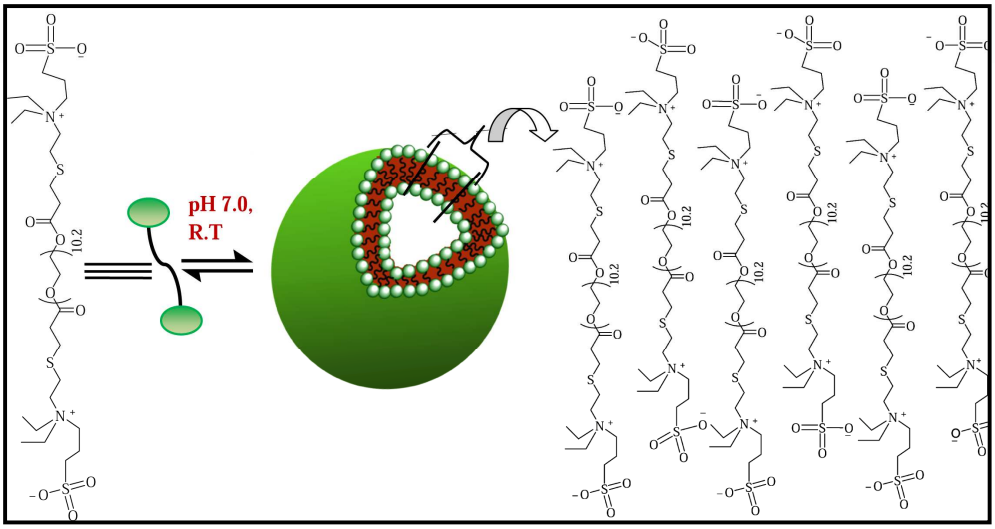

Figure 5.2.9 Schematic of monolayer vesicle formation by PEGDMS molecules.

5.2.8 Dye entrapment studies

The results of **Cal** encapsulation by the monolayer vesicles of PEGDMS are presented in **Figure 5.2.10**. The encapsulation of **Cal** was confirmed by the presence of small peak immediately after the void region in the chromatogram (see **Figure 5.2.10(a))**. This clearly suggests the presence of aqueous core within the monolayer vesicles formed by the pH-silent bolaamphiphile. The fluorescence spectra of free **Cal** in water and vesicle-entrapped **Cal** are depicted in **Figure 5.2.10(b)**. It is observed that the fluorescence intensity of **Cal** is quenched due to confinement within the vesicles. These experiments demonstrate the existence of vesicles in solutions of PEGDMS as observed with PEGDPC amphiphile.

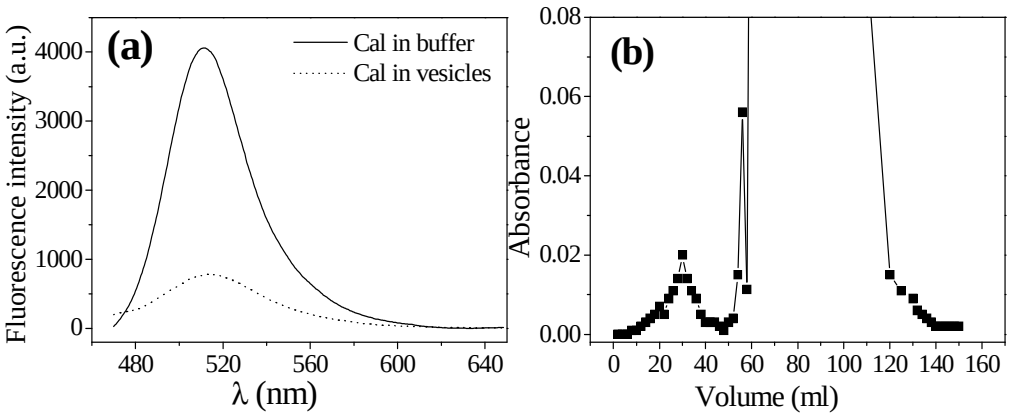

Figure 5.2.10 (a) Gel filtration profile showing separation of the **Cal**-entrapped (small peak) vesicles of PEGDMS from the corresponding free dye, and (b) fluorescence spectra of **Cal**-entrapped vesicles (20 mM PEGDMS) along with the one with unentrapped vesicles.

5.2.9 Stability of the monolayer vesicles

Since the quaternary ammonium and sulfonate groups are silent to solution pH change, the vesicles of PEGDMS bolaamphiphile is expected to be pH-silent. As the sulfonate group remains deprotonated in all the pH, no notable changes was observed in the

microenvironment and morphology of the aggregates. The same I_1 / I_3 value and *r* value at very low pH suggests that the local environment around the probe molecule remains the same even at low pH. For further confirmation, DLS measurement (**Figure 5.2.6**) and TEM analysis (**Figure 5.2.7(d)**) were performed with 2 mM PEGDMS at pH 3.0. As expected, no characteristic change was observed in the morphology or size distribution of the vesicles. This indicates that the monolayer vesicles are highly stable toward pH variation.

The ζ-potential values of the vesicles were measured to further examine the stability against flocculation and coagulation. Thus, ζ-potential value of the vesicles in 5 mM PEGDMS solution was found to be −5.02 mV and 10 mM PEGDMS shows −7.11 mV in pH 7.0 buffer. The results indicate that at pH 7.0 the surface charge is slightly negative which has already been described for other zwitterionic surfactants having sulfonate headgroups. Although the whole molecule of PEGDMS is electronically neutral, the anionic properties on the terminal end may be stronger because of the charge density distribution on the ionic head. It may be understood that the charge density of the quaternary ammonium part located in the middle part on the chain of PEGDMS is scattered along the molecule chain, while the charge density of the anionic sulfonate group located in the terminal end is concentrated. Therefore, the zwitterionic PEGDMS molecule can be treated like a slightly charged anionic surfactant in pH 7.0 buffer. Similar viewpoints have also been reported by Florenzano, Qin and Chorro et al. [52-54].

Since the zwitterionic vesicles have tendencies to precipitate out from solution, turbidity (τ) measurement of the surfactant solution (2 mM, pH 7.0) was monitored over a period of two months at 400 nm to assure vesicle stability. However, the plot in **Figure 5.2.11(a)** shows only a slight increase in turbidity for the surfactant solution and can be attributed to the formation and growth of the vesicles. This is supported by the size distribution profiles (inset of **Figure 5.2.11(a)**) of the surfactant solution at different time intervals. The monolayer vesicles in 2 mM PEGDMS solution are thus found to be highly stable even after two months.

The fluorescence anisotropy of DPH probe solubilized in the monolayer vesicle of PEGDMS was also monitored with increasing NaCl concentration to investigate whether

there is any effect of salt on the monolayer vesicles. The plot in **Figure 5.2.11(b)** shows quite increase of *r* value with the increase in [NaCl]. The increase of *r* value of DPH suggests that the monolayer membranes become more rigid with the increase in NaCl concentration. The size distribution histogram of 10 mM PEGDMS in the presence of 200 mM NaCl has been depicted as inset in **Figure 5.2.11(b)**. It can be observed that the size of the monolayer vesicles also increases in presence of NaCl. The increase of membrane rigidity and size of the monolayer vesicles can be attributed to the decrease in head-group repulsions which is slightly negatively charged in pH 7.0 buffer.

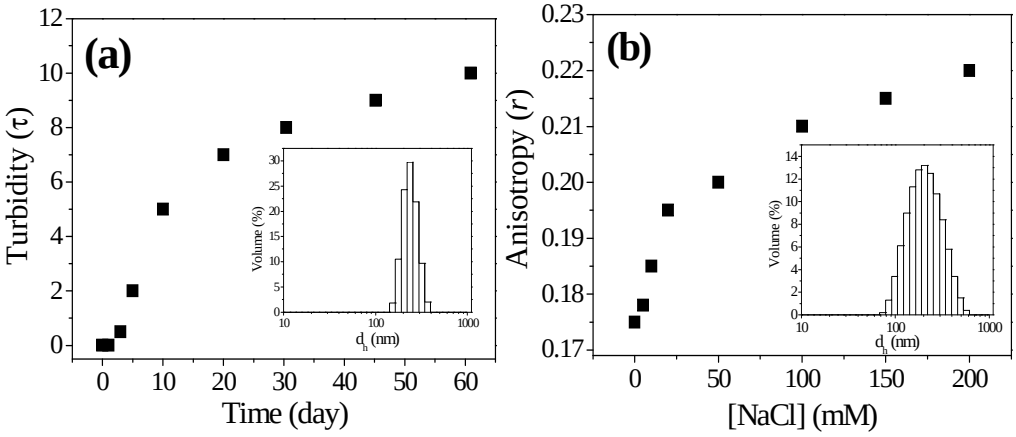

Figure 5.2.11 Plots of (a) variation of turbidity of the vesicles with aging time in neutral pH at room temperature (inset: Size distribution histograms of 2 mM PEGDMS after 60 days of sample preparation) (b) variation of anisotropy (*r*) of DPH versus NaCl concentration (mM) using 10 mM PEGDMS solution at 25 ^{o}C (inset: size distribution histogram of 10 mM PEGDMS in the presence of 200 mM NaCl).

5.2.10 Summary

In summary, a novel zwitterionic bolaamphiphile with PEG as spacer has been developed and characterized. The surface activity and the solution behavior of the amphiphiles were investigated in pH 7.0 at 25 ^{o}C. The results of various experiments suggest spontaneous formation small unilamellar vesicles in neutral, acidic, and basic buffers at room

temperature. The thermodynamic parameters suggest that the driving force behind the aggregate formation is the hydrophobic interaction among the PEG chains. Since the zwitterionic head group of PEGDMS contains charged sulfobetaine groups, the stability of the vesicles was observed to be independent of pH. The monolayer vesicles were found to be sufficiently stable under physiological conditions for a longer period of time.

References

[1] Fuhrhop, H. J.; David, H. H.; Mathieu, J.; Liman, U.; Winter, J. H.; Boekemat, E. Bolaamphiphiles and Monolayer Lipid Membranes Made from 1,6,19,24-Tetraoxa-3,21-cyclohexatriacontadiene- 2,5,20,23–tetrone. *J. Am. Chem. Soc.* **1986**, *108*, 1785-1791.

[2] Bohme, P.; H, -G. Hicke.; Boettcher, C.; Fuhrhop,-H. J. Reactive and Rigid Monolayers of Bisaroyl Azide Diamide Bolaamphiphiles on Polyacrylonitrile Surfaces *J. Am. Chem. Soc.* **1995**, *117*, 5824-5828.

[3] Escamilla, G. H.; Newkome, G. R. Bolaamphiphiles: From Golf Balls to Fibers. *Angew. Chem. Int. Ed.* **1994**, *33(19)*, 1937-1940.

[4] Fuhrhop, -H. J.; Fritsch, D. Bolaamphiphiles Form Ultrathin, Porous and Unsymmetric Monolayer Lipid Membranes. *Acc Chem Res* **1986**, *19*, 130-137.

[5] Mao, G.; Tsao, Y. H.; Tirrell, M.; Davis, T. H.; Hessel, V.; Van, J. E. Monolayers of Bolaform Amphiphiles: Influence of Alkyl Chain Length and Counterions. *Langmuir* **1994**, *10(11)*, 4174-4184.

[6] Fuhrhop, -H. J.; Wang, T. Bolaamphiphiles. *Chem. Rev.* **2004**, *104*, 2901-2937.

[7] Kunitake, T.; Okahata, Y. Formation of Stable Monolayer Membranes and Related Structures
in Dilute Aqueous Solution from Two-headed Ammonium Amphiphiles. *J. Am. Chem. Soc.* **1979**, *101*, 5231-5234.

[8] Newkome, R.; Lin, X. F.; Chen, Y. X.; Escamilla, G. H. Two-Directional Cascade Polymer Synthesis: Effects of Core Variation. *J. Org. Chem.* **1993**, *58*, 3123-3129.

[9] Fuhrhop, J. H.; Spiroski, D.; Boettcher, C. Molecular Monolayer Rods and Tubules Made of .Alpha.-(L-lysine),.omega.-(amino) Bolaamphiphiles. *J. Am. Chem. Soc.* **1993**, *115*, 1600-1601.

[10] Shimizu, T.; Masuda, M. Stereochemical Effect of Even−Odd Connecting Links on Supramolecular Assemblies Made of 1-Glucosamide Bolaamphiphiles. *J. Am. Chem. Soc.* **1997**, *119*, 2812-2818.

[11] Roussel, M.; Lognone, V.; Plusquelleca, D.; Benvegnu, T. Monolayer Lipid Membrane-Forming Dissymmetrical Bolaamphiphiles Derived from Alginate Oligosaccharides. *Chem. Commun.* **2006**, *34*, 3622–3624.

[12] Guilbot, J.; Benvegnu, T.; Legros, N.; Pluspuellec, D. Efficient Synthesis of Unsymmetrical Bolaamphiphiles for Spontaneous Formation of Vesicles and Disks with a Transmembrane Organization. *Langmuir* **2001**, *17*, 613-618.

[13] Shimizu, T.; Iwaura, R.; Masuda, M.; Hanada, T.; Yase, K. Internucleobase-Interaction-Directed Self-Assembly of Nanofibers from Homo- and Heteroditopic 1,*ω*-Nucleobase Bolaamphiphiles. *J. Am. Chem. Soc.* **2001**, *123*, 5947-5955.

[14] Iwaura, R.; Yoshida, K.; Masuda, M.; Yase, K.; Shimizu, T. Spontaneous Fiber Formation and Hydrogelation of Nucleotide Bolaamphiphiles. *Chem. Mater.* **2002**, *14*, 3047-3053.

[15] Yin, S.; Song, B.; Liu, G.; Wang, Z.; Zhang, X. Self-Organization of Polymerizable Bolaamphiphiles Bearing Diacetylene Mesogenic Group. *Langmuir* **2007**, *23*, 5936-5941.

[16] Kobayashi, H.; Amaike, M.; Jung, J. H.; Friggeri, A.; Shinkai, S.; Reinhoudt, D. N. Organogel or Polymer Gel; Facilitated Gelation of a Sugar-Based Organic Gel by the Addition of a Boronic Acid-Appended Polymer. *Chem. Commun.* **2001**, 1038-1039.

[17] Shimizu, T.; Kogiso, M.; Masuda, M. Noncovalent Formation of Polyglycine II-Type Structure by Hexagonal Self-Assembly of Linear Polymolecular Chains. *J. Am. Chem. Soc.* **1997**, *119*, 6209-6210.

[18] Shimizu, T.; Kogiso, M.; Masuda, M. Vesicle Assembly in Microtubes. *Nature* **1996**, *383*, 487-488.

[19] Claussen, C. R.; Rabatic, M. B.; Stupp. I. S. Aqueous Self-Assembly of Unsymmetric Peptide Bolaamphiphiles into Nanofibers with Hydrophilic Cores and Surfaces. *J. Am. Chem. Soc*. **2003**, *125*, 12680-12681.

[20] Ambrosi, M.; Fratini, E.; Alfredsson, V.; Ninham, W. B.; Giorgi, R.; Nostro, L. P.; Baglioni, P. Nanotubes from a Vitamin C-Based Bolaamphiphile. *J. Am. Chem. Soc*. **2006**, *128*, 7209-7214.

[21] Ray, S.; Das, A. K.; Banerjee, A. Self-Assembly Fibrillar Network Gels of Simple Surfactants in Organic Solvents. *Chem Mater* **2007**, *19*, 1633-1639.

[22] Fariya, M.; Jain, A.; Dhawan, V.; Shah, S.; Nagarsenker, S. M. Bolaamphiphiles: A Pharmaceutical Review. *Adv Pharm Bull* **2015**, *4*, 483-491.

[23] Ghosh, R.; Dey, J. Vesicle Formation by L-Cysteine-Derived Unconventional Single- Tailed Amphiphiles in Water: A Fluorescence, Microscopy, and Calorimetric Investigation. *Langmuir* **2014**, *30*, 13516-13524.

[24] Ghosh, R.; Dey, J. Aggregation Behavior of Poly(ethylene glycol) Chain-Containing Anionic Amphiphiles: Thermodynamic, Spectroscopic and Microscopic Studies. *Journal of Colloid and Interface Science* **2015**, *451*, 53-62.

[25] Rosen, J. M.; Mathias, H. J.; Davenport, L. Aberrant Aggregation Behavior in Cationic Gemini Surfactants Investigated by Surface Tension, Interfacial Tension, and Fluorescence Methods. *Langmuir* **1999,** *15*, 7340-7346.

[26] Rosen, M.; Li, F. The Relationship between the Interfacial Properties of Surfactants and Their Toxicity to Aquatic Organisms. *Environ. Sci. Technol.* **2001**, *35*, 954-959.

[27] Ghosh, R.; Dey, J. Vesicle-to-Micelle Transition in Aqueous Solutions of L-Cysteine- Derived Carboxylate Surfactants Containing Both Hydrocarbon and Poly(ethylene glycol) Tails. *Langmuir* **2017**, *33*, 543−552.

[28] Garidel, P.; Hildebrand, A.; Neubert, R.; Blume, A. Thermodynamic Characterization of Bile Salt Aggregation as a Function of Temperature and Ionic Strength Using Isothermal Titration Calorimetry. *Langmuir* **2000,** *16*, 5267-5275.

[29] Majhi, P.; Moulik, S. Energetics of Micellization: Reassessment by a High-Sensitivity Titration Microcalorimeter. *Langmuir* **1998**, *14*, 3986-3990.

[30] Bhattacharya, S.; Haldar, J. Thermodynamics of Micellization of Multiheaded Single-Chain Cationic Surfactants. *Langmuir* **2004**, *20*, 7940-7947.

[31] Laskar, P.; Dey, J.; Ghosh, K. S. Evaluation of Zwitterionic Polymersomes Spontaneously Formed by pH-Sensitive and Biocompatible PEG Based Random

Copolymers as Drug Delivery Systems. *Colloids and Surfaces B: Biointerfaces* **2016**, *139*, 107–116.

[32] Tao, W.; Liu, Y.; Jiang, B.; Yu, S. Huang, W.; Zhou, Y.; Yan. D. A Linear-Hyperbranched Supramolecular Amphiphile and Its Self-Assembly into Vesicles with Great Ductility. *J. Am. Chem. Soc.* **2012**, *134*, 762−764.

[33] Naploli, A.; Valentini, M.; Tirelli, N.; Muller, M.; Hubbell, A. J. Oxidation-Responsive Polymeric Vesicles. *Nat. Mater.* **2004**, *3*, 183-189.

[34] Kalyanasundaram, K.; Thomas, J. K. Environmental Effects on Vibronic Band Intensities in Pyrene Monomer Fluorescence and Their Application in Studies of Micellar Systems. *J. Am. Chem. Soc.* **1977**, *99*, 2039-2044.

[35] Kalyansundaram, K. *Photophysics of Microheterogeneous Systems*; Academic Press: New York, **1988**.

[36] Zana, R.; Martin, I.; Lévy, H. Alkanediyl-α,ω-bis(dimethylalkylammonium bromide). 7. Fluorescence Probing Studies of Micelle Micropolarity and Microviscosity. *Langmuir* **1997**, *13*, 21-27.

[37] Roy, S.; Mohanty, A.; Dey, J. Microviscosity of Bilayer membranes of some N-Acylamino Acid Surfactants determined by Fluorescence Probe Method. *Chem. Phys. Lett*. **2005**, *414*, 23-27.

[38] Lakowicz, J. R. *Principles of Fluorescence Spectroscopy*; Plenum Press: New York, **1983**; p 132.

[39] Cehelnik, E. D.; Cundall, R. B.; Lockwood, J. R.; Palmer, T. F. Solvent and Temperature Effects on the Fluorescence of all-trans-1,6-diphenyl-1,3,5-hexatriene. *J. Phys. Chem.* **1975**, 79, 1369-1376.

[40] Debye, P. *Polar Molecules*; Dover: New York, **1929**.

[41] Roy, S.; Khatua, D.; Dey, J. Giant vesicles of a Single-Tailed Chiral Cationic Surfactant, (1R,2S)-(–)-*N*-Dodecyl-*N*-methylephedrinium Bromide, in Water. *J. Colloid Interface Sci*.**2005**, *292*, 255–264.

[42] Shankar, B. V.; Patanaik, A. pH-Dependent Chiral Vesicles from Enantiomeric Sodium 2,3-Bis(decyloxy)succinate in Aqueous Solution. *Langmuir* **2007**, *23*, 3523-3529.

[43] Horbaschek, K.; Hoffmann, H.; Thunig, C. Formation and Properties of Lamellar Phases in Systems of Cationic Surfactants and Hydroxy-Naphthoate. *J. Colloid Interface Sci*. **1998**, *206*, 439-456.

[44] Ghosh, A.; Dey, J. Physicochemical Characterization and Tube-like Structure Formation of a Novel Amino Acid-Based Zwitterionic Amphiphile N-(2-Hydroxydodecyl)-L-valine in Water. *J. Phys. Chem. B* **2008**, *112*, 6629–6635.

[45] Bhattacharya, S.; Biswas, J. Vesicle and Stable Monolayer Formation from Simple "Click" Chemistry Adducts in Water. *Langmuir* **2011**, *27*, 1581-1591.

[46] Bhattacharya, S.; Ghanashyam Acharya, N. S. Vesicle and Tubular Microstructure Formation from Synthetic Sugar-linked Amphiphiles. Evidence of Vesicle Formation from Single-chain Amphiphiles Bearing a Disaccharide Headgroup. *Langmuir* **2000**, *16*, 87−97.

[47] Böckmann, R. A.; Hac, A.; Heimburg, T.; Grubmüller, H. Effect of Sodium Chloride on a Lipid Bilayer. *Biophys. J.* **2003**, *85*, 1647-1655.

[48] Gurtovenko, A. A.; Vattulainen, I. Effect of NaCl and KCl on Phosphatidylcholine and Phosphatidylethanolamine Lipid Membranes: Insight from Atomic-Scale Simulations for Understanding Salt-Induced Effectsin the Plasma Membrane. *J. Phys. Chem. B* **2008**, *112*, 1953-1962.

[49] Bhattacharya, S.; Biswas, J. Vesicle and Stable Monolayer Formation from Simple "Click" Chemistry Adducts in Water. *Langmuir* **2011**, *27*, 1581–1591.

[50] Bhattacharya, S.; De, S.; Subramanian, M. Synthesis and Vesicle Formation from Hybrid Bolaphile/ Amphiphile Ion-Pairs. Evidence of Membrane Property Modulation by Molecular Design. *J. Org. Chem.* **1998,** *63*, 7640-7651.

[51] Ghosh, R.; Dey, J. An Unconventional Zwitterionic Bolaamphiphile Containing PEG as Spacer Chain: Surface Tension and Self-Assembly Behavior. *Langmuir* **2017**, 33, 7741−7750.

[52] Florenzano, F. H.; Dias, L. G. Critical Micelle Concentration and Average Aggregation Number Estimate of Zwitterionic Amphiphiles: Salt Effect. *Langmuir* **1997**, *13*, 5756−5758.

[53] Chorro, M.; Kamenka, N.; Faucompre, B.; Partyka, S.; Lindheimer, M.; Zana, R. Micellization and Adsorption of a Zwitterionic Surfactant N-dodecyl Betaine: Effect of Salt. *Colloids Surf., A* **1996**, *110*, 249−261.

[54] Qin, X.; Liu, M.; Zhang, X.; Yang, D. Proton NMR Based Investigation of the Effects of Temperature and NaCl on Micellar Properties of CHAPS. *J. Phys. Chem. B* **2011**, *115*, 1991−1998.

Chapter 6
Conclusions and Scope for Future Studies

6.1 Conclusions

The work presented in this dissertation was focused on development of biocompatible amphiphilic molecules having PEG of different chain lengths as tail(s) (or spacer) covalently linked with anionic or zwitterionic group(s) as head. One of the objectives of this work was to demonstrate that though low-molecular-weight PEG chain is hydrophilic in nature, it could behave as a hydrophobic tail when covalently attached to an ionic head group. Therefore, a series of molecules with an ionic (anionic or zwitterionic) head covalently attached to a single or double PEG chains of different lengths was synthesized and characterized for the first time in the literature. Two novel bolaamphiphiles with zwitterionic head groups linked by a PEG spacer were also developed in this work. A comparison of the self-assembly properties of the amphiphiles has been made in Table 6.1.

The solution behavior of these molecules suggests that they are less surface active in comparison to their corresponding hydrocarbon chain analogues which means these molecules are amphiphilic in nature. Despite having so-called polar PEG chain(s) these molecules also self-assemble spontaneously in aqueous solution at room temperature above a very low critical concentration. The self-assembly formation is driven by the positive entropy change in the system and hence hydrophobic effect. This behavior is similar to those of conventional hydrocarbon chain surfactants. In other words, the PEG chain behaves like a hydrocarbon tail. It is important to note that amphiphiles with zwitterionic head group(s) formed small unilamellar vesicles (SUVs) irrespective of PEG chain length, but the sulfonate amphiphile with long PEG tail, due to the helicity of longer PEG chain in water, formed small micelles. In contrast, the double PEG-tailed sulfonate amphiphiles formed unilamellar vesicles irrespective of PEG chain length. In all the single and double PEG-tailed amphiphiles, the bilayer membrane of vesicles or core of micelles is constituted by the PEG chains. The bilayer membrane and the micellar core are less polar and more viscous. But the micropolarity of the bilayer membrane is slightly greater than those constituted by hydrocarbon chains of conventional

amphiphiles. Thus these vesicular (or micellar) aggregates can solubilize molecules of moderate polarity and hence can find applications in drug delivery.

Further, this is the first time, two novel bolaamphiphiles constituted by so-called polar PEG chain as spacer and L-cysteine or sulfobetaine as zwitterionic head groups (PEGDPC and PEGDMS) have been developed. Both types of bolaforms have been shown to be moderately surface active, showing their amphiphilic character. Both types of bolaforms form monolayer vesicles in water at room temperature. The PEG spacer constitutes the monolayer and hence the monolayer is slightly more polar than in the cases of bolaforms containing hydrocarbon chain as spacer.

Interestingly, when a PEG as well as a hydrocarbon chain (or cholesterol moiety) is attached to the same anionic group, the resulting molecule (CPOLE, CPMYS, CPCF3, and CPCF11) behaves like a conventional surfactant and the PEG chain acts as the head group. Unlike conventional surfactants, these carboxylate surfactants produced bilayer vesicles in water at low concentrations (above the *cmc* value), but they exhibit vesicle-to-micelle transition in concentrated solution. However, as in the case of hydrocarbon surfactants, the vesicle bilayer is constituted by the hydrocarbon chains or cholesterol moieties. The PEG chains oriented toward the surface not only impart stability to vesicles, but also act as stealth to be less recognized by the blood components and thereby increasing the lifetime of vesicles in the body circulation.

The sulfonate amphiphiles with two PEG tails exhibit NaCl and L-lysine-induced vesicle-to-tube and vesicle-to-micelle transition, respectively, at room temperature which can be exploited in drug delivery applications. It is important to note that none of these amphiphiles exhibit clouding phenomenon even at a temperature as high as 80 ^{o}C. In fact, the aggregates formed in room temperature were observed to be stable at the physiological temperature. In contrast, the carboxylate amphiphiles containing both PEG and hydrocarbon (or cholesterol) chains exhibit clouding of the solution of pH <3 at a temperature sufficiently above physiological temperature. Thus, the vesicles or micelles being sufficiently small (200-300 nm) and stable under physiological conditions can be used as injectable drug delivery systems. On the other hand, the vesicles of zwitterionic single-chain amphiphiles and bolaamphiphiles ($mPEG_{300}$-Cys and PEGDPC) containing

L-cysteine as head group(s) which exhibit pH-responsive behavior can find applications as pH-triggered drug release vehicles.

Table 6.1 A comparison of different properties, for example, surface activity (pC_{20})**,** critical micelle concentration (*cmc*), microviscosity (η_m)**,** micropolarity index (I_1/I_3), mean hydrodynamic diameter (d_h) and morphology of aggregates of the amphiphiles in pH 7.0 buffer at 25 ^oC.

Amphiphile	**pC_{20}**	***cmc*** (mM)	**η_m** (mPa s)	(I_1/I_3)	**d_h** (nm)	**Morphology**
$mPEG_{300}$-Cys	2.28	1.0 ± 0.07	65	1.56	~50, ~250	ULV*
$mPEG_{1100}$-Cys	2.36	0.2 ± 0.03	79	1.46	~50, ~250	ULV
PEGS1	2.30	2.0 ± 0.1	46	1.61	~300	ULV
PEGS2	2.42	0.86 ± 0.11	22	1.56	~5	Micelles
DPEGS1	-	0.15 ± 0.02	48	1.65	~50, ~400	ULV
DPEGS2	-	0.07 ± 0.03	39	1.70	~250	ULV
CPOLE	5.25	0.01, 0.11	22	1.02	~5	Spherical micelles
CPMYS	4.84	0.03, 0.16	26	1.02	~10	Disk-like micelles
CPCF3	4.45	0.002	540	0.93	~250	ULV
CPCF11	4.67	0.005	485	1.00	~300	ULV
PEGDPC	2.3	0.6	70	1.38	~300	Monolayer vesicles
PEGDMS	2.4	0.52	49	1.36	~180	Monolayer vesicles

* ULV = unilamellar vesicles

6.2 Contributions

- A series of novel amphiphilic molecules with striking properties have been developed.
- PEG molecule acting as tail of the amphiphiles has been reported for the first time.

- Spontaneous unilamellar stable vesicle formation by the single as well as double PEG-tailed amphiphiles without any external stimuli has been reported for the first time.
- It has been demonstrated when both PEG and hydrocarbon chain (or cholesterol) are covalently linked with L-cysteine head group, the resulting amphiphiles behave like conventional surfactant.
- Zwitterionic bolaamphiphiles containing low-molecular-weight PEG as spacer chain have been reported for the first time.
- Also spontaneous formation of monolayer vesicles by the bolaamphphiles has been demonstrated.
- The results of this work have shown that the small unilamellar vesicles (SUVs) can be used for encapsulation and release of hydrophobic as well as moderately polar drugs in drug delivery applications.

6.3 Scope for future studies

The present work can be further extended to develop a large number of biocompatible amphiphiles by conjugating PEG with different amino acids, especially with pH-sensitive functionality. The gemini surfactants constituting of two PEG tails and two ionic or zwitterionic heads can also be synthesized and a comparison of their solution behavior with those of conventional gemini surfactants can be made. Further, it would be interesting to investigate the interactions of these PEG based amphiphiles with oppositely charged conventional surfactants in solution. The present investigation could also be extended to molecular modeling to understand the self-assembly processes of these amphiphiles in water. A detailed *in vitro* and *in vivo* evaluation of drug-loaded vesicles produced by these amphiphiles is also required. Applications of PEG based nanostructures in developing products for daily-use should be studied.

List of Publications

- **Ghosh, R** and Dey, J.* An Unconventional Zwitterionic Bolaamphiphile Containing PEG as Spacer Chain: Surface Tension and Self-Assembly Behavior. ***Langmuir*** **2017**, 33, 7741−7750.

- **Ghosh, R** and Dey, J.* Vesicle-to-Micelle Transition in Aqueous Solutions of L-Cysteine-Derived Carboxylate Surfactants Containing Both Hydrocarbon and Poly(ethylene glycol) Tails. ***Langmuir*** **2017**, 33, 543−552.

- **Ghosh, R** and Dey, J.* Aggregation Behavior of Poly(ethylene glycol) Chain-Containing Anionic Amphiphiles: Thermodynamic, Spectroscopic and Microscopic Studies; ***Journal of Colloid and Interface Science*** **2015**, 451, 53–62.

- **Ghosh, R** and Dey, J.* Vesicle Formation by L-Cysteine-Derived Unconventional Single-Tailed Amphiphiles in Water: A Fluorescence, Microscopy and Calorimetric Investigation; ***Langmuir*** **2014**, 30 (45), 13516–13524.

- **Ghosh, R** and Dey, J.* Unusual Solution Behavior and Aggregation Properties of PEG-Based Double-Tailed Surfactants in Water. **(Manuscript to be submitted)**

- **Ghosh, R** and Dey, J.* Spontaneous Aggregate Formation by Poly(ethylene glycol)-containing Zwitterionic Amphiphiles at Room Temperature: A Fluorescence, Microscopy, and Calorimetric Investigation. **(Manuscript to be submitted)**

- **Ghosh, R** and Dey, J.* pH-induced Micelle to Vesicle Transition by Cholesterol-PEG containing Double-Headed Amphiphiles. **(Manuscript under preparation)**

Conferences

- Poster presentation at **"252nd American Chemical Society National Meeting"** organized by American Chemical Society (ACS) at Philadelphia, PA, USA, 21-25thAugust, 2016.

- Poster presentation at **"Challenges in Organic Materials and Supramolecular Chemistry (ISACS18)"** organized by Royal Society of Chemistry (RSC) at Indian Institute of Science, Bangalore, India, 19 – 21st November, 2015.

- Poster presentation at **"5th Asian Conference on Colloid and Interface Science (ACCIS 2013)"** organized by American Chemical Society (ACS) and Department of Chemistry, University of North Bengal, Darjeeling, India, 20- 23rd November, 2013.

- Poster Presentation at **"Research Scholars' Day (RSD 2015)"** organized by Department of Chemistry, IIT Kharagpur, West Bengal, India, 2nd August, 2015.

- Poster Presentation at **"Research Scholars' Day (RSD 2013)"** organized by Department of Chemistry, IIT Kharagpur, West Bengal, India, 29th July, 2013.